

UCLA

UCLA Electronic Theses and Dissertations

Title

Development of Chemical Patterning: Toward the Realization of Functional Neurotransmitter Chips

Permalink

<https://escholarship.org/uc/item/5xq747q1>

Author

CAO, HUAN

Publication Date

2015

Peer reviewed|Thesis/dissertation

UNIVERSITY OF CALIFORNIA

Los Angeles

Development of Chemical Patterning:
Toward the Realization of Functional Neurotransmitter Chips

A dissertation submitted in partial satisfaction of the requirements for the degree of
Doctor of Philosophy in Chemistry

by

Huan Hien Nam Cao

2015

© Copyright by

Huan Hien Nam Cao

2015

ABSTRACT OF THE DISSERTATION

Development of Chemical Patterning:
Toward the Realization of Functional Neurotransmitter Chips

by

Huan Hien Nam Cao

Doctor of Philosophy in Chemistry

University of California, Los Angeles, 2015

Professor Paul S. Weiss, Chair

G-Protein-coupled receptors (GPCRs) embedded in native neuronal membranes transduce interneuronal signals *via* molecular recognition of small-molecule neurotransmitters. Alterations in chemical communication pathways involving these molecules have been associated with the causes and treatments of neurological and neuropsychiatric disorders. As a result, GPCR-ligand interactions have been extensively investigated. However, conventional radioligand binding methods for interrogating these interactions suffer from laborious protocols needed to label each ligand, as well as cost and safety concerns associated with working with radioactivity. Moreover, traditional methods are not amenable to multiplexing. To address these challenges, we investigated self-assembled monolayers (SAMs) as a means to tether small-molecule neurotransmitters to solid substrates for capturing biomolecules, including GPCRs, from solution. Bovine serum albumin was used to reduce nonspecific biomolecule-substrate binding;

thus improving biomolecule-probe recognition. We developed and advanced new patterning strategies to interrogate relative binding of biomolecules to ligand-functionalized *vs.* unfunctionalized regions and to enable multiplexing on bioactive substrates. Microfluidics was utilized to generate multiplexed substrates by spatially addressing different small-molecule probes to individual channels. The resulting arrays were used to capture and to sort antibodies and GPCRs from complex mixtures according to ligand affinities. We invented chemical lift-off lithography to achieve highly precise biomolecule patterning with sub-30 nm feature sizes. The key step here relies on covalent interactions at stamp/substrate interfaces to enable molecule removal upon stamp release. We discovered that chemical lift-off generated a new class of surface defects for molecular insertion. By varying the pre-lift-off SAM compositions, we controlled surface densities and hybridization of inserted thiolated DNAs and improved target hybridization compared to the conventional backfilling method. We improved surface functionalization strategies by investigating ligand conjugation to surface tethers under two conditions – pre-assembly *vs.* post-assembly. We found the former showed consistent and improved recognition of antibodies compared to the latter. Our next proximal goals will be to use the bioactive substrates developed here to identify high-affinity synthetic neurotransmitter receptors by screening nucleic acid combinatorial libraries. Once selected, these receptors will be used as molecular recognition elements in bioelectronic nanosensors to enable *in vivo* neurotransmitter sensing.

The dissertation of Huan Hien Nam Cao is approved.

Anne M. Andrews

Mark S. Cohen

Paul S. Weiss, Committee Chair

University of California, Los Angeles

2015

Table of Contents

Chapter 1. Multiplexed Nano-Biosensors for Neurotransmitter Measurements at Neural

Synapses

1.1 Introduction to Receptor-Neurotransmitter Recognition Complexes

1.2 Design Motifs Dictating Small-Molecule Neurotransmitter-Functionalized

Substrates

1.2.1 Diluting Surface Coverage of Neurotransmitter-Functionalized

Alkanethiols to Reduce Nonspecific Substrate-Interactions of Biomolecules

1.2.2 Tailoring Ligand Specificity to Enable Selective Recognition of

Biomolecules

1.2.3 Chemical Patterning of Neurotransmitter-Functionalized Alkanethiols to

Enable Multiplexed Screening of Biomolecular Receptors

1.2.3.A Microcontact Insertion Printing

1.2.3.B Microfluidics

1.2.3.C Chemical Lift-Off Lithography

1.3 References

Chapter 2. Patterning Small-Molecule Biocapture Surfaces: Microcontact Insertion

Printing vs. Photolithography

2.1 Abstract

2.2 Introduction

2.3 Materials and Methods

2.4 Results and Discussions

2.4.1 Patterning Small-Molecule Ligands via Self-Assembly-Assisted

Photolithography

2.4.2 Patterning Small-Molecule Ligands via Insertion-Directed Self-Assembly-

Assisted Photolithography

2.4.3 Patterning Small-Molecule Ligands via Microcontact Insertion Printing

2.4.4 Small-Molecule Ligand-Functionalized Substrates for Studying

Competitive Recognition of Mixed Biomolecules from Solution

2.5 Conclusions and Prospects

2.6 Supplementary Experiments and Figures

2.7 References

Chapter 3. Small-Molecule Arrays for Sorting G-Protein-Coupled Receptors

3.1 Abstract

3.2 Introduction

3.3 Materials and Methods

3.4 Results and Discussions

3.4.1 Neurotransmitter Arrays for Sorting Mixed Antibody

3.4.2 Surface-Bound Ligands Mimicking Endogenous Neurotransmitters for

Sorting Native G-Protein-Coupled Receptors

3.5 Conclusions and Prospects

3.6 Supplementary Experiments and Figures

3.7 References

Chapter 4. Subtractive Patterning *via* Chemical Lift-Off Lithography

4.1 Abstract

4.2 Introduction

4.3 Materials and Methods

4.4 Results and Discussions

4.4.1 Chemical Nature of the Lift-Off Process

4.4.2 Patterning Alkanethiol Monolayers and Underlying Substrates with Chemical Lift-Off Lithography

4.4.3 Chemical Lift-Off Nanolithography and Multiple Lift-Off Process

4.4.4 Investigating Molecular Diffusion Following Lift-Off and “Fast” Chemical Lift-Off Lithography

4.5 Conclusions and Prospects

4.6 Supplementary Experiments and Figures

4.7 References

Chapter 5. Toward Multiplexed Biocapture Substrates *via* Chemical Lift-Off Lithography

5.1 Abstract

5.2 Introduction

5.3 Materials and Methods

5.4 Results and Discussions

5.4.1 Patterning Biorecognition Over Multiple Scales

5.4.2 Multiplexed Substrates

5.4.3 Capturing Native Membrane-Associated Receptors

5.5 Conclusions and Prospects

5.6 Supplementary Experiments and Figures

5.7 References

Chapter 6. Enabling Multiplexed Small-Molecule Patterning *via* Pre-Functionalized Molecules

6.1 Abstract

6.2 Introduction

6.3 Materials and Methods

6.4 Results and Discussions

6.4.1 Synthesis of Pre-Functionalized Molecules

6.4.2 Patterning Pre- vs. Post-Functionalized Molecules with Lift-Off

Lithography

6.4.3 Direct Comparisons between Pre- and Post-Functionalized Approaches

6.4.4 Multiplexed Neurotransmitter Pre-Functionalized Substrates

6.5 Conclusions and Prospects

6.6 Supplementary Experiments and Figures

6.7 References

Chapter 7. Controlled DNA Patterning by Chemical Lift-Off Lithography: Matrix Matters

7.1 Abstract

7.2 Introduction

7.3 Materials and Methods

7.4 Results and Discussions

7.4.1 Chemical Lift-Off Lithography Facilitates Probe DNA Insertion and Target DNA Hybridization

7.4.2 Oligo(Ethylene Glycol)-Terminated Alkanethiols Reduce DNA Insertion

7.4.3 Chemical Lift-Off Reduces DNA-Substrate Interactions and Improves DNA Hybridization

7.4.4 Backfilling Reduces Inserted DNA on Post-Lift-Off Alkanethiol SAMs

7.4.5 DNA Arrays Patterned *via* Lift-Off Lithography Using Longer Functionalized Alkanethiols

7.4.6 Spectroscopic Evidence for Lift-Off-Induced Conformation Changes in Oligo(Ethylene Glycol) Moieties

7.4.7 Mixed MCU/TEG SAMs Modulate DNA Surface Coverage

7.5 Conclusions and Prospects

7.6 Supplementary Experiments and Figures

7.7 References

Chapter 8. Fabrication of High Performance Ultrathin In₂O₃ Film Field-Effect Transistors and Biosensors Using Chemical Lift-Off Lithography

8.1 Abstract

8.2 Introduction

8.3 Materials and Methods

8.4 Results and Discussions

8.4.1 Preparation and Characterization of Ultrathin In₂O₃ Film on SiO₂/Si Substrates

8.4.2 Fabricating Micrometer-Scale FET Devices with Chemical Lift-Off

Lithography

8.4.3 Fabricating Submicrometer-Scale FET Devices with Chemical Lift-Off

Lithography

8.4.4 Fabricating FET-Based Aptamer Biosensors for *In Vitro* Dopamine Sensing

8.5 Conclusions and Prospects

8.6 Supplementary Experiments and Figures

8.7 References

Chapter 9. Prospects to the Realization of Functional Neurotransmitter Chips

9.1 Research Highlights and Prospects

9.1.1 Neurochip Project

9.1.2 Chemical Patterning

9.2 References

9.3 Full Publication List

Acknowledgments

I would like to show my greatest appreciation and thankfulness to my advisors, Professors Paul S. Weiss and Anne M. Andrews for their guidance, support, and encouragement throughout my graduate training both at the Pennsylvania State University (PSU) and the University of California, Los Angeles (UCLA). Their invaluable coaching and insightful experiences not only gave inspiration in my research but also helped prepare me well for the important next steps in life as I continue to work toward an independent academic career. I especially thank Anne for improving my writing (the journey of “comments reduction” to publication) and for her willingness to meet (sometimes for hours) to discuss experimental details. Besides being academic advisors, they are my friends whose care and support are always there when I need them. They have been a great support to help me make the transition from PSU to UCLA as smooth as possible. In particular, I would like to thank Anne for helping me pay the first-month housing rent at UCLA when my new bank account was not activated yet at that time. It would not be possible for me to secure my apartment in Westwood, Los Angeles, CA, if I did not have Anne’s help. Finally, my family and I are grateful to both Paul and Anne for standing by me when I had to go through a serious, distressful personal ordeal at UCLA.

My graduate training would have been tiresome and strenuous without my friends and colleagues. I am grateful for Dr. Mitchell J. Shuster and Dr. Amit Vaish for helping me to get started with my graduate research. I am also thankful for the enjoyable friendship with Professor Sarawut Cheunkar (King Mongkut’s University of Technology Thonburi), Mr. Andrew I. Guttentag, and Mr. Jeffrey J. Schwartz. Our scientific discussions, whether in the laboratory or over a dinner table, have always been exciting and challenging. Moreover, I want to show

appreciation to all members of the Weiss and Andrews' groups for their continuous support in work and daily life.

Regarding the neurochip project, I want to thank Ms. Nako Nakatsuka for having the patience to work with me and for giving me the pleasure to gain experience in mentoring younger graduate students. Not only I am proud to have the opportunity to mentor. Nako through her early years in graduate school, but I am also proud of her for her performance in course work and her excellent achievement in our neurochip project. In addition, I am so grateful to work with Professor Wei-Ssu Liao (National Taiwan University) during my research experience at UCLA. He and I worked together to produce exciting scientific innovations. In 2012, I had the honor to work with him to invent chemical lift-off lithography, which was published in *Science* and highlighted in several media sources. Together, we carried the neurochip project to a new phase where neurotransmitter-functionalized substrates were capable of sorting native membrane-associated protein receptors from solution.

In addition, I would like to recognize the funding agencies that made my research endeavors possible. I gratefully acknowledge funding from the National Science Foundation (ECS-0335765, CHE-1013042, and ECCS-1202231), the Kavli Foundation, the U.S. Department of Energy (DE-SC-0005025), the National Institutes of Health, the UCLA Semel Institute for Neuroscience and Human Behavior, the California Nanosystems Institute, and the UCLA Weil Endowment Fund for Research.

I also want to thank the Nano and Pico Characterization Lab and the Integrated Systems Nanofabrication Cleanroom at the California NanoSystems Institute (CNSI), and the UCLA Molecular Instrumentation Center for the use of their facilities. In particular, I would like to thank the staff of CNSI, particularly Dr. Adam Z. Stieg, Dr. Ghassan Malek, and Ms. Lorna

Tokunaga for their helpful insight and support. I also grateful to Prof. Andre Nel for the use of his fluorescent microscope throughout my graduate work at UCLA.

Last but not least, I would like to say my biggest “thank-you” to my family and in particular, my parents, Mr. Cao Bach Van and Mrs. Le Thi Minh Hien, and my great aunt, Ms. Le Thi Xuan Hoa. Without their immense, unceasing support and love, I would not be where I am today. They have accompanied me every single step along my graduate training. The sacrifices they made were too enormous to be measured by any earthly scale. They were so proud to see me attending the UCLA Chemistry and Biochemistry Department’s hooding ceremony. I love my parents dearly and I thank God for giving me the honor to be their only son.

Finally, I want to thank the Lord, my Savior, who always guides me and protects me from harm in this life. There was time when I faltered, but my Lord picked me up and gave me hope to keep going again. In particular, He has reserved for me the woman of my life. Thank-you, Lord, for allowing me to meet my wife, Mrs. Ho Nguyen Thanh Truc. She has been my first and only love, my best friend forever. She has been so patient with me, and was willing to make the sacrifices to come and to stay with me. Her care, support, and most of all love have nurtured and invigorated me to go through the final step in completing my graduate training. I love you, Truc, more than words can say.

Biographical Sketch

Huan Hien Nam Cao came to the United States of America as a high school exchange student in 2003. After completing his high school education, he attended Marshall University, Huntington, WV where he completed an undergraduate degree in chemistry. There, he joined the research group of Professor Michael L. Norton in the Department of Chemistry in 2005. His undergraduate research was aimed at designing and implementing strategies to anchor DNA templates to Au nanostructures patterned on Si/SiO₂ substrates to enable site-directed functionalization of nanoelectronic components for bioelectronics and related applications. He received several academic awards and honors, including a Summer Undergraduate Research Experience (S.U.R.E) fellowship supported by the West Virginia Research Challenge Fund in 2006 and the Chang and Chung Kong Scholar two-year scholarship supported by the Department of Chemistry at Marshall University. He earned his Bachelor of Science degree in Chemistry (*summa cum laude*) in 2008. He co-authored several publications, one of which was published in the *Journal of Chemical Physics* in 2008 featuring studies of impedance measurements on a DNA junction.

In 2008, he began his graduate education at the Pennsylvania State University, University Park, PA. He joined the research groups of Professor Paul S. Weiss from the Department of Chemistry and Professor Anne M. Andrews from the Department of Neuroscience. There, he received an Incoming Graduate Student award from the Department of Chemistry in 2009 for his excellence in teaching and course work. In 2010, he transferred to University of California, Los Angeles with his advisors to continue his graduate studies. In 2011, he had the honor of receiving a NeuroImaging training fellowship supported by the National Institutes of Health. His graduate research has been focused on creating multiplexed arrays of small-molecule probes for the

capture and sorting biomolecules. He developed advanced lithographic techniques and in 2012, he co-invented chemical lift-off lithography to enable precise biomolecule patterning down to 30 nm feature sizes. The work was published in *Science*. He also worked with microfluidics to generate small-molecule arrays for sorting G-protein-coupled receptors (published in the *Journal of Physical Chemistry C* in 2013) and used lift-off lithography to regulate DNA surface density and improve DNA hybridization (published in *ACS Nano* in 2015).

Chapter 1

Multiplexed Nano-Biosensors for Neurotransmitter Measurements at Neural Synapses

1.1 Introduction to Receptor-Neurotransmitter Recognition Complexes

Despite the advances that have been made in medicine to date, combating brain disorders is an increasingly important health issue to address because of the rising numbers of people diagnosed with depression, anxiety disorders, schizophrenia, and Alzheimer's and Parkinson's diseases. For example, the National Institute of Mental Health reported that in 2013, depression disorders affected nearly 16 million adults aged 18 or older in the United States alone.¹ In addition, the Parkinson's Disease Foundation reported that approximately one million Americans are currently living with Parkinson's disease as of 2015.² These rising statistics reveal an urgent need to develop preventive measures and more effective therapeutic treatments for neuropsychiatric and neurological disorders. However, tackling these diseases is a daunting challenge because we still do not comprehend the structural and functional complexity of the human brain. Although an adult human brain only takes up on average about 1-3% of the total body weight, it contains billions of neurons and trillions of interconnected neural networks that regulate all normal brain functions.^{3,4} When we understand the mechanisms underlying these intricate interneuronal connectomes, then biomedical scientists will be able to devise preventive measures and new treatments for brain diseases. Thus, over the years, interdisciplinary efforts spanning numerous scientific fields have joined together in attempts to shed light on the mechanisms of brain functions with a specific focus on gaining understanding of how information is encoded in the signaling between neurons.⁵⁻¹⁰

Neural communication is both electrical and chemical in nature. Signals transmitted between neurons are mediated by chemical interactions between signaling molecules called neurotransmitters and G-protein-coupled receptors (GPCRs) that are embedded in the cell membranes of neurons. Electrical signals are generated upon receiving incoming stimuli. They

are transported *via* dendrites, across the cell body and to the axon by carefully regulated ion channels. As electrical signals reach the ends of neural axons, they trigger the release of neurotransmitters into nanoscale gaps (~20 nm) between neurons called synapses (Fig. 1-1A). Neurotransmitter molecules (typically ~200-300 MW) diffuse across synapses and are recognized by large GPCR binding partners (typically ~100,000 MW) expressed by neighboring neurons. Once captured, neurotransmitters activate G-proteins and subsequent second messenger systems to regulate cellular and physiological functions in the brain. Thus, the formation of GPCR-neurotransmitter complexes is essential to communication between neurons.¹¹⁻¹³

Because of the ability to recognize small-molecule neurotransmitters, GPCRs have become popular targets for drug molecules.^{14,15} In fact, drug molecules have been used to investigate their effects on regulating neural activities at synapses.¹⁴⁻¹⁶ Behavioral and biochemical studies have provided knowledge on drug effects involving specific GPCRs and have helped to identify new drugs for novel therapeutic treatments in neurology and

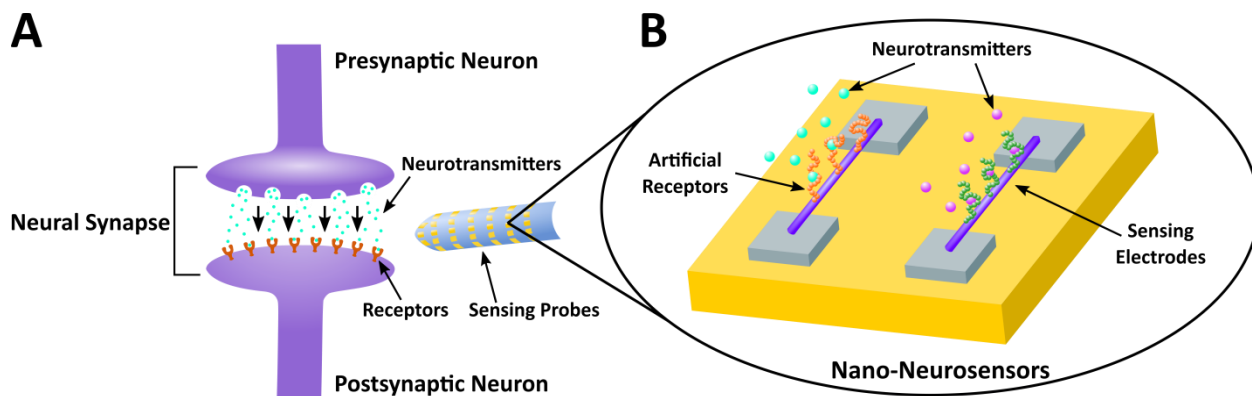


Figure 1-1. Schematic diagram (not to scale) illustrating neurotransmission at neural synapses and neurotransmitter measurements enabled by nano-neurosensors. **(A)** As presynaptic neurons release neurotransmitters into the synapse, they diffuse across and are captured by membrane-associated receptors on the surface of postsynaptic neurons. **(B)** Neurotransmitters can also be captured by artificial receptors tethered to sensing electrodes and the resulting recognition can be transduced into electrical readout signals.

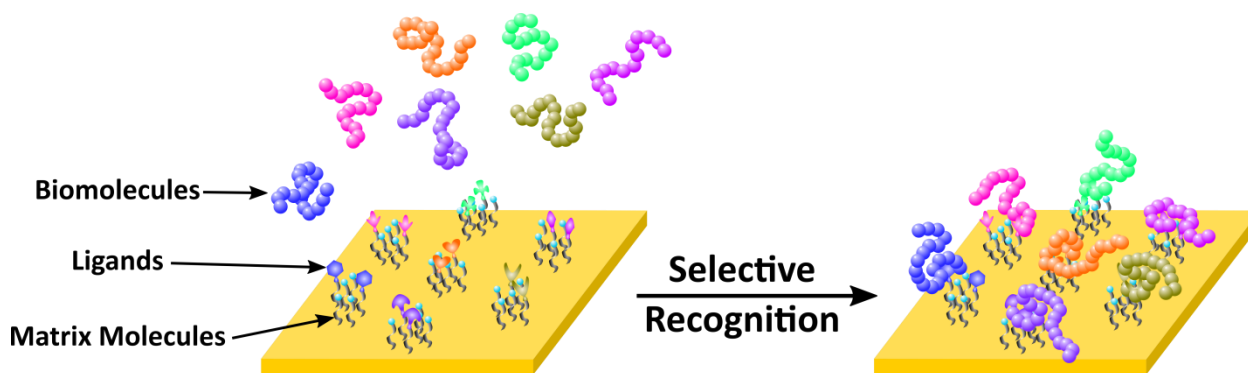
psychiatry.¹⁷⁻¹⁹ Today, with the advent of imaging technology, powerful brain imaging techniques such as magnetic resonance imaging (MRI), positron emission tomography (PET), and functional MRI (fMRI) are used to study brain function.²⁰⁻²² Although brain imaging techniques have provided a large database for both functional and structural information about the human brain, only limited information about GPCR functions, mainly through the use of PET imaging, can be gleaned *via* these methodologies. For example, fMRI measures changes in local blood flow in specific brain regions and correlates that activity with neural responses.²³ Alternately, PET enables imaging of radiotracer binding to receptors and transporters, and also brain glucose utilization.^{24,25} The key point missing in these methodologies is the direct investigation of molecular interactions between GPCRs and their neurotransmitters.^{26,27} In addition, current brain imaging techniques are limited in terms of multiplexed measurements and poor spatial resolution, which are highly disadvantageous for investigating neural activity at the level of nanoscale synapses.^{28,29} Thus, developing novel tools capable of high chemical and spatial resolution to enable such investigations are urgently needed to elucidate molecular interactions between GPCRs and small molecules underlying neural information processing.^{8,9,30}

To address this challenge, we aim to generate multiplexed nanoscale sensors to enable neurotransmitter detection and measurement *in vivo*. Our group has developed advanced lithographic techniques to enable the precise placement of field-effect-transistor (FET)-based biosensors on the surfaces of electrodes in a highly parallel fashion.³¹ Molecular recognition elements (*i.e.*, artificial receptors) are tethered to the FET surfaces to detect changes in neurotransmitter concentrations in the extracellular space at high spatial resolution (Fig. 1-1B). Receptor-neurotransmitter recognition is then transduced into electrical readouts. Aptamer-based artificial receptors screened from combinatorial libraries will be used to recognize different

neurotransmitters selectively and to enable multiplexed *in situ* measurements of neurotransmitters at high spatial and temporal resolution. Because this type of FET-biosensor can be produced at the nanoscale, large numbers of FETs can be packed into small areas on sensing electrodes to reduce the diffusion time from the points of neurotransmitter release to the points of detection (ns- μ s compared to ms-s as currently required for *in vivo* sensing).^{32,33} This will enable high temporal resolution of real-time electrical measurements to capture the dynamics of neurotransmitter release and reuptake. Moreover, these nanosensors will enable highly sensitive neurotransmitter detection due to their intrinsic electrical amplification upon molecular recognition.³³ Thus, our ultimate goal is to use nano-neurosensors to capture chemical dynamics of neurotransmitter activities between neurons in brain circuits to understand how information is encoded in neurotransmitter signaling. Shedding light on this process will provide a neurochemical basis not only to comprehend complex human behaviors but also to distinguish disease states from healthy states, thereby providing insights needed to develop preventive and therapeutic strategies against neurological and neuropsychiatric disorders.

1.2 Design Motifs Dictating Small-Molecule Neurotransmitter-Functionalized Substrates

To enable neurotransmitter measurements for biosensing applications, receptors with high affinity and selectivity for small-molecule ligands are desired. We combine advanced self-assembly surface chemistries, microfluidics, and innovative chemical patterning methods to generate multiplexed platforms decorated with surface-tethered small-molecule ligands capable of high-throughput screening to identify potential artificial receptors for neurosensing purposes (Fig. 1-2). Because native receptors recognize small-molecules in solution, specific surface chemistries need to be discovered and optimized to enable effective and efficient biological recognition at solid/liquid interfaces that mimic solution-phase binding. My thesis focuses on discovering these design rules to enable biological recognition between surface-tethered small-molecule ligands and large biomolecular binding partners at the solid/liquid interface. Application of these design rules enables the development of *functional* neurotransmitter-functionalized self-assembled monolayer-modified substrates (“neurochips”) capable of multiplexed screening to identify artificial neurosensing receptors.



Multiplexed Receptor-Screening Platform

Figure 1-2. Schematic diagram (not to scale) illustrating multiplexed screening platforms decorated with surface-tethered ligands, which recognize biomolecules from solution according to ligand affinities.

Because receptor-ligand binding takes place on surfaces, we also utilized and developed a repertoire of lithographic methods, *i.e.*, microcontact insertion printing (μ CIP), microfluidics, and chemical lift-off lithography, to pattern ligand-functionalized substrates.³⁴⁻³⁸ Because the unfunctionalized regions serve as the internal reference to interrogate relative binding between the background areas absent of ligands and the ligand-functionalized regions, differences in biomolecular recognition between these two regions are classified as “pattern-specific binding.” On the other hand, if patterned substrates are challenged with target and nontarget biomolecular receptors, differences in binding to the patterned substrates between these two biomolecules are classified as “target-specific binding” or binding selectivity.

1.2.1 Diluting Surface Coverage of Neurotransmitter-Functionalized Alkanethiols to Reduce Nonspecific Substrate-Interactions of Biomolecules

Our group employed alkanethiol molecules as the surface linkers to tether neurotransmitters to Au substrates. Alkanethiol self-assembled monolayers (SAMs) are advantageous for studying biomolecule-ligand binding on solid substrates.³⁹⁻⁴¹ These molecules can be anchored to Au surfaces *via* thiol head groups, which form thiol-Au bonds (Fig. 1-3).⁴¹ The aliphatic backbones of alkanethiols form van der Waals interactions between neighboring molecules to promote monolayer formation. Previous studies have shown that alkanethiol SAM formation is composed of an initial fast step (several seconds) where alkanethiols spontaneously assemble on Au surfaces followed by a slower step (hours to days) where these molecules undergo surface rearrangement to form well-packed monolayers.⁴¹ However, even for well-ordered alkanethiol SAMs, surface defects can still be detected with scanning probe microscopy and other methods.⁴²⁻⁴⁴ Because these defect sites are susceptible to *molecular insertion* by other

alkanethiols, we are able to use them to advantage (*vide infra*) to address challenging issues in biomolecular recognition.

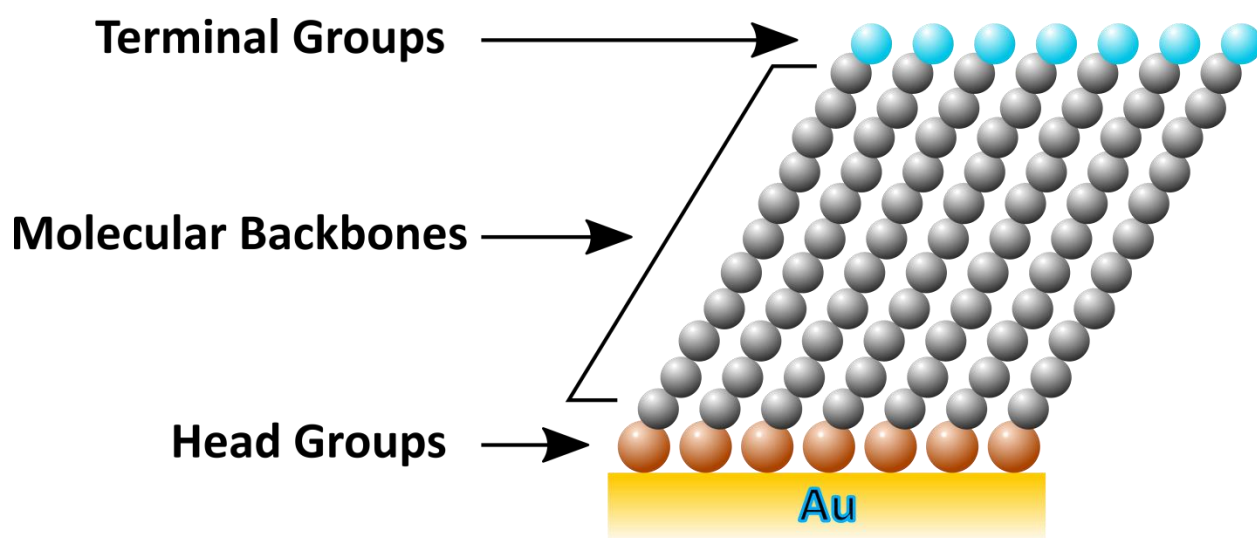


Figure 1-3. Schematic diagram illustrating alkanethiol self-assembled monolayers on Au substrates. Alkanethiols consists of thiol head groups forming thiol-Au bonds, molecular backbones forming van der Waals interactions with neighboring molecules, and terminal groups amenable to chemical functionalization.

The terminal groups of alkanethiols are amenable to chemical functionalization. For example, some terminal groups, such as carboxyls, primary amines, aldehydes, alkynes, azides, and hydrazines can be used for functionalization to small molecules, peptides, or proteins through standard coupling chemistries.^{41,45,46} Moreover, alkanethiols terminated with oligo(ethylene glycol) moieties are known to resist nonspecific binding of biomolecules on substrates.⁴⁷⁻⁴⁹ Thus, mixed monolayers of alkanethiol tethers and oligo(ethylene glycol)-modified matrix molecules are often used to enhance specific binding of biomolecules to ligand-modified tethers while reducing nonspecific binding of biomolecules to the protein-resistant backgrounds.⁵⁰ Low surface coverages (<10%) of tethers were found to improve *specific binding* (specific binding for patterned substrates) of biomolecules compared to higher tether surface coverages (>80%).⁵¹ Because scanning probe microscopy studies showed that alkanethiols can separate into domains according to chemical similarities, diluting ligand-tethered alkanethiols in a protein-resistant background reduces phase separation and steric interactions between surface-bound ligands, enabling improved specific binding.⁵²⁻⁵⁴ Other studies also showed that high densities of surface-bound ligands increase the probability of nonspecific binding of biomolecules through multivalent interactions.⁵⁵⁻⁵⁷

Alternately, our group achieved specific biomolecule capture on ligand-modified substrates by diluting tethering molecules *via* molecular insertion into defects in protein-resistant SAMs (Fig. 1-4A).^{58,59} In this approach, we inserted amine- or carboxyl-terminated alkanethiol tethers into preformed oligo(ethylene glycol)-modified SAMs on Au substrates.^{58,60,61} The inserted molecules were then functionalized with small-molecule neurotransmitters through standard coupling chemistries (Fig. 1-4B).^{62,63} Insertion-directed functionalization of

neurotransmitters overcomes not only steric hindrance and nonspecific interactions due to phase separation, but also the size-mismatch problem of protein-ligand pairs.

Considering the sizes of biomolecules (ranging from a few nanometers for proteins to tens of nanometers for membrane-associated proteins), it is difficult for these large molecules to approach substrates particularly when ligand-tethered molecules are clustered together. The binding of one biomolecule to a ligand-tethered molecule will exclude the binding of additional biomolecules due to the physical dimensions of the captured biomolecule on the substrate. Thus, by isolating tethering molecules through insertion-directed assembly, each ligand-tethered molecule is well separated ($\sim 1\text{-}3$ nm for the size of protein receptors, *e.g.*, streptavidin) to enable efficient biomolecule binding (Fig. 1-4C).^{64,65} Moreover, we also incorporated additional ethylene glycol moieties into the tethering molecules to render them longer than the protein-

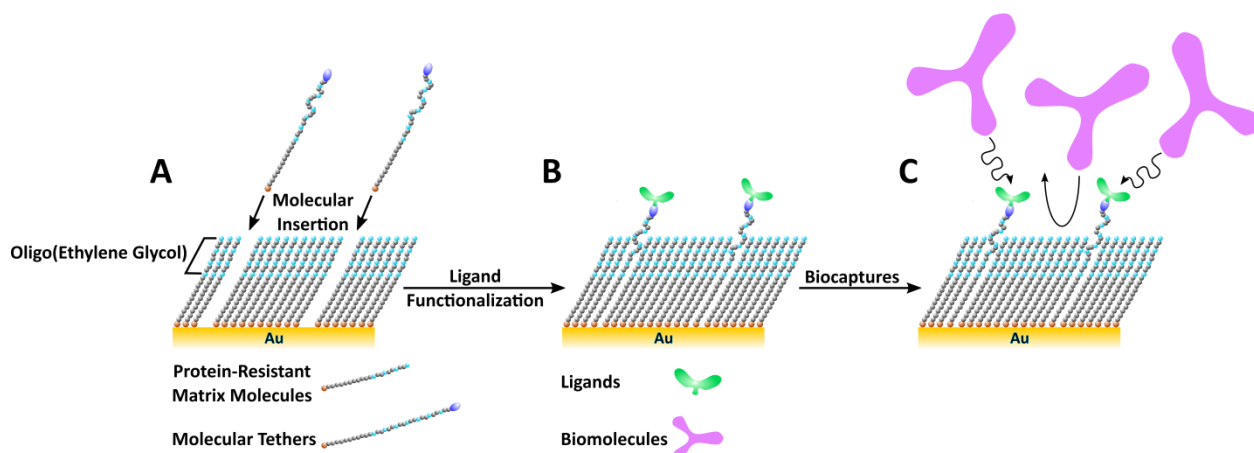


Figure 1-4. Schematic diagram (not to scale) illustrating insertion-functionalization of Au substrates for biomolecule captures. **(A)** Molecular tethers are inserted into the defect sites of preformed oligo(ethylene glycol)-terminated alkanethiols, which are known to resist nonspecific protein adsorption. **(B)** Terminal groups of molecular tethers are functionalized with ligands of interest (*i.e.*, small-molecule neurotransmitters). **(C)** The resulting surface-tethered ligands are well isolated and protrude beyond the protein-resistant matrix to enable effective recognition of target biomolecules (the squiggled arrows), while the protein-resistant background repels biomolecules (the curved arrow).

resistant matrix molecules to access the binding pockets of biomolecules (Scheme 1-1A).⁵⁸ The use of additional oligo(ethylene glycol) moieties also helps reduce nonspecific interactions of protein receptors.^{35,58}

1.2.2 Tailoring Ligand Specificity to Enable Selective Recognition of Biomolecules

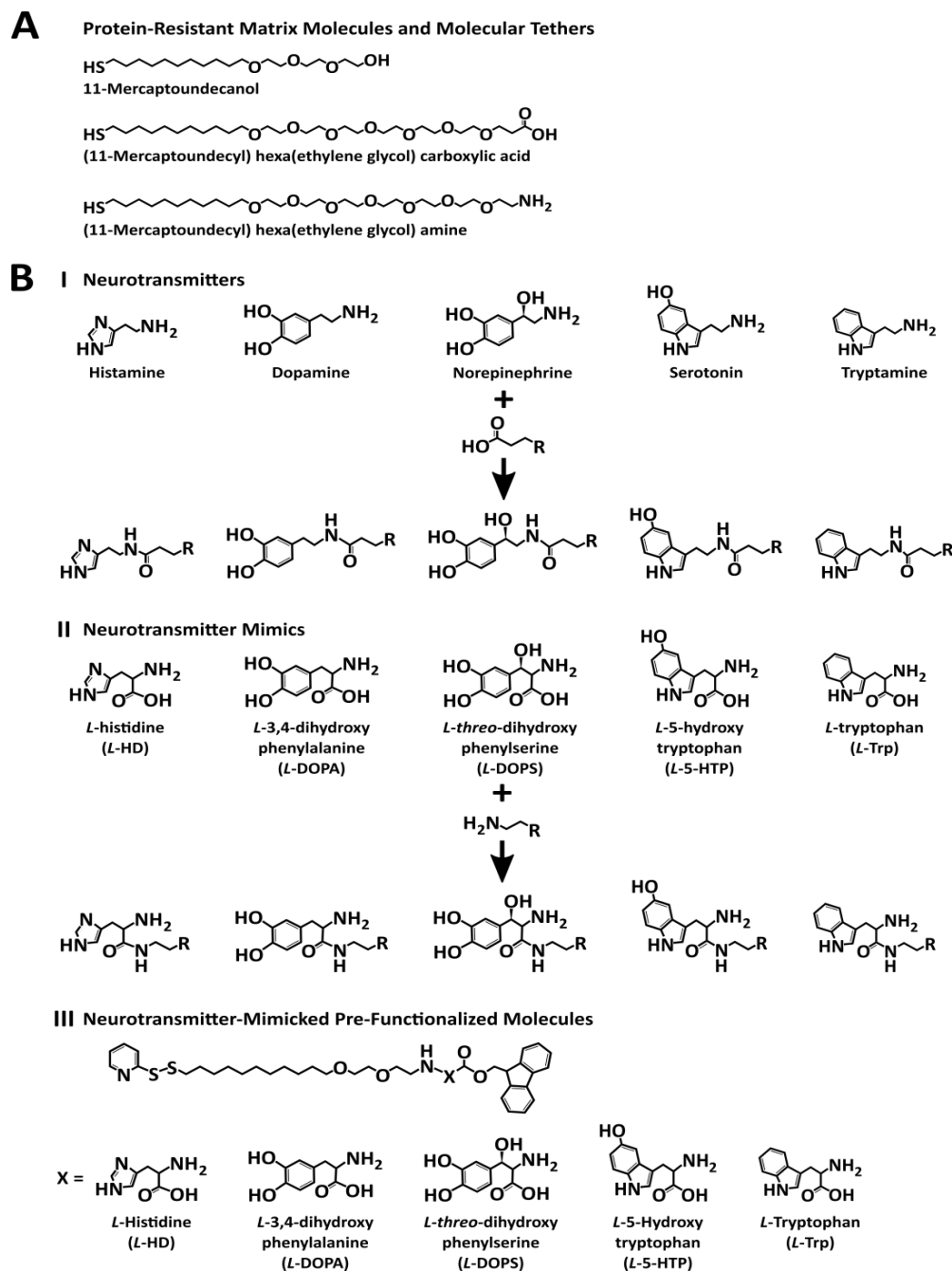
During signal transmission at neural synapses, neurotransmitters released from pre-synaptic neurons are recognized by GPCRs on the cell membranes of post-synaptic neurons. These GPCR-neurotransmitter interactions take place under the condition where the neurotransmitters are in their free form.^{60,66,67} In other words, they are not bound to a solid surface, and thus all of their essential functional epitopes are available for recognition by GPCRs. Small-molecule neurotransmitters used in our early experiments were tethered to substrates through amide bonds formed between the amino groups on neurotransmitters and the terminal carboxyl groups on the tethering alkanethiols (Scheme 1-1BI).^{58,59} However, we discovered that although this functionalization approach facilitated the capture of antibodies on neurotransmitter-modified substrates, it failed to do so with native membrane-associated receptors.⁶⁰ The latter are evolved to recognize free solution neurotransmitters.

To address this difficulty, we noted that these small molecules are biogenic amine neurotransmitters in which the amino moiety is a common motif among them.⁶⁸ However, because we have used these amines to tether neurotransmitters to substrates, they are no longer available for receptor binding. Thus, we hypothesized that using an alternate strategy where the surface-tethered molecules following functionalization retained the essential epitopes for biorecognition, the neurotransmitter-modified substrates would be able to capture native GPCRs. We tested this hypothesis by replacing the neurotransmitters with their biological precursor

molecules, which introduced additional carboxyl groups for surface tethering instead of using the amine groups (Scheme 1-1BII). This new approach enabled the surface-bound precursor molecules to mimic neurotransmitters in solution with the amino moieties exposed for capturing GPCRs. For example, we showed that surface-tethered serotonin and dopamine neurotransmitters were able to capture their respective antibodies but failed to do so with their native membrane-associated receptors.⁵⁸⁻⁶⁰ In contrast, precursors of serotonin and dopamine, *i.e.*, *L*-5-hydroxytryptophan (*L*-5-HTP) and *L*-3,4-dihydroxyphenylalanine (*L*-DOPA), respectively, tethered to the substrates were able to capture *L*-5-HTP and *L*-DOPA antibodies and serotonin and dopamine membrane-associated receptors, respectively.^{35,60}

1.2.3 Chemical Patterning of Neurotransmitter-Functionalized Alkanethiols to Enable Multiplexed Screening of Biomolecular Receptors

One of the methods used to detect biomolecule binding on surfaces is fluorescence microscopy. A fluorescence assay is used in which secondary antibodies tagged with fluorophores are used to visualize primary antibodies captured on substrates.^{69,70} To visualize antibody binding on neurotransmitter-tethered alkanethiol SAM-modified substrates with fluorescence microscopy, we have developed several chemical-patterning strategies. Because patterning enables placement of tethering molecules on substrates in a spatially defined manner, specific binding of biomolecules can be visualized and quantified through the fluorescence contrast between ligand-functionalized and unfunctionalized regions. Moreover, patterning can generate arrays of small-molecule ligands enabling multiplexed measurement of biomolecule binding.⁷¹



Scheme 1-1. List of (A) matrix and tethering molecules, (BI,II) reaction diagrams of neurotransmitters/neurotransmitter mimics conjugated with tethering molecules, and (BIII) list of neurotransmitter-mimicked pre-functionalized molecules. Amide bond formation is the common chemical motif in the conjugation schemes BI, BII, and BIII. (BI,II) Amines/carboxyls of neurotransmitters/neurotransmitter mimics reacted with carboxyl/amine-terminated tethering molecules, respectively. (BIII) Similarly, carboxyls of neurotransmitter mimics reacted with amine-terminated tethering molecules in the pre-functionalization scheme.

1.2.3.A Microcontact Insertion Printing

The ability to self-assemble alkanethiols on Au substrates enables these molecules to be used as molecular inks in microcontact printing (μ CP) to create molecular patterns (Fig. 1-5A).⁷² Rubber stamps made of polydimethylsiloxane (PDMS) with topographic features, which are replicated from the relief features on silicon master molds, are inked with alkanethiols, and then brought into conformal contact with Au substrates. Wherever the stamp contacts the substrate, alkanethiols diffuse from the stamp to the substrate to form a monolayer on the surface. However, the longer the contact time, the more likely alkanethiols will diffuse beyond the contact region.⁷³ In some cases, longer contact times are preferable because the printed monolayers can serve as molecular resists to protect the underlying Au substrates against chemical etching for device fabrication purposes.⁷⁴⁻⁷⁷ In addition, volatile alkanethiols residing in the recesses of the stamp topography can reach the noncontact areas through gas-phase deposition. These phenomena render the printed patterns blurred or indiscernible because alkanethiol diffusion causes the printed features to merge and gas-phase deposition causes noncontact areas to be populated with alkanethiols.^{78,79} Thus, modified versions of μ CP have been developed to overcome these difficulties.

Our group developed μ CIP in which Au substrates pre-existing with alkanethiol SAMs, instead of bare Au substrates, are used as printing templates (Fig. 1-5B).³⁸ During conformal contact, alkanethiols from the rubber stamp are stochastically inserted into intrinsic SAM defects in the preformed monolayers. This approach allows the preformed alkanethiol monolayer to act as a physical barrier against both lateral diffusion of alkanethiols on Au surfaces and gas-phase deposition in noncontact areas. Moreover, the stochastic nature of insertion enables spacing

between alkanethiol tethers on the preformed SAM matrix. Preparation and processing of the matrix defines the types of monolayer defects into which new molecules will be inserted.^{37,42,43,80-82} For example, our group demonstrated that μ CIP enabled insertion-directed assembly of tethering alkanethiols that can be later functionalized with small-molecule neurotransmitters.⁵⁸⁻⁶¹

Using microcontact insertion printing to generate patterned surfaces and fluorescence microscopy to visualize biomolecule binding, I discovered that passivating the background with oligo(ethylene glycol) moieties was not sufficient to reduce nonspecific binding of fluorescently labeled secondary antibodies to surfaces to acceptable levels (<10% of total binding). Because of the need to visualize and to quantify patterned-specific primary antibody binding to surface-bound neurotransmitters, fluorescently labeled secondary antibodies were necessary to tag the bound primary antibodies. However, to ensure that the patterned-specific fluorescence resulted from the binding of primary antibodies, control experiments were carried out in which substrates were exposed only to fluorescently labeled secondary antibodies. These experiments showed that the amount of nonspecific binding from fluorescently labeled secondary antibodies was greater than 20% of the total (primary + secondary antibody) binding. However, when I first passivated the patterned surfaces with bovine serum albumin, I discovered that I could reduce nonspecific binding to <10%.^{35,59} This was a significant finding because it not only improved the pattern quality visually, but also enabled the quantification of antibody-specific binding. The details of this work are described in Chapter 2.

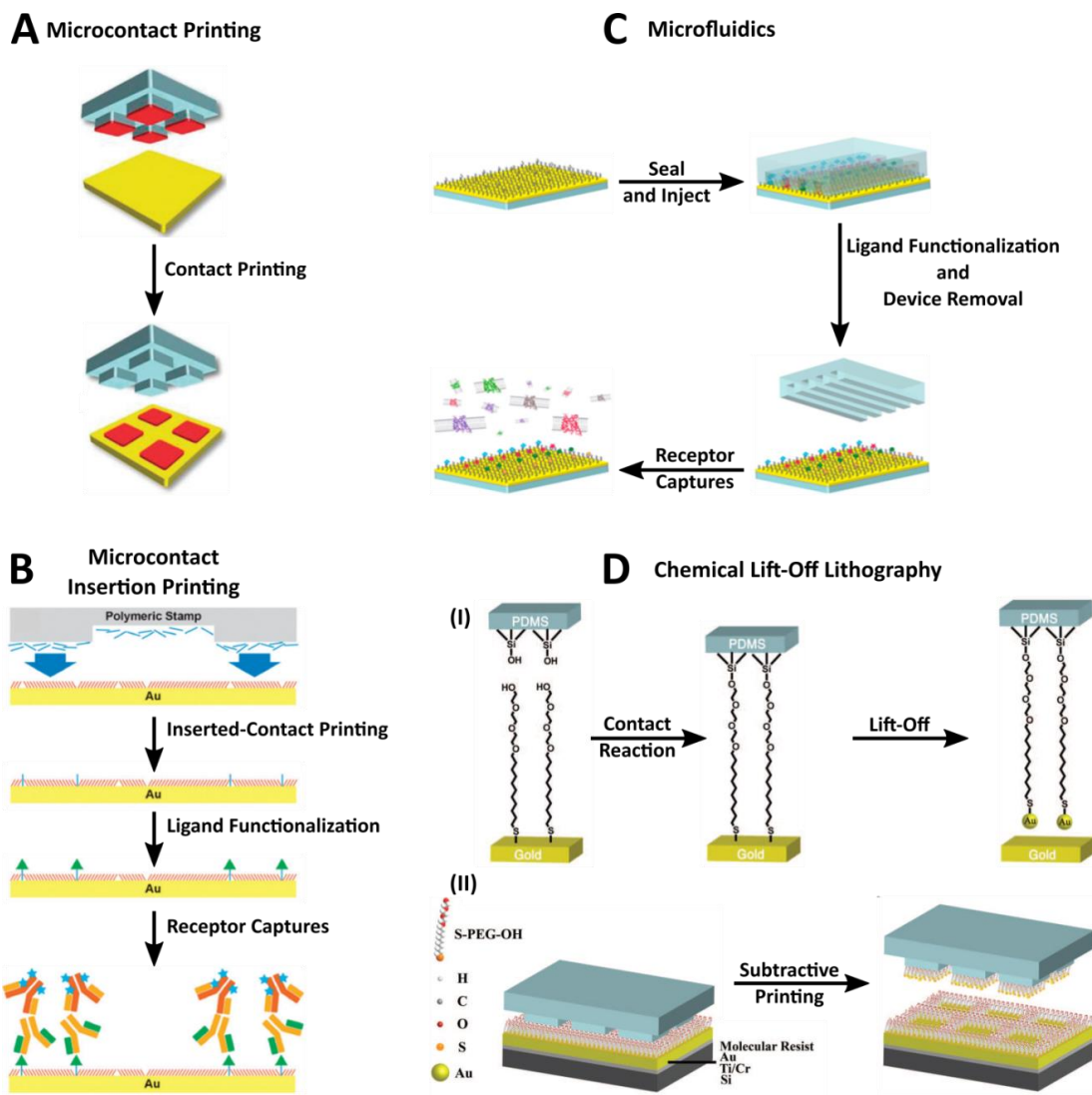


Figure 1-5. Schematic diagrams (not to scale) illustrating different chemical patterning methods including (A) microcontact printing, (B) microcontact insertion printing, (C) microfluidics, and (D) chemical lift-off lithography. A polydimethylsiloxane (PDMS) stamp with predefined relief features is used in (A) to print molecules onto bare Au substrates or in (B) to insert molecules into a preformed self-assembled monolayer (SAM). Patterned molecules can then be functionalized with ligands for biocapture. (C) Alternately, a PDMS mold with microscale conduits is used to pattern ligand functionalization on the top of oligo(ethylene glycol)-terminated alkanethiol (S-PEG-OH) SAMs diluted with tethering molecules during initial deposition. (D) A PDMS stamp can also be activated with oxygen plasma to undergo contact reaction with S-PEG-OH molecules during conformal contact on SAMs. Because of strong covalent stamp/SAM interactions, stamp removal causes SAM molecules and underlying Au atoms to be removed from substrates. (A), (B), (C), and (D) are reprinted with permission from references 31, 53, 29, and 28, respectively.

The success of μ CIP in patterning neurotransmitter-tethered alkanethiols for biorecognition led us to attempt multiplexed patterning with μ CIP. To achieve this, substrates need to be insertion-printed sequentially. Following each printing step, the inserted tethers need to be functionalized with a different type of small-molecule neurotransmitter. The downside of this approach is that the functionalization with one ligand can alter the functionalization of a previous ligand already tethered on the substrates.⁵⁹ Thus, multiplexed patterning with μ CIP is limited by the need to devise compatible serial functionalization chemistries.

1.2.3.B Microfluidics

To circumvent limitations of μ CIP when used for multiplexing, I used microfluidics to generate patterns of multiple small-molecule neurotransmitters on individual substrates (Fig. 1-5C).³⁵ This approach involves the use of PDMS microfluidic devices consisting of multiple micrometer-wide channels. Upon conformal contact with the substrates, each channel serves as a micro-incubator enabling neurotransmitter functionalization with surface tethers as different neurotransmitter solutions are injected into different channels. Thus, multiple neurotransmitters can be functionalized simultaneously on the same substrates without the need to devise compatible serial functionalization chemistries.

Using microfluidics, I was able to generate multiplexed platforms that were used to sort complex mixtures of antibodies and GPCRs from solutions.³⁵ This work is described in Chapter 3. Although surface chemistries were controlled by employing oligo(ethylene glycol) moieties to reduce nonspecific substrate-biomolecule interactions and microfluidics were used to circumvent sequential ligand functionalization, moderately large cross-reactivity (~30%) of

biomolecules to nontarget ligands continued to be observed. Further experiments showed that the cross-reactivity might stem from the antibodies themselves. Additionally, optimization of different conditions such as pH, solvent, temperature, and reaction time for individual ligands was still needed. Variations in these conditions might also facilitate cross-reactivity with nontarget molecules. Therefore, an approach that enables differential functionalization of substrates with small-molecule ligands would permit facile production of multiplexed systems, including ligands sensitive to various protection/deprotection chemistries.

For this purpose, the Kasko laboratory of the UCLA Department of Bioengineering synthesized a library of oligo(ethylene glycol)alkyl pyridyl disulfide tethering molecules pre-functionalized with neurotransmitter precursor molecules (Scheme 1-1BIII) through a novel organic synthesis procedure. Because these novel materials are conjugated with ligands prior to surface assembly, the need to devise compatible serial functionalization chemistries for each molecule is circumvented. These pre-assembly neurotransmitter-functionalized molecules were found to display more consistent antibody binding and equivalent or improved specific binding compared to the post-assembly functionalization approach. This work is detailed in Chapter 6.

1.2.3.C Chemical Lift-Off Lithography

In contrast to the previous patterning methods, which add molecules to substrates, we invented chemical lift-off lithography to pattern substrates *via* subtractive patterning (Fig. 1-5D).³⁴ In this novel approach, PDMS stamps are treated with oxygen plasma to generate surface siloxyls reactive towards hydroxyl-terminated alkanethiol SAM-modified Au substrates during conformal contact. Because the covalent stamp/SAM interactions are stronger than Au-Au bonds, removing the stamps lifts off SAM molecules along with underlying Au atoms. The

newly exposed Au regions in the subtracted areas can then be inserted with small-molecule ligand-tethered alkanethiols for biocapture. In addition, the exposed regions can be subjected to wet chemical etching to transfer the molecular patterns to the underlying substrates. Because molecules are removed from the surface, common problems associated with microcontact printing, *i.e.*, lateral diffusion and gas-phase deposition of inks are circumvented with chemical lift-off. Chapter 4 is focused on this work.

Using chemical lift-off, multiplexed patterns of surface-tethered small-molecule bioactive probes were fabricated to enable sorting of biomolecules from complex mixtures of protein solutions. This work is described in Chapter 5. In addition, I discovered that lift-off lithography did not remove all alkanethiol molecules in the contact regions. The remaining alkanethiols advantageously act as spacers to regulate the densities of the inserted oligonucleotides.⁸³ I found that SAM conformations of the remaining alkanethiols regulate access of DNA to the Au substrate surfaces. Compare to other DNA assembly methods, chemical lift-off creates a new class of surface defects that are favorable for insertion of thiolated DNAs, controlling DNA surface densities, and improving DNA hybridization. This work is the focus of Chapter 7. Lastly, in combination with sol-gel chemistry, lift-off lithography was used to fabricate highly sensitive field-effect-transistor-based biosensors capable of detecting the small-molecule neurotransmitter dopamine down to physiological subnanomolar concentrations.³¹ This work is described in Chapter 8.

1.3 References

1. National Institute of Mental Health. Major Depression among Adults. Published Online: 2013. <http://www.nimh.nih.gov/health/statistics/prevalence/major-depression-among-adults.shtml> (accessed Sep 16, 2015).
2. Parkinson's Disease Foundation. Statistics on Parkinson's. Published Online: 2015. http://www.pdf.org/en/parkinson_statistics (accessed Sep 16, 2015).
3. Hartmann, P.; Ramseier, A.; Gudat, F.; Mihatsch, M. J.; Polasek, W.; Geisenhoff, C. Normal-Weight of the Brain in Adults, Referred to Age, Sex, Height and Body-Weight. *Pathologie* **1994**, *15*, 165-170.
4. Herculano-Houzel, S. The Human Brain in Numbers: A Linearly Scaled-Up Primate Brain. *Front. Hum. Neurosci.* **2009**, *3*, 1-11.
5. Jorgenson, L. A.; Newsome, W. T.; Anderson, D. J.; Bargmann, C. I.; Brown, E. N.; Deisseroth, K.; Donoghue, J. P.; Hudson, K. L.; Ling, G. S. F.; MacLeish, P. R.; Marder, E.; Normann, R. A.; Sanes, J. R.; Schnitzer, M. J.; Sejnowski, T. J.; Tank, D. W.; Tsien, R. Y.; Ugurbil, K.; Wingfield, J. C. The BRAIN Initiative: Developing Technology to Catalyse Neuroscience Discovery. *Philos. Trans. R. Soc. Lond. B Biol. Sci.* **2015**, *370*, 8-19.
6. Alivisatos, A. P.; Chun, M.; Church, G. M.; Deisseroth, K.; Donoghue, J. P.; Greenspan, R. J.; McEuen, P. L.; Roukes, M. L.; Sejnowski, T. J.; Weiss, P. S.; Yuste, R. The Brain Activity Map. *Science* **2013**, *339*, 1284-1285.
7. Weiss, P. S. Brain Activity Mapping Project: Applying Advances in Nanoscience and Nanotechnology to Neuroscience. *ACS Nano* **2013**, *7*, 1825-1826.

8. Alivisatos, A. P.; Andrews, A. M.; Boyden, E. S.; Chun, M.; Church, G. M.; Deisseroth, K.; Donoghue, J. P.; Fraser, S. E.; Lippincott-Schwartz, J.; Looger, L. L.; Masmanidis, S.; McEuen, P. L.; Nurmikko, A. V.; Park, H.; Peterka, D. S.; Reid, C.; Roukes, M. L.; Scherer, A.; Schnitzer, M.; Sejnowski, T. J.; Shepard, K. L.; Tsao, D.; Turrigiano, G.; Weiss, P. S.; Xu, C.; Yuste, R.; Zhuang, X. W. Nanotools for Neuroscience and Brain Activity Mapping. *ACS Nano* **2013**, *7*, 1850-1866.
9. Andrews, A. M.; Schepartz, A.; Sweedler, J. V.; Weiss, P. S. Chemistry and the BRAIN Initiative. *J. Am. Chem. Soc.* **2014**, *136*, 1-2.
10. Andrews, A. M. The BRAIN Initiative: Toward a Chemical Connectome. *ACS Chem. Neurosci.* **2013**, *4*, 645-645.
11. McCorvy, J. D.; Roth, B. L. Structure and Function of Serotonin G Protein-Coupled Receptors. *Pharmacol. Ther.* **2015**, *150*, 129-142.
12. Gellynck, E.; Heyninck, K.; Andressen, K. W.; Haegeman, G.; Levy, F. O.; Vanhoenacker, P.; Van Craenenbroeck, K. The Serotonin 5-HT₇ Receptors: Two Decades of Research. *Exp. Brain Res.* **2013**, *230*, 555-568.
13. Thathiah, A.; De Strooper, B. The Role of G Protein-Coupled Receptors in the Pathology of Alzheimer's Disease. *Nat. Rev. Neurosci.* **2011**, *12*, 73-87.
14. Allen, J. A.; Roth, B. L. Strategies to Discover Unexpected Targets for Drugs Active at G Protein-Coupled Receptors. *Annu. Rev. Pharmacol. Toxicol.* **2011**, *51*, 117-144.
15. Thompson, M. D.; Burnham, W. M.; Cole, D. E. C. The G Protein-Coupled Receptors: Pharmacogenetics and Disease. *Crit. Rev. Clin. Lab. Sci.* **2005**, *42*, 311-392.
16. Congreve, M.; Marshall, F. The Impact of GPCR Structures on Pharmacology and Structure-Based Drug Design. *Br. J. Pharmacol.* **2010**, *159*, 986-996.

17. Leopoldo, M.; Lacivita, E.; Berardi, F.; Perrone, R.; Hedlund, P. B. Serotonin 5-HT₇ Receptor Agents: Structure-Activity Relationships and Potential Therapeutic Applications in Central Nervous System Disorders. *Pharmacol. Ther.* **2011**, *129*, 120-148.
18. Dalet, F. G. E.; Guadalupe, T. F. J.; del Carmen, C. H. M.; Humberto, G. A. C.; Antonio, S. U. M. Insights into the Structural Biology of G-Protein Coupled Receptors Impacts Drug Design for Central Nervous System Neurodegenerative Processes. *Neural Regener. Res.* **2013**, *8*, 2290-2302.
19. Yang, H. Y.; Thompson, A. B.; McIntosh, B. J.; Altieri, S. C.; Andrews, A. M. Physiologically Relevant Changes in Serotonin Resolved by Fast Microdialysis. *ACS Chem. Neurosci.* **2013**, *4*, 790-798.
20. Sarvari, M.; Kocsis, P.; Deli, L.; Gajari, D.; David, S.; Pozsgay, Z.; Hegedus, N.; Tihanyi, K.; Liposits, Z. Ghrelin Modulates the fMRI BOLD Response of Homeostatic and Hedonic Brain Centers Regulating Energy Balance in the Rat. *PLoS One* **2014**, *9*, e97651
21. Demmer, O.; Gourni, E.; Schumacher, U.; Kessler, H.; Wester, H. J. PET Imaging of CXCR4 Receptors in Cancer by a New Optimized Ligand. *ChemMedChem* **2011**, *6*, 1789-1791.
22. Seung-Hyun, Y.; Dan, H.; Lee, E.; Eunjung, K.; Eun-Kyung, L.; Young Han, L.; Seungjoo, H.; Jin-Suck, S.; Yong-Min, H.; Jaemoon, Y.; Sahng Wook, P. Galactosylated Manganese Ferrite Nanoparticles for Targeted MR Imaging of Asialoglycoprotein Receptor. *Nanotechnology* **2013**, *24*, 475103.

23. Essig, M.; Schoenberg, S. O.; Schlemmer, H. P.; Metzner, R.; van Kaick, G. Functional Magnetic Resonance Imaging in Neuroradiology. *Radiologe* **2000**, *40*, 849-857.
24. Loane, C.; Politis, M. Positron Emission Tomography Neuroimaging in Parkinson's Disease. *Am. J. Transl. Res.* **2011**, *3*, 323-341.
25. Rocchi, L.; Niccolini, F.; Politis, M. Recent Imaging Advances in Neurology. *J. Neurol.* **2015**, *262*, 2182-2194.
26. Swinney, D. C.; Anthony, J. How Were New Medicines Discovered? *Nat. Rev. Drug Discovery* **2011**, *10*, 507-519.
27. Swinney, D. C. Biochemical Mechanisms of Drug Action: What Does It Take for Success? *Nat. Rev. Drug Discovery* **2004**, *3*, 801-808.
28. Menon, R. S.; Kim, S. G. Spatial and Temporal Limits in Cognitive Neuroimaging with fMRI. *Trends Cogn. Sci.* **1999**, *3*, 207-216.
29. Meyer-Lindenberg, A. From Maps to Mechanisms through Neuroimaging of Schizophrenia. *Nature* **2010**, *468*, 194-202.
30. Andrews, A. M.; Weiss, P. S. Nano in the Brain: Nano-Neuroscience. *ACS Nano* **2012**, *6*, 8463-8464.
31. Kim, J.; Rim, Y. S.; Chen, H. J.; Cao, H. H.; Nakatsuka, N.; Hinton, H. L.; Zhao, C. Z.; Andrews, A. M.; Yang, Y.; Weiss, P. S. Fabrication of High-Performance Ultrathin In₂O₃ Film Field-Effect Transistors and Biosensors Using Chemical Lift-Off Lithography. *ACS Nano* **2015**, *9*, 4572-4582.
32. Shin, K. S.; Lee, K.; Kang, J. Y.; Chui, C. O. Novel T-Channel Nanowire FET with Built-in Signal Amplification for pH Sensing. *Int. Elec. Devices Meet.* **2009**, *2009*, 555-558.

33. Shin, K. S.; Lee, K.; Park, J. H.; Kang, J. Y.; Chui, C. O. Schottky Contacted Nanowire Field-Effect Sensing Device With Intrinsic Amplification. *IEEE Electron Device Lett.* **2010**, *31*, 1317-1319.
34. Liao, W. S.; Cheunkar, S.; Cao, H. H.; Bednar, H. R.; Weiss, P. S.; Andrews, A. M. Subtractive Patterning *via* Chemical Lift-Off Lithography. *Science* **2012**, *337*, 1517-1521.
35. Liao, W. S.; Cao, H. H.; Cheunkar, S.; Shuster, M. J.; Altieri, S. C.; Weiss, P. S.; Andrews, A. M. Small-Molecule Arrays for Sorting G-Protein-Coupled Receptors. *J. Phys. Chem. C* **2013**, *117*, 22362-22368.
36. Saavedra, H. M.; Mullen, T. J.; Zhang, P. P.; Dewey, D. C.; Claridge, S. A.; Weiss, P. S. Hybrid Strategies in Nanolithography. *Rep. Prog. Phys.* **2010**, *73*, 036501.
37. Claridge, S. A.; Liao, W. S.; Thomas, J. C.; Zhao, Y. X.; Cao, H. H.; Cheunkar, S.; Serino, A. C.; Andrews, A. M.; Weiss, P. S. From the Bottom Up: Dimensional Control and Characterization in Molecular Monolayers. *Chem. Soc. Rev.* **2013**, *42*, 2725-2745.
38. Mullen, T. J.; Srinivasan, C.; Hohman, J. N.; Gillmor, S. D.; Shuster, M. J.; Horn, M. W.; Andrews, A. M.; Weiss, P. S. Microcontact Insertion Printing. *Appl. Phys. Lett.* **2007**, *90*, 063114.
39. Mrksich, M. Using Self-Assembled Monolayers to Understand the Biomaterials Interface. *Curr. Opin. Colloid Interface Sci.* **1997**, *2*, 83-88.
40. Gooding, J. J.; Mearns, F.; Yang, W. R.; Liu, J. Q. Self-Assembled Monolayers into the 21st Century: Recent Advances and Applications. *Electroanalysis* **2003**, *15*, 81-96.

41. Love, J. C.; Estroff, L. A.; Kriebel, J. K.; Nuzzo, R. G.; Whitesides, G. M. Self-Assembled Monolayers of Thiolates on Metals as a Form of Nanotechnology. *Chem. Rev.* **2005**, *105*, 1103-1169.
42. Bumm, L. A.; Arnold, J. J.; Cygan, M. T.; Dunbar, T. D.; Burgin, T. P.; Jones, L.; Allara, D. L.; Tour, J. M.; Weiss, P. S. Are Single Molecular Wires Conducting? *Science* **1996**, *271*, 1705-1707.
43. Cygan, M. T.; Dunbar, T. D.; Arnold, J. J.; Bumm, L. A.; Shedlock, N. F.; Burgin, T. P.; Jones, L.; Allara, D. L.; Tour, J. M.; Weiss, P. S. Insertion, Conductivity, and Structures of Conjugated Organic Oligomers in Self-Assembled Alkanethiol Monolayers on Au{111}. *J. Am. Chem. Soc.* **1998**, *120*, 2721-2732.
44. Gannon, G.; Greer, J. C.; Larsson, J. A.; Thompson, D. Molecular Dynamics Study of Naturally Occurring Defects in Self-Assembled Monolayer Formation. *ACS Nano* **2010**, *4*, 921-932.
45. Christman, K. L.; Enriquez-Rios, V. D.; Maynard, H. D. Nanopatterning Proteins and Peptides. *Soft Matter* **2006**, *2*, 928-939.
46. Wendeln, C.; Ravoo, B. J. Surface Patterning by Microcontact Chemistry. *Langmuir* **2012**, *28*, 5527-5538.
47. Ostuni, E.; Yan, L.; Whitesides, G. M. The Interaction of Proteins and Cells with Self-Assembled Monolayers of Alkanethiolates on Gold and Silver. *Colloids Surf., B* **1999**, *15*, 3-30.
48. Zhu, B.; Eurell, T.; Gunawan, R.; Leckband, D. Chain-Length Dependence of the Protein and Cell Resistance of Oligo(Ethylene Glycol)-Terminated Self-Assembled Monolayers on Gold. *J. Biomed. Mater. Res.* **2001**, *56*, 406-416.

49. Kankate, L.; Werner, U.; Turchanin, A.; Golzhauser, A.; Grossmann, H.; Tampe, R. Protein Resistant Oligo(Ethylene Glycol) Terminated Self-Assembled Monolayers of Thiols on Gold by Vapor Deposition in Vacuum. *Biointerphases* **2010**, *5*, 30-36.
50. Hudalla, G. A.; Murphy, W. L. Using "Click" Chemistry to Prepare SAM Substrates to Study Stem Cell Adhesion. *Langmuir* **2009**, *25*, 5737-5746.
51. Perez-Luna, V. H.; O'Brien, M. J.; Opperman, K. A.; Hampton, P. D.; Lopez, G. P.; Klumb, L. A.; Stayton, P. S. Molecular Recognition between Genetically Engineered Streptavidin and Surface-Bound Biotin. *J. Am. Chem. Soc.* **1999**, *121*, 6469-6478.
52. Lewis, P. A.; Smith, R. K.; Kelly, K. F.; Bumm, L. A.; Reed, S. M.; Clegg, R. S.; Gunderson, J. D.; Hutchison, J. E.; Weiss, P. S. The Role of Buried Hydrogen Bonds in Self-Assembled Mixed Composition Thiols on Au{111}. *J. Phys. Chem. B* **2001**, *105*, 10630-10636.
53. Smith, R. K.; Nanayakkara, S. U.; Woehle, G. H.; Pearl, T. P.; Blake, M. M.; Hutchison, J. E.; Weiss, P. S. Spectral Diffusion in the Tunneling Spectra of Ligand-Stabilized Undecagold Clusters. *J. Am. Chem. Soc.* **2006**, *128*, 9266-9267.
54. Stranick, S. J.; Parikh, A. N.; Tao, Y. T.; Allara, D. L.; Weiss, P. S. Phase-Separation of Mixed-Composition Self-Assembled Monolayers into Nanometer-Scale Molecular Domains. *J. Phys. Chem.* **1994**, *98*, 7636-7646.
55. Kwon, Y.; Han, Z. Z.; Karatan, E.; Mrksich, M.; Kay, B. K. Antibody Arrays Prepared by Cutinase-Mediated Immobilization on Self-Assembled Monolayers. *Anal. Chem.* **2004**, *76*, 5713-5720.
56. Lahiri, J.; Isaacs, L.; Grzybowski, B.; Carbeck, J. D.; Whitesides, G. M. Biospecific Binding of Carbonic Anhydrase to Mixed SAMs Presenting Benzenesulfonamide

- Ligands: A Model System for Studying Lateral Steric Effects. *Langmuir* **1999**, *15*, 7186-7198.
57. Lahiri, J.; Isaacs, L.; Tien, J.; Whitesides, G. M. A Strategy for the Generation of Surfaces Presenting Ligands for Studies of Binding Based on an Active Ester as a Common Reactive Intermediate: A Surface Plasmon Resonance Study. *Anal. Chem.* **1999**, *71*, 777-790.
58. Shuster, M. J.; Vaish, A.; Szapacs, M. E.; Anderson, M. E.; Weiss, P. S.; Andrews, A. M. Biospecific Recognition of Tethered Small Molecules Diluted in Self-Assembled Monolayers. *Adv. Mater.* **2008**, *20*, 164-167.
59. Shuster, M. J.; Vaish, A.; Cao, H. H.; Guttentag, A. I.; McManigle, J. E.; Gibb, A. L.; Martinez, M. M.; Nezarati, R. M.; Hinds, J. M.; Liao, W.-S.; Weiss, P. S.; Andrews, A. M. Patterning Small-Molecule Biocapture Surfaces: Microcontact Insertion Printing vs. Photolithography. *Chem. Commun.* **2011**, *47*, 10641-10643.
60. Vaish, A.; Shuster, M. J.; Cheunkar, S.; Singh, Y. S.; Weiss, P. S.; Andrews, A. M. Native Serotonin Membrane Receptors Recognize 5-Hydroxytryptophan-Functionalized Substrates: Enabling Small-Molecule Recognition. *ACS Chem. Neurosci.* **2010**, *1*, 495-504.
61. Vaish, A.; Shuster, M. J.; Cheunkar, S.; Weiss, P. S.; Andrews, A. M. Tuning Stamp Surface Energy for Soft Lithography of Polar Molecules to Fabricate Bioactive Small-Molecule Microarrays. *Small* **2011**, *7*, 1471-1479.
62. Xia, N.; Xing, Y.; Wang, G. F.; Feng, Q. Q.; Chen, Q. Q.; Feng, H. M.; Sun, X. L.; Liu, L. Probing of EDC/NHSS-Mediated Covalent Coupling Reaction by the Immobilization of Electrochemically Active Biomolecules. *Int. J. Electrochem. Sci.* **2013**, *8*, 2459-2467.

63. Wang, C.; Yan, Q.; Liu, H. B.; Zhou, X. H.; Xiao, S. J. Different EDC/NHS Activation Mechanisms between PAA and PMAA Brushes and the following Amidation Reactions. *Langmuir* **2011**, *27*, 12058-12068.
64. Christman, K. L.; Requa, M. V.; Enriquez-Rios, V. D.; Ward, S. C.; Bradley, K. A.; Turner, K. L.; Maynard, H. D. Submicron Streptavidin Patterns for Protein Assembly. *Langmuir* **2006**, *22*, 7444-7450.
65. Neish, C. S.; Martin, I. L.; Henderson, R. M.; Edwardson, J. M. Direct Visualization of Ligand-Protein Interactions Using Atomic Force Microscopy. *Br. J. Pharmacol.* **2002**, *135*, 1943-1950.
66. Seeber, M.; De Benedetti, P. G.; Fanelli, F. Molecular Dynamics Simulations of the Ligand-Induced Chemical Information Transfer in the 5-HT_{1A} Receptor. *J. Chem. Inf. Comput. Sci.* **2003**, *43*, 1520-1531.
67. Congreve, M.; Langmead, C. J.; Mason, J. S.; Marshall, F. H. Progress in Structure Based Drug Design for G Protein-Coupled Receptors. *J. Med. Chem.* **2011**, *54*, 4283-4311.
68. Hsiao, J. K.; Potter, W. Z.; Agren, H.; Owen, R. R.; Pickar, D. Clinical Investigation of Monoamine Neurotransmitter Interactions. *Psychopharmacology* **1993**, *112*, S76-S84.
69. Ono, K.; Kimura, S.; Nakano, M.; Naruse, T. Detection of Heterogeneity of Cu, Zn-Superoxide Dismutase with Monoclonal-Antibodies and the Establishment of a Highly Sensitive Fluorescence Sandwich Enzyme-Linked-Immuno-sorbent-Assay. *FEBS Lett.* **1991**, *282*, 115-118.
70. Van Loon, A. M.; Van Der Logt, J. T. M.; Heessen, F. W. A.; Van Der Veen, J. Enzyme Linked Immuno Sorbent Assay That Uses Labeled Antigen for Detection of Immuno Globulin M and a Antibodies in Toxoplasmosis Comparison with Indirect Immuno

- Fluorescence and Double Sandwich Enzyme Linked Immuno Sorbent Assay. *J. Clin. Microbiol.* **1983**, *17*, 997-1004.
71. MacBeath, G.; Koehler, A. N.; Schreiber, S. L. Printing Small Molecules as Microarrays and Detecting Protein-Ligand Interactions en Masse. *J. Am. Chem. Soc.* **1999**, *121*, 7967-7968.
72. Whitesides, G. M.; Ostuni, E.; Takayama, S.; Jiang, X. Y.; Ingber, D. E. Soft Lithography in Biology and Biochemistry. *Annu. Rev. Biomed. Eng.* **2001**, *3*, 335-373.
73. Srinivasan, C.; Mullen, T. J.; Hohman, J. N.; Anderson, M. E.; Dameron, A. A.; Andrews, A. M.; Dickey, E. C.; Horn, M. W.; Weiss, P. S. Scanning Electron Microscopy of Nanoscale Chemical Patterns. *ACS Nano* **2007**, *1*, 191-201.
74. Mehlich, J.; Miyata, Y.; Shinohara, H.; Ravoo, B. J. Fabrication of a Carbon-Nanotube-Based Field-Effect Transistor by Microcontact Printing. *Small* **2012**, *8*, 2258-2263.
75. Das, R. N.; Lin, H. T.; Lauffer, J. M.; Markovich, V. R. Printable Electronics: Towards Materials Development and Device Fabrication. *Circuit World* **2011**, *37*, 38-45.
76. Hovestad, A.; Rendering, H.; Maijenburg, A. W. Patterned Electrodeposition of Interconnects Using Microcontact Printing. *J. Appl. Electrochem.* **2012**, *42*, 753-761.
77. Lauer, L.; Ingebrandt, S.; Scholl, M.; Offenhausser, A. Aligned Microcontact Printing of Biomolecules on Microelectronic Device Surfaces. *IEEE Trans. Biomed. Eng.* **2001**, *48*, 838-842.
78. Gannon, G.; Larsson, J. A.; Greer, J. C.; Thompson, D. Quantification of Ink Diffusion in Microcontact Printing with Self-Assembled Monolayers. *Langmuir* **2009**, *25*, 242-247.

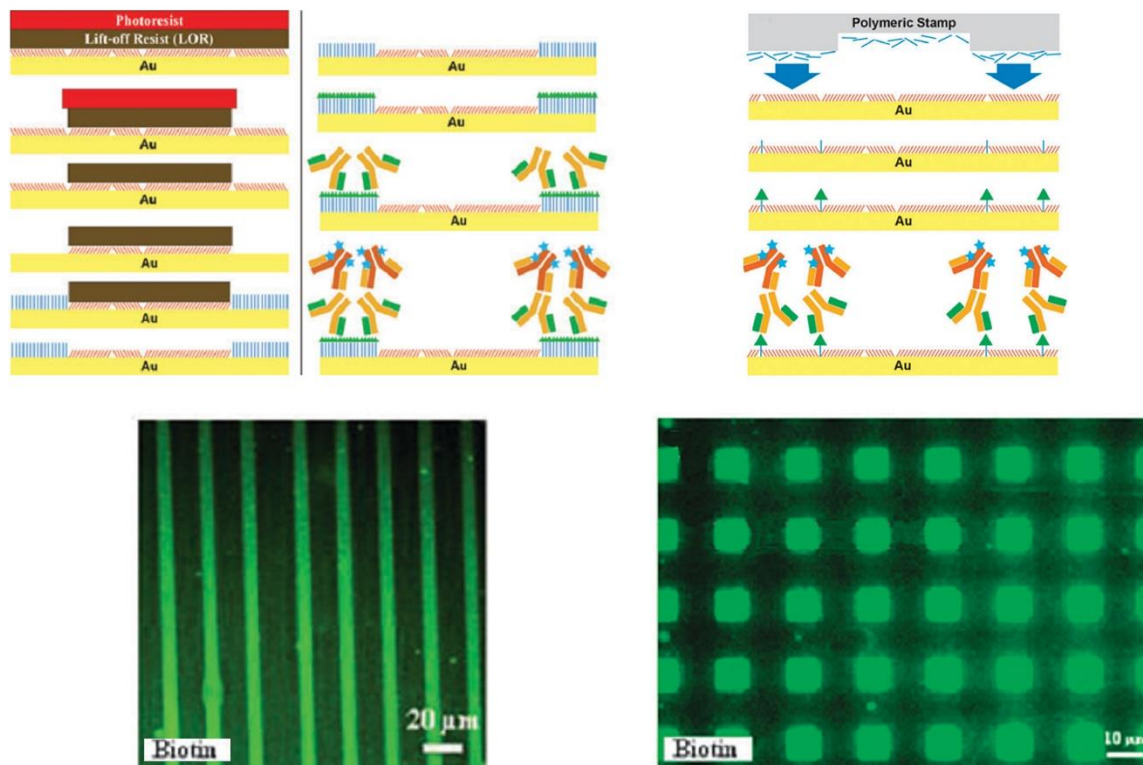
79. Sharpe, R. B. A.; Burdinski, D.; Huskens, J.; Zandvliet, H. J. W.; Reinhoudt, D. N.; Poelsema, B. Spreading of 16-Mercaptohexadecanoic Acid in Microcontact Printing. *Langmuir* **2004**, *20*, 8646-8651.
80. Saavedra, H. M.; Barbu, C. M.; Dameron, A. A.; Mullen, T. J.; Crespi, V. H.; Weiss, P. S. 1-Adamantanethiolate Monolayer Displacement Kinetics Follow a Universal Form. *J. Am. Chem. Soc.* **2007**, *129*, 10741-10746.
81. Donhauser, Z. J.; Price, D. W.; Tour, J. M.; Weiss, P. S. Control of Alkanethiolate Monolayer Structure Using Vapor-Phase Annealing. *J. Am. Chem. Soc.* **2003**, *125*, 11462-11463.
82. Lewis, P. A.; Donhauser, Z. J.; Mantooth, B. A.; Smith, R. K.; Bumm, L. A.; Kelly, K. F.; Weiss, P. S. Control and Placement of Molecules *via* Self-Assembly. *Nanotechnology* **2001**, *12*, 231-237.
83. Cao, H. H.; Nakatsuka, N.; Serino, A. C.; Liao, W.-S.; Cheunkar, S.; Yang, H.; Weiss, P. S.; Andrews, A. M. Controlled DNA Patterning by Chemical Lift-Off Lithography: Matrix Matters. *ACS Nano* **2015**, *9*, 11439-11454.

Chapter 2

Patterning Small-Molecule Biocapture Surfaces: Microcontact Insertion Printing *vs.* Photolithography

The information in this chapter was published in *Chemical Communications* **2011**, *47*, 10641-10643 and has been reproduced here in its entirety.

Authors: Shuster, M. J.; Vaish, A.; Cao, H. H.; Guttentag, A; McManigle, J.; Gibb, A.;
Martinez, M.; Nezarati, R.; Hinds, J.; Liao, W. S.; Weiss P. S.; Andrews, A. M.



2.1 Abstract

Chemical patterns prepared by self-assembly, combined with soft lithography or photolithography, are directly compared. Pattern fidelity can be controlled in both cases but patterning at the low densities necessary for small-molecule probe capture of large biomolecule targets is better accomplished using μ CIP. Surfaces patterned by μ CIP are used to capture biomolecule binding partners for the small molecules dopamine and biotin.

2.2 Introduction

A broad range of techniques are currently employed to produce chemical patterns on surfaces to fabricate arrays for the selective capture of biological targets.¹ For small-molecule capture, dilute probe coverage is necessary to facilitate selective molecular recognition by large binding partners.^{2,3} Small-molecule microarrays are important for investigating numerous biological processes mediated by interactions with large biomolecules.^{3,4} Serial techniques, such as electron-beam lithography,⁵ scanning probe lithography,⁶ and spotting,⁷ are difficult to scale up. By contrast, parallel techniques, such as photolithographic chemical patterning and soft lithography, produce surface features simultaneously, enabling rapid processing of large surface areas.

Here, we evaluate two different methods of chemical patterning. The first involves a hybrid approach combining photolithography and self-assembly, which produces patterns with sharp features, high resolution, and pattern alignment.^{8,9} Photolithography can be used to pattern SAMs by utilizing a patterned physical barrier to protect pre-existing monolayers.⁸ As a result, domains of differing chemical compositions can be formed with no intercalation. Photolithography is compared to μ CIP.⁹⁻¹¹ The latter is a soft-lithography-based technique wherein molecules are inserted into defect sites in SAMs using patterned PDMS stamps. In both patterning methods, we leverage insertion-directed self-assembly^{10,12} to create mixed monolayers having dilute coverage of one chemically distinct terminal group within a matrix of hydroxyl-terminated oligo(ethylene glycol)alkanethiol (OEG) to minimize nonspecific binding of proteins.^{13,14} Thiols pre-functionalized with a biological epitope, as well as *in situ* chemical functionalization, are used to create bioactive surfaces.¹¹

2.3 Materials and Methods

Chemicals. 23-(9-Mercaptononyl)-3,6,9,12,15,18,21-heptaoxatricosanoic acid (HEG) and 1-(9-ercaptononyl)-3,6,9-trioxaundecan-11-ol (TEG) were purchased from Toronto Research Chemicals (Toronto, ON, Canada). 1-(9-Mercaptononyl)-3,6,9,12,15,18-hexa-oxaundecan-11-biotin (BEG) was purchased from ProChimia (Sopot, Poland). *N*-Hydroxysuccinimide (NHS), *N*-ethyl-*N*-(dimethylaminopropyl)-carbodiimide (EDC), 5-hydroxytryptamine hydrochloride (5-HT), 3,4-hydroxytyramine hydrochloride (3,4-dihydroxyphenylethylamine; dopamine; DA), and bovine serum albumin (BSA) were obtained from Sigma-Aldrich (St. Louis, MO, USA). Commercial grade ethanol (EtOH) was from Pharmaco-AAPER (Brookfield, CT, USA). Rabbit anti-serotonin polyclonal antibodies and rabbit anti-dopamine polyclonal antibodies were procured from Millipore (Temecula, CA, USA). AlexaFluor 488-labeled goat anti-rabbit antibodies (absorbance max at 495 nm, emission max at 519 nm), AlexaFluor 546-labeled goat anti-rabbit antibodies (absorbance max at 556 nm, emission max at 573 nm), streptavidin, and AlexaFluor 488-tagged streptavidin (absorbance max at 494 nm, emission max at 521 nm) were purchased from Invitrogen (Carlsbad, CA, USA). Fluorescein isothiocyanate (FITC)-tagged anti-streptavidin polyclonal antibodies were purchased from Abcam (Cambridge, MA, USA).

Substrate formation. Metalized surfaces were fabricated by thermal evaporation of either 5 nm Cr and 15 nm Au on glass microscopy slides (photolithographic patterning) or 10 nm Cr and 100 nm Au on Si wafers (soft lithography patterning) (SiliconQuest, Santa Clara, CA, USA) using an electron beam evaporator (Kurt Lesker Inc., Clairton, PA, USA). Both metals were deposited at a rate of 1 Å/sec. Substrates were flame-annealed with a hydrogen flame immediately prior to monolayer formation.

Monolayer preparation. Self-assembled monolayers were prepared by exposing Au surfaces to a 1 mM solution of either TEG or HEG. After patterning by photolithography or μ CIP, surfaces with HEG were exposed to a solution of 15 mM NHS and 25 mM EDC for 1 h to create an activated ester bond between NHS and the carboxyl group of the HEG molecules on the surfaces. The NHS acts as a leaving group in the presence of the primary amine of 5-HT or DA, resulting in amide bond formation between 5-HT or DA and HEG and tethering of 5-HT or DA to surfaces only in regions containing carboxyl-terminated oligo(ethylene glycol) thiols.^{S1} Both 5-HT and DA solutions were prepared at 25 mM in phosphate-buffered saline (PBS). For 5-HT, PBS pH was 9.5, and samples were incubated at room temperature for 4 h. For DA, PBS pH was 6.75, and samples were incubated at 4 °C overnight. The lower temperature and pH for DA, which necessitates the longer incubation time, is required to reduce spontaneous oxidation in solution. In cases where BEG was used in place of HEG, the biotin epitope was attached to the thiol molecules by the manufacturer.

Photolithographic patterning. Photolithography on monolayers was accomplished using a bilayer resist stack and a series of pattern transfer techniques, as described elsewhere.^{S2} Briefly, a resist stack consisting of a non-photosensitive lift-off resist (LOR 5A, MicroChem Corp., Newton, MA) on the bottom and a photoresist (Shipley 3012, Shipley Company, Marlborough, MA) on the top was spin-coated on SAMs. Samples were then exposed to 365 nm light at a power of 12 mW·cm⁻² using a contact aligner (MA-6, Karl Suss America, Inc., Waterbury Center, VT, USA), and patterns were transferred to the LOR during photoresist development. The photoresist was removed with an acetone rinse because of its instability under standard self-assembly conditions. The LOR then acted as a mask during UV-ozone exposure, which removed the SAMs in regions not protected by the LOR. A different thiol species (TEG or HEG)

was then deposited on the newly exposed Au by immersing samples in a 1 mM thiol solution in EtOH, and the LOR was subsequently removed using a 2% tetramethyl ammonium hydroxide solution, leaving a patterned monolayer. A total of eight samples were prepared and analyzed using this technique, with five of the eight samples prepared with an initial TEG monolayer and three prepared with an initial HEG monolayer.

Stamp preparation. PDMS stamps were prepared by mixing Dow Corning Sylgard 184 oligomer with the catalyst at a 10:1 ratio by weight. The mixture was then degassed, poured onto a silanized Si master wafer, and degassed again. This preparation was then baked at 75 °C for 24 h, after which the cured PDMS was removed from the wafer and cut into 1 cm × 2 cm squares. Stamps were cleaned by soaking in hexane for 1.5 h three times, followed by baking at 75 °C for 24 h to remove absorbed hexane.

Soft lithography by microcontact insertion printing. Immediately prior to use, stamps were sonicated in a 50/50 mixture EtOH and 18.2 MΩ deionized water for 30 min, then pressed onto a clean Si wafer to remove surface contaminants. Subsequently, stamps were exposed to an oxygen plasma for 12 s using a Harrick plasma cleaner (Ithaca, NY, USA) operated under low radio frequency power (6.8 W) to create an intermediate hydrophilic surface to facilitate ink transfer from stamps to substrates.^{S3} A 3 mM solution of either HEG or BEG was pipetted onto the patterned side of the stamp and allowed to sit for 60 s. The stamp was then dried and placed into firm contact with a substrate on which a TEG monolayer had already been assembled. Stamps stayed in contact with SAMs for printing for 1 h. The HEG or BEG molecules insert into the monolayer only where the PDMS stamp makes direct contact with the surface, resulting in low densities of HEG or BEG molecules distributed in patterns reflecting the topography of the PDMS stamp. The stamp was subsequently removed, and samples were rinsed with EtOH and

dried under a stream of nitrogen, resulting in patterned monolayers. Experiments with HEG and BEG samples were repeated 3-5 times.

Fluorescence microscopy. Patterned, chemically functionalized samples were exposed to solutions of primary antibodies that were specific for either 5-HT or DA epitopes or to streptavidin, which binds to biotin, followed by a rinse with deionized water. Surfaces were then exposed to solutions of fluorescently tagged antibodies with affinity for primary antibodies or streptavidin. In all cases, 1% (w/v) BSA was added to solutions to minimize nonspecific binding. Both fluorescently labeled and unlabeled streptavidin were used for biocapture experiments. In experiments shown in Fig. 2-3, AlexaFluor 488-labeled streptavidin was used to simplify the incubation process and to rule out antibody cross reactivity.

Samples were examined using an inverted Nikon TE300 optical microscope (Melville, NY, USA) with a 40× objective and a xenon arc lamp light source. Filter cubes appropriate for the different fluorophores were used for fluorescence imaging. Photolithographically assisted chemical patterning samples, which were prepared on transparent thin Au on glass substrates, were also imaged using transmitted visible light.

Nonspecific binding analysis. Nonspecific binding patterns were difficult to observe on control samples, *i.e.*, samples where primary antibodies were omitted. We used the statistical toolbox of Matlab (MathWorks, Natick, MA, USA) to perform principal component analysis (PCA) on fluorescence intensity data to gain information about the magnitude of nonspecific binding compared to specific binding. Principal component analysis provides a method for deconstructing a data set into an orthogonal set of basis vectors (principal components, PCs) ordered by the contribution of each PC to the variance of the data. To accomplish this for analysis of an image, a matrix is created in which the position of the pixel intensity data in the

matrix is spatially correlated to the pixel location in the image. Using this matrix as a data set, the mean of each column of the matrix is subtracted from each entry in that column to adjust the column data mean to zero. The covariance matrix is then calculated and its eigenvectors determined. The square root of the eigenvalue associated with each eigenvector is proportional to the variance correlated with that eigenvector. To determine how many PCs are necessary to account for a chosen percentage of the variance, a cumulative sum of the eigenvalues, arranged from greatest to least, divided by the sum of all eigenvalues, is performed. The number of eigenvalues necessary to reach a desired threshold indicates the necessary number of PCs. We used a 90% threshold for the analysis presented below. Because PCA has no free parameters, it provides an objective method to assess correlations in a data set. In the case of image analysis and images with high contrast, patterns require only a small number of PCs to account for the majority (60% to 90%) of the variance in the pixel intensities of the images. Conversely, low-contrast patterns or images without a clear pattern require a substantially greater number of PCs to reach the same variance threshold.

Analysis of 21 images of samples prepared using μ CIP indicates that over 90% of the variance of well-defined, relatively uniform patterns, such as those seen in Figs. 2-2D and 2-2E in the main text, can be explained using less than 1% of the PCs (10 PCs in a 1024×1024 pixel image). By contrast, for control samples with low nonspecific binding, where patterns were faint or not discernable, upwards of 10% of all principal components were needed to reach a 90% variance threshold.

Although this analysis does not allow determination of nonspecific binding levels per se, it provides a method for comparing specific *vs.* nonspecific binding. Patterns that do not meet the 1% PC criteria for reaching a 90% variance threshold can be regarded as spurious, *i.e.*, low

specific binding. Moreover, control sample images that do not require greater than 10% of PCs to reach a 90% variance threshold indicate failure of the control experiment, *i.e.*, high nonspecific binding.

2.4 Results and Discussions

2.4.1 Patterning Small-Molecule Ligands via Self-Assembly-Assisted Photolithography

Previously, photolithography combined with self-assembly was used to pattern bi- and tri-component SAMs of methyl-, carboxyl-, and amino-terminated alkanethiols.^{8,9} Here, we expand this technique to pattern biologically relevant OEGs to form SAMs terminated with hydroxyl (TEG) and carboxyl (HEG) groups, depicted schematically in Fig. 2-1A, left. Surfaces patterned by photolithography employ chemical functionalization to attach the small-molecule neurotransmitter serotonin (5-hydroxytryptamine) to HEG.² The resulting surfaces are shown schematically in Fig. 2-1A, right. Fluorescently tagged secondary antibodies were used to

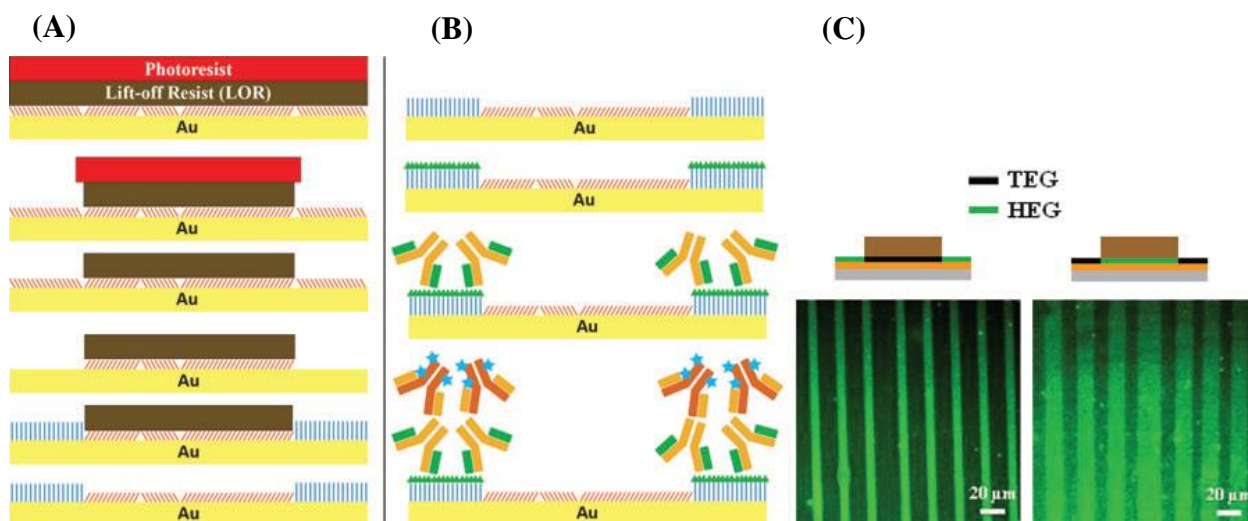


Figure 2-1. Patterned monolayer preparation using photolithography. (A) Schematic of lift-off resist (LOR)-based monolayer patterning, chemical functionalization, and antibody capture. Regions protected by the LOR retain the molecular identity of the initial monolayer after patterning. UV ozone treatment is used to remove SAMs in the exposed regions.

Unprotected regions are backfilled or inserted to form a new SAM with a different composition. Comparison of fluorescence microscopy images of samples prepared by starting with (B) a TEG monolayer, which was then backfilled with a HEG monolayer vs. those starting with (C) a HEG monolayer, then backfilled with a TEG monolayer. The HEG molecules were functionalized with serotonin. Antibody capture is more prevalent in serotonin-functionalized regions.

visualize primary anti-serotonin antibodies captured in serotonin-functionalized regions. Fig. 2-1B and C show representative samples created using this photolithographic method each with a different initial SAM. Regardless of the initial SAM, samples displayed a fluorescent pattern concurrent with the HEG serotonin-functionalized SAM regions. Pattern reversal demonstrates that the fluorescent patterns result from the surface chemistry, *i.e.*, antibodies bind to regions of serotonin functionalization.

While these results demonstrate the extension of photolithographically patterned monolayers beyond simple alkanethiols, we discovered that the surfaces initially produced by this method were not suited for selective molecular recognition. Patterns created with densely packed regions of HEG, with or without serotonin functionalization (Supplementary Information, Fig. 2-S1A and 2-S1B, respectively), demonstrated significant capture of fluorescently labeled secondary antibodies, even in the absence of primary antibodies, indicating a high degree of nonspecific binding. We attribute nonspecific antibody recognition to the high densities of functional groups in the patterned regions.²

2.4.2. Patterning Small-Molecule Ligands *via* Insertion-Directed Self-Assembly-Assisted Photolithography

One strategy to overcome high nonspecific binding is to insert HEG molecules into TEG SAMs to produce low-density coverage of small-molecule probes.^{2,3,11} To accomplish this, exposure of LOR-patterned substrates to UV-ozone to remove the initial TEG SAMs in the exposed regions was omitted, while all other aspects of the process remained the same. The LOR prevented insertion of HEG tethers in the masked regions, while insertion took place at defect sites in the SAMs in the exposed regions. However, samples prepared in this manner displayed a

fluorescence pattern that was reversed from that shown in Fig. 2-1B, with less fluorescence in probe-functionalized regions than in LOR-protected TEG monolayer regions, which should resist nonspecific binding (see the ESI, Fig. 2-S1C). We attribute this finding to residual LOR remaining on the surface even after removal by tetramethyl ammonium hydroxide. By contrast, minimal residual LOR is expected to be present in the inserted (patterned) regions, because in these areas, LOR was removed during photolithographic development. Residual LOR appears to interfere with the protein-resistant properties of TEG SAM regions, leading to nonspecific binding greater than the signal from specific binding to the dilute serotonin epitopes, and thereby, pattern reversal.

2.4.3. Patterning Small-Molecule Ligands *via* Microcontact Insertion Printing

More severe methods to remove the LOR completely are likely to disrupt TEG surfaces, which would also lead to considerable nonspecific binding. Instead, a method of patterning with minimal impact to the surface chemistry is preferred to preserve surface properties intended to reduce nonspecific binding.^{14,15} To this end, μ CIP,^{10,11} which obviates the need for exposure of surfaces to photolithography chemicals, was utilized. The process by which patterned surfaces were prepared using this technique is depicted schematically in Fig. 2-2A. In μ CIP, a polymeric stamp inked with the thiol molecules to be inserted is brought into contact with a pre-formed SAM. Insertion of the inked thiols occurs in regions where the stamp makes direct contact with the surface. Probe functionalization chemistry then can be performed on the terminal groups of the inserted molecules. Surfaces prepared in this manner are exposed to biomolecule targets to investigate selective capture.

Here, stamps having 10 μm or 25 μm posts with 10 μm or 25 μm spacing, respectively, were used for surface patterning. The resulting surfaces are depicted schematically in Fig. 2-2B and C. Biotin-terminated oligo(ethylene glycol) thiol (BEG) was investigated initially because of strong binding interactions between biotin and streptavidin. In Fig. 2-2D, surfaces patterned with biotin demonstrate capture of streptavidin from solution. Fluorescence intensity line scans show that pattern size and spacing are commensurate with the geometry of the stamp. Line scans also demonstrate the high level of contrast between regions where insertion occurred *via* stamping and regions where only the protein-resistant TEG monolayer is present. Control samples were patterned by microcontact insertion printing of BEG but were exposed only to fluorescently tagged anti-streptavidin antibodies with streptavidin omitted. Anti-streptavidin antibodies have low affinity for both biotin and TEG, and no patterns were observed under these circumstances. These results support the conclusion that patterns are due to the specific recognition of surface-

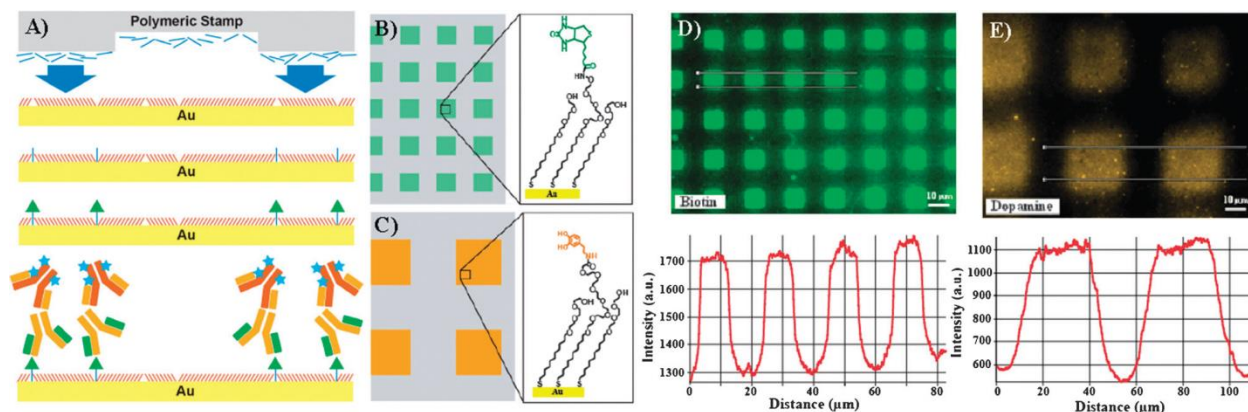


Figure 2-2. Fluorescence microscopy of specific antibody recognition of patterned surfaces. Schematics of (A) the microcontact insertion printing process, (B) 10 μm squares of inserted biotinylated-OEG, and (C) 25 μm squares of inserted carboxyl-terminated OEG functionalized *in situ* with dopamine. (D) Biotinylated OEG patterned *via* μCIP binds streptavidin with high affinity. (E) Similarly, carboxyl-terminated OEG functionalized with dopamine captures anti-dopamine antibodies. FITC-tagged anti-streptavidin antibodies and AlexaFluor 546-tagged anti-rabbit secondary antibodies were used for visualization. The double lines indicate the areas used for fluorescence line scans of the respective surfaces.

tethered biotin by streptavidin, which was captured from solution and visualized by subsequent binding of fluorescent anti-streptavidin antibodies.

Samples were also patterned by μ CIP using a HEG ink solution followed by *in situ* functionalization with the small-molecule neurotransmitter dopamine (3,4-dihydroxyphenylethylamine; DA) using a similar coupling chemistry to that previously developed for serotonin.² Dopamine was used here because it is an important neurotransmitter involved in the control of movement and reward-related behavior. Anti-DA antibody affinity for DA is expected to be similar to anti-serotonin antibody affinity for serotonin. Anti-DA antibodies bind selectively to regions where DA epitopes are present (Fig. 2-2E); fluorescence intensity line scans correlate with the expected patterns with consistent intensity across the fluorescently labeled squares. No pattern is observed for DA-functionalized samples exposed to fluorescent secondary antibodies where primary antibodies were omitted. This suggests that binding site densities produced by μ CIP provide sufficient sites for specific binding yet are within the range needed to control nonspecific binding.

2.4.4. Small-Molecule Ligand-Functionalized Substrates for Studying Competitive Recognition of Mixed Biomolecules from Solution

While the data in Fig. 2-2 show that specific capture occurs on surfaces patterned by μ CIP, truly effective surfaces must discriminate between high and low affinity targets in complex environments. To determine the capabilities of surfaces fabricated by μ CIP to capture high affinity binding partners selectively, both BEG- and DA-patterned substrates were exposed to a mixture of AlexaFluor 488-labeled streptavidin and anti-DA antibodies, followed by AlexaFluor 546-tagged anti-rabbit antibodies. As seen in Fig. 2-3A and B, BEG-functionalized

surfaces only bind streptavidin in the patterned regions, as evidenced by the presence of a fluorescent pattern only at the emission wavelength corresponding to AlexaFluor 488. Moreover, DA-patterned surfaces (Fig. 2-3C and D) show patterned protein capture only at an emission wavelength corresponding to the AlexaFluor 546 secondary antibodies, while no pattern is observed at the wavelength corresponding to streptavidin binding. These results suggest that surfaces prepared by μ CIP using either pre- or *in situ*-functionalized small molecules distinguish between protein binding partners based on differences in affinity.

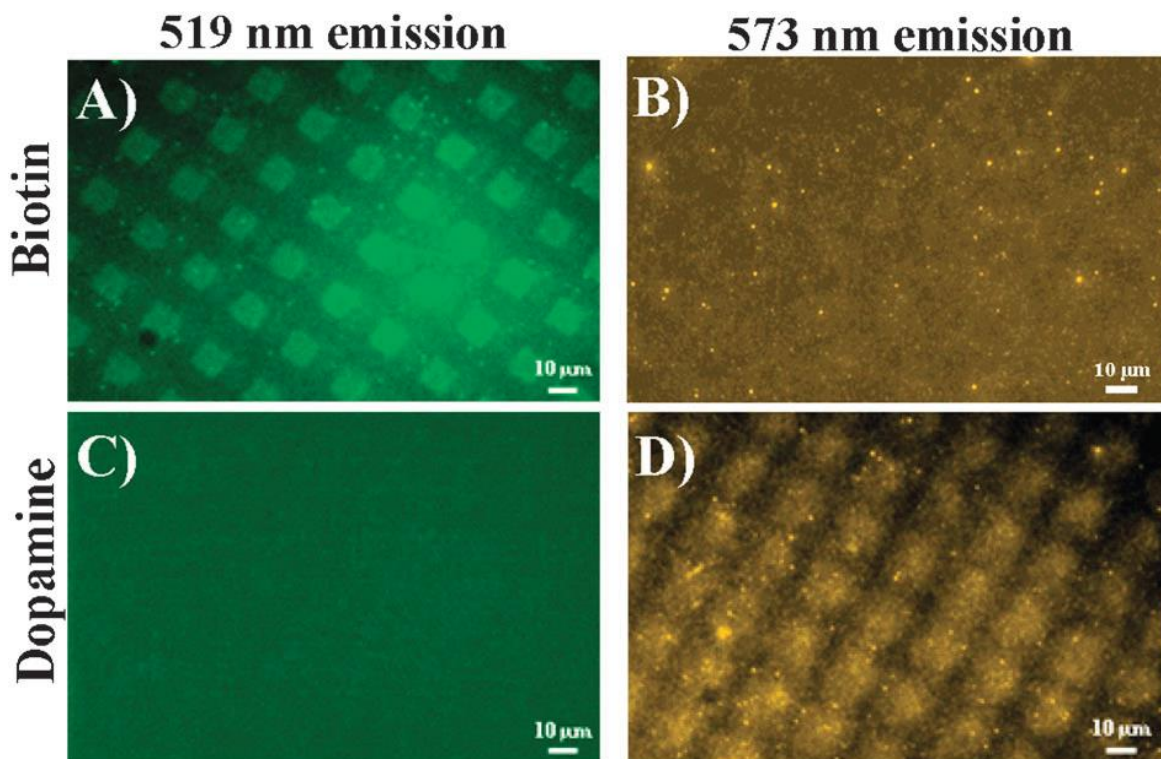


Figure 2-3. Fluorescence microscopy of antibody recognition in complex environments. Biotin- and dopamine-functionalized surfaces were exposed to a combination of AlexaFluor 488-tagged streptavidin and anti-dopamine antibodies raised in rabbit, followed by AlexaFluor 546-tagged anti-rabbit antibodies. Patterned protein capture is apparent for biotin-functionalized surfaces in (A) at the AlexaFluor 488 emission maximum but not in (B), at the AlexaFluor 546 emission maximum. Conversely, dopamine-functionalized surfaces show no protein capture (C) at the AlexaFluor 488 wavelength, while in (D), a pattern is apparent at the AlexaFluor 546 wavelength.

2.5 Conclusions and Prospects

Using μ CIP, chemical patterns were fabricated that not only captured large-molecule binding partners with high affinity for the corresponding small-molecule epitopes, but these surfaces enabled separation based on binding partner affinities. In contrast, photolithographically assisted chemical patterning is relatively unfavorable for creating dilute small-molecule functionalized surfaces having low nonspecific binding.

In addition to limiting nonspecific binding, small-molecule-functionalized capture surfaces fabricated *via* μ CIP offer tailored surface chemical compositions at the nanoscale through control of insertion parameters, precise lithographic control of structures at the micron scale through stamp geometry, and scalability at the centimeter scale. The ability to create patterned, small-molecule-functionalized surfaces using a wider variety of epitopes, *i.e.*, serotonin, dopamine, and biotin, represents a key step toward multiplexed microarrays capable of screening biomolecule binding partners in parallel. Multiplexed surfaces will expedite high-throughput screening for drug discovery, proteomics, and studies of binding interactions from a heterogeneous milieu.¹⁶

2.6 Supplementary Experiments and Figures

Limitations of photolithographically patterned small-molecule capture surfaces.

Although photolithographically assisted chemical patterning is capable of creating spatially separated regions of different functional molecules, specific capture of high-affinity binding partners by surface-tethered small-molecule probes was difficult to accomplish. High-density regions of small-molecule-functionalized probes were associated with high levels of nonspecific adsorption of antibodies (Fig. 2-S1A). Even without functionalization, high-density regions of HEG exhibit nonspecific binding of antibodies (Fig. 2-S1B). To overcome this, low-density small-molecule-functionalized regions were created using insertion-directed self-assembly. However, disruption of the protein-resistant properties of TEG regions by residual LOR resulted in fluorescent patterns with a reversal of the expected contrast (Fig. 2-S1C).

While the biotin-streptavidin complex is an excellent test system, binding affinity is on the order of 10^{-14} M, making it amongst the highest affinity interactions found in nature and thus, not wholly representative of common biological interactions. In contrast, neurotransmitters have affinities, when tethered to surfaces, for their cognate antibodies on the order of 10^{-9} M.^{S4} The ability to capture binding partners selectively with binding affinities in the nanomolar range suggests that μ CIP will be useful for many applications of biological interest.

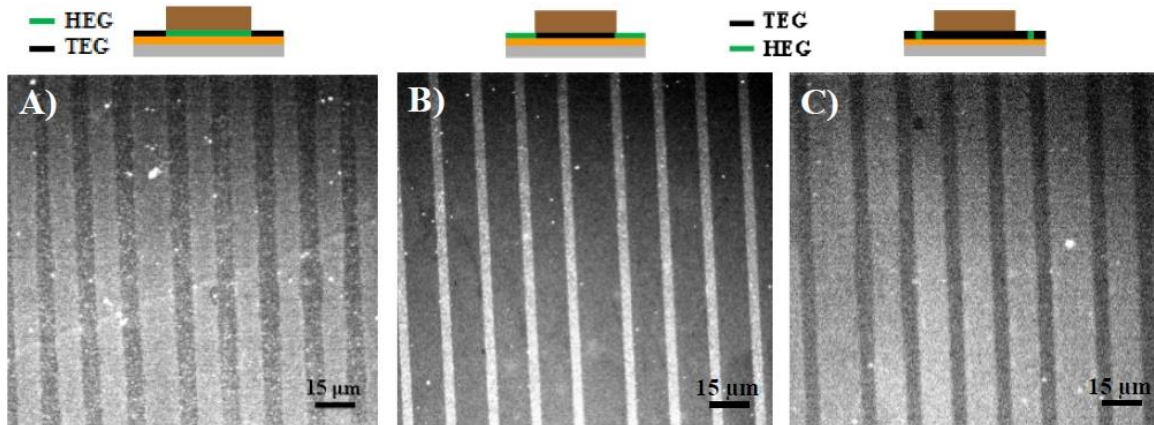


Figure 2-S1. Limitations of photolithographically patterned small-molecule capture surfaces. (A) Samples were prepared by creating densely packed SAMs of HEG followed by backfilling in unprotected regions with protein-resistant TEG. Regions containing HEG were functionalized with serotonin. These surfaces captured fluorescently tagged secondary antibodies in the serotonin functionalized HEG regions in the absence of primary anti-serotonin antibodies, indicating high nonspecific binding in the densely functionalized regions. (B) Self-assembled monolayers of TEG were formed first, and HEG was backfilled in the photolithographically exposed regions. In this case, HEG was left unfunctionalized. Fluorescently tagged secondary antibodies showed recognition of densely packed regions of HEG in the absence of serotonin functionalization and primary anti-serotonin antibodies, indicating a high degree of nonspecific binding. (C) Samples were prepared by forming monolayers of TEG followed by insertion of HEG into the unprotected regions, rather than backfilling. These samples showed an inverted contrast pattern such that TEG regions were brighter than serotonin-functionalized HEG regions after exposing surfaces to anti-serotonin primary antibodies and fluorescently tagged secondary antibodies. We hypothesize this type of pattern is due to residual LOR remaining in the protected TEG regions resulting in high nonspecific binding, which is greater than specific binding in the HEG inserted regions. For all images, wider stripes are the regions initially protected by the LOR.

2.7 References

1. MacBeath, G.; Koehler, A. N.; Schreiber, S. L. Printing Small Molecules as Microarrays and Detecting Protein-Ligand Interactions en Masse. *J. Am. Chem. Soc.* **1999**, *121*, 7967-7968.; Braunschweig, A. B.; Huo, F.; Mirkin, C. A. Molecular Printing. *Nature Chem.* **2009**, *1*, 353-358.; Smith, R. K.; Lewis, P. A.; Weiss, P. S. Patterning Self-Assembled Monolayers. *Prog. Surf. Sci.* **2004**, *75*, 1-68.; Saavedra, H. M.; Mullen, T. J.; Zhang, P.; Dewey, D. C.; Claridge, S. A.; Weiss, P. S. Hybrid Strategies in Nanolithography. *Rep. Prog. Phys.* **2010**, *73*, 036501.
2. Shuster, M. J.; Vaish, A.; Szapacs, M. E.; Anderson, M. E.; Weiss, P. S.; Andrews, A. M. Biospecific Recognition of Tethered Small Molecules Diluted Is Self-Assembled Monolayers. *Adv. Mater.* **2008**, *20*, 164-167.
3. Vaish, A.; Shuster, M. J.; Cheunkar, S.; Singh, Y. S.; Weiss, P. S.; Andrews, A. M. Native Serotonin Membrane Receptors Recognize 5-Hydroxytryptophan-Functionalized Substrates: Enabling Small-Molecule Recognition. *ACS Chem. Neurosci.* **2010**, *1*, 495-504.
4. Szapacs, M. E.; Mathews, T. A.; Tessarollo, L.; Lyons, W. E.; Mamounas, L. A.; Andrews, A. M. Exploring the Relationship Between Serotonin and Brain-Derived Neurotrophic Factor: Analysis of BDNF Protein and Extraneuronal 5-HT in Mice with Reduced Serotonin Transporter or BDNF Expression. *J. Neurosci. Methods* **2004**, *140*, 81-92.; Vu, T. Q.; Chowdhury, S.; Muni, N. J.; Qian, H. H.; Standaert, R. F.; Pepperberg, D. R. Activation of Membrane Receptors by a Neurotransmitter Conjugate Designed for Surface Attachment. *Biomaterials* **2005**, *26*, 1895-1903.

5. Christman, K. L.; Schopf, E.; Broyer, R. M.; Li, R. C.; Chen, Y.; Maynard, H. D. Positioning Multiple Proteins at the Nanoscale with Electron Beam Cross-Linked Functional Polymers. *J. Am. Chem. Soc.* **2009**, *131*, 521-527.
6. Lee, K. B.; Park, S. J.; Mirkin, C. A.; Smith, J. C.; Mrksich, M. Protein Nanoarrays Generated by Dip-Pen Nanolithography. *Science* **2002**, *295*, 1702-1705.
7. Fang, Y.; Frutos, A. G.; Lahiri, J. Membrane Protein Microarrays. *J. Am. Chem. Soc.* **2002**, *124*, 2394-2395.
8. Anderson, M. E.; Srinivasan, C.; Hohman, J. N.; Carter, E. M.; Horn, M. W.; Weiss, P. S. Combining Conventional Lithography with Molecular Self-Assembly for Chemical Patterning. *Adv. Mater.* **2006**, *18*, 3258-3260.
9. Srinivasan, C.; Mullen, T. J.; Hohman, J. N.; Anderson, M. E.; Dameron, A. A.; Andrews, A. M.; Dickey, E. C.; Horn, M. W.; Weiss, P. S. Scanning Electron Microscopy of Nanoscale Chemical Patterns. *ACS Nano* **2007**, *1*, 191-201.
10. Mullen, T. J.; Srinivasan, C.; Hohman, J. N.; Gillmor, S. D.; Shuster, M. J.; Horn, M. W.; Andrews, A. M.; Weiss, P. S. Microcontact Insertion Printing. *Appl. Phys. Lett.* **2007**, *90*, 063114.
11. Vaish, A.; Shuster, M. J.; Cheunkar, S.; Weiss, P. S.; Andrews, A. M. Tuning Stamp Surface Energy for Soft Lithography of Polar Molecules to Fabricate Bioactive Small-Molecule Microarrays. *Small* **2011**, *7*, 1471-1479.
12. Kim, M.; Hohman, J. N.; Cao, Y.; Houk, K. N.; Ma, H.; Jen, A. K. Y.; Weiss, P. S. Creating Favorable Geometries for Directing Organic Photoreactions in Alkanethiolate Monolayers. *Science* **2011**, *331*, 1312-1315.; Kumar, A. S.; Ye, T.; Takami, T.; Yu, B.-C.; Flatt, A. K.; Tour, J. M.; Weiss, P. S. Reversible Photo-Switching of Single

- Azobenzene Molecules in Controlled Nanoscale Environments. *Nano Lett.* **2008**, *8*, 1644-1648.; Moore, A. M.; Yeganeh, S.; Yao, Y.; Claridge, S. A.; Tour, J. M.; Ratner, M. A.; Weiss, P. S. Polarizabilities of Adsorbed and Assembled Molecules: Measuring the Conductance through Buried Contacts. *ACS Nano* **2010**, *4*, 7630-7636.
13. Chapman, R. G.; Ostuni, E.; Yan, L.; Whitesides, G. M. Preparation of Mixed Self-Assembled Monolayers (SAMs) That Resist Adsorption of Proteins Using the Reaction of Amines with a SAM That Presents Interchain Carboxylic Anhydride Groups. *Langmuir* **2000**, *16*, 6927-6936.
14. Lahiri, J.; Isaacs, L.; Tien, J.; Whitesides, G. M. A Strategy for the Generation of Surfaces Presenting Ligands for Studies of Binding Based on an Active Ester as a Common Reactive Intermediate: A Surface Plasmon Resonance Study. *Anal. Chem.* **1999**, *71*, 777-790.
15. Lahiri, J.; Ostuni, E.; Whitesides, G. M. Patterning Ligands on Reactive SAMs by Microcontact Printing. *Langmuir* **1999**, *15*, 2055-2060.; Qin, D.; Xia, Y.; Whitesides, G. M., Soft Lithography for Micro- and Nanoscale Patterning. *Nat. Protoc.* **2010**, *5*, 491-502.; Mrksich, M.; Whitesides, G. M. Patterning Self-Assembled Monolayers Using Microcontact Printing - A New Technology for Biosensors. *Trends Biotechnol.* **1995**, *13*, 228-235.
16. Millet, L. J.; Stewart, M. E.; Nuzzo, R. G.; Gillette, M. U. Guiding Neuron Development with Planar Surface Gradients of Substrate Cues Deposited Using Microfluidic Devices. *Lab Chip* **2010**, *10*, 1525-1535.; Zhang, H.; Shepherd, J. N. H.; Nuzzo, R. G. Microfluidic Contact Printing: A Versatile Printing Platform for Patterning Biomolecules on Hydrogel Substrates. *Soft Matter* **2010**, *6*, 2238-2245.

Experimental Procedure References

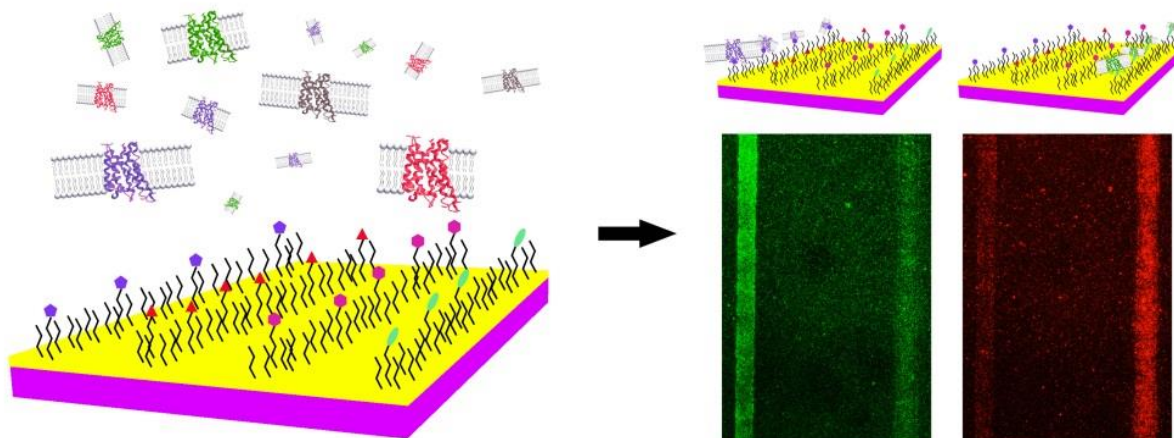
- S1. Shuster, M. J.; Vaish, A.; Szapacs, M. E.; Anderson, M. E.; Weiss, P. S.; Andrews, A. M. Biospecific Recognition of Tethered Small Molecules Diluted in Self-Assembled Monolayers. *Adv. Mater.* **2008**, *20*, 164-167.
- S2. Anderson, M. E.; Srinivasan, C.; Hohman, J. N.; Carter, E. M.; Horn, M. W.; Weiss, P. S. Combining Conventional Lithography with Molecular Self-Assembly for Chemical Patterning. *Adv. Mater.* **2006**, *18*, 3258-3260.
- S3. Vaish, A.; Shuster, M. J.; Cheunkar, S.; Weiss, P. S.; Andrews, A. M. Tuning Stamp Surface Energy for Soft Lithography of Polar Molecules to Fabricate Bioactive Small-Molecule Microarrays. *Small* **2011**, *7*, 1471-1479.
- S4. Wang, T.; Muthuswamy, J. Immunosensor for Detection of Inhibitory Neurotransmitter γ -Aminobutyric Acid Using Quartz Crystal Microbalance. *Anal. Chem.* **2008**, *80*, 8576-8582.

Chapter 3

Small-Molecule Arrays for Sorting G-Protein-Coupled Receptors

The information in this chapter was published in *Journal of Physical Chemistry C* **2013**, *117*,
22362-22368 and has been reproduced here in its entirety.

Authors: Liao, W.-S.; Cao, H. H.; Cheunkar, S.; Shuster, M. J.; Altieri, S. C.;
Weiss, P. S.; Andrews, A. M.



3.1 Abstract

Precise self-assembled monolayer chemistries and microfluidic technology are combined to create small-molecule biorecognition arrays. Small-molecule neurotransmitters or precursors are spatially encoded on monolayer-modified substrates. This platform enables multiplexed screening of G-protein-coupled receptors (GPCRs) from complex media *via* protein-ligand interactions. Preserving access to all epitopes of small molecules is critical for GPCR recognition. The ability to address multiple small molecules on solid substrates and to sort protein mixtures based on specific affinities is a critical step in creating biochips for proteomic applications.

3.2 Introduction

G-protein-coupled receptors (GPCRs) are membrane-associated proteins that are critical to intracellular signaling and cell-to-cell communication in the peripheral and central nervous systems.¹⁻³ Altered GPCR expression and function play key roles in the causes and treatment of psychiatric and neurological disorders, including major depressive disorder, schizophrenia, Alzheimer's disease, and Parkinson's disease.⁴⁻⁶ Consequently, GPCRs are important targets for biomedical research and drug discovery and design.⁷⁻¹²

For more than 40 years, GPCRs have been investigated using equilibrium binding methods involving radiolabeled endogenous ligands or drugs.^{13,14} While invaluable in terms of enabling current understanding of interactions between numerous GPCRs and their binding partners, this approach is limited by the need to develop radiolabeling chemistries for each ligand, as well as the risks and costs associated with the use of radioactive materials.¹⁵ Moreover, GPCRs must be individually interrogated in solution-phase assays using laborious protocols, although high-throughput versions of these assays have recently been developed for large-scale work.¹⁶ To address challenges associated with conventional methods, advanced surface chemistries have been combined with microspotting technology to generate GPCR microarrays for investigating GPCR-drug interactions.^{17,18} Membrane proteins are immobilized on solid substrates, sometimes with prior solubilization to remove membrane lipids to reduce steric hindrance.^{19,20} Notably, immobilization and solubilization can permanently alter the structure and function of receptors.²¹⁻²³

Conversely, libraries of drugs and their derivatives can be tethered to solid substrates and used for high-throughput screening to identify potential biomolecule targets and to enable investigation of binding affinities for many protein-ligand pairs simultaneously.^{11,24,25} For drug

design, multiplexed small-molecule arrays are important *in vitro* screening tools for identifying drug candidates suitable for *in vivo* testing, thus guiding, improving, and streamlining experimentation before clinical trials. However, multiplexed small-molecule arrays have not been successfully demonstrated for GPCR screening. A problem commonly encountered is the size mismatch between small-molecule ligands and GPCR binding partners, the latter of which are bulky due to overall protein size and the presence of membrane fragments needed to stabilize native receptor conformations.²⁶

Several studies have demonstrated that free small-molecule ligands require all epitopes to participate in membrane protein recognition.²⁶⁻²⁸ Thus, we have investigated tethering small molecules *via* ectopic functional groups to mimic free ligands and to enable bioselective recognition of large biomolecule binding partners.²⁶ We have demonstrated strategies for selectively capturing serotonin (5-hydroxytryptamine; 5-HT) GPCRs *via* the small-molecule precursor *L*-5-hydroxytryptophan (*L*-5-HTP), which approximates free 5-HT when tethered *via* its carboxyl group in a dilute manner to SAM-modified substrates.^{26,29}

Previously, we used μ CIP³⁰ to pattern small molecules in a dilute manner on SAM-modified substrates.³¹ Isolated probes patterned using μ CIP show selective molecular recognition of antibody and receptor binding partners and can capture cognate antibodies from dual antibody mixtures.³¹ However, multiplexed patterning *via* μ CIP was limited by the need to devise compatible serial functionalization chemistries. Here, we patterned substrates using parallel functionalization with multiple small molecules. Each type of small molecules was physically restricted to separate microfluidic channels. This strategy enabled multiple biomolecule binding partners to be captured in a spatially encoded manner.

The work of Lahiri and co-workers has shown that GPCRs microspotted on chemically modified glass substrates are active *via* a fluorescence guanosine triphosphate (GTP) γ S assay for G-protein activity.^{18,32} The GPCRs captured on the platform described here could also be tested for G-protein activity, which would enable on-chip functional assays. Moreover, in addition to fluorescence microscopy used to visualize GPCR binding in the present study, we have also shown that functionalized thin (10-15 nm) Au layers can be used to detect binding by fluorescence spectroscopy.³³ Here, we significantly advance small-molecule capture surface strategies by placing multiple small-molecule mimics in specified locations on single substrates (Figure 3-1). Microfluidic channels are used to address small-molecule ligands to specific locations on SAM-modified Au substrates producing microarrays for sorting GPCRs from mixtures based on ligand specificities. The GPCRs used here were not solubilized to facilitate native biological conformations and ligand recognition.^{18,26} We first examined mixtures of antibodies raised against specific biogenic amine small-molecule neurotransmitters. Next, platforms functionalized with multiple neurotransmitter precursors were screened for selective GPCR binding and for sorting mixtures containing two GPCRs.

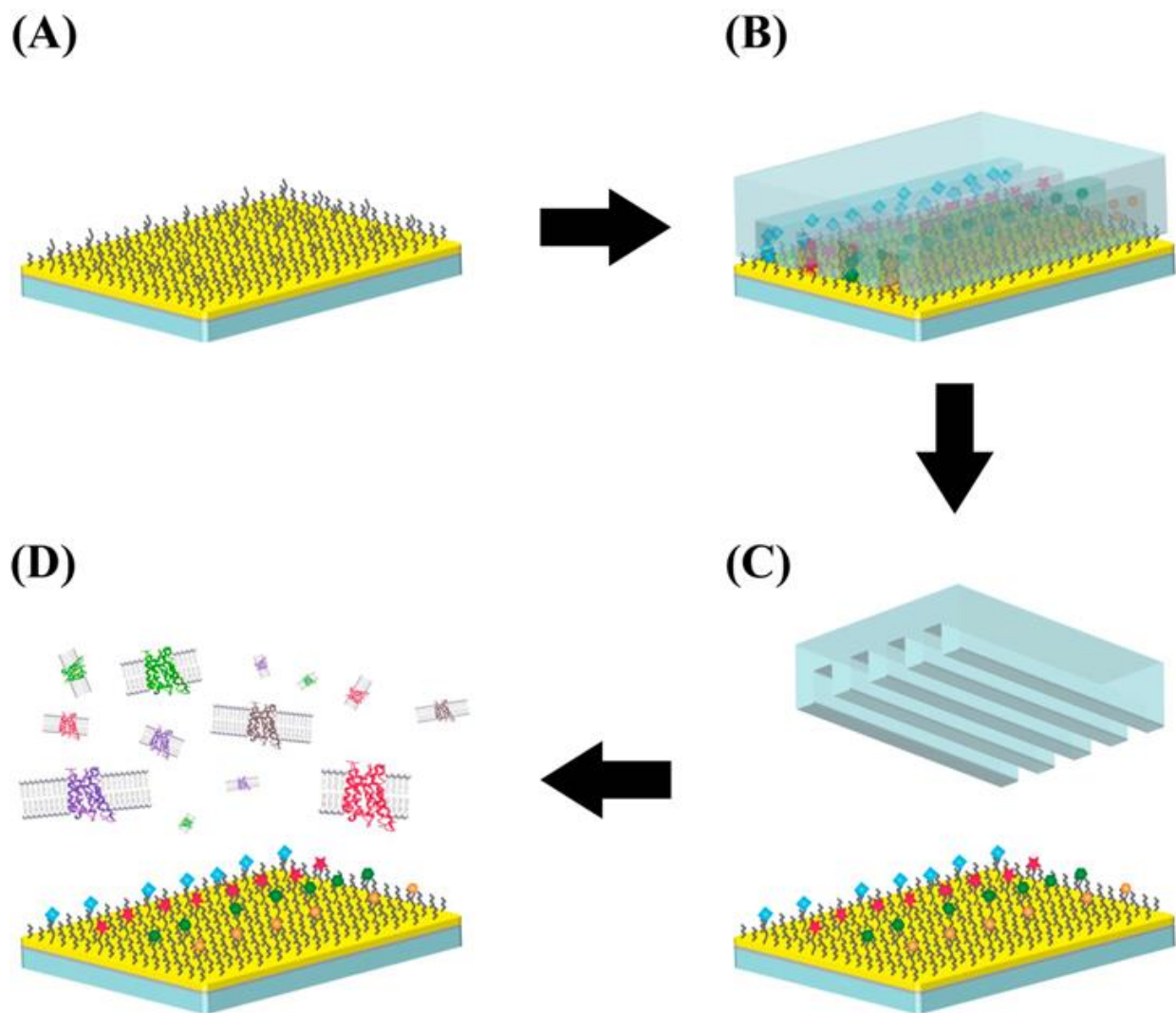


Figure 3-1. Schematic illustrating the small-molecule array fabrication process.

(A) Molecules with extended functional tail groups are self-assembled in a dilute manner on a Au substrate. (B) A PDMS microfluidic device is sealed to the substrate enabling multiplexed surface functionalization inside the fluidic channels. (C) The PDMS microfluidic device is removed revealing spatially encoded molecules on the substrate. (D) The substrate is challenged with solutions containing multiple biomolecule binding partners enabling sorting *via* different specificities for tethered small molecules.

3.3 Materials and Methods

Materials. D,L-Norepinephrine (NE) hydrochloride $\geq 97\%$, histamine (HA) dihydrochloride $\geq 99\%$, bovine serum albumin (BSA) lyophilized, *N*-hydroxysuccinimide (NHS) 98%, *N*-(3-dimethylaminopropyl)-*N'*-ethylcarbodiimide hydrochloride (EDC) commercial grade, 4-methylpiperidine 96%, and *N,N*-dimethylformamide ACS reagent $\geq 99.8\%$ were purchased from Sigma Aldrich (St. Louis, MO). The Fmoc-protected biological precursors to 5-HT and dopamine, 9-fluorenylmethoxycarbonyl-5-hydroxy-L-tryptophan (Fmoc-*L*-5-HTP) and Fmoc-3,4-dihydroxy-L-phenylalanine (Fmoc-*L*-DOPA), were purchased from AnaSpec Eurogentec (Fremont, CA). The Fmoc-protected biological precursor to HA, Fmoc-His-OH (Fmoc-*L*-HD), was purchased from Bachem Americas, Inc. (Torrance, CA). Absolute, anhydrous, ACS/USP grade ethanol was purchased from PHARMCO-AAPER (Oakland, CA). Deionized water was obtained from an in-house Millipore water purifier (Billerica, MA).

The following primary antibodies were purchased from Abcam, Inc. (Cambridge, MA): rabbit polyclonal anti-noradrenaline antibody (whole antiserum), mouse monoclonal anti-histamine antibody (1 mg/mL), mouse monoclonal [SG2-D1a] anti-dopamine D₁ receptor antibody, chicken polyclonal anti- β_2 adrenergic receptor antibody, and rabbit polyclonal anti-histamine H₁ receptor antibody. Secondary antibodies, AlexaFluor 350 goat anti-mouse, AlexaFluor 546 goat anti-mouse, and AlexaFluor 488 goat anti-rabbit IgG highly cross-adsorbed antibodies (2 mg/mL), were purchased from Invitrogen (Carlsbad, CA). Membrane preparations containing human histamine H₁ receptors (5 $\mu\text{g}/\mu\text{L}$ protein concentration) or human dopamine D₁ receptors (4 $\mu\text{g}/\mu\text{L}$ protein concentration) expressed in Chinese hamster ovary (CHO-K1) cells and nontransfected CHO-K1 cell membranes (10 mg/mL protein concentration) were purchased from Perkin-Elmer, Inc. (Waltham, MA). Hydroxyl-terminated tri(ethylene

glycol)undecanethiol (TEG) and carboxyl-terminated hexa(ethylene glycol)undecanethiol (HEG) were purchased from Toronto Research Chemicals Inc. (Toronto, ON, Canada). Amine-terminated hexa(ethylene glycol)undecanethiol (AEG) was purchased from Prochimia (Sopot, Poland).

Neurotransmitter Spatial Addressing for Antibody Sorting. Substrates (100 nm of Au on 5 nm of Ti on Si, Platypus, Madison, WI) were exposed to an 80/20 ethanolic solution of 0.48 mM TEG and 0.12 mM HEG for ~16 h to form dilute carboxyl-terminated SAMs. An aqueous solution containing 25 mM NHS and 30 mM EDC was incubated with SAM-modified Au substrates for 1 h. This step converts the carboxyls of HEG to NHS-ester moieties, which are then reacted with the primary amines on the small-molecule probes NE and HA to form amide bonds.

Polydimethylsiloxane microfluidic devices were fabricated using standard photolithography-fabricated masters. A 10:1 mass ratio of SYLGARD® 184 silicone elastomer base and curing agent (Ellsworth Adhesives, Germantown, WI) was thoroughly mixed, degassed under vacuum and cured in an oven at 70 °C overnight. Devices were soaked in 10 mg/mL of BSA in phosphate-buffered saline (PBS) ($[\text{KH}_2\text{PO}_4] = 10 \text{ mM}$, $[\text{Na}_2\text{HPO}_4] = 49 \text{ mM}$, $[\text{NaCl}] = 137 \text{ mM}$, $[\text{KCl}] = 2.7 \text{ mM}$; pH 7.4) for 1 h to block nonspecific protein adsorption sites. Microfluidics devices were then rinsed with DI water and dried with nitrogen before being brought into conformal contact with NHS-activated SAM-modified Au substrates. All antibodies and receptors were used as purchased and were dissolved in PBS pH 7.4.

Phosphate buffer (PB) ($[\text{KH}_2\text{PO}_4] = 10 \text{ mM}$, $[\text{K}_2\text{HPO}_4] = 40 \text{ mM}$; pH 7.4) was used to dissolve NE, while PB ($[\text{KH}_2\text{PO}_4] = 0.73 \text{ mM}$, $[\text{K}_2\text{HPO}_4] = 499 \text{ mM}$; pH 9.5) was used to dissolve HA and 5-HT. For antibody sorting experiments, HA (100 mM) was first injected and

incubated in several microfluidic channels such that there was always one channel filled with PB on either side of the HA channels. After 2 h incubation of HA or PB in some channels, NE (2 mM) was injected into the remaining empty channels and incubated for another 3 h. After surface modification steps, microfluidic devices were removed from the platforms. The remaining unreacted NHS-activated carboxyls on HEG in SAMs were hydrolyzed by rinsing platforms with PB at pH 9.5 for 1 min. Platforms were then rinsed with DI water, incubated with 10 mg/mL of BSA for 5 min, and rinsed again with DI water before incubating with antibodies.

Primary and secondary antibodies were diluted 1:200 and 1:100 in PBS pH 7.4, respectively. Each antibody was incubated with small-molecule arrays for 20 min, and DI water was used to rinse substrates between steps. Substrates were exposed to thoroughly mixed solutions containing both NE and HA primary antibodies prepared immediately before use, followed by solutions containing both AlexaFluor 488 goat anti-rabbit and AlexaFluor 350 goat anti-mouse IgG secondary antibodies (Table 3-S1, Supporting Information).

Neurotransmitter Precursor Spatial Addressing for Screening and Sorting GPCRs.

Substrates coated with Au were exposed to 95/5 ethanolic solutions of 0.48 mM TEG and 0.025 mM AEG for 16 h to form dilute amine-terminated SAMs. Microfluidic devices fabricated from PDMS were first treated for 30 s in an oxygen-plasma cleaner (Harrick Plasma, Ithaca, NY; 18 W, 10 psi oxygen pressure) and then brought into conformal contact with amine-terminated SAM-modified Au substrates. For screening GPCR binding, solutions containing either 30 mM Fmoc-protected *L*-5-HTP, Fmoc-protected *L*-DOPA, or Fmoc-protected *L*-HD were combined with 30 mM NHS/EDC in 60/40 DMF/water. For sorting GPCR mixtures, solutions containing either 20 mM Fmoc-*L*-HD or 35 mM Fmoc-*L*-DOPA were combined with 20 mM NHS/EDC or 35 mM NHS/EDC, respectively, in 60/40 DMF/water. Solutions containing each

probe molecule were then injected into different microfluidic channels and incubated for 20 min. Activated NHS-esters on the probes were used to form amide bonds with the primary amines of AEG. The Fmoc protecting groups were used to prevent intermolecular reactions with other probe molecule activated esters.

Once surface functionalization was carried out, the microfluidic devices were peeled off the substrates. The Fmoc moieties were removed from surface-bound probes by incubating with 20% 4-methylpiperidine in water for 15 min. After rinsing with copious amounts of DI water, platforms were incubated with 10 mg/mL of BSA for 5 min to block nonspecific adsorption sites. Platforms were rinsed again with DI water prior to incubation with receptors and antibodies.

The preparation protocol for antibodies to visualize receptor binding was similar to that used for the antibody capture experiments. Copious amounts of DI water were used to rinse the small-molecule arrays between protein incubation steps. Briefly, platforms for GPCR-ligand screening experiments were first incubated with a solution containing 80 μ g of human histamine H₁ for 1 h. Platforms were then sequentially challenged with chicken polyclonal anti- β_2 adrenergic receptor antibody, rabbit polyclonal anti-histamine H₁ receptor antibody, and AlexaFluor 488 goat anti-rabbit IgG secondary antibody. Anti- β_2 adrenergic receptor antibodies were used to mask nonspecific adsorption sites introduced by bound receptor-membrane complexes and to alleviate nonspecific binding of receptor antibodies to surface-bound tethers. Each antibody incubation step was 15 min.

For GPCR sorting experiments, 80 μ g of membrane-associated human histamine H₁ receptors and 80 μ g of membrane-associated dopamine D₁ receptors were thoroughly mixed in solution immediately before use. Platforms were incubated with GPCR solutions for 1 h followed by sequential incubation with chicken polyclonal anti- β_2 adrenergic receptor antibody

(to reduce nonspecific binding), rabbit polyclonal anti-histamine H₁ receptor antibody, AlexaFluor 488 goat anti-rabbit IgG secondary antibody, mouse monoclonal [SG2-D1a] anti-dopamine D₁ receptor antibody, and AlexaFluor 546 goat anti-mouse IgG secondary antibody.

Statistical Analyses. Data were initially analyzed by Student t-tests (2-group comparisons) or analysis of variance (ANOVA; multiple group comparisons) using GraphPad Prism (GraphPad Software Inc., San Diego, USA). Following ANOVA, pair-wise comparisons were carried out using Tukey's multiple comparisons. Fluorescence intensities are reported as means \pm standard errors of the means with probabilities $P < 0.05$ considered statistically significant.

3.4 Results and Discussions

3.4.1 Neurotransmitter Arrays for Sorting Mixed Antibody

Wafers composed of Si coated with 100-nm-thick Au films served as substrates for tethering small-molecule ligands. Substrates were exposed to ethanolic solutions of 80/20 hydroxyl-terminated tri(ethylene glycol)alkanethiol (TEG) and carboxyl-terminated hexa(ethylene glycol)alkanethiol (HEG) to form SAMs bearing dilute carboxyl-terminated moieties. Oligo(ethylene glycol) (OEG) terminal groups reduce nonspecific protein adsorption.^{31,34,35} Additionally, substrates were briefly exposed (~5 min) to bovine serum albumin (BSA) (10 mg/mL) before incubating with antibodies or receptors.³¹ We have found that using both protein-resisting OEGs and BSA blocking substantially reduces nonspecific protein adsorption.

The free carboxyl groups of the extended tethers of HEG molecules were first activated by exposure to an aqueous mixture of *N*-hydroxysuccinimide (NHS) and *N*-(3-dimethylaminopropyl)-*N'*-ethylcarbodiimide (EDC) to create NHS-activated carboxyls of HEG, enabling amide bond formation with small-molecule primary amines (Figure 3-2A).^{26,31,35} A PDMS device with microfluidic channels was then brought into conformal contact with each NHS-activated SAM, and aqueous solutions containing individual ligands were injected into different channels. Control channels were injected with phosphate buffer (PB; pH 9.0) in the absence of ligands. Microfluidic devices were removed from substrates after ligand incubation, and the platforms were rinsed with PB to facilitate hydrolysis of the remaining unreacted surface-tethered NHS-esters.^{36,37} Afterward, platforms were rinsed with copious amounts of deionized (DI) water prior to protein exposure.

We expanded the small-molecule library described in our previous work by selecting two additional neurotransmitters, norepinephrine (NE; 4-[(1R)-2-amino-1-hydroxyethyl]-benzene-1,2-diol) and histamine (HA; 2-(1H-imidazol-4-yl)-ethanamine), for surface functionalization.^{26,31,35} Following functionalization with NE and HA, substrates were incubated with solutions containing a mixture of primary antibodies to determine whether antibodies would sort to regions of the substrate functionalized with the cognate neurotransmitter. Primary antibody-ligand interactions were visualized using fluorescently tagged secondary antibodies specific for each primary antibody (Table 3-S1, Supporting Information). Substrates were imaged at two different wavelengths corresponding to secondary antibody emission wavelengths. As shown in Figure 3-2B, the high-intensity green and blue lanes represent total (specific + nonspecific) binding of NE and HA antibodies to the corresponding tethered ligands. The dark middle lanes show lack of antibody binding in the absence of tethered ligands and demonstrate that TEG-functionalized substrates resist nonspecific protein adsorption.^{31,34,35} Low nonspecific recognition of HA by NE antibodies (6%) and modest nonspecific recognition of NE by HA antibodies (30%) were observed (right lane in Figure 3-2B and left lane in Figure 3-2C, respectively). To investigate the origins of this nonspecific binding, substrates were exposed to fluorescently tagged secondary antibodies in the absence of primary antibodies. No detectable fluorescence intensity was observed in any lane (Figures 3-S2C, D, Supporting Information), indicating that the binding of HA antibodies to NE was due to HA primary antibody cross-reactivity.

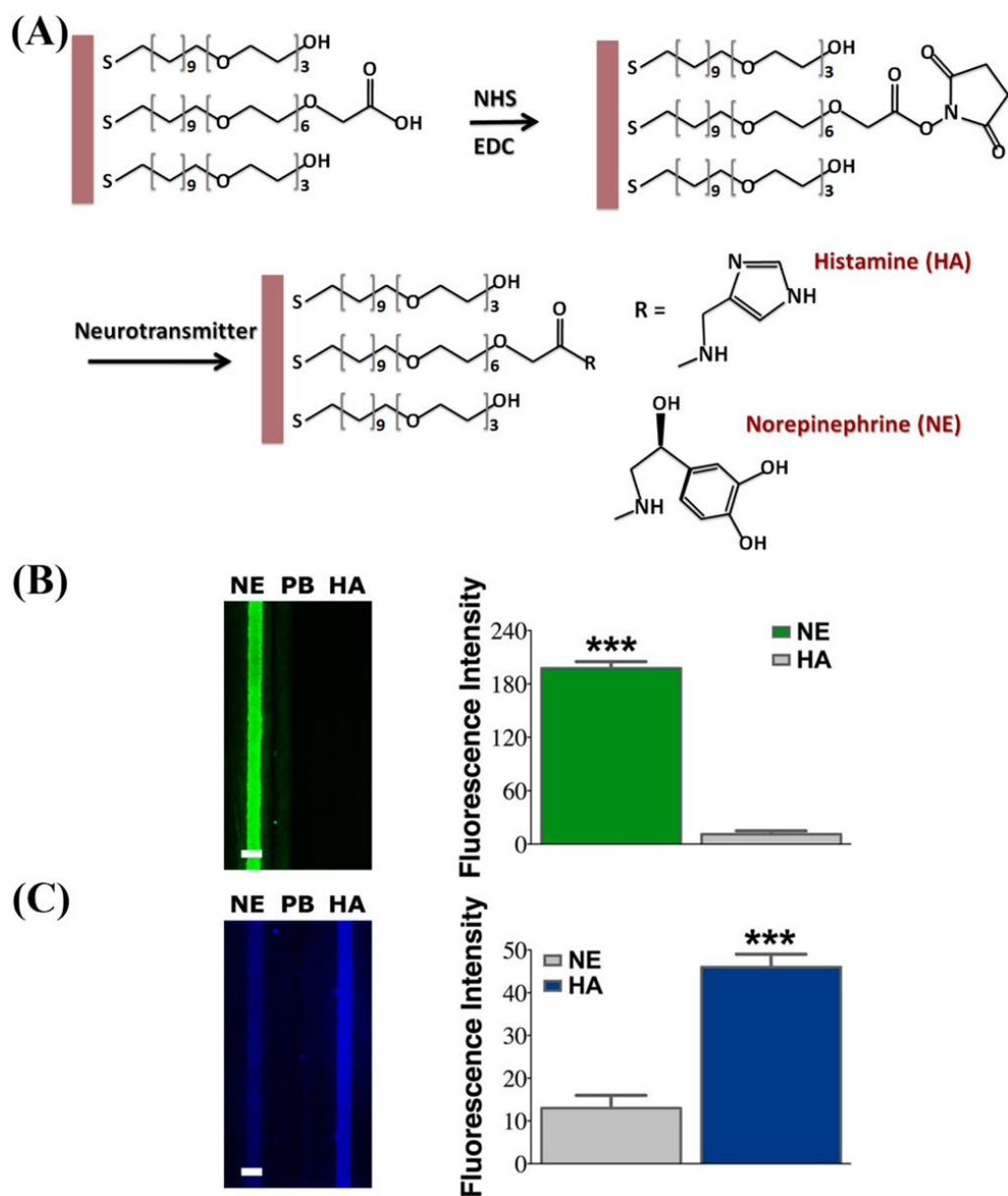
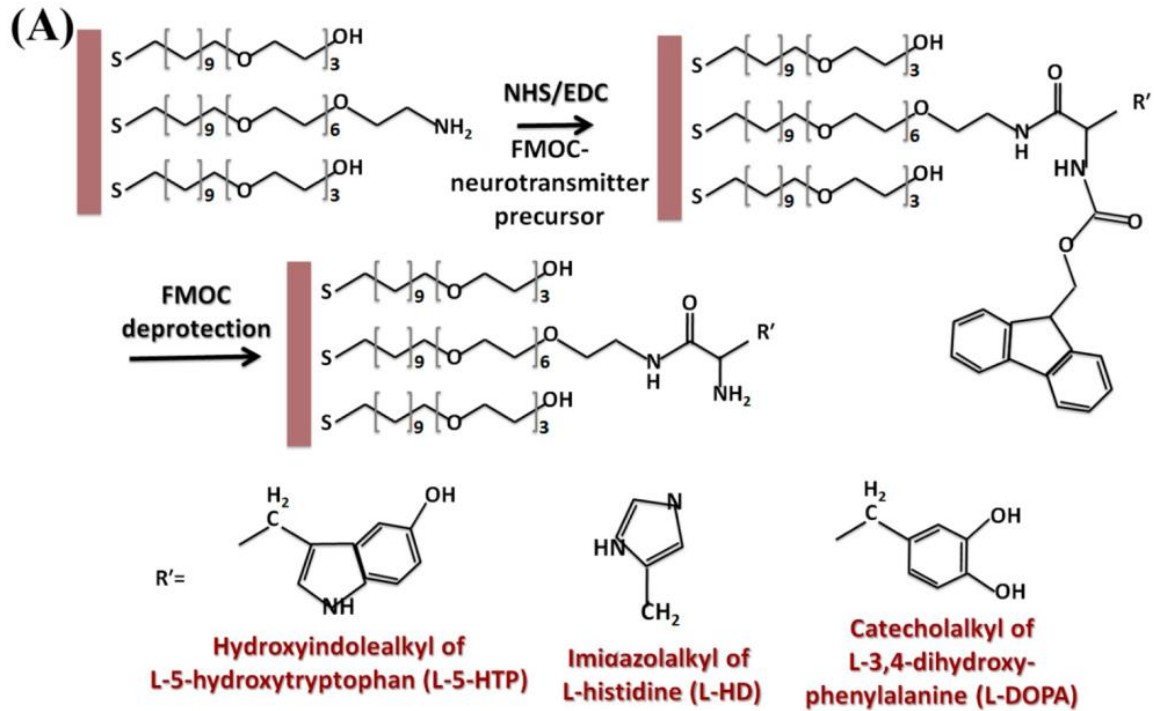


Figure 3-2. (A) Schematic of surface functionalization chemistries for histamine (HA) and norepinephrine (NE). (B,C) (Left) Representative fluorescence images and (right) fluorescence intensity graphs for NE and HA antibody sorting. High fluorescence intensity in the NE lane (AlexaFluor 488; emission 519 nm) (top image) vs. the HA lane (AlexaFluor 350; emission 442 nm) (bottom image) indicates that antibodies against NE and HA sort to surface-tethered NE and HA, respectively. Left lane: NE; middle lane: blank (no surface-tethered ligands); right lane: HA. Error bars represent standard errors of the means with $N=4$ substrates per group. The means for total vs. nonspecific binding are significantly different for NE antibody binding [$t(6)=67$, $***P < 0.001$] and HA antibody binding [$t(6)=18$, $***P < 0.001$]. Scale bars are 50 μm .

3.4.2 Surface-Bound Ligands Mimicking Endogenous Neurotransmitters for Sorting Native G-Protein-Coupled Receptors

In the extracellular space, all functional groups associated with free small-molecule neurotransmitters are available for GPCR recognition.^{6,38} However, the tethered small molecules used in the antibody sorting experiments described above are not expected to recognize GPCRs effectively because one of the key functional groups, the primary amine, is used to tether the neurotransmitters to substrates.²⁶ We have shown that by utilizing small-molecule analogs containing all epitopes necessary for recognizing GPCRs, plus an additional functional group for tethering, surface-immobilized species mimic free ligands and capture GPCRs.^{26,29,31}

Here, we used *L*-histidine (*L*-HD) and *L*-3,4-dihydroxyphenylalanine (*L*-DOPA), in addition to *L*-5-hydroxytryptophan (*L*-5-HTP), which we have demonstrated previously, in tethering reactions to approximate the free neurotransmitters histamine, 3,4-dihydroxyphenylethylamine (dopamine), and serotonin, respectively. The former are the native biological precursors to HA, dopamine, and 5-HT. They not only preserve all native epitopes for receptor recognition but also contain additional carboxyl moieties for surface tethering. The surface conjugation steps are illustrated in Figure 3-3A. Briefly, an ethanolic solution of 95/5 TEG and amine-terminated hexa(ethylene glycol)alkanethiol (AEG) was used to self-assemble the longer amine-terminated molecules at low density in TEG SAMs.²⁹ A lower tethering alkanethiol ratio than that used in the antibody sorting experiments was employed to dilute tethered ligands further, providing better access to large GPCRs with associated membrane fragments. A mixture of NHS/EDC in 60/40 DMF/DI water was used to activate carboxyl groups on 9-fluorenylmethyloxycarbonyl (Fmoc)-protected precursor molecules.^{26,29}



(B) L-5-HTP L-HD Blank L-DOPA

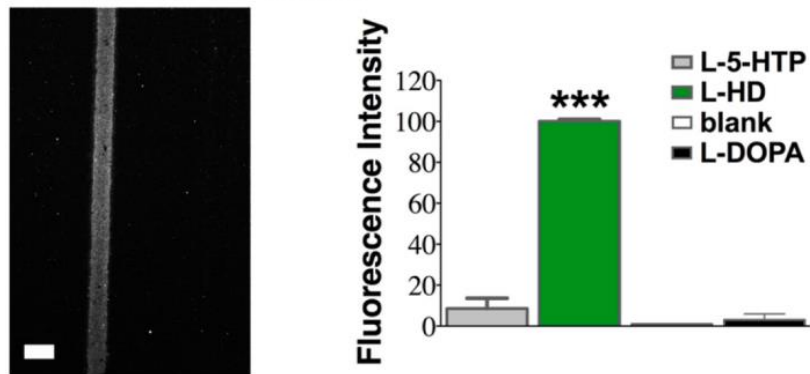


Figure 3-3. (A) Schematic of surface functionalization chemistry for *L*-5-hydroxytryptophan (*L*-5-HTP), *L*-histidine (*L*-HD), and *L*-3,4-dihydroxyphenylalanine (*L*-DOPA). (B) (Left) Representative fluorescence image and (right) fluorescence intensity graph. High fluorescence intensity was observed for the *L*-HD lane (AlexaFluor 488; emission 519 nm) indicating specific capture of histamine H_1 receptors compared to lanes functionalized with other neurotransmitter precursors. Left to right: *L*-5-HTP, *L*-HD, blank (no surface-tethered ligands), and *L*-DOPA. Error bars represent standard errors of the means with $N=5$ substrates. Mean fluorescence intensities across lanes are significantly different [$F(3,16)=280$; $P<0.001$]. *** $P<0.001$ between mean *L*-HD fluorescence intensity and *L*-5-HTP, blank, and *L*-DOPA fluorescence intensities. Scale bars are 50 μ m.

Microfluidic PDMS devices were sealed against SAM-modified substrates. Activated precursor solutions were immediately injected and incubated in the microfluidic channels enabling amide bond formation with the primary amines of AEG in SAMs. The Fmoc protecting groups prevented primary amine intermolecular reactions with NHS-activated carboxyl groups.^{26,29} After peeling off the microfluidic devices, 4-methylpiperidine was used to remove Fmoc from tethered precursor molecules.^{26,29} Substrates were then rinsed with DI water and dried with nitrogen gas.

The spatially encoded multifunctionalized substrates were used to investigate receptor recognition of small-molecule neurotransmitter mimics. Cell membrane fragments containing human histamine H₁ receptors isolated from transfected Chinese hamster ovary (CHO)-K1 cell lines were incubated with surfaces functionalized with *L*-5-HTP, *L*-HD, and *L*-DOPA. A H₁ anti-receptor antibody was used to recognize bound receptors. Fluorescently tagged secondary antibodies were used to visualize primary antibodies associated with bound receptors (Table 3-S2, Supporting Information). The significantly greater fluorescence intensity in the *L*-HD-functionalized lane (second from the left; Figure 3-3B) compared with the adjacent lanes indicated biospecificity of H₁ receptor recognition of immobilized *L*-HD mimicking free HA.

Furthermore, surfaces having tethered *L*-HD and *L*-DOPA were challenged with solutions containing mixtures of human histamine H₁ and dopamine D₁ GPCRs isolated from transfected CHO-K1 cell lines. Figure 3-4 displays high-intensity green and red lanes illustrating total binding by H₁ and D₁ receptors to the corresponding lanes functionalized with *L*-HD and *L*-DOPA. Moderate nonspecific binding was observed in the green fluorescence image for the *L*-DOPA lane (35%) and in the red fluorescent image for the *L*-HD lane (40%). Control experiments were carried out using CHO-K1 cell membranes from nontransfected cell lines, *i.e.*,

membranes without H₁ or D₁ GPCRs, followed by exposure to anti-receptor antibodies and fluorescently tagged secondary antibodies. Low fluorescence intensity was observed in all lanes (Figures 3-S3C, D, Supporting Information) suggesting that nonspecific binding observed in Figure 3-4 stemmed from some affinity of anti-H₁ receptor antibodies with *L*-HD and anti-D₁ receptor antibodies with *L*-DOPA. Nonetheless, this small-molecule array experiment demonstrates that GPCRs in complex mixtures can be sorted to particular regions on solid substrates *via* specific GPCR-ligand interactions. The receptor screening results demonstrated in Figures 3-3 and 3-4 further indicate that additional epitopes introduced to the surface-tethered ligands do not lead to surface-tethering-induced orientation and crowding problems affecting receptor binding. Rather, the presence of the additional epitope restores the bioselectivity of the small-molecule arrays toward membrane protein targets.

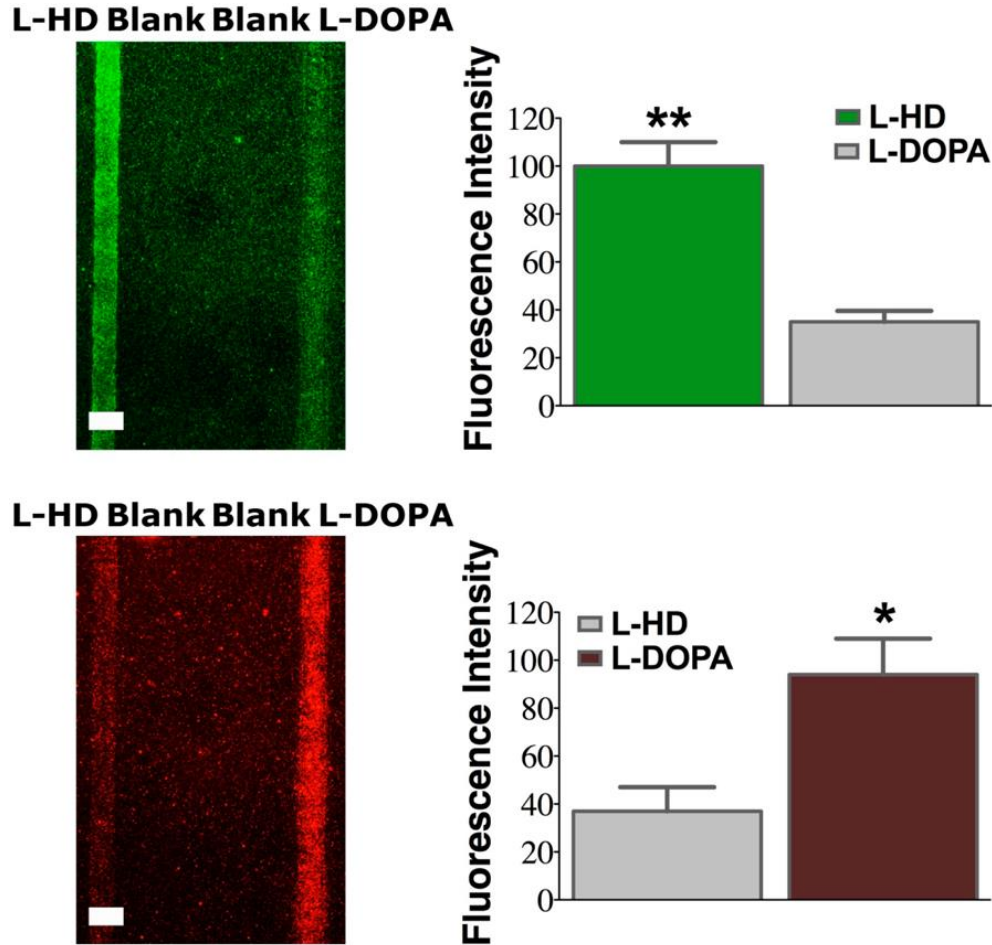


Figure 3-4. (Left) Representative fluorescence images and (Right) fluorescence intensity graphs for sorting human histamine H₁ and human dopamine D₁ receptor mixtures. Left lane: *L*-histidine (*L*-HD). Two middle lanes: blank (no surface-tethered ligands). Right lane: *L*-3,4-dihydroxyphenylalanine (*L*-DOPA). Substrates were imaged at two different wavelengths to visualize the *L*-HD lanes (AlexaFluor 488; emission 519 nm) (top image) and the *L*-DOPA lanes (AlexaFluor 546; emission 573 nm) (bottom image). Fluorescence intensities indicate sorting of histamine H₁ and dopamine D₁ receptors to the corresponding surface-tethered ligands. Error bars represent standard errors of the means with $N=3$ samples per group. Mean intensities are significantly different for green [$t(4)=6.2$, $**P<0.01$] and red [$t(4)=3.5$, $*P<0.05$] fluorescence data. Scale bars are 50 μm .

3.5 Conclusions and Prospects

The capability to sort multiple nonsolubilized GPCRs from complex media, in combination with minimal fluorescence background, suggests that this platform can be used not only to screen biological preparations containing native molecules for “orphan” GPCRs but also to identify novel synthetic binding partners, such as neuropeptides from phage display libraries or aptamers to serve as artificially receptors, with relevance to therapeutic development and biosensing applications.^{39–43}

3.6 Supplemental Experiments and Figures

Supplemental Experiments. Experiments to investigate sources of nonspecific binding for NE and HA antibodies were carried out using the same procedures described in the *Antibody Sorting* experimental section with the exception that primary antibodies were omitted. The results are shown in fig. 3-S1. Experiments to investigate the origins of nonspecific binding in receptor-ligand screening and sorting experiments were conducted using the same procedures described in the *Screening and Sorting GPCRs* experimental section with the exception that CHO-K1 cell membranes lacking transfected H₁ and D₁ receptors were used. The results are shown in figs. 3-S2 and 3-S3.

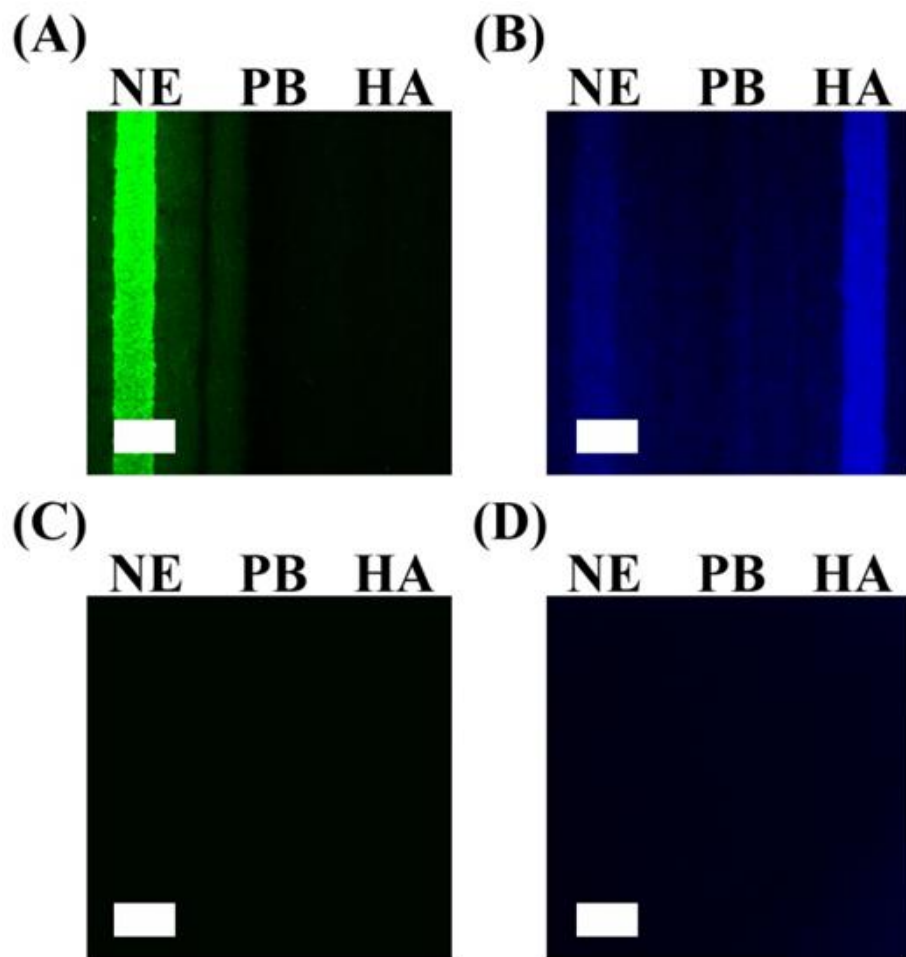


Figure 3-S1. Norepinephrine (NE) and histamine (HA) antibody sorting (corresponding to fig. 3-2). A substrate was prepared as described in the experimental sections and cut to produce two identical halves. **(A,B)** One half of the substrate was challenged with anti-noradrenaline and anti-histamine primary antibodies simultaneously, followed by a combination of AlexaFluor 488 and AlexaFluor 350 secondary antibodies. In **(A)**, the substrate was imaged at 519 nm, the emission wavelength to detect secondary antibody binding to NE primary antibodies. In **(B)**, the substrate was imaged at 442 nm, the emission wavelength to detect secondary antibody binding to HA primary antibodies. **(C,D)** The other half of the substrate was challenged with secondary antibodies alone and imaged as in **(A,B)**. Fluorescence was not detected at either secondary antibody emission wavelength when primary antibodies were omitted indicating minimal nonspecific adsorption of secondary antibodies. Left lanes: NE; middle lanes: blank (no surface-tethered ligands); right lanes: HA. Scale bars are 50 μm . The substrate shown in **(A,B)** is the same as depicted in fig. 3-2 **(B,C)**.

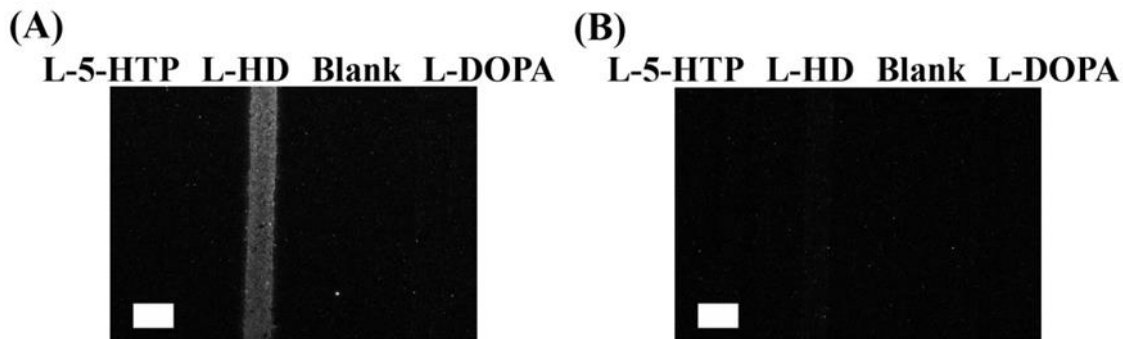


Figure 3-S2. Histamine H₁ receptor screening (corresponding to fig. 3-3).

A substrate was prepared as described in the experimental section and cut to produce two identical halves. **(A)** One half of the substrate was challenged with histamine H₁ receptors, anti-β₂ adrenergic receptor antibodies (to block nonspecific sites introduced by bound receptor-membrane complexes), anti-histamine H₁ receptor primary antibodies, and AlexaFluor 488 secondary antibodies. Imaging was carried out at 519 nm to detect secondary antibody binding. **(B)** The other half of the substrate was challenged with nontransfected CHO-K1 cell membranes, anti-β₂ adrenergic receptor antibodies, anti-histamine H₁ receptor primary antibodies, and AlexaFluor 488 secondary antibodies and imaged at 519 nm. Fluorescence is not detected in **(B)** indicating little to no nonspecific binding of primary and secondary antibodies when histamine H₁ receptors are not present in CHO-K1 cell membranes. Left to right: *L*-5-hydroxytryptophan (*L*-5-HTP); *L*-histidine (*L*-HD); blank (absence of surface-tethered ligands); and *L*-3,4-dihydroxyphenylalanine (*L*-DOPA). Scale bars are 50 μm. The substrate shown in **(A)** is the same as depicted in fig. 3-3 **(B)**.

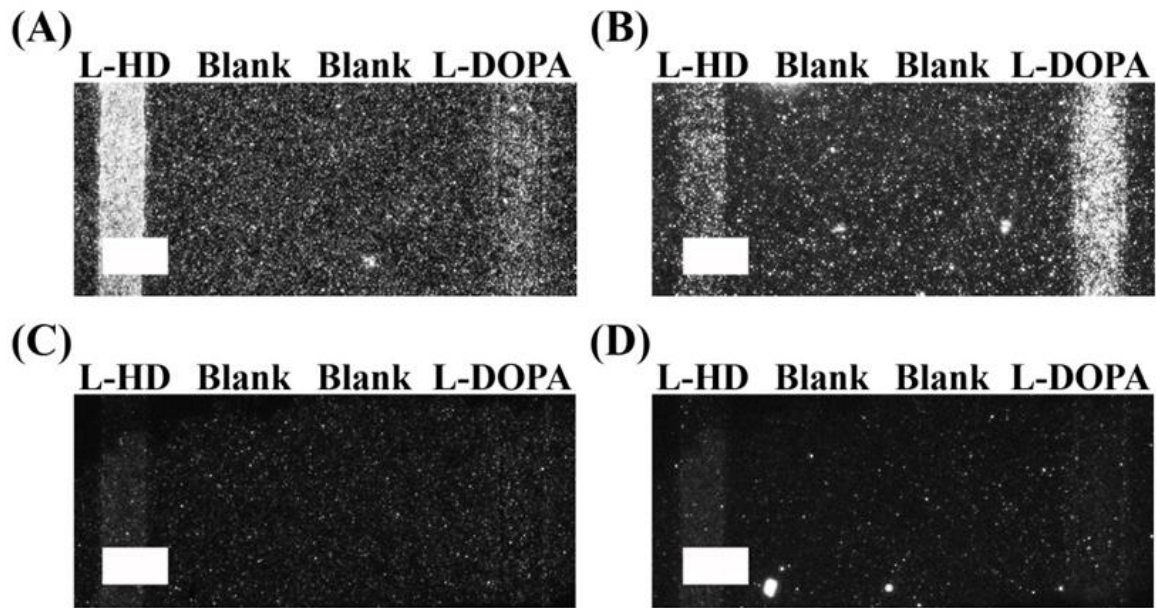


Figure 3-S3. Histamine H₁ and dopamine D₁ receptor sorting (corresponding to fig. 3-4).

A substrate was prepared as described in the experimental sections and cut to produce two identical halves. **(A,B)** One half of the substrate was challenged sequentially with a solution containing a mixture of histamine H₁ and dopamine D₁ receptors, anti- β_2 adrenergic receptor antibodies (to block nonspecific sites introduced by bound receptor-membrane complexes), anti-histamine H₁ receptor primary antibodies, AlexaFluor 488 secondary antibodies, anti-dopamine D₁ receptor primary antibodies, and AlexaFluor 546 secondary antibodies. In **(A)**, the substrate was imaged at 519 nm to visualize secondary antibodies bound to anti-H₁ receptor primary antibodies, which bind to H₁ receptors. In **(B)**, the substrate was imaged at 573 nm to visualize secondary antibodies bound to anti-D₁ receptor primary antibodies, which recognize D₁ receptors. **(C,D)** The other half of the substrate was challenged with nontransfected CHO-K1 cell membranes, anti- β_2 adrenergic receptor antibodies, both primary antibodies, and both secondary antibodies. Low fluorescence intensity was detected in **(C)** and **(D)**, indicating some nonspecific binding of primary and *secondary* antibodies in the absence of H₁ and D₁ receptors. Left lanes: *L*-histidine (*L*-HD); middle lanes: blank (absence of surface-tethered ligands); right lanes: *L*-3,4-dihydroxyphenylalanine (*L*-DOPA). Scale bars are 50 μ m. The substrate shown in **(A,B)** is the same as depicted in fig. 3-4.

Table 3-S1. Visualization strategy for antibody binding to tethered neurotransmitters

Surface-Bound Ligands	Primary Antibodies	Secondary Antibodies
Norepinephrine (NE)	Rabbit polyclonal anti-noradrenaline	AlexaFluor [®] 488 goat anti-rabbit IgG
Histamine (HA)	Mouse monoclonal anti-histamine	AlexaFluor [®] 350 goat anti-mouse IgG

Table 3-S2. Visualization strategy for GPCR binding to tethered neurotransmitter precursors

Surface-Bound Ligands	Receptors	Primary Antibodies	Secondary Antibodies
<i>L</i> -histidine (<i>L</i> -HD)	Human histamine H ₁	Rabbit polyclonal anti-histamine H ₁ receptor	AlexaFluor [®] 488 goat anti-rabbit IgG
<i>L</i> -3,4-dihydroxyphenylalanine (<i>L</i> -DOPA)	Human dopamine D ₁	Mouse monoclonal anti-dopamine D ₁ receptor	AlexaFluor [®] 546 goat anti-mouse IgG
<i>L</i> -5-hydroxytryptophan (<i>L</i> -5-HTP)	N/A	N/A	N/A

3.7 References

1. Granier, S.; Kobilka, B. A New Era of GPCR Structural and Chemical Biology. *Nat. Chem. Biol.* **2012**, *8*, 670–673.
2. Jean-Alphonse, F.; Hanyaloglu, A. C. Regulation of GPCR Signal Networks via Membrane Trafficking. *Mol. Cell. Endocrinol.* **2011**, *331*, 205–214.
3. Wettschureck, N.; Offermanns, S. Mammalian G Proteins and Their Cell Type Specific Functions. *Physiol. Rev.* **2005**, *85*, 1159–1204.
4. Catapano, L. A.; Manji, H. K. G Protein-Coupled Receptors in Major Psychiatric Disorders. *Biochim. Biophys. Acta* **2007**, *1768*, 976–993.
5. Thathiah, A.; De Strooper, B. The Role of G Protein-Coupled Receptors in the Pathology of Alzheimer's Disease. *Nat. Rev. Neurosci.* **2011**, *12*, 73–87.
6. Gainetdinov, R. R.; Premont, R. T.; Bohn, L. M.; Lefkowitz, R. J.; Caron, M. G. Desensitization of G Protein-Coupled Receptors and Neuronal Functions. *Annu. Rev. Neurosci.* **2004**, *27*, 107–144.
7. Wise, A.; Gearing, K.; Rees, S. Target Validation of G-Protein Coupled Receptors. *Drug Discovery Today* **2002**, *7*, 235–246.
8. Overington, J. P.; Al-Lazikani, B.; Hopkins, A. L. How Many Drug Targets Are There? *Nat. Rev. Drug Discovery* **2006**, *5*, 993–996.
9. Eglen, R. M.; Reisine, T. New Insights into GPCR Function: Implications for HTS. *Methods Mol. Biol.* **2009**, *552*, 1–13.
10. Dencker, D.; Thomsen, M.; Wörtwein, G.; Weikop, P.; Cui, Y.; Jeon, J.; Wess, J.; Fink-Jensen, A. Muscarinic Acetylcholine Receptor Subtypes as Potential Drug Targets for the

- Treatment of Schizophrenia, Drug Abuse, and Parkinson's Disease. *ACS Chem. Neurosci.* **2011**, *3*, 80–89.
11. Wang, C.; Jiang, Y.; Ma, J.; Wu, H.; Wacker, D.; Katritch, V.; Han, G. W.; Liu, W.; Huang, X.-P.; Vardy, E.; McCorvy, J. D.; Gao, X.; Zhou, X. E.; Melcher, K.; Zhang, C.; Bai, F.; Yang, H.; Yang, L.; Jiang, H.; Roth, B. L.; Cherezov, V.; Stevens, R. C.; Xu, H. E. Structural Basis for Molecular Recognition at Serotonin Receptors. *Science* **2013**, *340*, 610–614.
 12. Wacker, D.; Wang, C.; Katritch, V.; Han, G. W.; Huang, X.-P.; Vardy, E.; McCorvy, J. D.; Jiang, Y.; Chu, M.; Siu, F. Y.; Liu, W.; Xu, H. E.; Cherezov, V.; Roth, B. L.; Stevens, R. C. Structural Features for Functional Selectivity at Serotonin Receptors. *Science* **2013**, *340*, 615–619.
 13. Hulme, E. C.; Trevethick, M. A. Ligand Binding Assays at Equilibrium: Validation and Interpretation. *Br. J. Pharmacol.* **2010**, *161*, 1219–1237.
 14. Bylund, D. B.; Toews, M. L. Radioligand Binding Methods for Membrane Preparations and Intact Cells. *Methods Mol. Biol.* **2011**, *746*, 135–164.
 15. Takakura, H.; Hattori, M.; Takeuchi, M.; Ozawa, T. Visualization and Quantitative Analysis of G Protein-Coupled Receptor-Beta-Arrestin Interaction in Single Cells and Specific Organs of Living Mice Using Split Luciferase Complementation. *ACS Chem. Biol.* **2012**, *7*, 901–910.
 16. Glickman, J. F.; Schmid, A.; Ferrand, S. Scintillation Proximity Assays in High-Throughput Screening. *Assay Drug Dev. Technol.* **2008**, *6*, 433–455.

17. Fang, Y.; Peng, J.; Ferrie, A. M.; Burkhalter, R. S. Air-Stable G-Protein-Coupled Receptor Microarrays and Ligand Binding Characteristics. *Anal. Chem.* **2006**, *78*, 149–155.
18. Hong, Y.; Webb, B. L.; Su, H.; Mozdy, E. J.; Fang, Y.; Wu, Q.; Liu, L.; Beck, J.; Ferrie, A. M.; Raghavan, S.; Mauro, J.; Carre, A.; Müller, D.; Lai, F.; Rasnow, B.; Johnson, M.; Min, H.; Salon, J.; Lahiri, J. Functional GPCR Microarrays. *J. Am. Chem. Soc.* **2005**, *127*, 15350–15351.
19. Navratilova, I.; Besnard, J.; Hopkins, A. L. Screening for GPCR Ligands Using Surface Plasmon Resonance. *ACS Med. Chem. Lett.* **2011**, *2*, 549–554.
20. Neumann, L.; Wohland, T.; Whelan, R. J.; Zare, R. N.; Kobilka, B. K. Functional Immobilization of a Ligand-Activated G-Protein-Coupled Receptor. *ChemBioChem* **2002**, *3*, 993–998.
21. Kirilovsky, J.; Steiner-Mordoch, S.; Selinger, Z.; Schramm, M. Lipid Requirements for Reconstitution of the Delipidated Beta-Adrenergic Receptor and the Regulatory Protein. *FEBS Lett.* **1985**, *183*, 75–80.
22. Bally, M.; Bailey, K.; Sugihara, K.; Grieshaber, D.; Voros, J.; Stadler, B. Liposome and Lipid Bilayer Arrays Towards Biosensing Applications. *Small* **2010**, *6*, 2481–2497.
23. Fruh, V.; IJzerman, A. P.; Siegal, G. How to Catch a Membrane Protein in Action: A Review of Functional Membrane Protein Immobilization Strategies and Their Applications. *Chem. Rev.* **2011**, *111*, 640–656.
24. MacBeath, G.; Koehler, A. N.; Schreiber, S. L. Printing Small Molecules as Microarrays and Detecting Protein–Ligand Interactions en Masse. *J. Am. Chem. Soc.* **1999**, *121*, 7967–7968.

25. Vegas, A. J.; Fuller, J. H.; Koehler, A. N. Small-Molecule Microarrays as Tools in Ligand Discovery. *Chem. Soc. Rev.* **2008**, *37*, 1385–1394.
26. Vaish, A.; Shuster, M. J.; Cheunkar, S.; Singh, Y. S.; Weiss, P. S.; Andrews, A. M. Native Serotonin Membrane Receptors Recognize 5-Hydroxytryptophan-Functionalized Substrates: Enabling Small-Molecule Recognition. *ACS Chem. Neurosci.* **2010**, *1*, 495–504.
27. Seeber, M.; De Benedetti, P. G.; Fanelli, F. Molecular Dynamics Simulations of the Ligand-Induced Chemical Information Transfer in the 5-HT_{1A} Receptor. *J. Chem. Inf. Comput. Sci.* **2003**, *43*, 1520–1531.
28. Congreve, M.; Langmead, C. J.; Mason, J. S.; Marshall, F. H. Progress in Structure Based Drug Design for G-Protein-Coupled Receptors. *J. Med. Chem.* **2011**, *54*, 4283–4311.
29. Vaish, A.; Shuster, M. J.; Cheunkar, S.; Weiss, P. S.; Andrews, A. M. Tuning Stamp Surface Energy for Soft Lithography of Polar Molecules to Fabricate Bioactive Small-Molecule Microarrays. *Small* **2011**, *7*, 1471–1479.
30. Mullen, T. J.; Srinivasan, C.; Hohman, J. N.; Gillmor, S. D.; Shuster, M. J.; Horn, M. W.; Andrews, A. M.; Weiss, P. S. Microcontact Insertion Printing. *Appl. Phys. Lett.* **2007**, *90*, 063114.
31. Shuster, M. J.; Vaish, A.; Cao, H. H.; Guttentag, A. I.; McManigle, J. E.; Gibb, A. L.; Martinez, M. M.; Nezarati, R. M.; Hinds, J. M.; Liao, W.-S.; Weiss, P. S.; Andrews, A. M. Patterning Small-Molecule Biocapture Surfaces: Microcontact Insertion Printing vs. Photolithography. *Chem. Commun.* **2011**, *47*, 10641–10643.
32. Fang, Y.; Frutos, A. G.; Lahiri, J. Membrane Protein Microarrays. *J. Am. Chem. Soc.* **2002**, *124*, 2394–2395.

33. Vaish, A.; Liao, W. S.; Shuster, M. J.; Hinds, J. M.; Weiss, P. S.; Andrews, A. M. Thin Gold Film-Assisted Fluorescence Spectroscopy for Biomolecule Sensing. *Anal. Chem.* **2011**, *83*, 7451–7456.
34. Lahiri, J.; Isaacs, L.; Tien, J.; Whitesides, G. M. A Strategy for the Generation of Surfaces Presenting Ligands for Studies of Binding Based on an Active Ester as a Common Reactive Intermediate: A Surface Plasmon Resonance Study. *Anal. Chem.* **1999**, *71*, 777–790.
35. Shuster, M. J.; Vaish, A.; Szapacs, M. E.; Anderson, M. E.; Weiss, P. S.; Andrews, A. M. Biospecific Recognition of Tethered Small Molecules Diluted in Self-Assembled Monolayers. *Adv. Mater.* **2008**, *20*, 164–167.
36. Grumbach, I. M.; Veh, R. W. Sulpho-*N*-hydroxysuccinimide Activated Long Chain Biotin. A New Microtitre Plate Assay for the Determination of Its Stability at Different pH Values and Its Reaction Rate with Protein Bound Amino Groups. *J. Immunol. Methods* **1991**, *140*, 205–210.
37. Nojima, Y.; Iguchi, K.; Suzuki, Y.; Sato, A. The pH-Dependent Formation of PEGylated Bovine Lactoferrin by Branched Polyethylene Glycol (PEG)-*N*-Hydroxysuccinimide (NHS) Active Esters. *Biol. Pharm. Bull.* **2009**, *32*, 523–526.
38. Schoneberg, T.; Schulz, A.; Gudermann, T. The Structural Basis of G-Protein-Coupled Receptor Function and Dysfunction in Human Diseases. *Rev. Physiol. Biochem. Pharmacol.* **2002**, *144*, 143–227.
39. Civelli, O.; Saito, Y.; Wang, Z.; Nothacker, H. P.; Reinscheid, R. K. Orphan GPCRs and Their Ligands. *Pharmacol. Ther.* **2006**, *110*, 525–532.

40. Pestourie, C.; Tavitian, B.; Duconge, F. Aptamers against Extracellular Targets for *in Vivo* Applications. *Biochimie* **2005**, *87*, 921–930.
41. Zhang, Y.; Wang, Z.; Parks, G. S.; Civelli, O. Novel Neuropeptides as Ligands of Orphan G Protein-Coupled Receptors. *Curr. Pharm. Des.* **2011**, *17*, 2626–2631.
42. Alivisatos, A. P. C., M.; Church, G. M.; Deisseroth, K.; Donoghue, J. P.; Greenspan, R. J.; McEuen, P. L.; Roukes, M. L.; Sejnowski, T. J.; Weiss, P. S.; Yuste, R. The Brain Activity Map. *Science* **2013**, *339*, 1284–1285.
43. Alivisatos, A. P.; Andrews, A. M.; Boyden, E. S.; Chun, M.; Church, G. M.; Deisseroth, K.; Donoghue, J. P.; Fraser, S. E.; Lippincott-Schwartz, J.; Looger, L. L.; Masmanidis, S.; McEuen, P. L.; Nurmikko, A. V.; Park, H.; Peterka, D. S.; Reid, C.; Roukes, M. L.; Scherer, A.; Schnitzer, M.; Sejnowski, T. J.; Shepard, K. L.; Tsao, D.; Turrigiano, G.; Weiss, P. S.; Xu, C.; Yuste, R.; Zhuang, X. W. Nanotools for Neuroscience and Brain Activity Mapping. *ACS Nano* **2013**, *7*, 1850–1866.

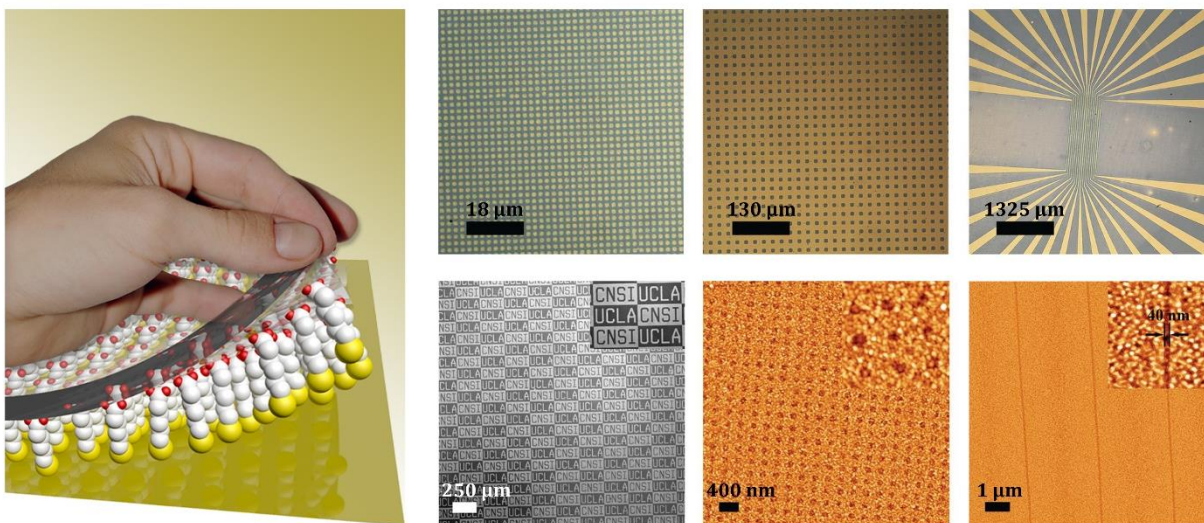
Chapter 4

Subtractive Patterning *via* Chemical Lift-Off Lithography

The information in this chapter was published in *Science* **2012**, 337, 1517-1521

and has been reproduced here in its entirety.

Authors: Liao, W.-S.; Cheunkar, S.; Cao, H. H.; Bednar, H.; Andrews, A. M.; Weiss, P. S.



4.1 Abstract

Conventional soft-lithography methods involving the transfer of molecular “inks” from polymeric stamps to substrates often encounter micrometer-scale resolution limits due to diffusion of the transferred molecules during printing. We report a “subtractive” stamping process in which silicone rubber stamps, activated by oxygen plasma, selectively remove hydroxyl-terminated alkanethiols from SAMs on Au surfaces with high pattern fidelity. The covalent interactions formed at the stamp-substrate interface are sufficiently strong to remove not only alkanethiol molecules but also Au atoms from the substrate. A variety of high-resolution patterned features were fabricated, and stamps were cleaned and reused many times without feature deterioration. The remaining SAM acted as a resist for etching exposed Au features. Monolayer backfilling into the lifted-off areas enabled patterned protein capture, and 40-nanometer chemical patterns were achieved.

4.2 Introduction

High-throughput molecular printing strategies with high feature resolution are central goals for lithography. However, progress has been impeded by the conflicting aims of large-area fabrication versus precision, and of convenience versus cost.¹⁻⁴ For instance, although photolithography enables patterning over large areas (centimeters), the prototyping process is time-consuming and resolution is restricted by light diffraction.¹⁻³ Patterning by electron beam lithography (EBL) or scanning probe lithography (SPL) techniques, such as dip-pen nanolithography, nanoshaving, and nanografting,⁵⁻⁷ produces high-resolution features (<10 nm and <100 nm for EBL and SPL, respectively),¹⁻³ but throughput is limited by serial processing speeds.

Soft-lithography strategies produce patterns over large areas at the micro- and nanoscales.^{1,3,4,8-10} Commercial polymers (such as, PDMS) are used as molds for pattern transfer *via* contact printing. The bas-relief pattern on a master mold is fabricated by photolithography for large-area patterning or EBL for high-resolution patterning.^{1,3} Once the master is generated, patterned features are negatively transferred to PDMS stamps, which are then “inked” with organic molecules, proteins, nanoparticles, or DNA.^{1,10-16}

Among the materials transferred, organic molecules such as alkanethiols and other related molecules, which form SAMs on Au substrates, can be readily subjected to chemical modification at the exposed terminal groups for capturing biomolecules.^{1,16-18} Moreover, SAMs serve as “molecular resists” against different wet etchants, enabling patterns to be transferred reproducibly to underlying substrates.¹⁹ However, the success of contact printing and related soft-lithography techniques is also limited by the chemistries and compatibility of the inks, stamps, and substrates.^{1,3,4} For example, lateral diffusion and gas-phase deposition of ink

molecules tend to reduce pattern fidelity,^{20,21} creating a resolution limit of ~100 nm for alkanethiols on Au.

To overcome the limitations of stamp feature replication in soft lithography, the general principles of contact printing must be modified to achieve sharp, stable, and reproducible chemical features on substrates.^{7,19,22,23} We transformed the conventional contact printing process such that the polymer stamp is activated and then used to lift off a preformed SAM resist. A strong contact-induced interaction at the stamp-SAM interface enables the transfer of sharp stamp features by mechanical desorption of resist only in the areas of stamp-substrate contact. The subtractive nature of this process precisely replicates features from the master mold.^{9,24} This approach, chemical lift-off patterning, facilitates the addition of different molecules into the lift-off areas to produce multicomponent patterned SAMs. It also enables the intact areas to act as an etch resist for the transfer of features to the underlying substrate. Moreover, stamps used for CLL can be cleaned and reused many times without deterioration.

4.3 Materials and Methods

Materials. Hydroxyl-terminated tri(ethylene glycol)undecanethiol (TEG) was purchased from Toronto Research Chemicals Inc., Canada. Biotin-terminated hexa(ethylene glycol)undecanethiol was purchased from Nanoscience Instruments Inc. (Phoenix, AZ). Methoxy-terminated tri(ethylene glycol)undecanethiol was purchased from Prochimia (Poland). Hydroxyl-terminated undecanethiol, methyl-terminated undecanethiol, iron nitrate, thiourea, and bovine serum albumin (BSA) were purchased from Sigma-Aldrich (St. Louis, MO). Streptavidin was purchased from Invitrogen Inc. (Carlsbad, CA). Anti-streptavidin antibody conjugated to fluorescein isothiocyanate (FITC) was purchased from Abcam Inc. (Cambridge, MA).

Chemical Lift-Off Process. Substrates consisted of 30-nm-thick Au evaporated on Si with a 5-nm Ti/Cr adhesion layer (Platypus, Madison, WI). Alkanethiols with different terminal groups were used to form SAMs on Au surfaces *via* incubation in 1 mM ethanolic solutions at room temperature for 18 h, except where noted. Polydimethylsiloxane stamps of different geometries were formed using standard photolithography-fabricated masters. A 10:1 mass ratio of SYLGARD[®] 184 silicone elastomer base and curing agent (Ellsworth Adhesives, Germantown, WI) was mixed thoroughly, degassed under vacuum, and cured at 60 °C overnight.^{17,18,47}

Stamps were activated by 30-s exposure to oxygen plasma (Harrick Plasma, Ithaca, NY) at a power of 18 W and an oxygen pressure of 10 psi to yield a fully hydrophilic reactive surface.^{17,25-27} Thereafter, stamps and SAM-modified substrates were brought into conformal contact for 5 min. Stamps were then carefully peeled away from substrates with stamp features transferred to the substrates. After lift-off, stamps were cleaned by wiping with lab tissues soaked in ethanol, additional rinsing with ethanol, and drying under nitrogen gas. Cleaned stamps

were sealed against clean glass slides for storage before additional patterning. Self-assembled monolayers and Au topographic features were characterized by tapping mode AFM (Dimension 5000, Bruker AXS, Santa Barbara, CA). Topographic AFM images were collected using Si cantilevers with a spring constant of 280 kHz (Veeco Instruments, Santa Barbara, CA). Bright-field optical images were obtained with an upright digital Nikon LV150 microscope (Nikon Instruments Inc., Melville, NY).

Biotin-Streptavidin Recognition Arrays. Biotinylated patterns were created by lifting off areas of initial hydroxyl-terminated tri(ethylene glycol)alkanethiol (TEG) SAMs to expose the Au substrates underneath, as described in fig. 4-1. Substrates were then exposed to a 90:10 molar ratio of TEG and biotin-terminated hexa(ethylene glycol)alkanethiol in ethanol for 18 h. Before streptavidin incubation, patterned substrates were exposed to 10 mg/mL BSA for 5 min to reduce nonspecific protein adsorption on biotinylated substrates.¹⁸ Patterned surfaces were incubated with 50 μ g/mL streptavidin for 20 min followed by 10 μ g/mL FITC-conjugated anti-streptavidin antibody for 20 min. Substrates were rinsed with deionized water between steps. Visualization of bound fluorophores was carried out using an inverted fluorescence microscope (Carl Zeiss MicroImaging, Inc., Thornwood, NY) with a fluorescence filter set (38 HE/high efficiency) having excitation and emission wavelengths at 470 ± 20 nm and 525 ± 25 nm, respectively.

Sub-100-nm features were created using the same lift-off process described above. As illustrated in fig. 4-4B, areas of pre-existing TEG SAM, which were in conformal contact with a PDMS stamp having 90 ± 5 -nm-diameter holes, were lifted off to expose the Au substrate underneath. The patterned substrates were then backfilled with 100% biotin-terminated alkanethiol for 1 h. Forty-nm features were achieved in the same manner using a PDMS stamp with 40 ± 2 nm channels. As shown in fig. 4-4C, bright fluorescent areas, representing biotin-

streptavidin, are separated by 40-nm lines representing areas of the original TEG SAM that were not lifted off. For double lift-off processing, the PDMS stamp was brought into conformal contact a second time but was shifted relative to its original contact position in the initial lift-off step (fig. 4-4D). Any TEG areas in the overlapping regions between hole features from the first and second lift-off steps remained intact, while TEG areas lying outside the overlapping hole regions were removed. The patterned surfaces were then backfilled with 100% biotin-terminated alkanethiol (fig. 4-4E). Patterned surfaces were incubated with 50 $\mu\text{g}/\text{mL}$ streptavidin for 30 min, rinsed with deionized water, and dried under nitrogen gas before AFM imaging.

Wet Chemical Etching. An aqueous solution of 20 mM iron nitrate and 30 mM thiourea was applied to post-lift-off substrates for 20 min to carry out selective wet etching of the exposed substrate areas after chemical lift-off lithography.¹⁹ Substrates were cleaned with deionized water and dried with nitrogen gas prior to imaging.

X-Ray Photoelectron Spectroscopy. All XPS data were collected using an AXIS Ultra DLD instrument (Kratos Analytical Inc., Chestnut Ridge, NY). A monochromatic Al K_{α} X-ray source (20 mA, 14 kV) with a 200 μm circular spot size and ultrahigh vacuum (10^{-9} torr) were used in all XPS experiments.¹⁷ Spectra were acquired at a pass energy of 80 mV for survey spectra and 20 mV for high resolution spectra of C 1s, S 2p, O 1s, and Au 4f regions using a 200 ms dwell time. Different numbers of scans were carried out depending on the difficulty of identifying each peak from background, ranging from 20 scans for C 1s to 100 for Au 4f.

Polydimethylsiloxane is an insulator; thus, a charge neutralizer (flood gun) was used to obtain signals. This has the effect of shifting peaks slightly from their expected regions (for C 1s this is 4-5 eV lower than the reference). Due to the small number of peaks and their separation, peak shifting did not affect identification. Peaks of interest had strong signals post-optimization.

No corrections were carried out during data collection to shift peaks back to particular regions or to scale peaks based on reference locations.

4.4 Results and Discussions

4.4.1 Chemical Nature of the Lift-Off Process

Alkanethiols with different terminal groups (Table 4-1) were used to form SAMs on Au-coated Si substrates. Soft-lithography stamps were created from PDMS to transfer features of different geometries from master molds (fabricated by standard photolithography and EBL techniques) to the molecular-resist layers.^{1,8,10} The CLL process is outlined schematically in Fig. 4-1. A PDMS stamp was first activated by exposure to oxygen plasma, yielding a fully hydrophilic and reactive surface.^{17,25-27} The stamp and SAM-modified substrate were then brought into conformal contact. The stamp was peeled away from the substrate, which removed resist molecules selectively in the areas contacted by the stamp, transferring stamp features with high resolution to the substrate.

On the basis of earlier work, we hypothesized that the Au-Au bonds in the substrate metal lattice, rather than the Au-S bonds between the substrate and alkanethiol, are preferentially broken during lift-off. The breaking of Au-Au bonds during SAM desorption has been a particular subject of controversy.^{6,28-32} The mobility of Au thiolates within SAMs^{29,33,34} indicates

Table 4-1. Alkanethiol molecules and terminal groups used in chemical lift-off

Alkanethiol	Chemical Formula
Hydroxyl-terminated tri(ethylene glycol)undecanethiol (TEG)	HS-(CH ₂) ₁₁ -(C ₂ H ₄ O ₃)-OH
Biotin-terminated hexa(ethylene glycol)undecanethiol	HS-(CH ₂) ₁₁ -(C ₂ H ₄ O) ₆ -NH-C ₁₀ H ₁₅ O ₂ N ₂ S
Hydroxyl-terminated undecanethiol	HS-(CH ₂) ₁₁ -OH
Methyl-terminated undecanethiol	HS-(CH ₂) ₁₁ -CH ₃
Methoxy-terminated tri(ethylene glycol)undecanethiol	HS-(CH ₂) ₁₁ -(C ₂ H ₄ O) ₃ -O-CH ₃

that weak Au-Au bonds are present at the substrate surface. Furthermore, recent studies show the presence of Au adatoms beneath SAMs, which leads to facile Au-Au bond breakage because of reduced coordination of the adatoms.³⁵⁻³⁸ We made a featureless, oxygen plasma-treated PDMS stamp and brought it into contact with a hydroxyl-terminated SAM-coated Au surface. After lift-off, a peak indicating the presence of Au was observed on the PDMS stamp surface by X-ray photoelectron spectroscopy (XPS; see spectra in fig. 4-S1). This finding is consistent with Au being removed from the underlying substrate.³⁹

The presence of Au on oxygen plasma-treated PDMS surfaces after chemical lift-off led us to propose that a contact-induced chemical reaction between the hydrophilic stamp surface and the molecular-resist layer results in Au-Au bond rupture during stamp removal. Studies have shown that oxygen plasma treatment yields siloxyl groups on PDMS stamp surfaces, which facilitate condensation reactions between Si-OH and hydroxyl groups on different oxides, such as Au, Ti, and Si to form Si-O-Au, Si-O-Ti, and Si-O-Si linkages, respectively.^{9,24,40-42} We anticipated that the same type of linkage (Si-O-SAM) would be established between Si-OH groups on oxygen plasma-treated PDMS stamp surfaces and hydroxyl-terminated groups on SAMs.

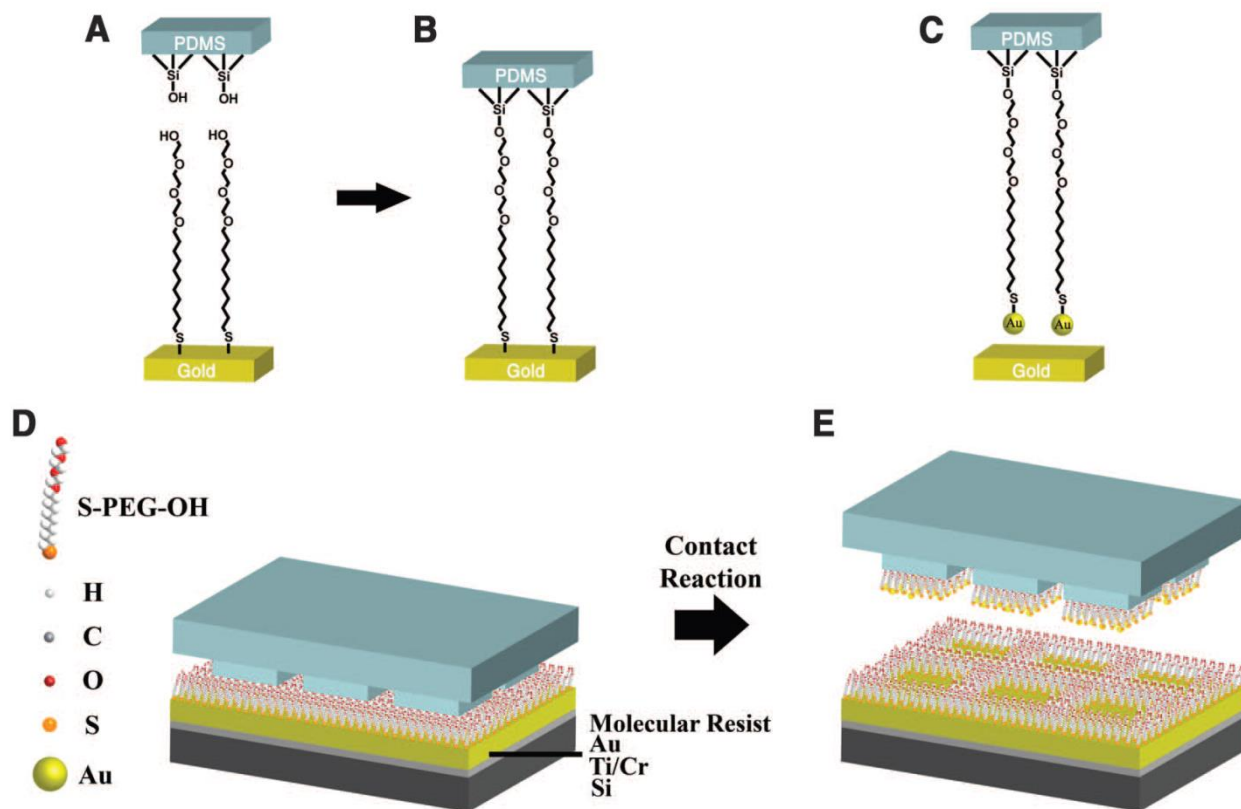


Figure 4-1. Schematic illustration of the molecular-resist lift-off process. (A) A polydimethylsiloxane (PDMS) stamp is activated by oxygen plasma treatment, producing hydrophilic siloxyl groups. (B) A surface-induced contact reaction is implemented *via* close contact between the stamp and hydroxyl-terminated molecules self-assembled on an Au substrate. (C) Stamp removal lifts off resist molecules and underlying Au. (D) In chemical lift-off lithography (CLL), a patterned PDMS stamp is brought into conformal contact with a self-assembled molecular resist. (E) Lift-off is limited to the stamp-contact regions.

To investigate the roles of the molecular resist tail groups in the CLL process, we assembled two different hydroxyl-terminated alkanethiol molecules, with and without oligo(ethylene glycol), as molecular resist monolayers (Table 4-1). Both provided good transfer of stamp features to SAM-coated Au substrates (Fig. 4-2 and Fig. 4-S5A). In contrast, when methoxy- or methyl-terminated alkanethiol molecules (Table 4-1) were tested under the same assembly and lift-off conditions, no detectable transfer of stamp features was found on SAM-coated Au surfaces (figs. 4-S5B and 4-S5C, respectively). Stamp features were not transferred when a hydrophilic PDMS stamp was used directly with a bare Au substrate (fig. 4-S5D). Thus, tail group reactivity dictates whether lift-off occurs *via* hydrophilic PDMS stamps.

Fourier-transform infrared reflection absorption spectroscopy (FT-IRRAS) was used to investigate the extent of lift-off occurring in a prototypical SAM. Spectral analysis indicated that

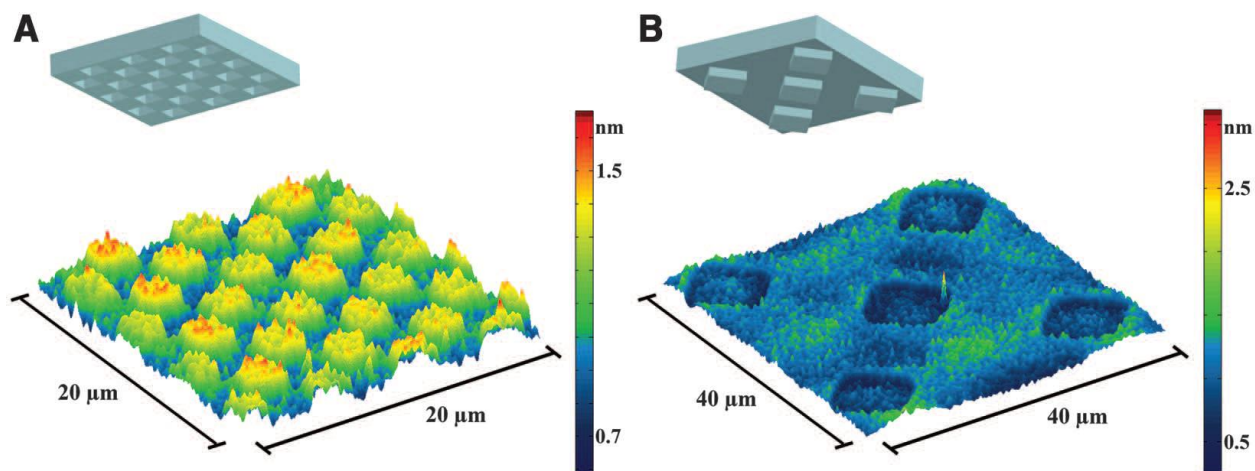


Figure 4-2. (A and B) Atomic force microscope topographic images of substrates patterned by CLL. Self-assembled monolayers of hydroxyl-terminated tri(ethylene glycol)alkanethiol on Au substrates were patterned using CLL and a PDMS stamp with depressed wells (**A**) ($2\ \mu\text{m} \times 2\ \mu\text{m}$) or a PDMS stamp with protruding posts (**B**) ($10\ \mu\text{m} \times 10\ \mu\text{m}$). Stamp geometries are illustrated above the images. Contact dwell time was 5 min. AFM topographical heights are shown in the scale bars to the right of each image.

75 to 80% of hydroxyl-terminated undecanethiol molecules are removed after the lift-off process (fig. 4-S6). Previous reactive patterning of hydrogen-bonding SAMs showed that this level of damage makes the SAM labile to complete displacement, and the hydrogen bonding in the intact areas prevents diffusion and thus pattern dissolution.⁴³ The terminal functionality of the initial SAM influences lift-off *via* the extent of the contact-induced reaction at the SAM-stamp interface. Lift-off from SAMs of hydroxyl-terminated TEG was sufficient to enable patterning of underlying substrates by wet etching and to produce patterned multicomponent SAMs capable of biorecognition (see below).

4.4.2 Patterning Alkanethiol Monolayers and Underlying Substrates with Chemical Lift-Off Lithography

Chemical patterns of TEG were characterized by atomic force microscopy (AFM) and bright-field optical microscopy, as shown in Figs. 4-2 and 4-3. Stamps with depressed well-like motifs or protruding posts were used to create different surface relief patterns. The stamp negative was produced in the resist, as molecules were removed (instead of added) by patterning. For example, islands of SAM resist remained when a stamp with a depressed relief was used; the areas surrounding the relief on the stamp contacted the SAM surface, and the molecular resist was removed in these areas during the lift-off step. The AFM topographic image in Fig. 4-2A illustrates the protruding SAM islands after patterning. By contrast, well-shaped features were observed on the substrate when a stamp with a protruding relief was used for patterning (Fig. 4-2B). In Fig. 4-2, AFM topography profiles indicate 2.0 ± 0.3 nm differences between lifted-off and unpatterned areas. The thickness of the TEG SAMs was 1.6 ± 0.1 nm by

ellipsometry. The difference can be accounted for by a single atomic layer of Au removed during the lift-off process.

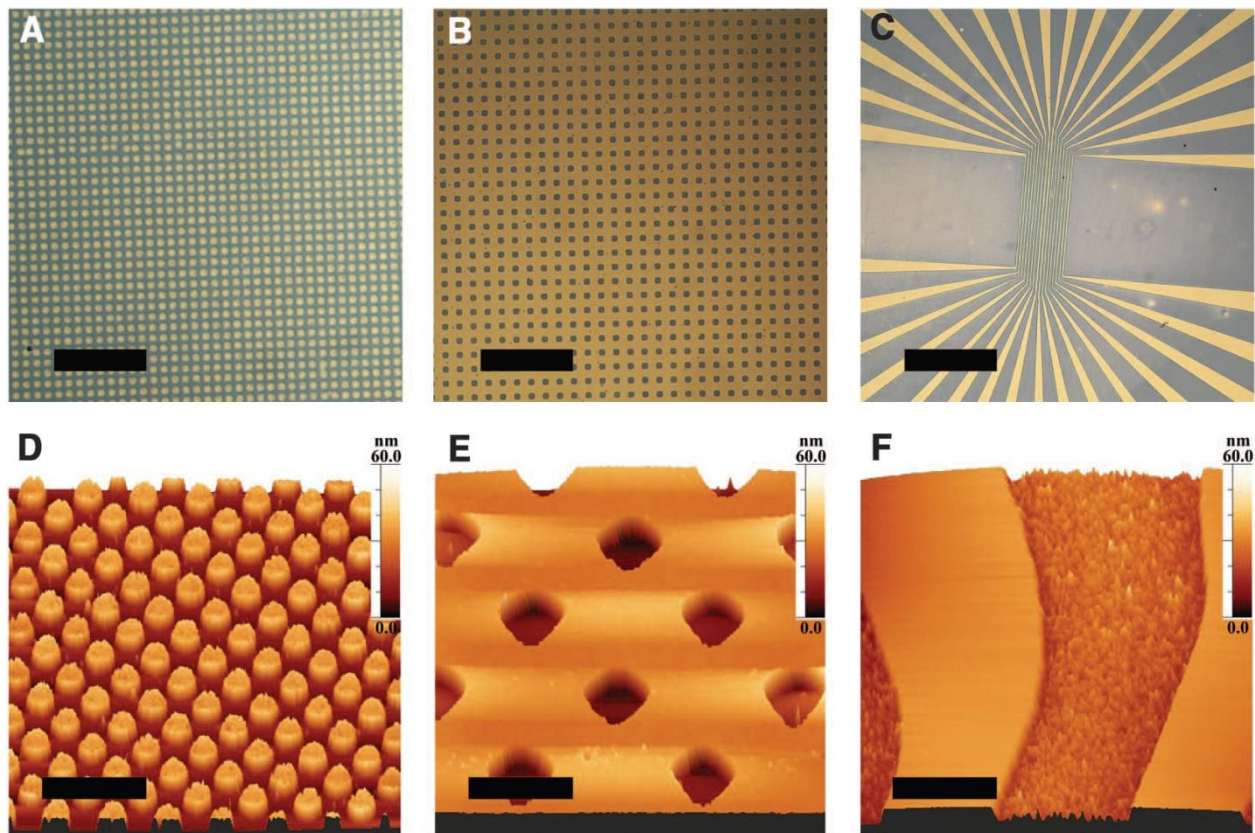


Figure 4-3. Patterning underlying Au substrates by CLL. Hydroxyl-terminated tri(ethylene glycol)undecanethiol was self-assembled on Au substrates. Lift-off lithography *via* activated PDMS stamps was used to produce a variety of patterns. Substrates were then chemically etched (Fe^{3+} /thiourea) to pattern the underlying metal by removing additional Au in the exposed regions. The SAM molecular resist was intact during imaging with bright-field microscopy and AFM. Patterns transferred by the molecular-resist lift-off process include (A and D) pillars, (B and E) wells, and (C and F) channels. Bright-field microscope images are shown in (A) to (C); corresponding AFM topography images are shown in (D) to (F). Scale bars, (A) 18 μm , (B) 130 μm , (C) 1325 μm , (D) 5 μm , (E) 15 μm , and (F) 17.5 μm . Atomic force microscopy topographical heights are shown in the upper right corners of (D) to (F).

We explored the use of the intact SAM areas as an unconventional resist to transfer patterns to the underlying material, Au, through selective wet chemical etching.^{19,44} Exposed areas of the Au surface were contacted by the etchant solution while the intact SAM molecular resist protected the remaining regions of Au. Etchant solutions removed exposed Au *via* oxidation by Fe³⁺, followed by complexation and dissolution of oxidized metal by thiourea.⁴⁵ A variety of patterns (inverse replicas of the PDMS stamp features) with features of different sizes were transferred, including lines, holes, and pillars (Fig. 4-3). The advantages of large patterning areas and high-fidelity features are apparent in the bright-field images (Fig. 4-3, A to C) and AFM topography images (Fig. 4-3, D to F), respectively. Differences in AFM heights indicate that features have been transferred to the level of the underlying substrate at a depth of 30 nm—the thickness of the original Au layer.

In addition to transferring patterns to SAMs and underlying Au substrates, CLL enables a SAM of a different composition to be assembled on the lift-off areas. Figure 4-4A shows a large-area, high-fidelity pattern of streptavidin binding to a biotinylated pattern created by lifting off areas of an initial TEG SAM to expose fresh Au substrate underneath. The substrate was then exposed to 90:10 TEG/biotin-terminated hexa(ethylene glycol)alkanethiol (Table 4-1) to produce a low-density biotinylated patterned SAM.^{17,18} Streptavidin was captured from solution by surface-tethered biotin. Bound streptavidin was detected by fluorescence microscopy of FITC-conjugated antibodies against streptavidin. The bright fluorescent regions in Fig. 4-4A and its inset display the lift-off areas where biotin-terminated alkanethiols were backfilled and used to capture streptavidin from solution. The dark regions display minimal fluorescence because of the absence of biotin-terminated alkanethiol and the resistance to nonspecific protein adsorption by TEG.^{17,46} The fabrication of biotin-streptavidin patterns demonstrates not only that CLL

transfers large-area, high-fidelity patterns to SAMs, but also that the Au areas exposed after lift-off are advantageous for producing multiplexed bioselective patterned surfaces.

4.4.3 Chemical Lift-Off Nanolithography and Multiple Lift-Off Process

To carry out nanometer-scale chemical patterning, we implemented the lift-off process for biotin-streptavidin described above, using a PDMS stamp with 90-nm well-like features (Fig. 4-4B). Areas surrounding the wells were lifted off and backfilled with biotin-terminated alkanethiol to capture streptavidin, whereas the areas inside the wells were not removed, producing TEG islands. In one method to achieve features smaller than 90 nm, a double lift-off strategy was used in which the PDMS stamp was twice brought into conformal contact with the substrate (Fig. 4-4E). The initial lift-off step removed the molecules in the areas surrounding the stamp wells, leaving the TEG SAM inside the wells intact. During the second lift-off step, the stamp was offset with respect to the first pattern. (This result was initially a serendipitous consequence of being unable to maintain exact registry between multiple stamping steps.) Additional areas of the TEG SAM were removed, depending on the amount of registration. The exposed Au surfaces resulting from both TEG removal steps were backfilled with biotin-terminated alkanethiol. Figure 4-4E illustrates decreasing registration associated with smaller feature sizes. The resulting intact TEG regions formed increasingly narrow marquis-shaped features with decreased spacing between biotin-streptavidin molecular recognition areas. Note that if conventional contact printing were used in this case, lateral diffusion of ink molecules would blur nanospaced features beyond detection by AFM.⁴⁷ In Fig. 4-4C, sharp features 40 ± 2 nm in width were directly fabricated using a stamp with 40-nm channels, indicating that we have not yet reached the resolution limit of the CLL method.

Exploring the effects of Au grain size will also be important for future mechanistic studies and possible further improvement of nanoscale feature resolution.

4.4.4 Investigating Molecular Diffusion Following Lift-Off and “Fast” Chemical Lift-Off

Lithography

Lateral diffusion of ink molecules, which occurs during increasing stamp contact times and/or molecular ink concentrations for additive printing methods on bare Au substrates, is avoided in CLL. Preformed well-ordered SAMs, strong intermolecular interactions between hydrophilic SAM molecules, and a diffusion barrier created by the Au step edges⁴⁸ formed during lift-off prevent pattern dissolution. Patterned TEG SAMs produced by CLL showed no discernable dissolution after 2 days under ambient storage conditions (fig. 4-S8). Furthermore, the backfilled multicomponent SAMs shown in Fig. 4-4 were produced by solution deposition of the second SAM component over 12 hours; sharp pattern features were produced even in this case, arguing against diffusion or dissolution of the original lift-off pattern.

We investigated the time needed for the contact-induced chemical reaction at the stamp-substrate interface by examining 1-min *versus* 5-min contact times between oxygen plasma-treated PDMS stamps and hydroxyl-terminated, alkanethiol-coated Au surfaces. Features were transferred even with 1-min contact times; however, shorter contact times resulted in poor features produced after wet etching. Additionally, pattern transfer was maintained with short SAM deposition times. Hydroxyl-terminated alkanethiol SAMs formed during 1 hour of deposition were found to provide good transfer of stamp features to Au substrates, comparable to transfer obtained from SAMs formed overnight. These findings demonstrate advantages associated with short contact and SAM formation times for facilitating robust, expeditious, and

high-throughput patterning by CLL. Ultimately, limits for SAM deposition and stamp contacts times will depend on the specific molecules used for SAM formation.

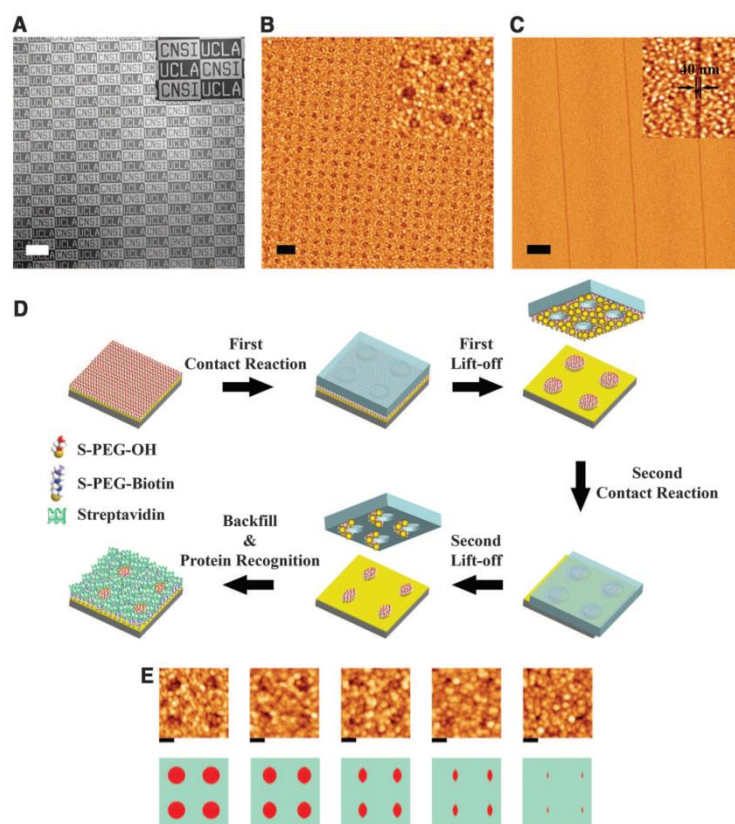


Figure 4-4. Large-area patterning of microscale and nanoscale features via CLL. (A) Tri(ethylene glycol)alkanethiol (TEG) self-assembled on an Au-coated substrate was subjected to the lift-off process using a PDMS stamp having “UCLA” characters as positive (protruding) features and “CNSI” characters as negative (depressed) features. After patterning, a new monolayer of 90% TEG/10% biotin-terminated oligo(ethylene glycol)alkanethiol (nominal solution ratio) was self-assembled on the exposed Au regions (“UCLA” characters and areas surrounding the “CNSI” characters). Bright areas indicate fluorescence associated with FITC-labeled anti-streptavidin antibody recognition of streptavidin bound to biotin. Dark areas display minimal fluorescence due to the protein-resistant characteristics of TEG. The fluorescent pattern is sharp and extends over a large substrate area ($>3 \text{ mm}^2$). Scale bar (main image), $250 \mu\text{m}$. (B) Au-coated substrates coated with TEG self-assembled monolayers were subjected to the lift-off process using a PDMS stamp with holes 90 nm in diameter. After patterning, a new monolayer of 100% biotin-terminated oligo(ethylene glycol)alkanethiol was self-assembled on the exposed Au regions (areas surrounding the resulting pillar features). Scale bar (main image), 400 nm. The inset shows a high-resolution AFM image of biospecific 90-nm circular features produced by CLL. (C) AFM images display biotin-streptavidin recognition areas separated by narrow line features. The inset shows a detailed AFM image of an individual line feature (width $40 \pm 2 \text{ nm}$) made using a stamp with 40-nm channels. Scale bar (main image), $1 \mu\text{m}$. (D) A PDMS stamp with holes 90 nm in diameter was brought into conformal contact once with a TEG SAM (upper left). In this case, substrates were stamped twice with decreasing registry (subsequent images from left to right). Patterned substrates were backfilled with biotin-terminated alkanethiol. (E) Topographic AFM images display decreasing feature sizes (from left to right): $90 \pm 5 \text{ nm}$, $80 \pm 3 \text{ nm}$, $50 \pm 2 \text{ nm}$, $30 \pm 3 \text{ nm}$, and $15 \pm 5 \text{ nm}$. Protruding (lighter) areas indicate biotin-streptavidin recognition. Shallow (darker) areas comprise intact TEG SAM. Scale bars are 100 nm.

4.5 Conclusions and Prospects

With this method, conventional nanolithographic patterning techniques such as photolithography and electron-beam lithography need only be used for the fabrication of stamp master molds. Once individual masters are produced, CLL can be implemented as a strategy for high-resolution, high-throughput, low-cost pattern fabrication. Because CLL enables patterns to be transferred to underlying substrates and can be used in a multiple-stamping strategy to produce patterns that are smaller than the actual stamp features, possible applications of CLL include the production of high-fidelity nanometer-scale patterns on Au substrates, as well as patterning of different materials such as Si, Ge, Pd, Pt, and graphene.

4.6 Supplementary Experiments and Figures

X-Ray Photoelectron Spectroscopy. The XPS spectra of PDMS stamps are shown in figs. 4-S1-S4. Figure 4-S1 shows Au 4f signature peaks at 78-86 eV indicating that layers of Au atoms were removed from the underlying substrate due to the contact reaction between an oxygen-plasma-treated stamp and a hydroxyl-terminated SAM on a Au surface. Figure 4-S3 obtained from oxygen plasma-treated PDMS in the absence of the contact reaction and lift-off processes displays no Au signature peaks, and serves as a background XPS spectrum. The XPS spectra of PDMS stamps without oxygen plasma treatment are shown in figs. 4-S2 and 4-S4. Figure 4-S2 indicates that removal of Au from the substrate was not detected when the lift-off process was carried out using a stamp that was not oxygen plasma treated and a hydroxyl-terminated SAM on the Au surface. Arguably, siloxyl groups might spontaneously form on the surface of PDMS stamps in the absence of oxygen plasma treatment. However, siloxyl groups are known to undergo rearrangement within the bulk PDMS and/or condensation such that oxygen plasma-treated stamps return to fully hydrophobic surfaces within a short period of time.⁴⁹ Thus, untreated stamps are not expected to have appreciable levels of siloxyl groups available for contact reactions. Figure 4-S4, which also displays no Au signature peaks, serves as a background XPS spectrum for the untreated PDMS alone in the absence of the lift-off process.

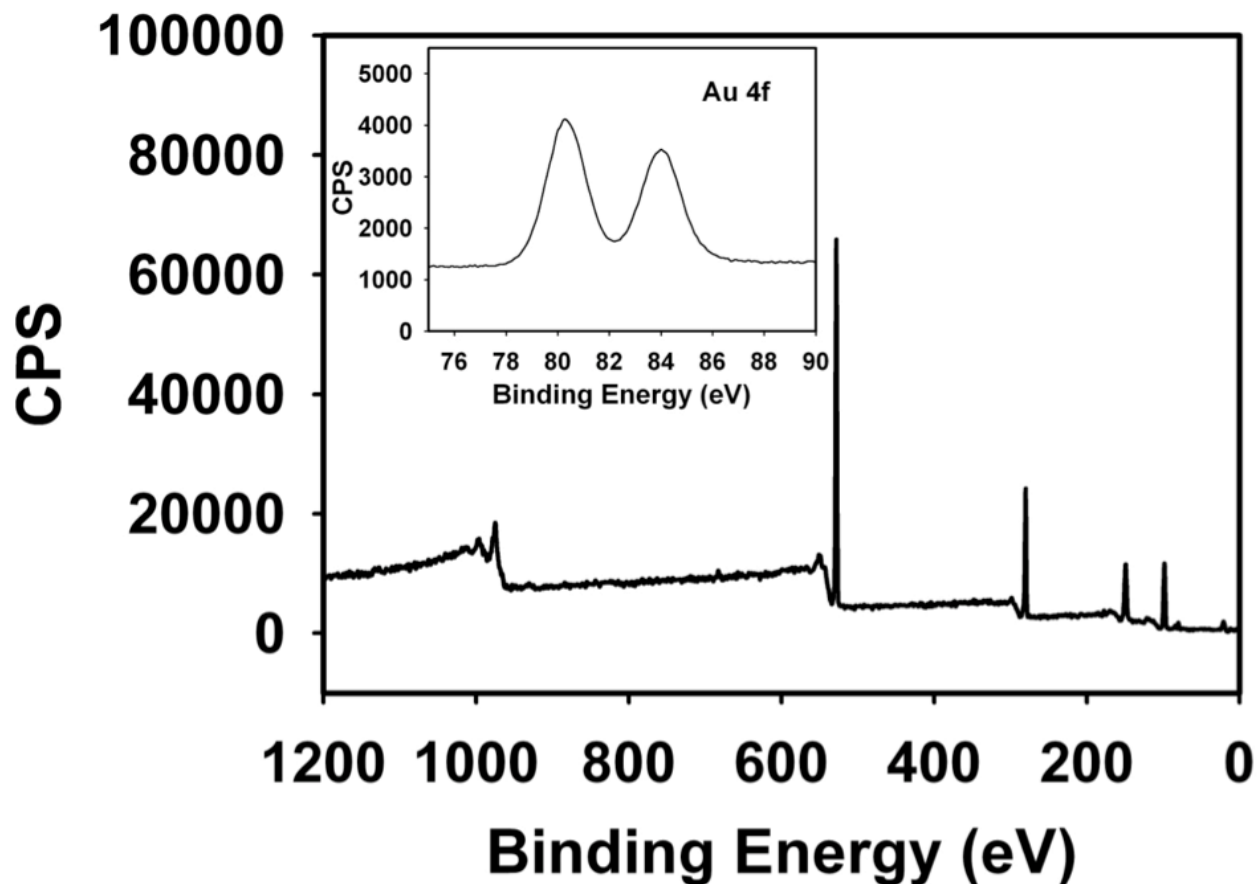


Figure 4-S1. X-ray photoelectron spectrum after lift-off from a hydroxyl-terminated SAM. An oxygen plasma-treated PDMS stamp was subjected to the contact reaction followed by the lift-off process. Peaks (Au 4f) indicate the presence of Au on the stamp surface after lift-off and are shown in the inset.

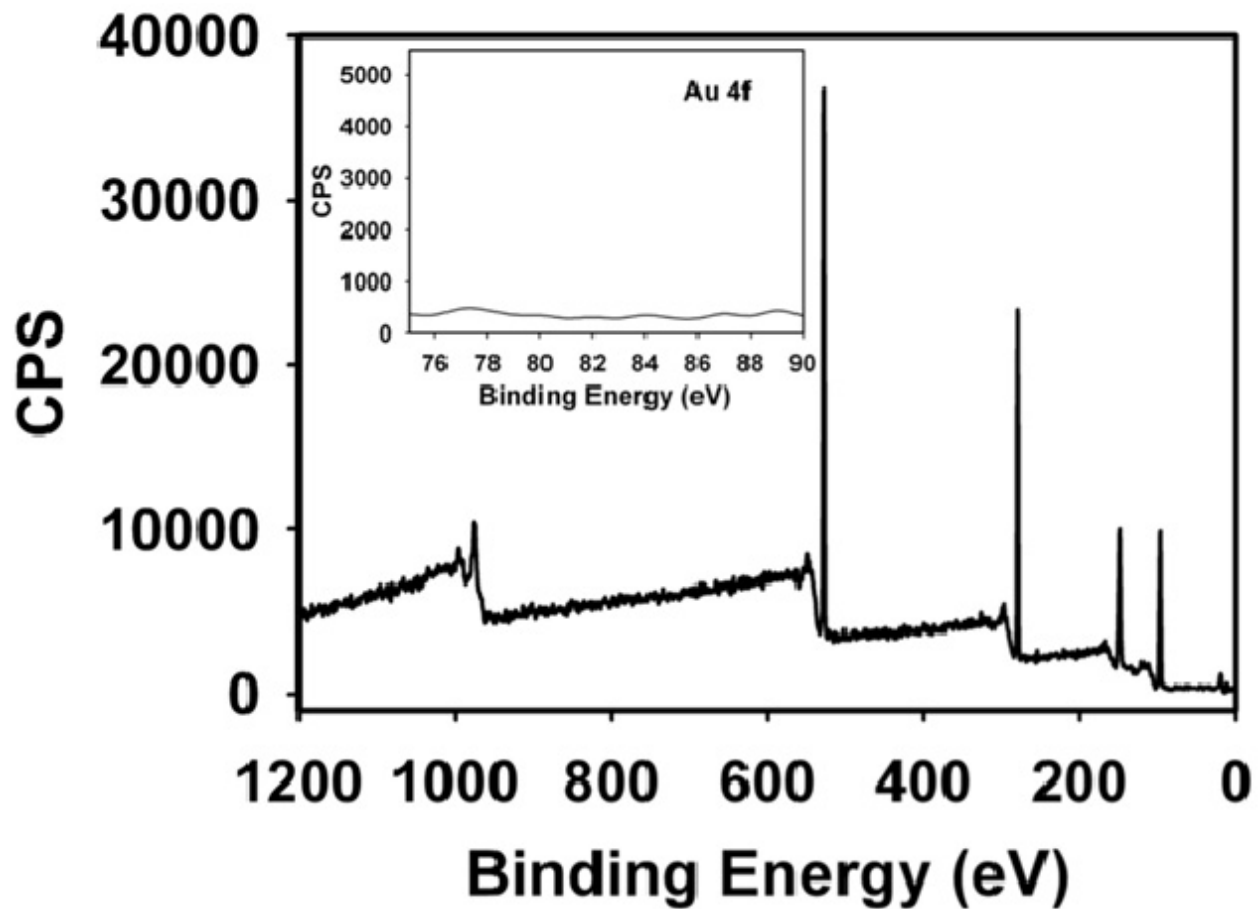


Figure 4-S2. Oxygen plasma treatment is necessary for lift-off. Here, a PDMS stamp was not treated with oxygen plasma prior to the contact reaction and lift-off processes. No Au 4f peaks are observed in the XPS spectrum, as shown in the inset, demonstrating that stamp activation is needed to observe lift-off of the molecular resist and removal of Au adatoms.

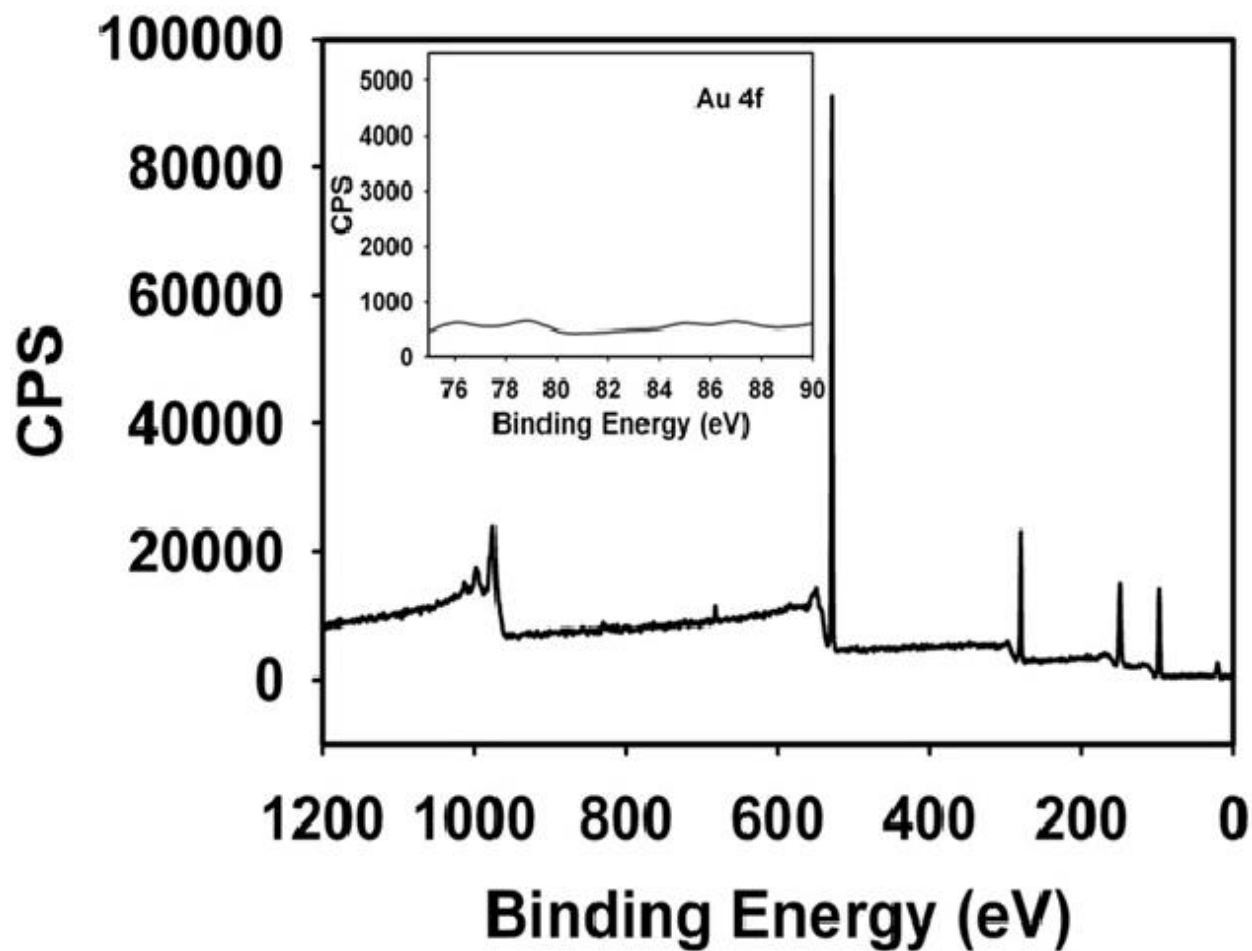


Figure 4-S3. X-ray photoelectron spectrum of a treated but unused PDMS stamp. A PDMS stamp was treated with oxygen plasma to make the surface fully hydrophilic, however, the stamp was not subjected to the contact reaction or lift-off processes. No Au 4f peaks are observed, as shown in the inset.

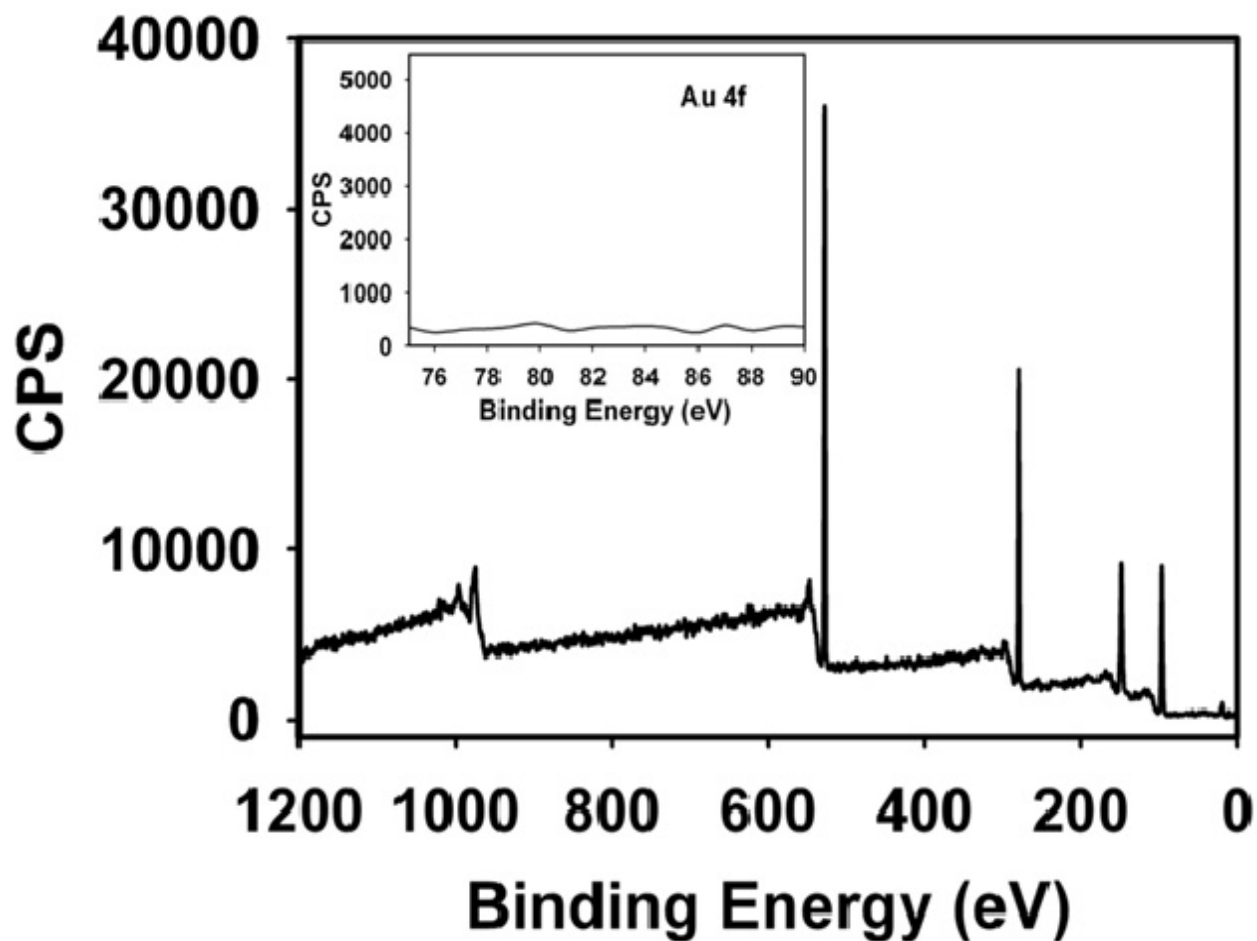


Figure 4-S4. X-ray photoelectron spectrum of an untreated and unused PDMS stamp. A PDMS stamp was not treated with oxygen plasma nor was it subjected to the contact reaction or lift-off processes. No Au 4f peaks are observed, as displayed in the inset.

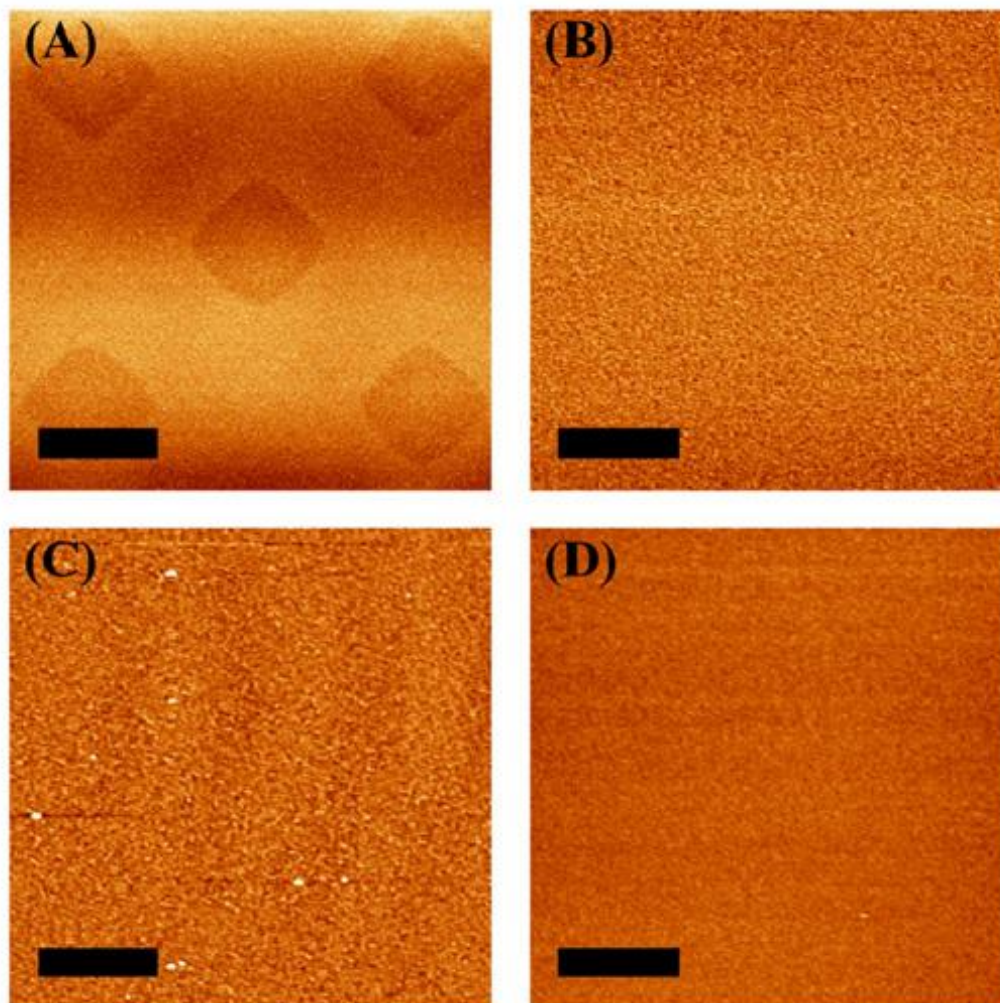


Figure 4-S5. Atomic force microscope topographic images of chemical lift-off lithography on different types of SAMs. Self-assembled monolayers of alkanethiols with different tail groups on Au substrates were investigated using chemical lift-off lithography and PDMS stamps with $10\text{-}\mu\text{m} \times 10\text{-}\mu\text{m}$ protruding posts. (A) Similar to TEG SAMs, monolayers of hydroxyl-terminated undecanethiol are patterned when contacted by oxygen plasma-treated PDMS stamps. By contrast, (B) a methoxy-terminated tri(ethylene glycol)undecanethiol SAM, (C) a methyl-terminated undecanethiol SAM, and (D) a bare Au substrate showed no evidence of patterning by lift-off lithography. Scale bars are $10\text{ }\mu\text{m}$.

Infrared Spectroscopy to Investigate the Extent of Lift-Off. Both Fourier-transform infrared reflection-absorption spectroscopy (FT-IRRAS) and polarization-modulation infrared reflection-absorption spectroscopy (PM-IRRAS) were carried out using a Thermo Nicolet 8700 FT-IR spectrometer (Thermo Electron Corp., Madison, WI) in reflectance mode using infrared light incident at 82° relative to the surface normal. Spectra with 1024 scans were collected in all cases. Before collecting FT-IRRAS spectra, the sample chamber was flushed with nitrogen gas to reduce the presence of water and CO₂. Additionally, deuterated dodecanethiol SAM-modified Au substrates were used as reference samples to subtract water and CO₂ contributions from experimental sample spectra. Since, the O-H stretching mode is relatively free of water interference, its peak area can be determined quantitatively.

The FT-IRRAS experiments were performed on hydroxyl-terminated SAM-coated Au substrates before and after the lift-off process to determine the lift-off yield resulting from the contact reaction at the stamp-SAM interface. An unpatterned, flat PDMS stamp was oxygen plasma-treated and used to produce the lift-off area for interrogation by FT-IRRAS. Spectra were collected in the range of 2500-3650 cm⁻¹ to monitor relative changes in peaks arising from O-H tail groups of hydroxyl-terminated SAMs. Before lift-off, a broad band centered around 3350 cm⁻¹ representing the O-H stretching modes and strong bands at 2800-3000 cm⁻¹ indicative of C-H stretching modes were observed as shown in representative spectra in fig. 4-S6. After lift-off, a decrease of 75-80% in the relative peak area was observed for the broad O-H stretching band. Weaker peak intensity decreases were observed for the C-H stretching bands. Pan and coworkers have shown that the IR intensity of the O-H stretching modes depends only on the surface coverage of hydroxyl-terminated alkanethiols, while that of the C-H stretching modes depends on both the surface coverage and the C-H dipole orientation.⁵⁰ Thus, a 75-80% decrease

in the peak area of the O-H stretching band reflects the actual decrease in the surface coverage of alkanethiols due to the lift-off process. Because the IR peak areas of the C-H stretching modes depend on both the surface coverage and the dipole orientation, it is possible that the remaining alkanethiol molecules that were not lifted off after the stamp-SAM contact reaction undergo rearrangement of the C-H dipoles to enhance the IR intensity/peak area. This would cancel out the reduction in C-H IR peak area due to the removal of alkanethiols *via* the lift-off process.

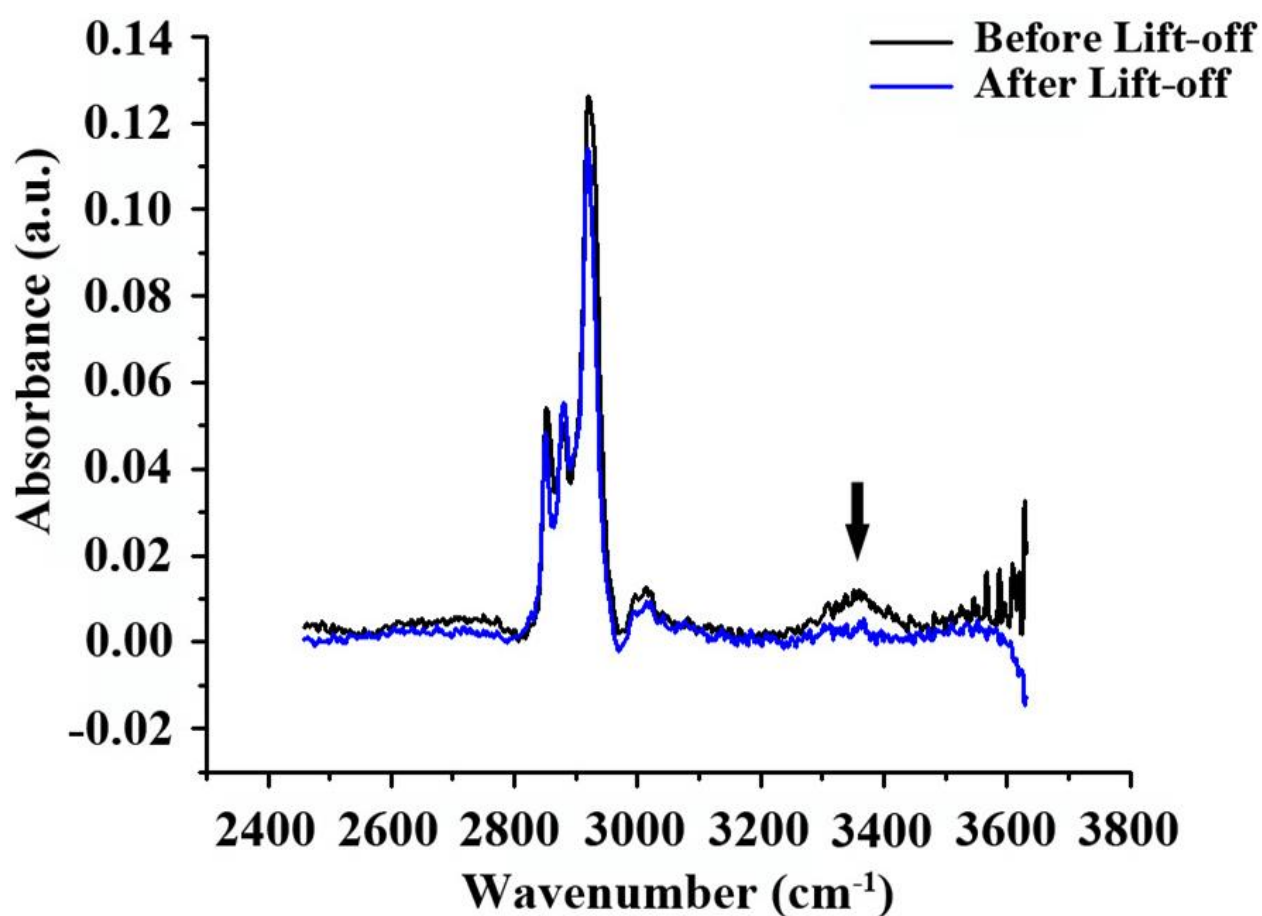


Figure 4-S6. Fourier-transform infrared reflection-absorption spectra of a hydroxyl-terminated SAM-coated Au substrate before and after the lift-off process. The broad hydroxyl stretch band (indicated by the black arrow) arising from the hydroxyl-terminated SAM molecules decreases in relative peak area, indicating 75-80% removal of alkanethiols after lift-off.

Thus, only a weak IR peak area decrease of the C-H stretching bands was observed in fig. 4-S6. The decrease in the peak area of the O-H stretching band enables a good estimation of the contact reaction lift-off yield for hydroxyl-terminated alkanethiols. Contact reaction lift-off yields may vary for different alkanethiols. A more thorough investigation of this phenomenon will be carried out in the future to reveal the reaction mechanism at the stamp-SAM interface by examining additional functional tail moieties.

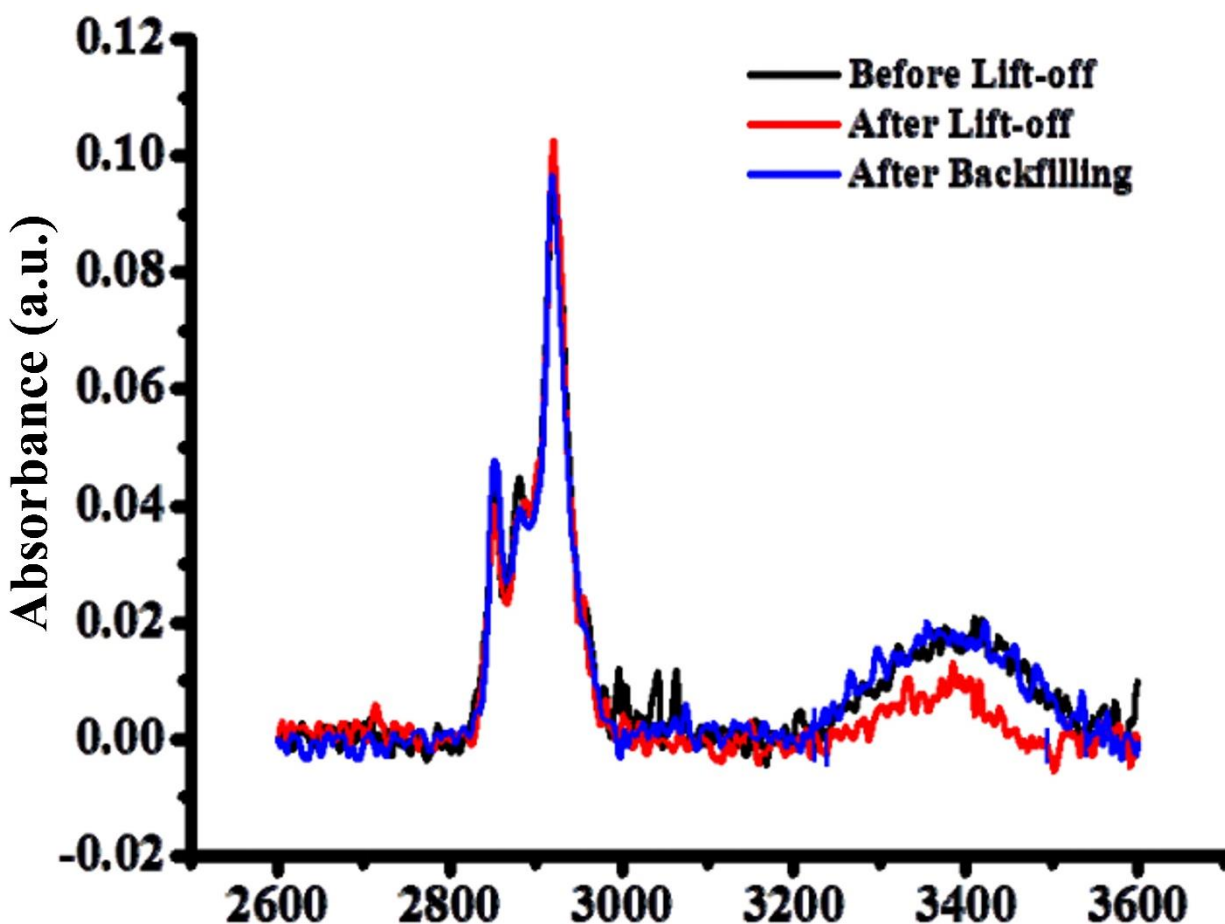


Figure 4-S7. Polarization-modulation infrared reflection-absorption spectra of a hydroxyl-terminated SAM-coated Au substrate before/after lift-off and after backfilling. The broad hydroxyl stretch centered around 3400 cm^{-1} of the hydroxyl-terminated alkanethiol SAM decreases after lift-off, due to the removal of hydroxyl-terminated alkanethiols and increases after backfilling, indicating hydroxyl-terminated alkanethiol refilling. By contrast, the C-H stretching modes stay constant, within experimental error.

Polarization-modulation infrared reflection-absorption spectroscopy was used to investigate the role of orientational changes in modulating the intensity of the C-H stretching peaks. In PM-IRRAS, both *p*-polarized and *s*-polarized radiation are modulated by a photoelastic modulator to reduce contributions to the spectra from water in the vapor phase above the substrates. As before, a featureless PDMS stamp was used to lift-off molecules from hydroxyl-terminated alkanethiol SAMs on Au substrates. After lift-off, the same hydroxyl-terminated alkanethiol molecules were backfilled into the exposed Au regions. Representative spectra are shown in fig. 4-S7. Similar to findings in FT-IRRAS experiments, only the broad O-H stretching peak area was reduced after lift-off; the C-H stretching peak was essentially unchanged. After the backfilling step, the O-H stretching peak returned to its pre-lift-off intensity. Again, the C-H stretch peak did not change, within experimental error. These results support the conclusion that the O-H intensity depends on surface coverage. By contrast, the C-H intensity, which depends on both surface coverage and dipole orientation, does not appear to be a good indicator of coverage. While similar conclusions are drawn from both the FT-IRRAS and PM-IRRAS data, conventional FT-IRRAS measurements are more quantitative, and are used to estimate the fraction of the monolayer removed here.

Effects of Diffusion. A hydroxyl TEG SAM-coated Au substrate was investigated by tapping-mode AFM immediately after lift-off. The substrate was subsequently stored under ambient conditions (in air at 25 °C) for two days and reinvestigated by AFM. The SAM features were found to remain intact on the substrate, and there was no obvious pattern dissolution, as shown in the comparative AFM topography images in fig. 4-S8.

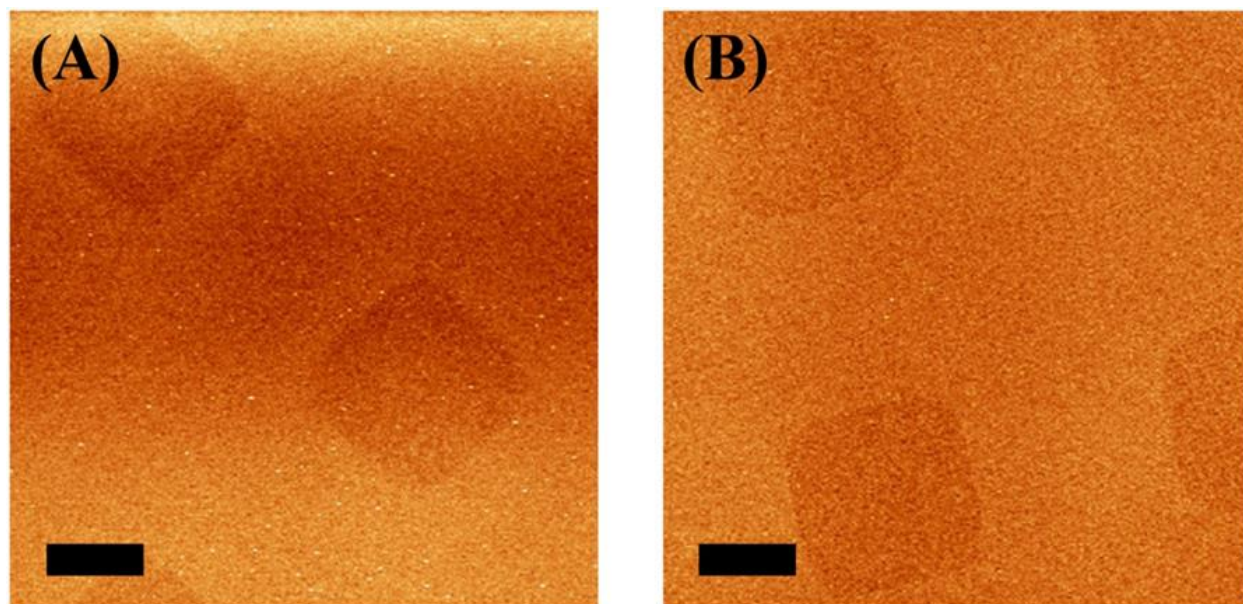


Fig. 4-S8. Atomic force microscope topographic images of TEG SAM hole features created by chemical lift-off lithography. PDMS stamps with $10\text{-}\mu\text{m} \times 10\text{-}\mu\text{m}$ protruding posts were used to lift-off areas of a TEG SAM on a Au substrate. **(A)** Freshly lifted-off TEG SAM hole features. **(B)** Lift-off TEG SAM features two days after storing under ambient conditions. Scale bars are $5\ \mu\text{m}$.

4.7 References

1. Gates, B. D.; Xu, Q. B.; Stewart, M.; Ryan, D.; Willson, C. G.; Whitesides, G. M. New Approaches to Nanofabrication: Molding, Printing, and Other Techniques. *Chem. Rev.* **2005**, *105*, 1171-1196.
2. Willson, C. G.; Roman, B. J. The Future of Lithography: SEMATECH Litho Forum 2008. *ACS Nano* **2008**, *2*, 1323-1328.
3. Saavedra, H. M.; Mullen, T. J.; Zhang, P.; Dewey, D. C.; Claridge, S. A.; Weiss, P. S. Hybrid Strategies in Nanolithography. *Rep. Prog. Phys.* **2010**, *73*, 036501.
4. Shim, W.; Braunschweig, A. B.; Liao, X.; Chai, J.; Lim, J. K.; Zheng, G.; Mirkin, C. A. Hard-Tip, Soft-Spring Lithography. *Nature* **2011**, *469*, 516-521.
5. Piner, R. D.; Zhu, J.; Xu, F.; Hong, S. H.; Mirkin, C. A. "Dip-Pen" Nanolithography. *Science* **1999**, *283*, 661-663.
6. Xu, S.; Laibinis, P. E.; Liu, G.-Y. Accelerating the Kinetics of Thiol Self-Assembly on Gold - A Spatial Confinement Effect. *J. Am. Chem. Soc.* **1998**, *120*, 9356-9361.
7. Xu, S.; Liu, G.-Y. Nanometer-Scale Fabrication by Simultaneous Nanoshaving and Molecular Self-Assembly. *Langmuir* **1997**, *13*, 127-129.
8. Xia, Y. N.; Whitesides, G. M. Soft Lithography. *Angew. Chem. Int. Edit.* **1998**, *37*, 550-575.
9. Li, X. M.; Peter, M.; Huskens, J.; Reinhoudt, D. N. Catalytic Microcontact Printing without Ink. *Nano Lett.* **2003**, *3*, 1449-1453.
10. Rogers, J. A.; Nuzzo, R. G. Recent Progress in Soft Lithography. *Mater. Today* **2005**, *8*, 50-56.

11. Wilbur, J. L.; Kumar, A.; Kim, E.; Whitesides, G. M. Microfabrication by Microcontact Printing of Self-Assembled Monolayers. *Adv. Mater.* **1994**, *6*, 600-604.
12. Chou, S. Y.; Krauss, P. R.; Renstrom, P. J. Imprint Lithography with 25-Nanometer Resolution. *Science* **1996**, *272*, 85-87.
13. Loo, Y. L.; Hsu, J. W. P.; Willett, R. L.; Baldwin, K. W.; West, K. W.; Rogers, J. A. High-Resolution Transfer Printing on GaAs Surfaces Using Alkane Dithiol Monolayers. *J. Vac. Sci. Technol., B* **2002**, *20*, 2853-2856.
14. Childs, W. R.; Nuzzo, R. G. Decal Transfer Microlithography: A New Soft-Lithographic Patterning Method. *J. Am. Chem. Soc.* **2002**, *124*, 13583-13596.
15. Kumar, A.; Whitesides, G. M. Features of Gold Having Micrometer to Centimeter Dimensions Can Be Formed through a Combination of Stamping with an Elastomeric Stamp and an Alkanethiol Ink Followed by Chemical Etching. *Appl. Phys. Lett.* **1993**, *63*, 2002-2004.
16. Christman, K. L.; Enriquez-Rios, V. D.; Maynard, H. D. Nanopatterning Proteins and Peptides. *Soft Matter* **2006**, *2*, 928-939.
17. Vaish, A.; Shuster, M. J.; Cheunkar, S.; Weiss, P. S.; Andrews, A. M. Tuning Stamp Surface Energy for Soft Lithography of Polar Molecules to Fabricate Bioactive Small-Molecule Microarrays. *Small* **2011**, *7*, 1471-1479.
18. Shuster, M. J.; Vaish, A.; Cao, H. H.; Guttentag, A. I.; McManigle, J. E.; Gibb, A. L.; Martinez, M. M.; Nezarati, R. M.; Hinds, J. M.; Liao, W.-S.; Weiss, P. S.; Andrews, A. M. Patterning Small-Molecule Biocapture Surfaces: Microcontact Insertion Printing vs. Photolithography. *Chem. Commun.* **2011**, *47*, 10641-10643.

19. McLellan, J. M.; Geissler, M.; Xia, Y. N. Edge Spreading Lithography and Its Application to the Fabrication of Mesoscopic Gold and Silver Rings. *J. Am. Chem. Soc.* **2004**, *126*, 10830-10831.
20. Srinivasan, C.; Mullen, T. J.; Hohman, J. N.; Anderson, M. E.; Dameron, A. A.; Andrews, A. M.; Dickey, E. C.; Horn, M. W.; Weiss, P. S. Scanning Electron Microscopy of Nanoscale Chemical Patterns. *ACS Nano* **2007**, *1*, 191-201.
21. Braunschweig, A. B.; Huo, F.; Mirkin, C. A. Molecular Printing. *Nature Chem.* **2009**, *1*, 353-358.
22. Xu, S.; Miller, S.; Laibinis, P. E.; Liu, G.-Y. Fabrication of Nanometer Scale Patterns within Self-Assembled Monolayers by Nanografting. *Langmuir* **1999**, *15*, 7244-7251.
23. Tiberio, R. C.; Craighead, H. G.; Lercel, M.; Lau, T.; Sheen, C. W.; Allara, D. L. Self-Assembled Monolayer Electron-Beam Resist on GaAs. *Appl. Phys. Lett.* **1993**, *62*, 476-478.
24. Loo, Y. L.; Willett, R. L.; Baldwin, K. W.; Rogers, J. A. Interfacial Chemistries for Nanoscale Transfer Printing. *J. Am. Chem. Soc.* **2002**, *124*, 7654-7655.
25. Lahiri, J.; Ostuni, E.; Whitesides, G. M. Patterning Ligands on Reactive SAMs by Microcontact Printing. *Langmuir* **1999**, *15*, 2055-2060.
26. Delamarche, E.; Geissler, M.; Bernard, A.; Wolf, H.; Michel, B.; Hilborn, J.; Donzel, C. Hydrophilic Poly(Dimethylsioxane) Stamps for Microcontact Printing. *Adv. Mater.* **2001**, *13*, 1164-1167.
27. Kaufmann, T.; Ravoo, B. J. Stamps, Inks and Substrates: Polymers in Microcontact Printing. *Polym. Chem.* **2010**, *1*, 371-387.

28. Wasserman, S. R.; Biebuyck, H.; Whitesides, G. M. Monolayers of 11-Trichlorosilylundecyl Thioacetate - A System That Promotes Adhesion between Silicon Dioxide and Evaporated Gold. *J. Mater. Res.* **1989**, *4*, 886-891.
29. Stranick, S. J.; Parikh, A. N.; Allara, D. L.; Weiss, P. S. A New Mechanism for Surface-Diffusion - Motion of a Substrate-Adsorbate Complex. *J. Phys. Chem.* **1994**, *98*, 11136-11142.
30. Stranick, S. J.; Atre, S. V.; Parikh, A. N.; Wood, M. C.; Allara, D. L.; Winograd, N.; Weiss, P. S. Nanometer-Scale Phase Separation in Mixed Composition Self-Assembled Monolayers. *Nanotechnology* **1996**, *7*, 438-442.
31. Skulason, H.; Frisbie, C. D. Detection of Discrete Interactions upon Rupture of Au Microcontacts to Self-Assembled Monolayers Terminated with -S(CO)CH₃ or -SH. *J. Am. Chem. Soc.* **2000**, *122*, 9750-9760.
32. Liu, M.; Amro, N. A.; Liu, G.-Y. Nanografting for Surface Physical Chemistry. *Annu. Rev. Phys. Chem.*, **2008**; *59*, 367-386.
33. Poirier, G. E.; Tarlov, M. J. The c(4x2) Superlattice of *n*-Alkanethiol Monolayers Self-Assembled on Au(111). *Langmuir* **1994**, *10*, 2853-2856.
34. Poirier, G. E.; Tarlov, M. J. Molecular Ordering and Gold Migration Observed in Butanethiol Self-Assembled Monolayers Using Scanning Tunneling Microscopy. *J. Phys. Chem.* **1995**, *99*, 10966-10970.
35. Maksymovych, P.; Sorescu, D. C.; Yates, J. T., Jr. Gold-Adatom-Mediated Bonding in Self-Assembled Short-Chain Alkanethiolate Species on the Au(111) Surface. *Phys. Rev. Lett.* **2006**, *97*, 146103.

36. Yu, M.; Bovet, N.; Satterley, C. J.; Bengio, S.; Lovelock, K. R. J.; Milligan, P. K.; Jones, R. G.; Woodruff, D. P.; Dhanak, V. True Nature of an Archetypal Self-Assembly System: Mobile Au-Thiolate Species on Au(111). *Phys. Rev. Lett.* **2006**, *97*, 166102.
37. Moore, A. M.; Mantooth, B. A.; Donhauser, Z. J.; Yao, Y.; Tour, J. M.; Weiss, P. S. Real-Time Measurements of Conductance Switching and Motion of Single Oligo(Phenylene Ethynylene) Molecules. *J. Am. Chem. Soc.* **2007**, *129*, 10352-10353.
38. Han, P.; Kurland, A. R.; Giordano, A. N.; Nanayakkara, S. U.; Blake, M. M.; Pochas, C. M.; Weiss, P. S. Heads and Tails: Simultaneous Exposed and Buried Interface Imaging of Monolayers. *ACS Nano* **2009**, *3*, 3115-3121.
39. When oxygen plasma treatment was omitted, a featureless PDMS stamp brought into contact with a hydroxyl-terminated, SAM-coated Au surface failed to produce XPS signature peaks indicative of Au lift-off (fig. 4-S2). Likewise, stamps that were either treated with oxygen plasma or left untreated but not subjected to the lift-off process had no indication of Au on the stamp surfaces (figs. 4-S3 and 4-S4, respectively).
40. Gou, H.-L.; Xu, J.-J.; Xia, X.-H.; Chen, H.-Y. Air Plasma Assisting Microcontact Deprinting and Printing for Gold Thin Film and PDMS Patterns. *ACS Appl. Mater. Interfaces* **2010**, *2*, 1324-1330.
41. Schueller, O. J. A.; Duffy, D. C.; Rogers, J. A.; Brittain, S. T.; Whitesides, G. M. Reconfigurable Diffraction Gratings Based on Elastomeric Microfluidic Devices. *Sensor Actuat. A-Phys.* **1999**, *78*, 149-159.
42. Duffy, D. C.; Schueller, O. J. A.; Brittain, S. T.; Whitesides, G. M. Rapid Prototyping of Microfluidic Switches in Poly(Dimethyl Siloxane) and Their Actuation by Electro-Osmotic Flow. *J. Micromech. Microeng.* **1999**, *9*, 211-217.

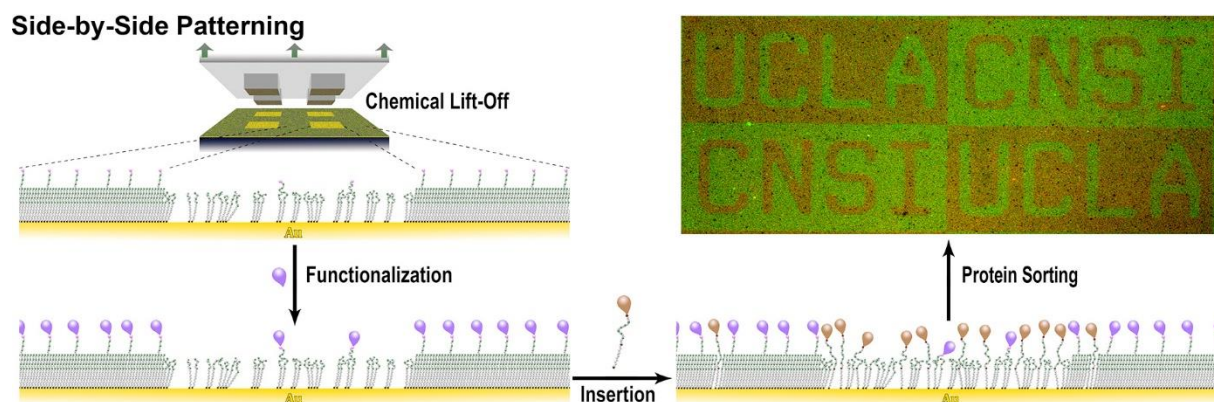
43. Saavedra, H. M.; Thompson, C. M.; Hohman, J. N.; Crespi, V. H.; Weiss, P. S. Reversible Lability by *in Situ* Reaction of Self-Assembled Monolayers. *J. Am. Chem. Soc.* **2009**, *131*, 2252-2259.
44. Liao, W.-S.; Chen, X.; Chen, J.; Cremer, P. S. Templating Water Stains for Nanolithography. *Nano Lett.* **2007**, *7*, 2452-2458.
45. Geissler, M.; Wolf, H.; Stutz, R.; Delamarche, E.; Grummt, U. W.; Michel, B.; Bietsch, A. Fabrication of Metal Nanowires Using Microcontact Printing. *Langmuir* **2003**, *19*, 6301-6311.
46. Prime, K. L.; Whitesides, G. M. Self-Assembled Organic Monolayers - Model Systems for Studying Adsorption of Proteins at Surfaces. *Science* **1991**, *252*, 1164-1167.
47. Dameron, A. A.; Hampton, J. R.; Smith, R. K.; Mullen, T. J.; Gillmor, S. D.; Weiss, P. S. Microdisplacement Printing. *Nano Lett.* **2005**, *5*, 1834-1837.
48. Stranick, S. J.; Kamna, M. M.; Weiss, P. S. Interactions and Dynamics of Benzene on Cu(111) at Low-Temperature. *Surf. Sci.* **1995**, *338*, 41-59.

Chapter 5

Toward Multiplexed Biocapture Substrates *via* Chemical Lift-Off Lithography

The information in the chapter is in preparation for submission
and is reproduced in its entirety here.

Authors: Cao, H. H.; Liao, W.-S.; Serino, A. C.; Cheunkar, S.; Yang, H.;
Weiss, P. S.; Andrews, A. M.



5.1 Abstract

Creating small-molecule addressable platforms for high-throughput screening and biosensing applications requires the precise placement of bioactive probes on solid substrates and the capability to capture and to sort targets from multi-component solutions. Here, chemical lift-off lithography was used to fabricate large-area, high-fidelity patterns of small-molecule probes. Lift-off lithography enabled precise patterning of biotin-streptavidin recognition from micrometer to sub-30-nm feature sizes. Subtractive patterning *via* lift-off further enabled multiplexed side-by-side patterns of small bioactive probes such that binding partners were directed to their cognate tethered ligands from complex mixtures. Moreover, small molecules mimicking endogenous neurotransmitters were patterned using lift-off to capture native human membrane-associated G-protein-coupled receptors. The ability to place bioactive probes precisely on substrates and to create multiplexed patterns of small molecules for sorting target mixtures according to ligand affinities is critical for fabricating biochips for proteomics and biosensing applications.

5.2 Introduction

Creating multiplexed functional biocapture platforms is essential for investigating biomolecule-ligand recognition for high-throughput screening and biosensing applications.¹⁻⁴ To achieve this, surface immobilization strategies are needed to anchor either biomolecules or ligands on solid substrates for capturing and sorting respective binding partners from solution phase. Immobilization of biomolecules on surfaces requires avoiding denaturation upon surface adsorption and favorable orientation for ligand binding.⁵⁻¹⁰ In contrast, surface tethering of small-molecule probes necessitates judicious selection of coupling chemistries and surface dilution to facilitate recognition by large biomolecule binding partners.^{6,11-16} For instance, the size mismatch between small-molecule neurotransmitters or amino acids and large antibody or receptor binding partners is 10-100-fold.¹⁷

The goal of small-molecule chemical patterning is the precise placement of multiple probes on substrates for the investigation of target binding specificity and selectivity.¹⁸⁻²⁰ However, the latter has been difficult to realize fully.^{21,22} To this end, we have developed a number of patterning methods to investigate relative biomolecule capture on small-molecule ligand-functionalized *vs.* unfunctionalized regions on substrates. We invented microcontact insertion printing (μ CIP) to pattern small-molecule neurotransmitters and precursor molecules mimicking endogenous neurotransmitters on alkanethiol SAM-modified Au substrates.²³⁻²⁵ In this patterning approach, molecular tethers are inserted into pre-formed SAMs and tethers are then functionalized on-chip with small-molecule probes. As an alternative to μ CIP, we have used microfluidics to generate multiplexed substrates.²⁶ In the latter, two-component SAMs having low proportions of tethering molecules (<10% solution concentration) were produced by solution co-deposition to achieve dilution of surface tethers.

Recently, we invented chemical lift-off lithography, wherein molecular patterning is achieved by removing alkanethiol SAM molecules from Au substrates.²⁷ In this approach, PDMS stamps are treated with oxygen plasma to generate siloxyls on stamp surfaces. These activated stamps are then brought into conformal contact with hydroxyl-terminated alkanethiol SAM-modified Au substrates to produce covalent interactions at stamp/SAM interfaces. The resultant interfacial interactions are stronger than the Au-Au bonds on Au substrates such that stamp lift-off causes alkanethiols and underlying Au atoms to be removed. We showed previously that post-lift-off regions could be inserted with biotin-functionalized alkanethiols to capture streptavidin. We also discovered that because lift-off removes only a portion of the preformed SAM molecules, the remaining molecules in the contact regions enabled controlled insertion of DNA probes for high-efficiency and tunable hybridization with target DNA.²⁸

Here, we continue to investigate the use of chemical lift-off lithography with the end-goal of producing multiplexed bioactive substrates in mind. We explore a wide range of feature shapes and sizes. Bifunctionalized substrates and the ability of small-molecule patterned substrates produced by lift-off lithography to recognize native G-protein-coupled receptor targets are also examined.

5.3 Materials and Methods

Materials. Silicon substrates having 100-nm-thick Au films overlaying 10-nm-thick Ti adhesive layers were purchased from Platypus Technologies (Madison, WI, USA). *N*-Hydroxysuccinimide (NHS), *N*-(3-dimethylaminopropyl)-*N'*-ethylcarbodiimide hydrochloride (EDC), *N,N*-dimethylformamide (DMF), 4-methylpiperidine, bovine serum albumin (BSA), and 0.01 M phosphate buffered saline (PBS) ([NaCl]=138 mM and [KCl]=2.7 mM) pH 7.4 were purchased from Sigma-Aldrich (St. Louis, MO, USA). Absolute, 200 proof, anhydrous, ACS/USP grade ethyl alcohol was purchased from PHARMCO-AAPER (Oakland, CA, USA). Deionized water (~18 M Ω) was obtained from a Millipore water purifier (Billerica, MA, USA). The Fmoc-protected biological precursors to serotonin and dopamine, *i.e.*, 9-fluorenylmethyloxycarbonyl-5-hydroxy-*L*-tryptophan (Fmoc-*L*-5HTP) and 9-fluorenylmethyloxycarbonyl-3,4-dihydroxy-*L*-phenylalanine (Fmoc-*L*-DOPA) were purchased from AnaSpec-Eurogentec (Fremont, CA, USA).

Streptavidin antibody (1 mg/mL) and AlexaFluor[®] 546 goat anti-mouse IgG (H+L) highly cross-adsorbed antibody (2 mg/mL) were purchased from Invitrogen (Carlsbad, CA, USA). Mouse polyclonal anti-serotonin_{1A} (5-HT_{1A}) receptor antibody (whole antiserum), rabbit polyclonal anti-dopamine D₁ receptor antibody (whole antiserum), mouse monoclonal anti-*L*-5-HTP antibody (1 mg/mL), mouse monoclonal anti-*L*-DOPA antibody (1 mg/mL), and fluorescein isothiocyanate (FITC)-conjugated rabbit polyclonal anti-streptavidin antibody (10 mg/mL) were purchased from Abcam Inc. (Cambridge, MA, USA). Native human 5-HT_{1A} receptor (6.4 μ g/ μ L total protein concentration) in human embryonic kidney 293 (HEK293) cell membranes and untransfected HEK293 cell membranes (10 mg/mL protein concentration) were purchased from Perkin Elmer, Inc. (Waltham, MA, USA). All proteins and antibodies were used

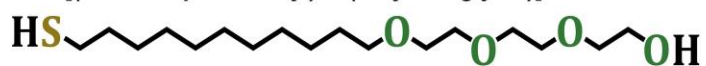
as received and incubated with substrates in 0.01 M PBS pH 7.4 at room temperature. Primary antibodies not labeled with fluorophores and fluorescently labeled secondary antibodies were diluted 1:200 and 1:100, respectively, in 0.01 M PBS pH 7.4.

(11-Mercaptoundecyl) tri(ethylene glycol) (TEG) (Chart 5-1) was purchased from Toronto Research Chemicals Inc. (Toronto, ON, Canada). Biotinylated hexa(ethylene glycol)undecanethiol (BEG) was purchased from Nanoscience Instruments Inc. (Phoenix, AZ, USA). (11-Mercaptoundecyl) hexa(ethylene glycol)amine (AEG) and (11-mercaptoundecyl) tri(ethylene glycol)methyl ether were purchased from Prochimia (Sopot, Poland).

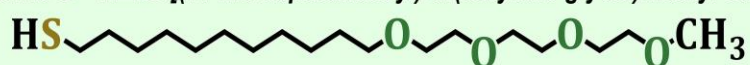
Substrate and stamp preparation. All Au substrates were hydrogen-flame annealed and followed by incubation with ethanolic solutions of alkanethiols. After monolayer formation, substrates were rinsed thoroughly with fresh ethanol and dried with nitrogen gas. Different feature shapes on PDMS stamps were produced from silicon master substrates, which were fabricated using standard photolithography. The process of stamp fabrication and details of oxygen plasma treatment have been published elsewhere.²⁵⁻²⁸

Briefly, a 10:1 mass ratio of *SYLGARD* 184 silicone elastomer base and curing agent (Ellsworth Adhesives, Germantown, WI, USA) was mixed thoroughly in a plastic cup, degassed under vacuum, cast onto master substrates in a plastic Petri dish, and cured in an oven at 70 °C overnight. Polymerized stamps were removed from the master substrates, cut into usable sizes, and treated with oxygen plasma (Harrick Plasma, power 18 W, and oxygen pressure 10 psi) for 30 s to produce hydrophilic reactive PDMS surfaces.^{25,27,28} After lift-off, stamps were rinsed with ethanol, wiped with Kimberly-Clark tissues soaked in ethanol, and dried with nitrogen gas. Cleaned stamps were sealed to clean glass slides for storage before additional use.

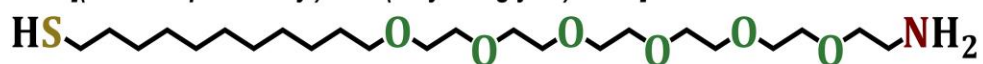
TEG [(11-mercaptoundecyl) tri(ethylene glycol)]



CH₃O-TEG [(11-mercaptoundecyl) tri(ethylene glycol)methyl ether]



AEG [(11-mercaptoundecyl) hexa(ethylene glycol)amine]



BEG [(11-mercaptoundecyl) hexa(ethylene glycol)biotin]

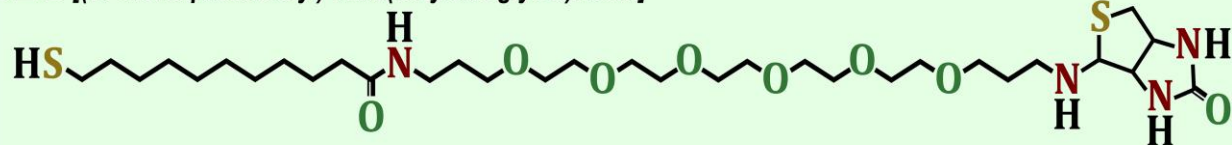


Chart 5-1. List of alkanethiols used in this study.

Streptavidin-Biotin Patterns. Substrates were incubated with ethanolic solutions of 0.5 mM TEG for ~17 h to form SAMs. The TEG SAM-modified substrates were then thoroughly rinsed with ethanol and dried with nitrogen gas. Oxygen plasma-treated PDMS stamps were placed in conformal contact with the substrates for 30 min to enable stamp/substrate contact reactions, which caused SAM molecules and underlying Au atoms to be removed from the contact areas once the stamps were released from the substrates. Microscale (~30- μ m features with ~30-60 μ m spacing) or nanoscale (200-nm circular features with 2- μ m pitch or 30-nm protruding line features with 3- μ m pitch) were used for patterning. After patterning, substrates were rinsed with ethanol and dried with nitrogen gas. The post-lift-off substrates were then inserted with 80/20 ethanolic solutions of 0.40 mM TEG and 0.1 mM BEG for 1 h. For nanoscale streptavidin-biotin patterning, 100% ethanolic solutions of 0.5 mM BEG were used for insertion into the post-lift-off TEG-modified substrates.

After rinsing with ethanol and drying with nitrogen gas, biotinylated substrates were incubated with 10 mg/mL of BSA for 5 min to block nonspecific protein adsorption sites, then with 50 μ g/mL of streptavidin for 20 min, and finally with 100 μ g/mL FITC-conjugated rabbit anti-streptavidin antibodies for 20 min to visualize streptavidin binding to surface-tethered biotin (Table 5-S1, Supporting Information). Copious deionized water was used to rinse substrates gently after each protein incubation step.

An inverted fluorescence microscope (Axio Observer.D1) was used to image substrates. A 38 HE/high efficiency filter-set with excitation and emission wavelengths at 470 ± 20 nm and 525 ± 25 nm, respectively was used to image streptavidin-biotin fluorescence patterns. A 43 HE/high efficiency filter-set with excitation and emission wavelengths at 550 ± 25 nm and

605 ± 70 nm, respectively was used to visualize antibody binding to *L*-DOPA or *L*-5-HTP on substrates (*vide infra*). Fluorescence images were collected using 10× or 20× objective lenses for microscale or nanoscale patterns, respectively.

Fluorescence intensities were determined with AxioVs40 version 4.7.1.0 software (Carl Zeiss MicroImaging, Inc., Thornwood, NY, USA). To measure fluorescence intensities resulting from periodic arrays of features (*i.e.*, patterns of square-shaped or stripe-shaped features), the heights of the fluorescence line scans were adjusted to be about the same as the patterned features. On average, five line scans were acquired per image. Fluorescence intensities were averaged for each line scan and then for each image. For images with more complex patterns (*i.e.*, UCLA/CNSI letter-shaped features), fluorescence intensities were measured using a histogram function and similarly defined areas over the bright and dark regions across all fluorescence images. Five fluorescence measurements were made for each bright and dark region per image. Fluorescence measurements were then averaged for each image.

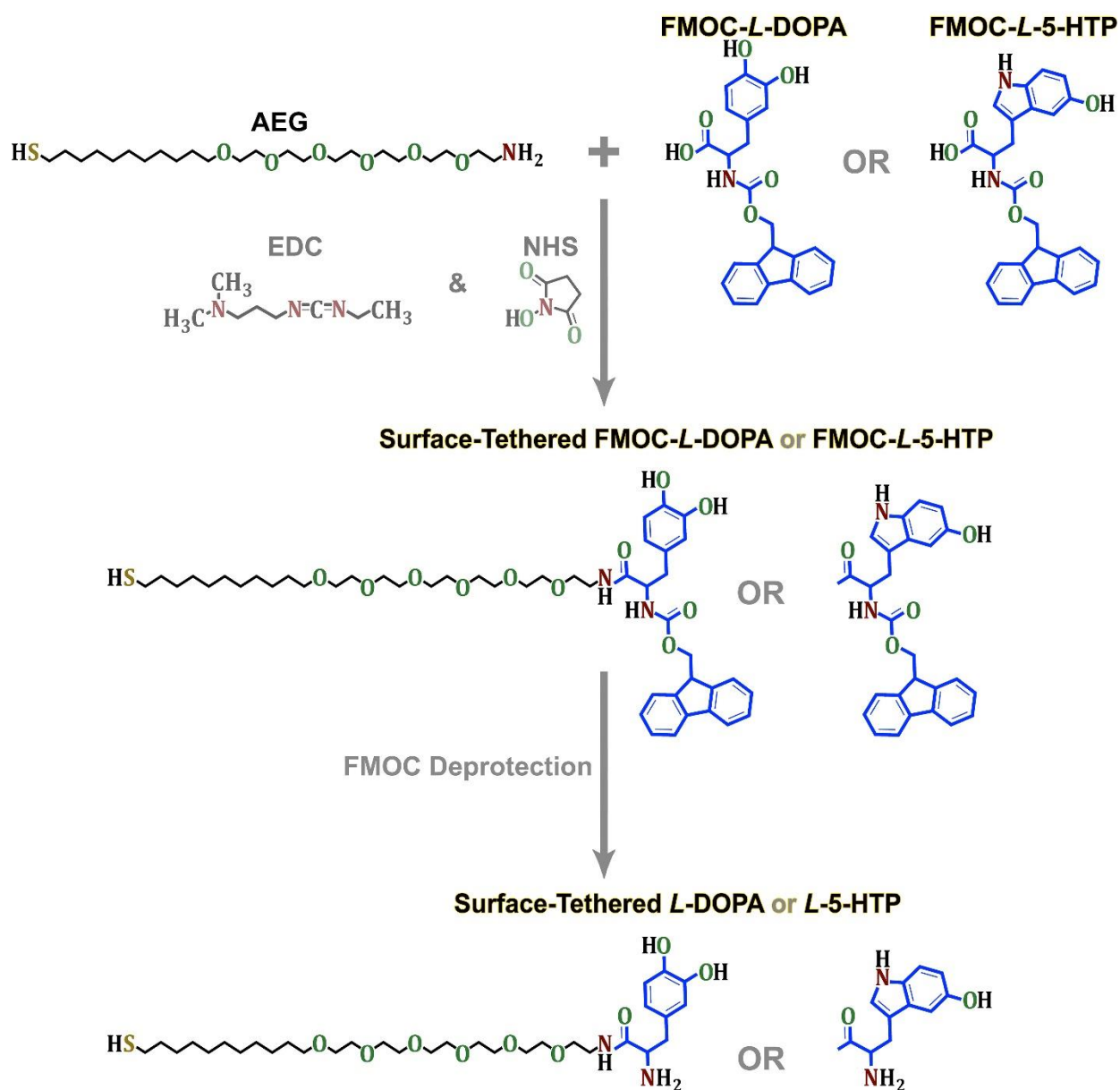
Streptavidin-biotin nanopatterns were also characterized *via* tapping-mode AFM (Dimension 5000, Bruker AXS, Santa Barbara, CA, USA). Topographic AFM images were collected using Si cantilevers with a spring constant of 48 N/m and a resonant frequency of 190 kHz (Veeco Instruments, Santa Barbara, CA, USA). The resulting images were processed with WSxM 4.0 Beta 6.4 software (Nanotec Electronica, Madrid, Spain).²⁹

Side-by-Side Patterning. Substrates were incubated with 90/10 ethanolic solutions of 0.45 mM TEG and 0.05 mM AEG for ~17 h to create dilute amine-terminated SAMs. Stamps were activated with oxygen plasma and brought into conformal contact with mixed SAM-modified substrates for 30 min to facilitate strong stamp/substrate interfacial interactions, which

removed SAM molecules upon releasing the stamps from the substrates. The post-lift-off substrates were rinsed with ethanol and dried with nitrogen gas.

For ligand functionalization, solutions of either 20 mM Fmoc-protected *L*-DOPA or 40 mM Fmoc-protected *L*-5-HTP were combined with 20 mM or 40 mM NHS/EDC, respectively, in 60/40 DMF/deionized water. This step was necessary to activate the carboxyl groups of *L*-DOPA and *L*-5-HTP with NHS esters for subsequent reaction with the amino moieties of AEG SAM molecules facilitating the formation of amide bonds (Scheme 5-1). Post-lift-off substrates were incubated with activated probe solutions for 4 h. Probe-modified substrates were then inserted with 90/10 ethanolic solutions of 0.45 mM TEG and 0.05 mM BEG for 1 h.

The Fmoc protecting groups were used to prevent intermolecular reactions between NHS-activated probe molecules. Removal of Fmoc protecting groups with 20% 4-methylpiperidine was carried out in deionized water for 20 min on-chip. After rinsing thoroughly with deionized water and drying with nitrogen gas, functionalized substrates were incubated with 10 mg/mL of BSA for 5 min, then with mixtures of streptavidin (50 μ g/mL) and either mouse monoclonal anti-*L*-DOPA primary antibody or mouse monoclonal anti-*L*-5-HTP primary antibody for 20 min, and finally with mixtures of FITC-conjugated rabbit polyclonal anti-streptavidin antibody (100 μ g/mL) and AlexaFluor[®] 546 goat anti-mouse IgG secondary antibody (20 μ g/mL) for another 20 min to visualize multiplexed protein patterns (Table 5-S1). Imaging was carried out as described above.



Scheme 5-1. Schematic illustrating surface functionalization chemistries.

N-Hydroxysuccinimide (NHS) and *N*-(3-dimethylaminopropyl)-*N'*-ethylcarbodiimide hydrochloride (EDC) were used to create NHS-ester activated carboxyl groups on 9-fluorenylmethoxycarbonyl (Fmoc)-protected 3,4-dihydroxy-*L*-phenylalanine (*L*-DOPA) and 5-hydroxy-*L*-tryptophan (*L*-5-HTP). The NHS esters were then reacted with the amino moieties on amine-terminated hexa(ethylene glycol)alkanethiol (AEG) to form amide bonds. Protecting groups were removed after ligand functionalization on substrates to reveal ligand epitopes essential for biorecognition.

Patterning Small Molecules Probes for Capturing Native Membrane-Associated Receptors. Dilute amine-terminated SAMs were produced by incubating substrates with 95/5 ethanolic solutions of 0.048 mM TEG and 0.025 mM AEG for ~17 h. These substrates were then brought into conformal contact for 30 min with the hydrophilic reactive surfaces of oxygen plasma-treated PDMS stamps (25×25 μm² square protruding features). Post-lift-off substrates were then functionalized with *L*-5-HTP and deprotection was carried out following the procedures described above in the previous section.

After rinsing with deionized water, substrates were incubated with 10 mg/mL BSA for 5 min to reduce nonspecific protein binding.^{24,26} The *L*-5-HTP-modified substrates were then incubated with 100 μg/μL native membrane-associated human 5-HT_{1A} receptors for 1 h. The associated cell membranes were not solubilized so as to retain native receptor conformations favorable for ligand recognition.^{8,26,30,31} Previously, we found that primary antibodies recognizing membrane-associated receptors also had weak affinity for surface-tethered probes.²⁶ Thus, after incubating with 5-HT_{1A} receptors, functionalized substrates were exposed to anti-dopamine D₁ receptor rabbit polyclonal blocking antibodies for 15 min to reduce nonspecific binding of anti-5-HT_{1A} receptor primary antibodies to surface-tethered *L*-5-HTP. Substrates were then incubated with mouse polyclonal anti-5-HT_{1A} receptor primary antibodies for 15 min and 20 μg/mL of AlexaFluor[®] 546 goat anti-mouse secondary antibodies for 15 min to visualize 5-HT_{1A} receptor binding (Table 5-S1). Substrates were rinsed with deionized water between protein incubation steps. The 43 HE fluorescence filter set was used to visualize the binding of 5-HT_{1A} receptors to patterns of surface-tethered *L*-5-HTP as described above.

X-Ray Photoelectron Spectroscopy. Featureless PDMS stamps were used for the chemical lift-off process. All XPS data were collected using an AXIS Ultra DLD instrument (Kratos Analytical Inc., Chestnut Ridge, NY, USA). A monochromatic Al K α X-ray source (10 mA for survey scans and 20 mA for high resolution scans, 15 kV) with a 200 μ m circular spot size and ultrahigh vacuum (10^{-9} Torr) were used.^{25,27} Spectra were acquired at a pass energy of 160 eV for survey spectra and 20 eV for high-resolution spectra of Au 4f regions using a 200-ms dwell time. Different numbers of scans were carried out depending on the sensitivity needed to differentiate each peak from background, ranging from 20 scans for C 1s to 100 for Au 4f.

Because PDMS is an insulator, a charge neutralizer (flood gun) was used to obtain signals from each element on PDMS stamps. As a result, peaks are shifted slightly from their expected regions (for C 1s this is 4-5 eV lower than the reference at 284.0 eV). Because the number of peaks of interest was small (only Au 4f peaks on PDMS samples), and they were well separated (\sim 4 eV), peak shifting did not affect identification. No corrections were therefore carried out during data collection to shift peaks back to particular regions or to scale peaks based on reference locations.

Statistical Analyses. Data were analyzed by Student's *t*-tests using GraphPad Prism 5.0 (GraphPad Software Inc., San Diego, USA). Fluorescence intensities are reported as means \pm standard errors of the means with probabilities $P < 0.05$ considered statistically significant.

5.4 Results and Discussions

5.4.1 Patterning Biorecognition over Multiple Scales

To demonstrate the versatility of chemical lift-off lithography as a biopatterning tool for creating high-density, small-molecule arrays beyond our initial findings,²⁷ we investigated the ability to pattern substrates with the small-molecule biotin (Figure 5-1A) over a wide variety of feature shapes and sizes. As shown in Figure 5-2A, differently shaped bright regions were indicative of specific recognition of surface-tethered biotin, *i.e.*, BEG (Chart 5-1), by streptavidin. The darker regions surrounding these microscale features were demonstrative of negligible nonspecific binding of streptavidin to the background matrix.

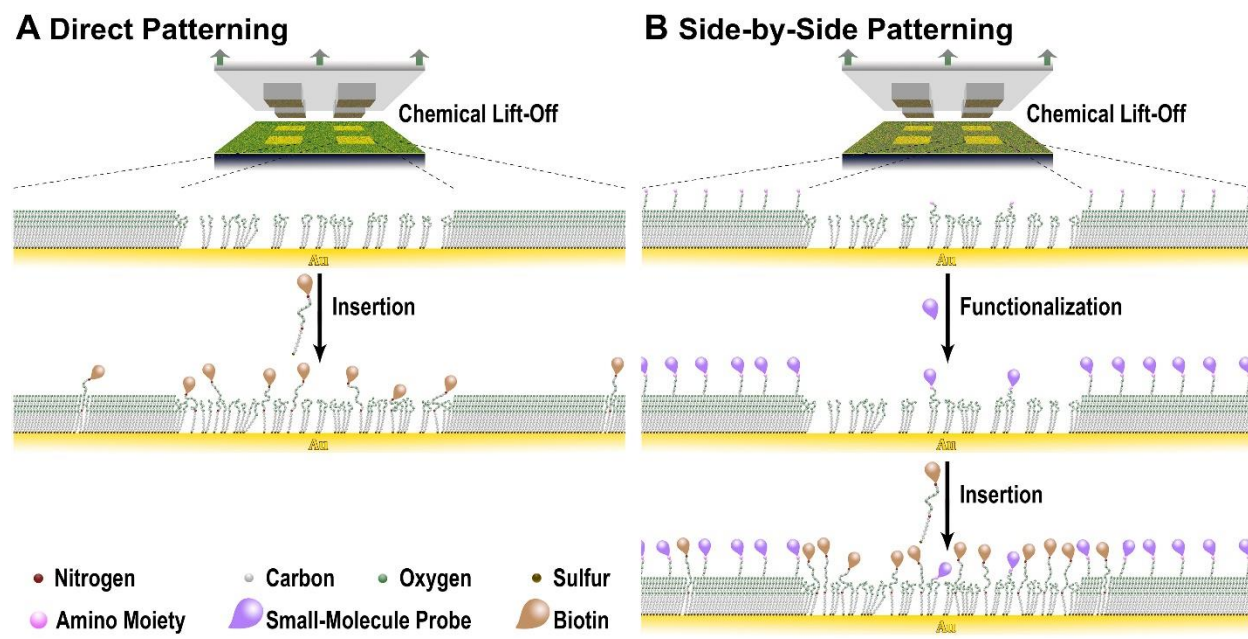


Figure 5-1. Schematic (not to scale) illustrating single and double patterning via chemical lift-off lithography. Preformed SAMs of either (A) hydroxyl-terminated tri(ethylene glycol)alkanethiol (TEG) or (B) mixed 90/10 TEG/amine-terminated hexa(ethylene glycol)alkanethiol (AEG) on Au substrates were chemically lifted off. In (A), substrates were inserted with biotin-terminated hexa(ethylene glycol)alkanethiols (BEG). In (B), substrates were first functionalized with small-molecule probes, *i.e.*, *L*-3,4-dihydroxyphenylalanine or *L*-5-hydroxytryptophan prior to BEG insertion to form side-by-side patterns.

A wide-area, bright, fluorescent nanodot array is shown against a dark TEG background in Figure 5-2B indicating specific streptavidin-biotin recognition but with 100-fold smaller patterned features. Nanodot features were measured by tapping-mode AFM and found to be 215 ± 3 nm (Figure 5-2C). A lack of measurable fluorescence was detected when similar substrates were incubated with FITC-labeled anti-streptavidin antibodies in the absence of streptavidin suggesting negligible nonspecific antibody binding (Figure 5-S1A,B).

Previously, we used chemical lift-off lithography to produce features as small as 40-nm through single lift-off; double lift-off lithography was needed to pattern 20-nm features.²⁷ Here, we achieved sub-30-nm feature resolution with single lift-off lithography using an inverse patterning strategy, *i.e.*, ultra-small features were produced by the non-contact areas. Tapping-mode AFM was needed to visualize these nanoscale patterns. As shown in Figure 5-2D, wide lines (~ 3 μm) with positive-height topographic features produced by streptavidin recognition of biotin are contrasted against narrow trenches with negative-height topography indicative of the non-lift-off TEG SAM regions. These negative features were measured by AFM to be 26 ± 1 nm (Figure 5-2E). These 26-nm feature sizes are within the Au-grain sizes on 100-nm polycrystalline Au films (~ 20 -50 nm), therefore, Au graininess might reduce the accuracy of feature size measurement.^{32,33} Nevertheless, this result suggests that it may be possible to use chemical lift-off lithography to produce sub-20-nm or even sub-10-nm features. Future nanopatterning experiments on ultra-flat Au films on mica substrates might help to achieve even smaller features and to provide improvement of nanoscale feature resolution.^{34,35}

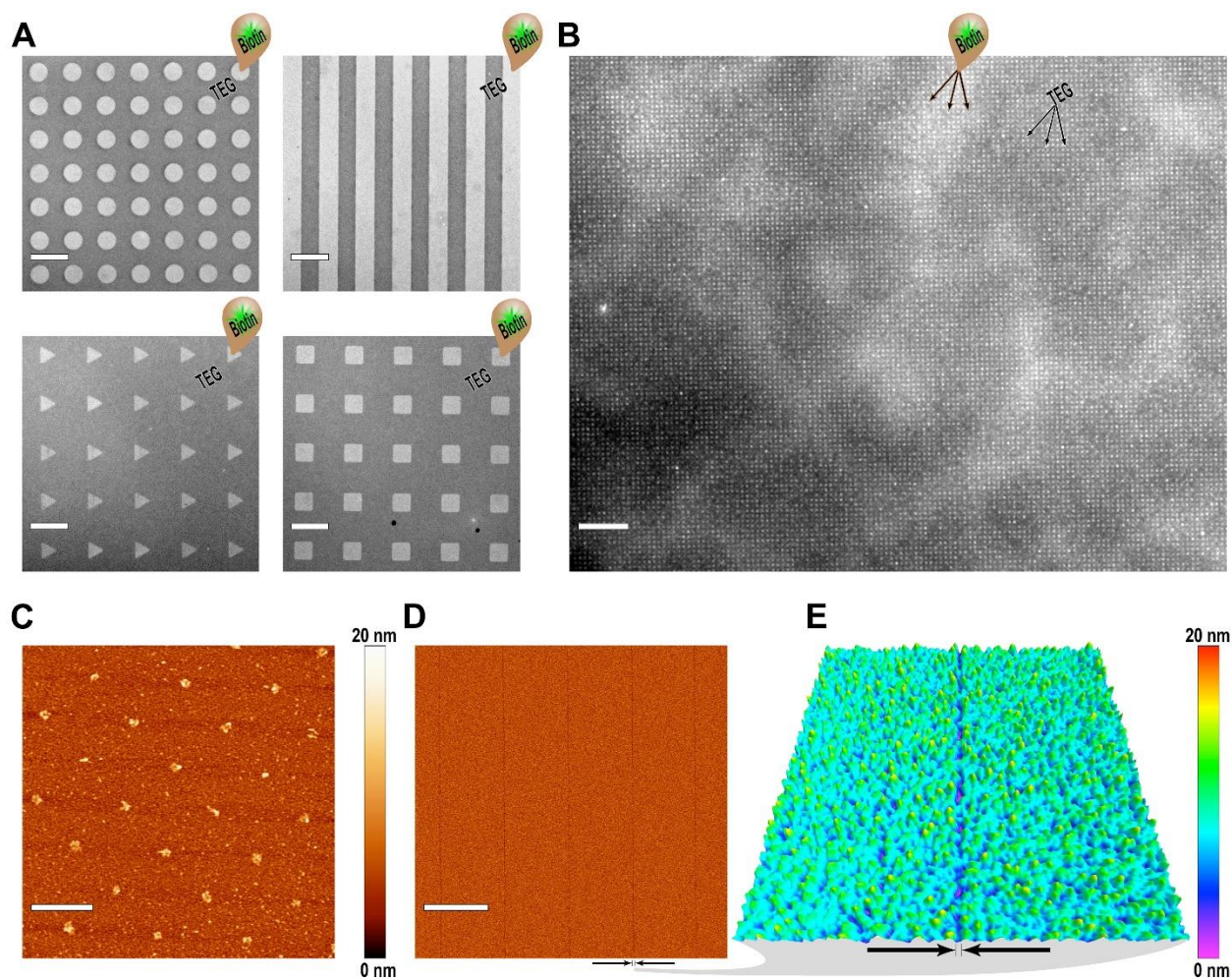


Figure 5-2. Representative images of streptavidin recognition on microscale and nanoscale biotin-patterned substrates. (A) Bright, microscale circular-, striped-, triangular-, or square-patterned regions or (B) nanoscale dots are visualized against dark surrounding hydroxyl-terminated tri(ethylene glycol)alkanethiol (TEG) backgrounds. Binding of streptavidin to surface-tethered biotin was visualized with fluorescein isothiocyanate (FITC)-labeled anti-streptavidin antibodies (excitation at 495 nm). Fluorescence images were recorded at an emission wavelength of 519 nm. (C) This atomic force microscopy (AFM) topography image shows an array of streptavidin-biotin nanodots. The dots are 215 ± 3 nm in diameter. In (D) and (E), AFM topographic images are of sub-30 nm wide lines on a streptavidin-biotin background, which are 26 ± 1 nm wide. The arrows help to show the locations of one line. Scale bars are 60 μm , 40 μm , 2 μm , and 3 μm for A, B, C, and D, respectively. Image dimension is 2 $\mu\text{m} \times 2 \mu\text{m}$ in E.

5.4.2 Multiplexed Substrates

Lift-off lithography was carried out on mixed 90/10 TEG/AEG SAMs and the remaining AEG tether molecules were functionalized with *L*-DOPA or *L*-5-HTP (Scheme 5-1). Afterwards, insertion of 90/10 TEG/BEG was carried out on functionalized post-lift-off substrates to create side-by-side biotin/*L*-DOPA or biotin/*L*-5-HTP bifunctional patterns (Figure 5-1B). The BEG or AEG molecules were in low abundance compared to TEG molecules to ensure dilution of surface-tethered *L*-DOPA, *L*-5-HTP, and biotin in the TEG background matrix. Mixed solutions of streptavidin and either anti-*L*-DOPA or anti-*L*-5-HTP primary antibodies were sorted *via* site-selective recognition of biotin *vs.* *L*-DOPA or biotin *vs.* *L*-5-HTP, respectively. Substrates were then exposed to mixed solutions of FITC-conjugated anti-streptavidin antibody and AlexaFluor® 546 secondary antibody for visualization of bound streptavidin and primary antibody bound to *L*-DOPA or *L*-5-HTP, respectively.

As shown in Figure 5-3A, at the fluorescence emission wavelength for FITC-conjugated anti-streptavidin antibody, bright wide channels (~75 μm) illustrate streptavidin-biotin recognition in stamp contact regions and in contrast to the dimmer narrow channels (~30 μm) where *L*-DOPA was functionalized in the non-contact areas. Conversely, in Figure 5-3B, at the fluorescence emission wavelength for AlexaFluor® 546 secondary antibody, bright narrow channels represent anti-*L*-DOPA antibody recognition of surface-functionalized *L*-DOPA against dim wide channels where biotin-captured streptavidin occurred.

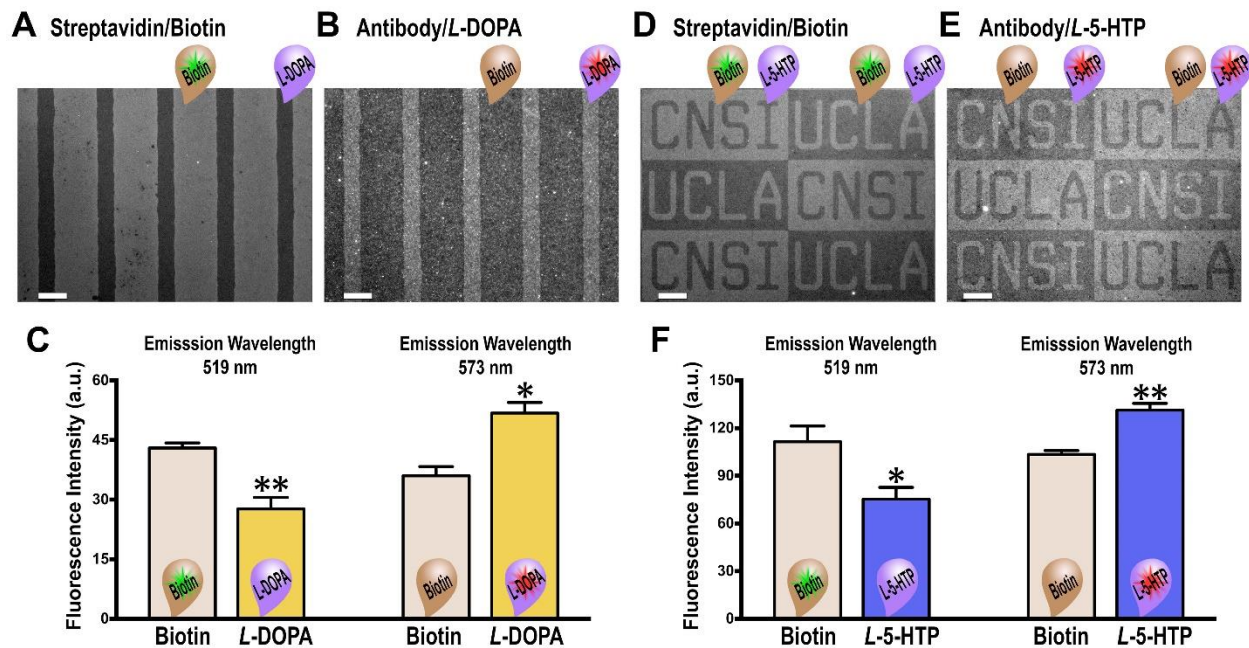


Figure 5-3. Target sorting on bifunctional substrates. Representative fluorescence images are shown for (A,B) biotin/*L*-DOPA and (D,E) biotin/*L*-5-HTP patterned substrates. Substrates were exposed to mixed solutions of streptavidin and anti-*L*-DOPA or anti-*L*-5-HTP primary antibodies followed by mixed fluorescein isothiocyanate (FITC)-conjugated anti-streptavidin antibodies (excitation at 495 nm) and AlexaFluor[®] 546 secondary antibodies (excitation at 556 nm), respectively. Substrates were then imaged at (A,D) 519 nm or (B,E) 573 nm emission wavelengths. In (C, left), significantly higher fluorescence intensities were measured in the wide-striped biotin-modified regions vs. the narrow-striped *L*-DOPA-modified regions [$t(4)=5$, $**P<0.01$] at the FITC emission wavelength. While in (C, right), higher fluorescence intensities were detected in the *L*-DOPA-modified narrow-striped regions vs. the wide-striped biotin-functionalized regions [$t(6)=3$, $*P<0.05$] at the AlexaFluor[®] 546 emission wavelength. Similarly, in (F, left), at the FITC emission wavelength, higher fluorescence intensities were observed within the UCLA letters and regions surrounding the CNSI letters [$t(4)=4$, $*P<0.05$], which were biotin-modified vs. surrounding the UCLA letters and within the CNSI letters, which were *L*-5-HTP-modified regions. In (F, right), opposite fluorescent intensity patterns were quantified at the AlexaFluor[®] 546 emission wavelength [$t(6)=6$, $**P<0.01$]. $N=3-4$ substrates per group. Scale bars are 50 μm .

Similarly, juxtaposed arrays of streptavidin-biotin and anti-*L*-5-HTP antibody/*L*-5-HTP fluorescence patterns are shown in Figure 5-3D and 5-3E, corresponding to the fluorescence wavelengths of FITC-conjugated anti-streptavidin antibody and AlexaFluor[®] 546 secondary antibody, respectively. Bright “UCLA” letters and bright regions surrounding the “CNSI” letters in Figure 5-3D represent streptavidin-biotin recognition. In contrast, the “CNSI” letters and bright areas surrounding the “UCLA” letters in Figure 5-3E represent anti-*L*-5HTP-antibody/*L*-5-HTP binding. Lack of fluorescence was observed when substrates were incubated with mixed solutions of FITC-conjugated anti-streptavidin antibody and AlexaFluor[®] 546 secondary antibody suggesting negligible nonspecific binding of the fluorescently labeled antibodies to bifunctional substrates (Figure 5-S2).

These results demonstrate that bifunctional small-molecule probe patterns produced *via* chemical lift-off lithography capture and sort large biomolecule targets from solution. Nonetheless, a few caveats need to be considered. Chemical lift-off has been shown to remove only 70% of TEG SAM molecules from Au substrates.²⁷⁻²⁸ Because Au-Au bonds are weaker than stamp/SAM and SAM/Au interactions, we used XPS to detect Au 4f signals resulting from the presence of underlying Au removed with TEG molecules. Here, lift-off lithography was carried out on mixed TEG/AEG SAMs. To test whether stamp contact also removes AEG molecules, we used flat PDMS stamps to carry out lift-off on AEG SAMs. Post-lift-off PDMS stamps from 100% AEG-modified Au substrates showed Au 4f XPS signals (Figure 5-S3A), indicating that AEG molecules are lift-able. Chemical lift-off experiments were also carried out on CH₃O-TEG SAMs, which were shown previously to be inert to chemical lift-off. The absence of Au 4f XPS peaks in Figure 5-S3B confirms that CH₃O-TEG molecules are not lift-able, in agreement with previous results.²⁷

Different tail groups (OH- in TEG vs NH₂- in AEG) and associated differences in intermolecular interactions between TEG and AEG molecules in mixed SAMs vs. each of these molecules in monocomponent SAMs might alter the lift-off yield for the SAMs used above. However, if we assume that lift-off removes ~70% of AEG molecules (similar to the lift-off yield for TEG molecules), a small percentage of AEG molecules will remain in the contact regions and these are expected to be functionalized with *L*-DOPA or *L*-5-HTP. This would result in a small amount of anti-*L*-DOPA or anti-*L*-5-HTP antibody binding in the lift-off regions, which are also functionalized with biotin, thereby reducing fluorescence contrast (and selectivity) between the contact and non-contact regions. Similarly, in the mono-functionalized substrates described above, small numbers of BEG molecules are expected to insert into native SAM defects in the non-contact regions reducing contrast between the lift-off and non-lift-off areas (Figure 5-1A).

In any case, sufficient contrast was observed for mono- and bifunctionalized substrates to yield convincing evidence of appropriate target sorting. Future work employing electrochemical reductive desorption will be useful to quantify surface-probe densities in the post-lift-off regions. This technique is sensitive to molecules with different functional groups and molecular interaction strengths causing various molecules to be desorbed at different electrochemical potentials.³⁶⁻³⁸ Moreover, substrates that also have adjacent regions devoid of small-molecule probes will enable relative specific and selective binding to be quantified to gain a better understanding of target behavior on bifunctionalized substrates.

Another caveat is with regard to the use of NHS/EDC coupling chemistry to tether *L*-DOPA or *L*-5-HTP to Au substrates. Here, possible side-product formation can occur so as to hydrolyze NHS-activated carboxylic acid groups on the tether molecules.^{39,40} This could result in

unreacted surface tethers having free carboxylate chain ends, which may contribute to nonspecific recognition by target proteins.^{41,42} The use of biotin pre-functionalized molecules, *i.e.*, BEG, circumvents potential disadvantages associated with on-chip surface coupling chemistries.

5.4.3 Capturing Native Membrane-Associated Receptors

Small-molecule *L*-5-HTP was singly patterned using lift-off lithography to investigate capture of native 5-HT_{1A} membrane-associated GPCRs. Because these receptors play critical roles in regulating serotonin neurotransmission in the central nervous system, they are pharmaceutical research targets for developing more effective treatments for neuropsychiatric disorders.⁴³⁻⁴⁵ In addition to conventional radioligand assays, recent efforts have been directed at using small-molecule-modified substrates to explore GPCR-ligand interactions and to screen for novel/artificial receptors.^{30,46,47} However, a common problem encountered with the latter approach is the size mismatch between small-molecule probes and GPCR binding partners due to the large size of the receptors themselves and the associated membrane fragments needed to stabilize native receptor conformations.^{14,26,31}

Several studies have shown that small-molecule probes require all epitopes to take part in receptor recognition.^{31,48,49} Previous studies from our group showed that the use of small-molecule precursors to neurotransmitters introduces an ectopic carboxyl group for surface tethering while preserving all epitopes essential for biorecognition.^{25,31} This strategy was combined with microcontact insertion printing or microfluidics to generate arrays of surface-tethered small molecules mimicking endogenous neurotransmitters to capture and to sort complex combination of GPCRs in mixed solutions.^{25-26,31}

Here, subtractive patterning was carried out on 95/5 TEG/AEG mixed SAMs. The AEG molecules were then functionalized with *L*-5-HTP, which is the biological precursor to the neurotransmitter serotonin, to investigate recognition by native human membrane-associated 5-HT_{1A} receptors isolated from transfected human embryonic kidney 293 cell lines.³¹ Anti-5-HT_{1A} receptor primary antibodies and AlexaFluor® 546-labeled secondary antibodies were used for visualizing receptor/*L*-5-HTP recognition patterns.

Mixed TEG/AEG SAMs were lifted-off and AEG molecules were functionalized with *L*-5-HTP. Fluorescent 5-HT_{1A} receptor/*L*-5HTP recognition patterns appear as bright non-lift-off areas surrounding arrays of dimmer lift-off square-shaped regions (Figure 5-4A). Fluorescence intensities in stamp-contact regions were significantly lower than in the non-contact regions (Figure 5-4B). Control experiments were carried out where similarly patterned substrates were

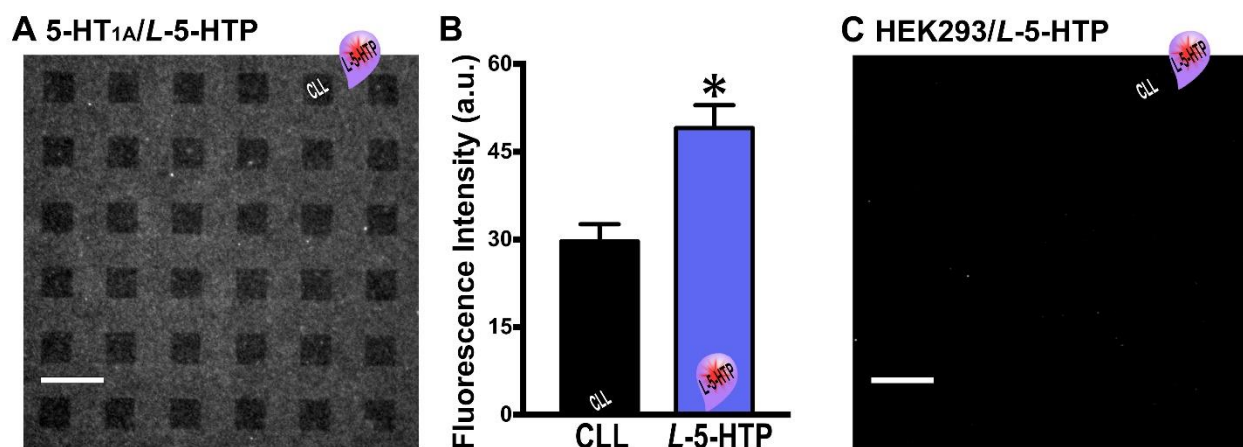


Figure 5-4. Native receptor capture. (A) Representative fluorescence image of an *L*-5-HTP-modified substrate exposed to HEK293 membranes from cells overexpressing 5-HT_{1A} receptors, anti-5-HT_{1A} receptor primary antibodies, and AlexaFluor® 546 secondary antibodies (excitation at 556 nm). (B) Mean fluorescence intensities were significantly different for stamp-contact vs noncontact regions [$t(4)=4, *P<0.05$]. Unobservable fluorescence in (C) suggests negligible nonspecific binding of primary and secondary antibodies to patterned substrates when 5-HT_{1A} receptors are not present in HEK293 cell membranes. Fluorescence images were recorded at an emission wavelength of 573 nm. $N=3$ substrates for each condition. Scale bars are 50 μ m.

exposed to HEK 293 cell membranes from untransfected cell lines not expressing 5-HT_{1A} receptors. Substrates were then incubated with anti-5-HT_{1A} receptor primary antibody and AlexaFluor[®] 546-labeled secondary antibody. Fluorescent patterns were not detectable (Figure 5-4C) indicating minimal nonspecific binding of HEK-cell-membranes to patterned *L*-5-HTP.

Overall, lift-off lithography appears to have some advantages for producing bifunctional substrates compared to our previous methods. For example, the need to carefully tune stamp surface properties so as to insert hydrophilic tether molecules *via* μ CIP is obviated.²⁵ Notably, a new class of defects, beyond the native SAM defects used in μ CIP, is created by lift-off. These additional defects enable greater numbers of tethers to be inserted and therefore, larger numbers of probes are conjugated to the patterned substrate regions. As such, specific binding of protein targets to patterned (or unpatterned regions) is maximized; sorting of protein targets to specific regions on bifunctionalized regions is also augmented. These improvements are evident even given the likely presence of small numbers of probes in non-target areas (Figure 5-1). When compared to the microfluidic approach, lift-off lithography avoids potential phase separation associated with solution deposition of multicomponent SAMs. The latter is hypothesized to contribute to the higher levels of nonspecific binding observed on bifunctional substrates patterned by microfluidics.²⁶

Nonetheless, chemical lift-off still requires successive ligand functionalization to produce multiplexed substrates. We are currently investigating overcoming this disadvantage *via* synthesis of tether molecules pre-functionalized with small-molecule probes. Advantages associated with pre-functionalized molecules, lift-off lithography, and microfluidics could then be combined to advance multiplexed biocapture surfaces further. Preformed 100% TEG SAMs

could be used for lift-off, in place of mixed SAMs, to avoid interference associated with remaining tether molecules in the lift-off regions. Microfluidics could then be used on post-lift-off substrates to insert multiple pre-functionalized molecules in parallel.

5.5 Conclusions and Prospects

Creating multiplexed substrates patterned with surface-tethered small-molecule probes to investigate target recognition for high-throughput affinity screening and biosensing is challenging. It requires the ability to place different bioactive small-molecules site-specifically on substrates and to capture and to sort targets from complex mixtures to the respective surface-tethered probes with low nonspecific binding to the background matrix and off-target probe regions. Here, we used subtractive patterning *via* chemical lift-off lithography to generate large-area micro- to nanoscale patterns of small-molecule probes. Notably, sub-30-nm biopatterning was feasible *via* a single lift-off step. Furthermore, small-molecule ligands were spatially encoded side-by-side on the same substrates to create multiplexed platforms such that protein/antibody binding partners were sorted to the correct probe locations from mixed protein solutions. Small molecules mimicking endogenous neurotransmitters patterned by lift-off lithography further enabled capture of native protein targets, *i.e.*, human 5-HT_{1A} membrane-associated receptors.

Ongoing efforts to optimize and to understand chemical lift-off lithography mechanistically (*e.g.*, precise lift-off yields), as well as to synthesize ligand pre-functionalized molecules for surface patterning are expected to improve specific binding and to circumvent shortcomings associated with tethers remaining in the lift-off regions. Generally, multiplexed patterning capabilities, the ability to produce sub-30-nm biopatterns, as well as recent fabrication of high-performance field-effect transistor-based biosensors *via* chemical lift-off lithography point to the versatility of this facile patterning method.^{1,50-52}

5.6 Supplementary Experiments and Figures

Experiments were carried out to investigate potential nonspecific binding associated with fluorescently tagged (secondary) antibodies, which may contribute to specific fluorescence signals arising from the binding of streptavidin or primary antibodies to biotin, 3,4-dihydroxy-*L*-phenylalanine (*L*-DOPA), or 5-hydroxy-*L*-tryptophan (*L*-5-HTP) functionalized substrates. These experiments were performed using the same procedures described in experimental sections in the main text with the exception that streptavidin and anti-*L*-DOPA/*L*-5-HTP primary antibodies were omitted. The results are shown in Figures 5-S1 and 5-S2.

X-ray photoelectron spectroscopy experiments were performed to investigate the removal of AEG molecules during chemical lift-off lithography. Flat, featureless PDMS stamps were used in place of patterned stamps to maximize the lift-off areas measured with XPS. Previously, the removal of TEG SAM molecules *via* lift-off lithography was determined by detecting Au 4f XPS signals resulting from Au atoms bound to the lifted-off alkanethiols on flat PDMS stamps.^{S1} Here, a similar process was carried out to determine whether AEG molecules could be removed with lift-off lithography (Figure 5-S3A). Control experiments were also performed on CH₃O-TEG SAMs (Figure 5-S3B), which were shown previously not to be amenable to chemical lift-off.

Table 5-S1. Visualization strategies for protein, antibody, and membrane-associated receptor binding to bioselective substrates.

Surface-Tethered Small-Molecule Probe	Protein Targets	Primary Antibodies	Secondary Antibodies
<i>L</i> -5-hydroxytryptophan (<i>L</i> -5-HTP)	Human 5-HT _{1A} R from HEK293 Cell Line N/A	Mouse Polyclonal Anti-5-HT _{1A} R Mouse Monoclonal Anti- <i>L</i> -5-HTP	AlexaFluor [®] 546 Goat Anti-Mouse IgG AlexaFluor [®] 546 Goat Anti-Mouse IgG
<i>L</i> -3,4-dihydroxyphenylalanine (<i>L</i> -DOPA)	N/A	Mouse Monoclonal Anti- <i>L</i> -DOPA	AlexaFluor [®] 546 Goat Anti-Mouse IgG
Biotin	Streptavidin	Rabbit Polyclonal FITC-Conjugated Anti-Streptavidin	N/A

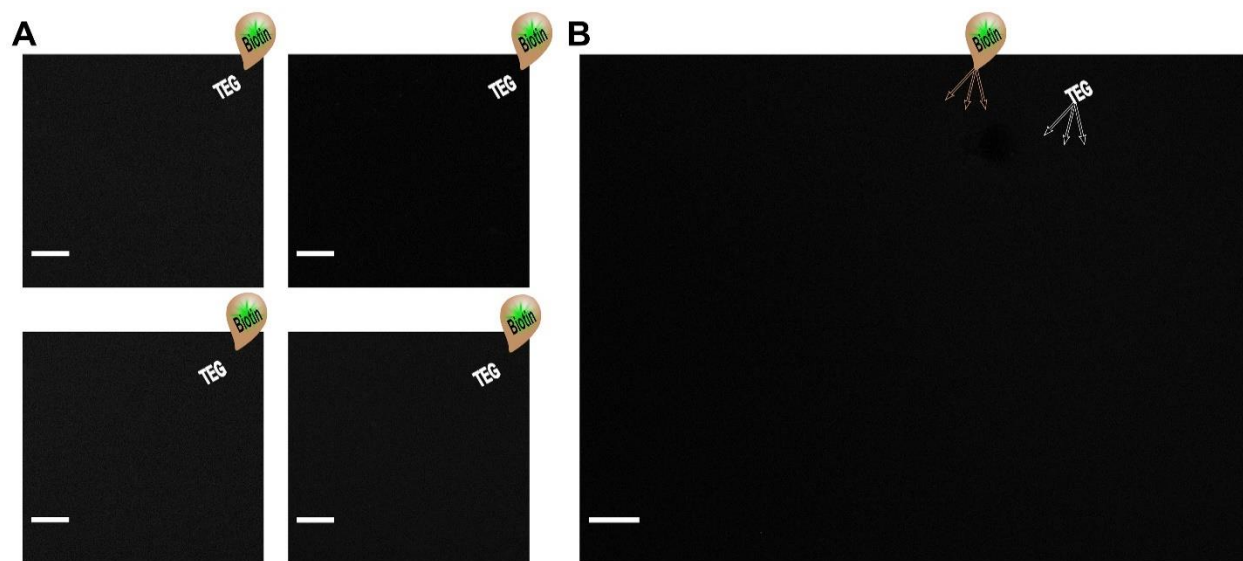


Figure 5-S1. Control experiments corresponding to Figure 5-2 in the main text. Representative fluorescence microscopy images showing nonspecific binding of fluorescein isothiocyanate (FITC)-conjugated anti-streptavidin antibodies (excitation at 495 nm) in the absence of streptavidin on (A) microscale and (B) nanoscale patterns of biotinylated hexa(ethylene glycol)undecanethiol-modified Au substrates. Undetectable fluorescence in all images indicates negligible nonspecific binding in the absence of streptavidin. Images were acquired at an emission wavelength of 519 nm. Scale bars are 60 μm in (A) and 40 μm in (B).

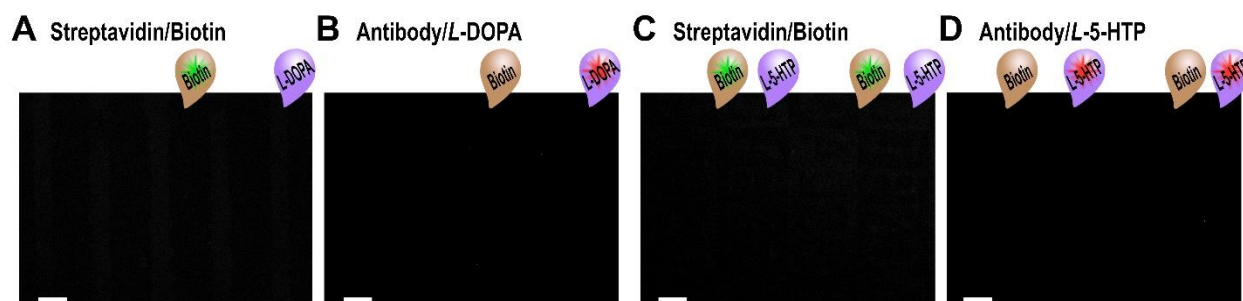


Figure 5-S2. Control experiments corresponding to Figure 5-3 in the main text. Representative fluorescence images displaying nonspecific binding from mixed solutions of fluorescein isothiocyanate (FITC)-conjugated anti-streptavidin antibody (excitation at 495 nm) and AlexaFluor 546[®] secondary antibody (excitation at 556 nm) in the absence of streptavidin, and anti-*L*-DOPA and anti-*L*-5-HTP primary antibodies on (A,B) biotin/*L*-DOPA and (C,D) biotin/*L*-5-HTP patterned surfaces. Substrates were imaged at emission wavelengths of 519 nm (A,C) or 573 nm (B,D). Negligible fluorescence signals were observed in all cases indicating minimal nonspecific binding of FITC-conjugated anti-streptavidin antibody or AlexaFluor 546[®] secondary antibody on the patterned substrates in the absence of streptavidin or primary antibodies. Scale bars are 50 μ m.

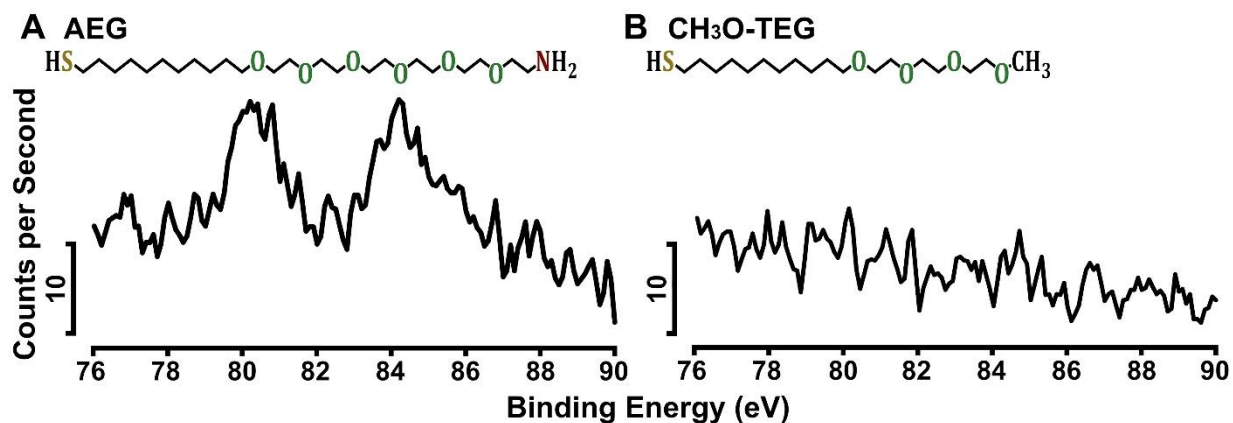


Figure 5-S3. Representative X-ray photoelectron spectroscopy (XPS) spectra of Au 4f peaks on flat, featureless PDMS stamps subjected to chemical lift-off on (A) (11-mercaptoundecyl) hexa(ethylene glycol)amine (AEG) and (B) (11-mercaptoundecyl) tri(ethylene glycol)methyl ether (CH₃O-TEG) self-assembled monolayers (SAMs). The presence of Au 4f XPS peaks in (A) at ~80 eV and 84 eV indicates that AEG molecules are amenable to chemical lift-off, while the absence of Au 4f XPS peaks in (B) shows that CH₃O-TEG molecules are inert to chemical lift-off.

5.7 References

1. MacBeath, G.; Koehler, A. N.; Schreiber, S. L., Printing Small Molecules as Microarrays and Detecting Protein-Ligand Interactions en Masse. *J. Am. Chem. Soc.* **1999**, *121*, 7967-7968.
2. LaFratta, C. N.; Walt, D. R., Very High Density Sensing Arrays. *Chem. Rev.* **2008**, *108*, 614-637.
3. Wittenberg, N. J.; Im, H.; Johnson, T. W.; Xu, X.; Warrington, A. E.; Rodriguez, M.; Oh, S.-H., Facile Assembly of Micro- and Nanoarrays for Sensing with Natural Cell Membranes. *ACS Nano* **2011**, *5*, 7555-7564.
4. Tu, S.; Jiang, H. W.; Liu, C. X.; Zhou, S. M.; Tao, S. C., Protein Microarrays for Studies of Drug Mechanisms and Biomarker Discovery in the Era of Systems Biology. *Curr. Pharm. Des.* **2014**, *20*, 49-55.
5. Fang, Y.; Frutos, A. G.; Lahiri, J., Membrane Protein Microarrays. *J. Am. Chem. Soc.* **2002**, *124*, 2394-2395.
6. Christman, K. L.; Enriquez-Rios, V. D.; Maynard, H. D., Nanopatterning Proteins and Peptides. *Soft Matter* **2006**, *2*, 928-939.
7. Wong, L. S.; Khan, F.; Micklefield, J., Selective Covalent Protein Immobilization: Strategies and Applications. *Chem. Rev.* **2009**, *109*, 4025-4053.
8. Fruh, V.; Ijzerman, A. P.; Siegal, G., How to Catch a Membrane Protein in Action: A Review of Functional Membrane Protein Immobilization Strategies and Their Applications. *Chem. Rev.* **2011**, *111*, 640-656.

9. Kwon, Y.; Han, Z.; Karatan, E.; Mrksich, M.; Kay, B. K., Antibody Arrays Prepared by Cutinase-Mediated Immobilization on Self-Assembled Monolayers. *Anal. Chem.* **2004**, *76*, 5713-5720.
10. Hodneland, C. D.; Lee, Y. S.; Min, D. H.; Mrksich, M., Selective Immobilization of Proteins to Self-Assembled Monolayers Presenting Active Site-Directed Capture Ligands. *Proc. Natl. Acad. Sci. U. S. A.* **2002**, *99*, 5048-5052.
11. Love, J. C.; Estroff, L. A.; Kriebel, J. K.; Nuzzo, R. G.; Whitesides, G. M., Self-Assembled Monolayers of Thiolates on Metals as a Form of Nanotechnology. *Chem. Rev.* **2005**, *105*, 1103-1169.
12. Wendeln, C.; Singh, I.; Rinnen, S.; Schulz, C.; Arlinghaus, H. F.; Burley, G. A.; Ravoo, B. J., Orthogonal, Metal-Free Surface Modification by Strain-Promoted Azide-Alkyne and Nitrile Oxide-Alkene/Alkyne Cycloadditions. *Chem. Sci.* **2012**, *3*, 2479-2484.
13. Nehilla, B. J.; Popat, K. C.; Vu, T. Q.; Chowdhury, S.; Standaert, R. F.; Pepperberg, D. R.; Desai, T. A., Neurotransmitter Analog Tethered to a Silicon Platform for Neuro-BioMEMS Applications. *Biotechnol. Bioeng.* **2004**, *87*, 669-674.
14. Vu, T. Q.; Chowdhury, S.; Muni, N. J.; Qian, H. H.; Standaert, R. F.; Pepperberg, D. R., Activation of Membrane Receptors by a Neurotransmitter Conjugate Designed for Surface Attachment. *Biomaterials* **2005**, *26*, 1895-1903.
15. Gussin, H. A.; Tomlinson, I. D.; Little, D. M.; Warnement, M. R.; Qian, H. H.; Rosenthal, S. J.; Pepperberg, D. R., Binding of Muscimol-Conjugated Quantum Dots to GABA_C Receptors. *J. Am. Chem. Soc.* **2006**, *128*, 15701-15713.

16. Shuster, M. J.; Vaish, A.; Szapacs, M. E.; Anderson, M. E.; Weiss, P. S.; Andrews, A. M., Biospecific Recognition of Tethered Small Molecules Diluted Is Self-Assembled Monolayers. *Adv. Mater.* **2008**, *20*, 164-167.
17. Claridge, S. A.; Schwartz, J. J.; Weiss, P. S., Electrons, Photons, and Force: Quantitative Single-Molecule Measurements from Physics to Biology. *ACS Nano* **2011**, *5*, 693-729.
18. Ganesan, R.; Kratz, K.; Lendlein, A., Multicomponent Protein Patterning of Material Surfaces. *J. Mater. Chem.* **2010**, *20*, 7322-7331.
19. Wendeln, C.; Rinnen, S.; Schulz, C.; Kaufmann, T.; Arlinghaus, H. F.; Ravoo, B. J., Rapid Preparation of Multifunctional Surfaces for Orthogonal Ligation by Microcontact Chemistry. *Chem. Eur. J.* **2012**, *18*, 5880-5888.
20. Wendeln, C.; Ravoo, B. J., Surface Patterning by Microcontact Chemistry. *Langmuir* **2012**, *28*, 5527-5538.
21. Bachas, L. G.; Meyerhoff, M. E., Theoretical-Models for Predicting the Effect of Bridging Group Recognition and Conjugate Substitution on Hapten Enzyme-Immunoassay Dose-Response Curves. *Anal. Biochem.* **1986**, *156*, 223-238.
22. Ishikawa, E.; Hashida, S.; Kohno, T., Development of Ultrasensitive Enzyme-Immunoassay Reviewed with Emphasis on Factors Which Limit the Sensitivity. *Mol. Cell. Probes* **1991**, *5*, 81-95.
23. Mullen, T. J.; Srinivasan, C.; Hohman, J. N.; Gillmor, S. D.; Shuster, M. J.; Horn, M. W.; Andrews, A. M.; Weiss, P. S., Microcontact Insertion Printing. *Appl. Phys. Lett.* **2007**, *90*, 063114.
24. Shuster, M. J.; Vaish, A.; Cao, H. H.; Guttentag, A. I.; McManigle, J. E.; Gibb, A. L.; Martinez, M. M.; Nezarati, R. M.; Hinds, J. M.; Liao, W.-S.; Weiss, P. S.; Andrews, A.

- M. Patterning Small-Molecule Biocapture Surfaces: Microcontact Insertion Printing vs. Photolithography. *Chem. Commun.* **2011**, 47, 10641-10643.
25. Vaish, A.; Shuster, M. J.; Cheunkar, S.; Weiss, P. S.; Andrews, A. M., Tuning Stamp Surface Energy for Soft Lithography of Polar Molecules to Fabricate Bioactive Small-Molecule Microarrays. *Small* **2011**, 7, 1471-1479.
26. Liao, W. S.; Cao, H. H.; Cheunkar, S.; Shuster, M. J.; Altieri, S. C.; Weiss, P. S.; Andrews, A. M., Small-Molecule Arrays for Sorting G-Protein-Coupled Receptors. *J. Phys. Chem. C* **2013**, 117, 22362-22368.
27. Liao, W.-S.; Cheunkar, S.; Cao, H. H.; Bednar, H. R.; Weiss, P. S.; Andrews, A. M., Subtractive Patterning *via* Chemical Lift-Off Lithography. *Science* **2012**, 337, 1517-1521.
28. Cao, H. H.; Nakatsuka, N.; Serino, A. C.; Liao, W.-S.; Cheunkar, S.; Yang, H.; Weiss, P. S.; Andrews, A. M., Controlled DNA Patterning by Chemical Lift-Off Lithography: Matrix Matters. *ACS Nano* **2015**, 9, 11439-11454.
29. Horcas, I.; Fernández, R.; Gómez-Rodríguez, J. M.; Colchero, J.; Gómez-Herrero, J.; Baro, A. M., WSXM: A Software for Scanning Probe Microscopy and a Tool for Nanotechnology. *Rev. Sci. Instrum.* **2007**, 78, 013705.
30. Hong, Y. L.; Webb, B. L.; Su, H.; Mozdy, E. J.; Fang, Y.; Wu, Q.; Liu, L.; Beck, J.; Ferrie, A. M.; Raghavan, S.; Mauro, J.; Carre, A.; Mueller, D.; Lai, F.; Rasnow, B.; Johnson, M.; Min, H. S.; Salon, J.; Lahiri, J. Functional GPCR Microarrays. *J. Am. Chem. Soc.* **2005**, 127, 15350-15351.
31. Vaish, A.; Shuster, M. J.; Cheunkar, S.; Singh, Y. S.; Weiss, P. S.; Andrews, A. M., Native Serotonin Membrane Receptors Recognize 5-Hydroxytryptophan-Functionalized

- Substrates: Enabling Small-Molecule Recognition. *ACS Chem. Neurosci.* **2010**, *1*, 495-504.
32. Melo, L. L.; Vaz, A. R.; Salvadori, M. C.; Cattani, M., Grain Sizes and Surface Roughness in Platinum and Gold Thin Films. *J. Metastable and Nanocrystalline Mater.* **2004**, *20-21*, 623-628.
33. Salvadori, M. C.; Melo, L. L.; Vaz, A. R.; Wiederkehr, R. S.; Teixeira, F. S.; Cattani, M., Platinum and Gold Thin Films Deposited by Filtered Vacuum Arc: Morphological and Crystallographic Grain Sizes. *Surf. Coat. Technol.* **2006**, *200*, 2965-2969.
34. Ruffino, F.; Torrisi, V.; Marletta, G.; Grimaldi, M. G., Atomic Force Microscopy Investigation of the Kinetic Growth Mechanisms of Sputtered Nanostructured Au Film on Mica: Towards a Nanoscale Morphology Control. *Nanoscale Res. Lett.* **2011**, *6*, 1-13.
35. Diebel, J.; Lowe, H.; Samori, P.; Rabe, J. P., Fabrication of Large-Scale Ultra-Smooth Metal Surfaces by a Replica Technique. *Appl. Phys. A: Mater. Sci. Process.* **2001**, *73*, 273-279.
36. Mullen, T. J.; Dameron, A. A.; Weiss, P. S., Directed Assembly and Separation of Self-Assembled Monolayers via Electrochemical Processing. *J. Phys. Chem. B* **2006**, *110*, 14410-14417.
37. Dameron, A. A.; Mullen, T. J.; Hengstebeck, R. W.; Saavedra, H. M.; Weiss, P. S., Origins of Displacement in 1-Adamantanethiolate Self-Assembled Monolayers. *J. Phys. Chem. C* **2007**, *111*, 6747-6752.
38. Kim, M.; Hohman, J. N.; Serino, A. C.; Weiss, P. S., Structural Manipulation of Hydrogen-Bonding Networks in Amide-Containing Alkanethiolate Monolayers via Electrochemical Processing. *J. Phys. Chem. C* **2010**, *114*, 19744-19751.

39. Xia, N.; Xing, Y.; Wang, G. F.; Feng, Q. Q.; Chen, Q. Q.; Feng, H. M.; Sun, X. L.; Liu, L., Probing of EDC/NHSS-Mediated Covalent Coupling Reaction by the Immobilization of Electrochemically Active Biomolecules. *Int. J. Electrochem. Sci.* **2013**, *8*, 2459-2467.
40. Sam, S.; Touahir, L.; Andresa, J. S.; Allongue, P.; Chazalviel, J. N.; Gouget-Laemmel, A. C.; de Villeneuve, C. H.; Moraillon, A.; Ozanam, F.; Gabouze, N.; Djebbar, S. Semiquantitative Study of the EDC/NHS Activation of Acid Terminal Groups at Modified Porous Silicon Surfaces. *Langmuir* **2010**, *26*, 809-814.
41. Sigal, G. B.; Bamdad, C.; Barberis, A.; Strominger, J.; Whitesides, G. M., A Self-Assembled Monolayer for the Binding and Study of Histidine Tagged Proteins by Surface Plasmon Resonance. *Anal. Chem.* **1996**, *68*, 490-497.
42. Lahiri, J.; Isaacs, L.; Tien, J.; Whitesides, G. M., A Strategy for the Generation of Surfaces Presenting Ligands for Studies of Binding Based on an Active Ester as a Common Reactive Intermediate: A Surface Plasmon Resonance Study. *Anal. Chem.* **1999**, *71*, 777-790.
43. Catapano, L. A.; Manji, H. K., G Protein-Coupled Receptors in Major Psychiatric Disorders. *Biochim. Biophys. Acta, Biomembr.* **2007**, *1768*, 976-993.
44. Richardson-Jones, J. W.; Craige, C. P.; Nguyen, T. H.; Kung, H. F.; Gardier, A. M.; Dranovsky, A.; David, D. J.; Guiard, B. P.; Beck, S. G.; Hen, R.; Leonardo, E. D. Serotonin-1A Autoreceptors Are Necessary and Sufficient for the Normal Formation of Circuits Underlying Innate Anxiety. *J. Neurosci.* **2011**, *31*, 6008-6018.
45. Altieri, S. C.; Garcia-Garcia, A. L.; Leonardo, E. D.; Andrews, A. M. Rethinking 5-HT_{1A} Receptors: Emerging Modes of Inhibitory Feedback of Relevance to Emotion-Related Behavior. *ACS Chem. Neurosci.* **2013**, *4*, 72-83.

46. Fang, Y.; Peng, J. L.; Ferrie, A. M.; Burkhalter, R. S., Air-Stable G Protein-Coupled Receptor Microarrays and Ligand Binding Characteristics. *Anal. Chem.* **2006**, *78*, 149-155.
47. Navratilova, I.; Besnard, J.; Hopkins, A. L., Screening for GPCR Ligands Using Surface Plasmon Resonance. *ACS Med. Chem. Lett.* **2011**, *2*, 549-554.
48. Seeber, M.; De Benedetti, P. G.; Fanelli, F., Molecular Dynamics Simulations of the Ligand-Induced Chemical Information Transfer in the 5-HT_{1A} Receptor. *J. Chem. Inf. Comput. Sci.* **2003**, *43*, 1520-1531.
49. Congreve, M.; Langmead, C. J.; Mason, J. S.; Marshall, F. H., Progress in Structure Based Drug Design for G Protein-Coupled Receptors. *J. Med. Chem.* **2011**, *54*, 4283-4311.
50. Lueking, A.; Horn, M.; Eickhoff, H.; Bussow, K.; Lehrach, H.; Walter, G., Protein Microarrays for Gene Expression and Antibody Screening. *Anal. Biochem.* **1999**, *270*, 103-111.
51. Mishina, Y. M.; Wilson, C. J.; Bruett, L.; Smith, J. J.; Stoop-Myer, C.; Jong, S.; Amaral, L. P.; Pedersen, R.; Lyman, S. K.; Myer, V. E.; Kreider, B. L.; Thompson, C. M. Multiplex GPCR Assay in Reverse Transfection Cell Microarrays. *J. Biomol. Screen.* **2004**, *9*, 196-207.
52. Cao, C.; Zhang, J.; Wen, X.; Dodson, S. L.; Dao, N. T.; Wong, L. M.; Wang, S.; Li, S.; Phan, A. T.; Xiong, Q., Metamaterials-Based Label-Free Nanosensor for Conformation and Affinity Biosensing. *ACS Nano* **2013**, *7*, 7583-7591.

Reference for Supporting Materials

S1. Liao, W. S.; Cheunkar, S.; Cao, H. H.; Bednar, H. R.; Weiss, P. S.; Andrews, A. M.

Subtractive patterning *via* chemical lift-off lithography. *Science* **2012**, *337*, 1517-1521.

Chapter 6

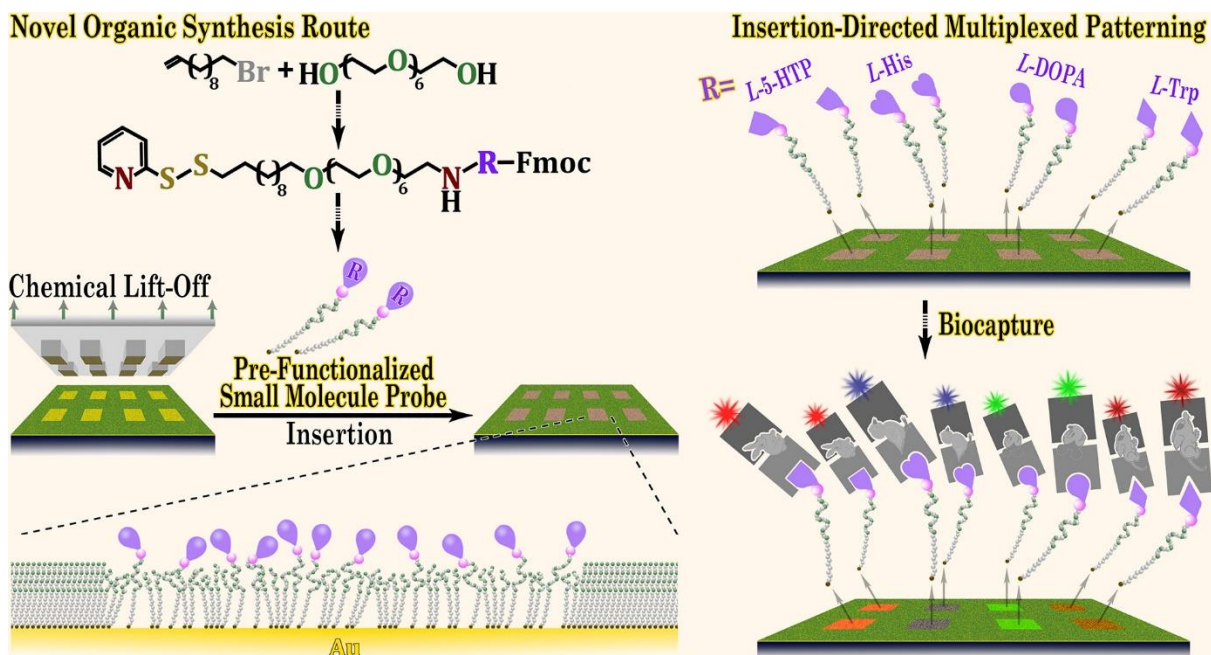
Enabling Multiplexed Small-Molecule Patterning *via* Pre-Functionalized Alkanethiols

The information in the chapter is in preparation for submission

and is reproduced in its entirety here.

Authors: Cao, H. H.; Deshayes, S.; Nakatsuka, N.; Yang, H.; Weiss, P. S.;

Kasko, A. M.; Andrews, A. M.



6.1 Abstract

Specific interactions between small molecules and biomolecules are important physiologically and for biosensing, diagnostic, and therapeutic applications. Small-molecules can be tethered to substrates through standard coupling chemistries. While convenient, these approaches mask one or more of the few small-molecule functional groups available for biorecognition. Moreover, for multiplexing, individual probes often require different surface functionalization chemistries and/or protection/deprotection strategies. Thus, when placing multiple probes on surfaces, functionalization chemistries need to be identified that preserve all functional groups and are sequentially compatible. Alternately, we demonstrate high-fidelity multiplexed surface patterning by coupling small-molecule neurotransmitter precursors to monodisperse oligo(ethylene glycol)alkyl disulfides during synthesis and *prior* to self-assembly on Au substrates. Chemical lift-off lithography was used to pattern multiplexed neurotransmitter-modified substrates. Pre-functionalized molecules exhibited improved antibody recognition and

specific binding compared to approaches where small-molecule neurotransmitters were functionalized to alkanethiols *after* surface assembly. Monoclonal but not polyclonal antibodies selectively differentiated pre-functionalized surface-tethered neurotransmitters from structurally related molecules that differed by as little as a hydroxyl group. These findings demonstrate that functionalization approaches that circumvent the need to devise sequential probe surface conjugation chemistries enable biomolecule recognition and reveal poor specificity of some types of biomolecule binding partners.

6.2 Introduction

Small-molecule interactions with large biomolecules are the primary *modus operandi* in many biosensing applications and high-throughput screening strategies.^{1,2} Because one of the partners needs to be tethered to a substrate to detect and to quantify molecular recognition by the other partner, a key obstacle is optimizing substrate-functionalization. Most often, large biomolecules are immobilized on substrates using a variety of strategies including liposome-based attachment, electrostatic interactions, or biotin-streptavidin linkage for molecular recognition by other biomolecule- or small-molecule-binding partners.³⁻¹⁰ Less often employed, yet no less important, is the reverse strategy wherein small-molecule probes are tethered to substrates to capture large biomolecule targets.^{11,12}

For over a decade, we have investigated the design rules for optimizing small-molecule surface tethering.¹³⁻¹⁸ We discovered that stochastic patterning at the molecular level *via* insertion-directed self-assembly is advantageous for spacing small molecules on substrates so that large biomolecule partners have ample access for binding.^{13,16,18} Others and we also found that controlling surface chemistries to reduce nonspecific substrate interactions is an important factor.^{15,16,19,20} We further demonstrated that linking chemistries employing ectopic functional groups to preserve small molecule functionality are tantamount to appropriate biomolecule recognition.^{14,16}

We have also invested in developing easily adoptable chemical patterning methods for substrates.^{14,15,21,22} Patterning enables relative binding between small-molecule-functionalized and unfunctionalized regions to be interrogated side-by-side on the same substrate. We have developed and utilized μ CIP to pattern small-molecule neurotransmitters within SAMs.^{15,16} Recently, we learned that by carefully controlling the surface chemistry of PDMS stamps, we

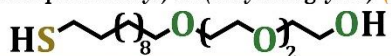
could insertion-print alkanethiol inks ranging in hydrophilicity.¹⁷ Moreover, we discovered that complete oxidation of PDMS stamps to produce highly hydrophilic stamp surfaces results in covalent interactions with hydroxyl-terminated SAM-modified substrates in the contact areas.²³ As a result, releasing stamps from substrates removes SAM molecules and a thin layer of Au substrate atoms leaving the exposed underlying Au available for self-assembly of different molecules. Using this lift-off lithography method, we generated streptavidin-recognition patterns on biotin-terminated SAM-modified substrates.²³

Previously, we attempted to fabricate multiplexed patterned substrates decorated with multiple small-molecule neurotransmitters¹⁵ to screen for high-affinity artificial molecular receptors, which can be used as recognition elements in biosensing applications.²⁴⁻²⁷ Multiplexed platforms are advantageous for investigating specific binding of target receptors to probe molecules in the context of cross-reactivity to similarly structured nontarget (interferent) molecules. However, initial attempts at using μ CIP to create multiplexed substrates suffered from the need to devise compatible successive small-molecule functionalization chemistries. This limitation is unavoidable when using μ CIP because this technique requires sequential insertion-directed patterning of tethering molecules in association with serial small-molecule functionalization steps. To circumvent this limitation, we employed microfluidics to generate small-molecule neurotransmitter arrays followed by sorting of mixtures of antibodies or native membrane-associated receptors to their cognate small-molecule partners.¹⁴ Because the latter approach physically restricts small-molecule functionalization to individual microfluidic channels, multiple neurotransmitters could be tethered to substrates using the same functionalization chemistries.

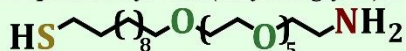
Although oligo(ethylene glycol) moieties were employed to reduce nonspecific substrate-biomolecule interactions and microfluidics were used to circumvent problems associated with sequential ligand functionalization, significant cross-reactivity (~30%) of biomolecules to nontarget probes was still observed.¹⁴ Control experiments revealed that cross-reactivity might stem from a lack of specificity of the biomolecules themselves. Specifically, we found that the primary antibodies used to label captured membrane-associated receptors also displayed nonspecific recognition of the surface-tethered small-molecule probes. Furthermore, recent studies suggest that surface conjugation chemistries (*e.g.*, NHS-EDC coupling chemistry) used to link small-molecule probes to tethering molecules on-chip suffer from the formation of side products and incomplete functionalization.²⁸⁻³⁰ These shortcomings likely contribute to the cross-reactivity to nontarget molecules that we observed.

In short, a better approach enabling functionalization with small-molecule probes is needed to produce multiply patterned substrates. Here, we generated a library of monodisperse oligo(ethylene glycol) alkyl pyridyl disulfide molecules pre-functionalized with small-molecule amino acids including *L*-histidine (*L*-HD), *L*-3,4-dihydroxyphenylalanine (*L*-DOPA), *L*-threo-3,4-dihydroxyphenylserine (*L*-DOPS), *L*-5-hydroxytryptophan (*L*-5-HTP), and *L*-tryptophan (*L*-Trp) (Scheme 6-1). The synthesis procedure is shown in Scheme 6-2. Because these novel molecules are conjugated with small-molecule probes *prior* to surface assembly, the need to devise compatible serial functionalization chemistries and to optimize reaction conditions for each probe on-chip was obviated.

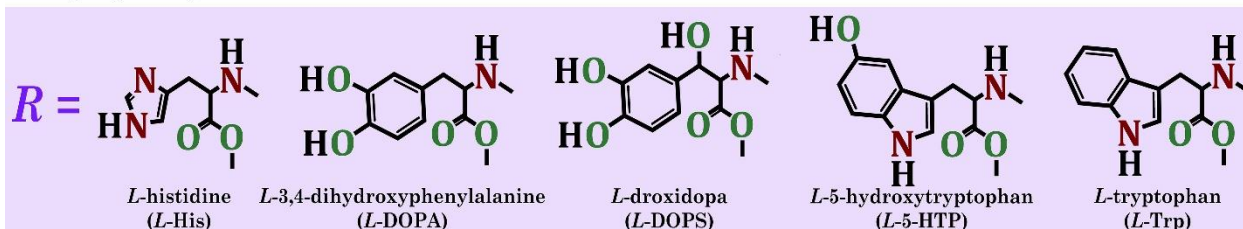
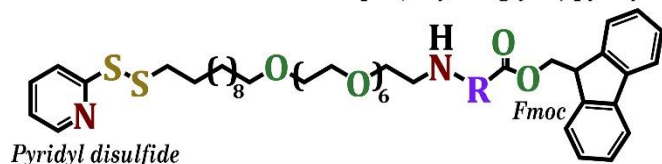
(11-Mercaptoundecyl) tri(ethylene glycol) (TEG)



11-Mercaptoundecyl hexa(ethylene glycol)amine (AEG)



Fmoc-neurotransmitter-terminated hepta(ethylene glycol) pyridyl disulfide (Fmoc-R-7EG-PDS)

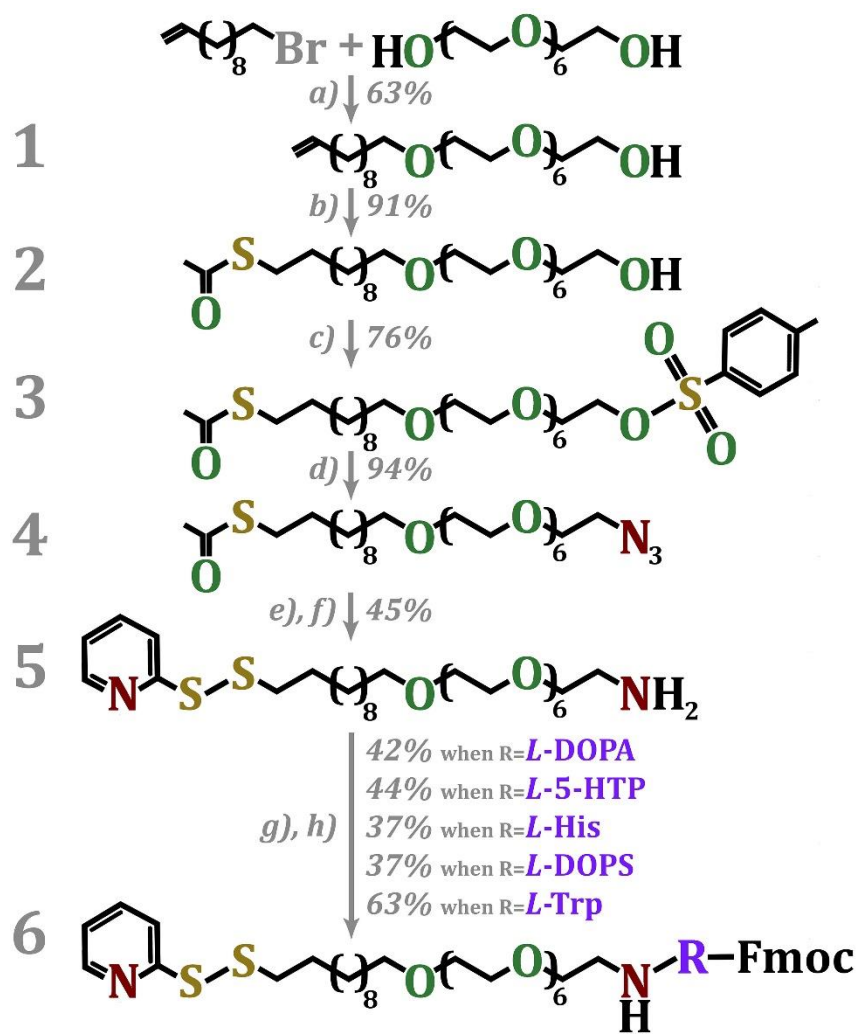


Scheme 6-1. Alkanethiols and neurotransmitter precursors. Neurotransmitter pre-functionalized molecules consist of pyridyl disulfide head groups for self-assembly on Au surfaces, oligo(ethylene glycol)undecyl backbones for resisting nonspecific binding of biomolecule targets, neurotransmitter tail groups for biomolecule capture, and 9-fluorenylmethyloxycarbonyl groups (Fmoc) for protecting the amino moieties of neurotransmitters during synthesis and self-assembly. The carboxyl groups of the amino acid precursors are linked to oligo(ethylene glycol)undecyl backbones *via* amide bonds.

With the exception of *L*-Trp, the small-molecule probes investigated are precursors to biogenic monoamine neurotransmitters having a biologically important primary amino motif needed for native receptor recognition.^{16,31,32} In our early studies, we directly ligated neurotransmitters to substrates *via* this amino group and observed antibody capture.^{13,18} In this arrangement, the amino motif was largely unavailable for recognition.^{13,14,16} However, by using the native amino acid precursors in Scheme 6-1, instead of the neurotransmitters themselves, we introduced an ectopic carboxyl moiety for surface tethering thereby preserving the amine moiety for biorecognition. We demonstrated that substrates functionalized with neurotransmitter precursors mimicked biologically active neurotransmitters and showed selective molecular recognition of the corresponding native membrane-associated receptors.^{14,16} Henceforth, we refer to these mimicking precursors as neurotransmitters (unless otherwise noted).

Herein, we used chemical lift-off lithography to generate patterned substrates modified with pre-functionalized or post-functionalized molecules.²³ (We refer to tethers pre-functionalized with neurotransmitters prior to self-assembly as “pre-functionalized molecules” and tethers that are first self-assembled and then functionalized with neurotransmitters as “post-functionalized molecules.”) Fluorescence microscopy was used to visualize antibody recognition of probes on substrates. Pre-functionalized molecules displayed consistent antibody recognition and equivalent (*e.g.*, *L*-DOPA) or improved specific binding (*e.g.*, *L*-5-HTP) compared to the post-functionalization approach. Double lift-off lithography was used to generate multiplexed substrates. We found that while monoclonal antibodies showed selective recognition of different surface-tethered pre-functionalized neurotransmitters, cross-reactivity occurred with polyclonal antibodies.³³ Thus, by controlling the surface conditions and chemistries of multiplexed biocapture platforms, biomolecule partners with high specificity for small-molecule probes can

be differentiated.^{34,35} We anticipate that the use of the pre-functionalized molecules developed here will enable identification of high-affinity artificial receptors targeting small-molecule neurotransmitters for use in biosensing applications.³⁵⁻³⁷



Scheme 6-2. Synthesis of Fmoc-neurotransmitter-7EG-pyridyl disulfide (Fmoc-R-7EG-PDS) compounds. **a)** 50% NaOH, 100 °C, 24 h; **b)** CH₃COSH, AIBN, MeOH, UV, 48 h, room temperature; **c)** TsCl, TEA, DCM, 24 h, room temperature; **d)** NaN₃, EtOH, 12 h, 85 °C; **e)** PH₃P, THF, 24 h, room temperature; **f)** 2-PDS, MeOH, 72 h, room temperature; **g)** Fmoc-NT, DIEA, HOBt, EDC, DCM (and/or DMF), 24 h, room temperature; and **h)** only for *L*-Trp and *L*-His, 20% TFA in DCM, 1 h, room temperature. Typical yields for each step are shown next to the arrows.

6.3 Materials and Methods

Materials. The Au films (100-nm-thick overlaying 10-nm-thick titanium adhesive layers) on silicon substrates were purchased from Platypus Technologies (Madison, WI, USA). The (11-mercaptopundecyl) tri(ethylene glycol) (TEG) was purchased from Toronto Research Chemicals Inc. (Toronto, ON, Canada). The (11-mercaptopundecyl) hexa(ethylene glycol)amine (AEG) was purchased from ProChimia Surfaces (Sopot, Poland). Threo-3,4-dihydroxyphenylserine (*L*-DOPS or *L*-droxidopa) was purchased from TCI America Inc. (Portland, OR, USA). Fluorenylmethyloxycarbonyl chloride (Fmoc-Cl) was purchased from Oakwood Products (West Columbia, SC, USA). Sodium carbonate (Na_2CO_3) was purchased from Fisher Scientific. Dichloromethane (DCM) was purchased from Fisher Scientific and was distilled over calcium hydride. 9-Fluorenylmethyloxycarbonyl-*L*-3,4-dihydroxyphenylalanine (Fmoc-*L*-DOPA-OH), 9-fluorenylmethyloxycarbonyl-5-hydroxy-*L*-tryptophan (Fmoc-*L*-5-HTP-OH), and *N*- α -(9-fluorenylmethyloxycarbonyl)-*N*-im-trityl-*L*-histidine (Fmoc-*L*-His(Trt)-OH) were purchased from AnaSpec-Eurogentec (Fremont, CA, USA). The *N*- α -(9-fluorenylmethyloxycarbonyl)-*N*-in-*tert*-butyloxycarbonyl-*L*-tryptophan (Fmoc-*L*-Trp(Boc)-OH) and hepta(ethylene glycol) molecules were purchased from ChemPep Inc. (Wellington, FL, USA). 11-Bromo-1-undecene, thioacetic acid (CH_3COSH), triethylamine (TEA), triphenylphosphine (Ph_3P), and *N,N*-diisopropylethylamine (DIEA) were purchased from Alfa Aesar (Ward Hill, MA, USA). *N*-Hydroxysuccinimide (NHS), *N*-(3-dimethylaminopropyl)-*N'*-ethylcarbodiimide hydrochloride (EDC), *N,N*-dimethylformamide (DMF), 4-methylpiperidine, bovine serum albumin (BSA), 0.01 M phosphate buffered saline (PBS) ([NaCl]=138 mM, [KCl]=2.7 mM, pH 7.4), and azobisisobutyronitrile (AIBN) were purchased from Sigma-Aldrich (St. Louis, MO, USA). 4-Toluenesulfonyl chloride (TsCl), 2,2'-dithiodipyridine (2-PDS),

ammonia (7 N in MeOH), and trifluoroacetic acid (TFA) were from Acros Organics (Geel, Belgium). Anhydrous tetrahydrofuran (THF), anhydrous methanol (MeOH), and sodium azide (NaN₃) were obtained from EMD Chemicals (Gibbstown, NJ, USA). Hydroxybenzotriazole (HOBt) was purchased from CreoSalus Inc. (Louisville, KY, USA). SYLGARD[®] 184 silicone elastomer kits were from Ellsworth Adhesives (Germantown, WI, USA). Absolute (200 proof) ethanol (EtOH) was purchased from Decon Laboratories, Inc. (King of Prussia, PA, USA). Deionized water (~18 MΩ) was obtained from a Millipore water purifier (Billerica, MA, USA).

Mouse monoclonal anti-*L*-3,4-dihydroxyphenylalanine antibody (ascites), rabbit polyclonal anti-*L*-5-hydroxytryptophan antibody (whole antiserum), rabbit polyclonal anti-*L*-histidine antibody (whole antiserum), and rat polyclonal anti-*L*-tryptophan antibody (pre-adsorbed antiserum) were purchased from Abcam Inc. (Cambridge, MA, USA). AlexaFluor[®] 546 goat anti-rabbit IgG (H+L) highly cross-adsorbed antibody (2 mg/mL), AlexaFluor[®] 568 goat anti-rat IgG (H+L) antibody (2 mg/mL), AlexaFluor[®] 488 goat anti-rabbit IgG (H+L) antibody (2 mg/mL), and AlexaFluor[®] 488 goat anti-mouse IgG (H+L) highly cross-adsorbed antibody (2 mg/mL) were purchased from Invitrogen (Carlsbad, CA, USA). All primary and secondary antibodies were diluted 1:200 and 1:100, respectively, with 0.01 M PBS pH 7.4 prior to incubation with substrates unless stated otherwise.

Synthesis of Pre-Functionalized Molecules. Pre-functionalized molecules contained monodisperse hepta(ethylene glycol) undecyl backbones (7EG) for resisting nonspecific protein binding, 9-fluorenylmethoxycarbonyl-protected neurotransmitters (Fmoc-R) for biomolecule capture, and pyridyl disulfides (PDS) as thiol protecting groups and for self-assembly on Au substrates (Scheme 6-1). Each of the neurotransmitter functionalized 7EG-pyridyl disulfides was synthesized according to Scheme 6-2.

Hepta(ethylene glycol) was monoetherified with 11-bromo-1-undecene. A large excess of hepta(ethylene glycol) was used to favor monosubstitution,³⁸ whereas a stoichiometric equivalent of both reagents generally yielded a statistical proportion of unmodified, mono-, and disubstituted molecules. Monoetherification was successfully achieved according to an established protocol³⁹ using a three-fold excess of hepta(ethylene glycol) compared to 11-bromo-1-undecene with a slight excess of 50% sodium hydroxide to give compound **1** in 63% yield. Next, the terminal olefin underwent a photoinitiated thiol-ene reaction with thioacetic acid in the presence of azobisisobutyronitrile (AIBN) to give compound **2** in good yield (91%). The terminal alcohol was then converted to a tosylate leaving group (compound **3**), which was subsequently reacted with sodium azide to provide compound **4** with a yield of 94%. The terminal azide group was reduced to a primary amine using triphenylphosphine, which also cleaved the thioacetate. The resulting free thiol was then protected with 2,2'-dithiodipyridine to give compound **5** with an overall yield of 45%.

The pyridyl disulfide moieties protected thiols from dimerization and other side reactions during the neurotransmitter coupling procedures. Pyridyl disulfides were selected because of their selectivity toward thiols and their reactivity to Au surfaces.⁴⁰ Finally, the terminal amine was coupled to Fmoc-R to form an amide bond using standard coupling agents (hydroxybenzotriazole (HOBt) and EDC in the presence of *N,N*-diisopropylethylamine, DIEA). The side-chain protecting groups of *L*-His and *L*-Trp, trityl (Trt) and *tert*-butyloxycarbonyl (Boc) groups, respectively, were removed with 20% trifluoroacetic acid (TFA) in dichloromethane (DCM). The final pre-functionalized molecules (Fmoc-NT-AEG-PDS) were obtained in 37-63% yield depending on the neurotransmitter R-group. Detailed synthesis information can be found in the first section of the Supporting Information.

Substrate Preparation and Stamp Fabrication. The Au substrates were hydrogen-flame annealed. They were then immersed in ethanolic solutions of 0.5 mM TEG for ~18 h to enable SAM formation. Substrates modified with TEG SAMs were rinsed thoroughly with ethanol and blown dry with nitrogen gas. The PDMS stamps were prepared by thoroughly mixing a 10:1 mass ratio of SYLGARD® 184 silicone elastomer base and curing agent, respectively, in a plastic cup. Mixtures were degassed under vacuum until all bubbles were removed and cast onto photolithography-fabricated silicon master substrates situated in plastic Petri dishes. Elastomeric mixtures and silicon masters were baked at 70 °C in an oven for ~20 h. The polymerized PDMS stamps were removed from the silicon masters and cut into appropriate sizes for easy handling.

Chemical Lift-Off Lithography. To prepare for lift-off lithography, PDMS stamps were exposed to oxygen plasma (power 18 W, oxygen pressure 10 psi, Harrick Plasma, Ithaca, NY, USA) for 40 s to generate reactive siloxyls on PDMS stamp surfaces. Activated stamps were immediately brought into conformal contact with TEG-modified Au substrates for ~17 h. After removing PDMS stamps from the substrates, ethanol was used to rinse post-lift-off substrates thoroughly. Patterned substrates were then submerged in ethanolic solutions of 0.5 mM pre-functionalized thiols for ~3 h, unless otherwise stated. Experiments were conducted with different insertion times (0.25-24 h) using *L*-DOPA pre-functionalized molecules (Fig. 6-S1). An early increase (0.5-3 h) followed by a slow rise (after 3 h) in fluorescence intensities suggests that insertion starts to saturate after 3 h (Fig. 6-S1 inset).

For post-functionalization, post-lift-off substrates were submerged in ethanolic solutions of 0.5 mM AEG molecules followed by neurotransmitter conjugation. To vary the amounts of inserted pre-functionalized thiols or AEG molecules, TEG molecules were co-incubated in different proportion such that the total solution concentrations were 1.0 mM and insertions times

were ~3 h. After insertion, substrates were rinsed with ethanol and blown dry with nitrogen gas. For neurotransmitters post-conjugated to surface tethers, substrates were incubated with 60/40 DMF/deionized water solutions of 35 mM Fmoc-protected neurotransmitter/NHS/EDC for ~3 h. Substrates were then rinsed thoroughly with ethanol and blown dry with nitrogen gas.

To generate double patterns of surface-tethered neurotransmitters with chemical lift-off lithography, PDMS stamps were used to lift-off TEG SAM molecules twice. After the first lift-off step, substrates were inserted with either surface tethers or pre-functionalized molecules. For the second lift-off step, PDMS stamps were used to lift-off TEG SAM molecules from spatially non-overlapping regions adjacent to the previously patterned regions on the same substrates. The post-double-lift-off substrates were then either inserted with surface tethers or pre-functionalized molecules, respectively. After each insertion step with tethering molecules, neurotransmitter conjugation was carried out.

To enable neurotransmitter epitopes to capture binding partners, Fmoc protecting groups were removed from surface-tethered neurotransmitters by immersing substrates in 20% 4-methylpiperidine in deionized water for 15 min. The Fmoc groups were used to protect amino moieties during chemical synthesis of pre-functionalized molecules. In addition, Fmoc groups protected amino moieties of neurotransmitter precursors from competing reactions with surface tethering molecules for NHS-activation of carboxyl groups of precursor molecules. After rinsing with deionized water, neurotransmitter-modified substrates were incubated with 10 mg/mL BSA solution for 5 min to reduce nonspecific adsorption of target proteins.¹⁴ Substrates were then completely submerged in plastic Petri dishes filled with deionized water. The substrates, held by a pair of tweezers, were then gently agitated side-to-side in the deionized water. This step was repeated once in fresh deionized water. This double rinsing step was used prior to exposing

substrates to protein solutions. Substrates were always covered with deionized water or protein solutions. Keeping the substrates wet reduced the likelihood for captured proteins to become denatured and dissociated from the substrates.

Antibody Binding. Primary and secondary antibodies were diluted 1:200 and 1:100 in 0.01 M PBS pH 7.4, respectively. All primary antibodies were incubated with substrates for 20 min, followed by incubation with fluorescently labeled secondary antibodies for 20 min. Antibody incubation was carried out at room temperature. During incubation of fluorescently labeled secondary antibodies, substrates in plastic Petri dishes were placed in the dark to reduce photobleaching of dye-labeled antibodies. An inverted fluorescence microscope (Axio Observer.D1) equipped with an AxioCam MRm charged-coupled device camera was used to image substrates (Carl Zeiss MicroImaging, Inc., Thornwood, NY, USA). Two fluorescence filter sets (38 HE/high efficiency), with excitation and emission wavelengths at 470 ± 20 nm and 525 ± 25 nm, respectively, and (43 HE/high efficiency) excitation and emission wavelengths at 550 ± 25 nm and 605 ± 70 nm, respectively, were used to visualize secondary antibody binding on substrates. Fluorescence images were collected using a 10 \times objective lens.

Fluorescence intensities were determined by performing line scans at a 30-pixel scanning width *via* AxioVs40 version 4.7.1.0 software (Carl Zeiss MicroImaging, Inc., Thornwood, NY, USA). On average, five fluorescence line scans were acquired per image. Fluorescence intensity was averaged for each line scan and then for each image. Specific fluorescence intensities measured on post-lift-off substrates are differences between fluorescence in the biorecognition regions (square features) and fluorescence intensity measured in the TEG background (absence of surface-tethered ligands).

Statistics. Fluorescence intensity data were evaluated by Student's *t*-tests (two-group comparisons) using Prism Version 5.02 (GraphPad Software Inc., San Diego, USA). Fluorescence intensities are reported as means \pm standard errors of the means with probabilities $P < 0.05$ considered statistically significant.

6.4 Results and Discussions

6.4.1 Synthesis of Pre-Functionalized Molecules

Previously, oligo(ethylene glycol)-modified alkanethiol surface tethers were self-assembled or inserted first on Au substrates followed by chemical modification with small-molecule probes. Here, we compared a different approach wherein neurotransmitter precursors were conjugated to surface tethers *prior* to self-assembly on Au substrates. The synthesis of pre-functionalized molecules is challenging because it requires bifunctional tethers and orthogonal coupling chemistries. Reactive amine terminal groups are necessary to form amide bonds with the carboxyl moieties of neurotransmitter precursors and thiol headgroups are required for self-assembly on Au substrates (Scheme 6-1).

Due to the high nucleophilicity of sulfur, thiols were protected during the coupling steps to avoid inter- and intramolecular thioesterification. Because the commercial availability of functional oligo(ethylene glycol)-terminated alkanethiol tethers is highly limited (and costly), a novel synthetic route was established as shown in Scheme 6-2. Although there have been reports in the literature regarding the synthesis of oligo(ethylene glycol)-terminated alkanethiols,^{38,39,41,42} few studies have reported the pre-functionalization of biologically active small molecules on these tethers.⁴³⁻⁴⁶ To the best of our knowledge, none of these studies reported pre-functionalization with neurotransmitters or their precursors.

6.4.2 Patterning Pre- vs. Post-Functionalized Molecules with Lift-Off Lithography

Chemical lift-off lithography was used to pattern TEG SAMs, which functioned as a protein-resistant background matrix (Fig. 6-1A). Following lithography, pre-functionalized molecules were inserted into the post-lift-off regions (Fig. 6-1B). For post-functionalization,

alkanethiol tethers were inserted into the post-lift-off regions. Functionalization with neurotransmitters *via* amide bond formation was then carried out directly on the substrates (Fig. 6-1C). Prior to antibody binding, Fmoc protecting groups were removed from pre-functionalized molecules to reveal epitopes essential for biomolecule recognition.

Oxygen plasma-treated PDMS stamps patterned with $25 \times 25 \mu\text{m}^2$ square-shaped protruding features separated by $25 \mu\text{m}$ spacing were used for chemical lift-off lithography. Because molecules are removed only in the stamp/SAM contact regions, patterns of negative, recessed squares were created on Au surfaces. Post-lift-off surfaces were exposed to varying nominal concentrations of TEG and pre-functionalized molecules or TEG and AEG tether molecules followed by post-functionalization. The goal of these experiments was to determine the insertion molecule compositions that result in maximal biomolecule/antibody recognition. Following surface functionalization, primary antibodies against each probe were then captured on the substrates.

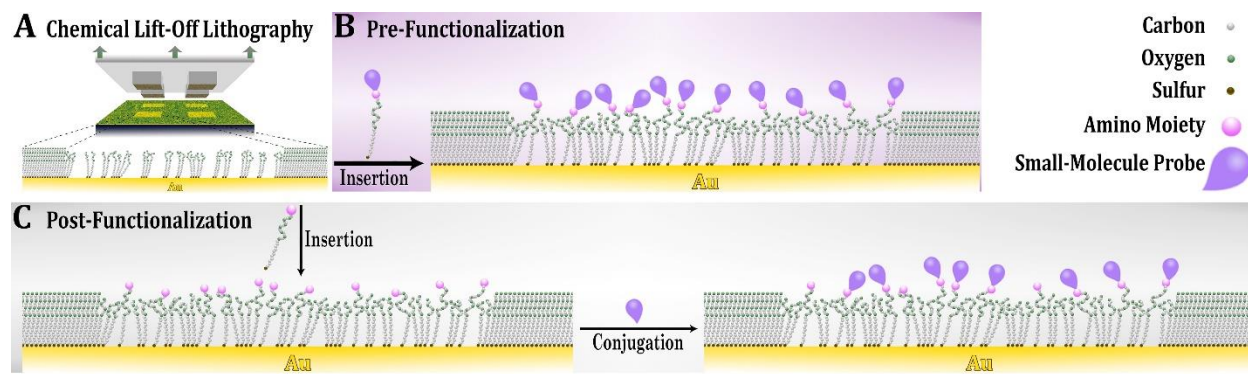


Figure 6-1. Schematics (not to scale) of patterning and functionalization strategies. (A) Polydimethylsiloxane stamps were treated with oxygen plasma to generate siloxyl groups for reaction with hydroxyl tri(ethylene glycol)-terminated alkanethiol (TEG) self-assembled monolayers (SAM) on Au surfaces. During stamp/SAM contact, stamps remove ~70% of TEG molecules and the associated underlying Au atoms in the contacted areas. (B) Tether molecules pre-functionalized with neurotransmitters or (C) tethers amenable to neurotransmitter post-functionalization were then inserted into post-lift-off regions.

Antibody binding was visualized *via* additional capture of fluorescently labeled secondary antibodies (Table 6-S1). Fluorescent arrays of square patterns against dark protein-resistant backgrounds of TEG SAMs resulted from antibody capture. As the ratios of *L*-DOPA or *L*-5-HTP pre-functionalized molecules were increased relative to TEG molecules, fluorescence signals also increased (Fig. 6-2A,B, left to right). Maximal fluorescence signals were observed at 100% pre-functionalized molecule ratios. In control experiments (Fig. 6-S2A,B), substrates were exposed to fluorescently labeled secondary antibodies without primary antibodies. Here, negligible fluorescence was detected indicating highly specific binding (>90%) on patterns containing *L*-DOPA or *L*-5-HTP pre-functionalized molecules.

Assuming equal chances of TEG *vs.* pre-functionalized molecule insertion on post-lift-off substrates, fluorescence signals would be hypothesized to increase linearly with increasing fractions of pre-functionalized molecules. (We assumed that primary antibody-probe binding followed a 1:1 stoichiometry such that fluorescence intensities in Figure 6-2 are directly related to the relative surface densities of probe molecules.) However, as quantified in Figure 6-3A and 6-3B, fluorescence signals were not linearly proportional to increasing fractions of pre-functionalized molecules. This nonlinear relationship suggests that surface adsorption and insertion of TEG molecules on post-lift-off substrates is favored over pre-functionalized molecules.⁴⁷⁻⁴⁹

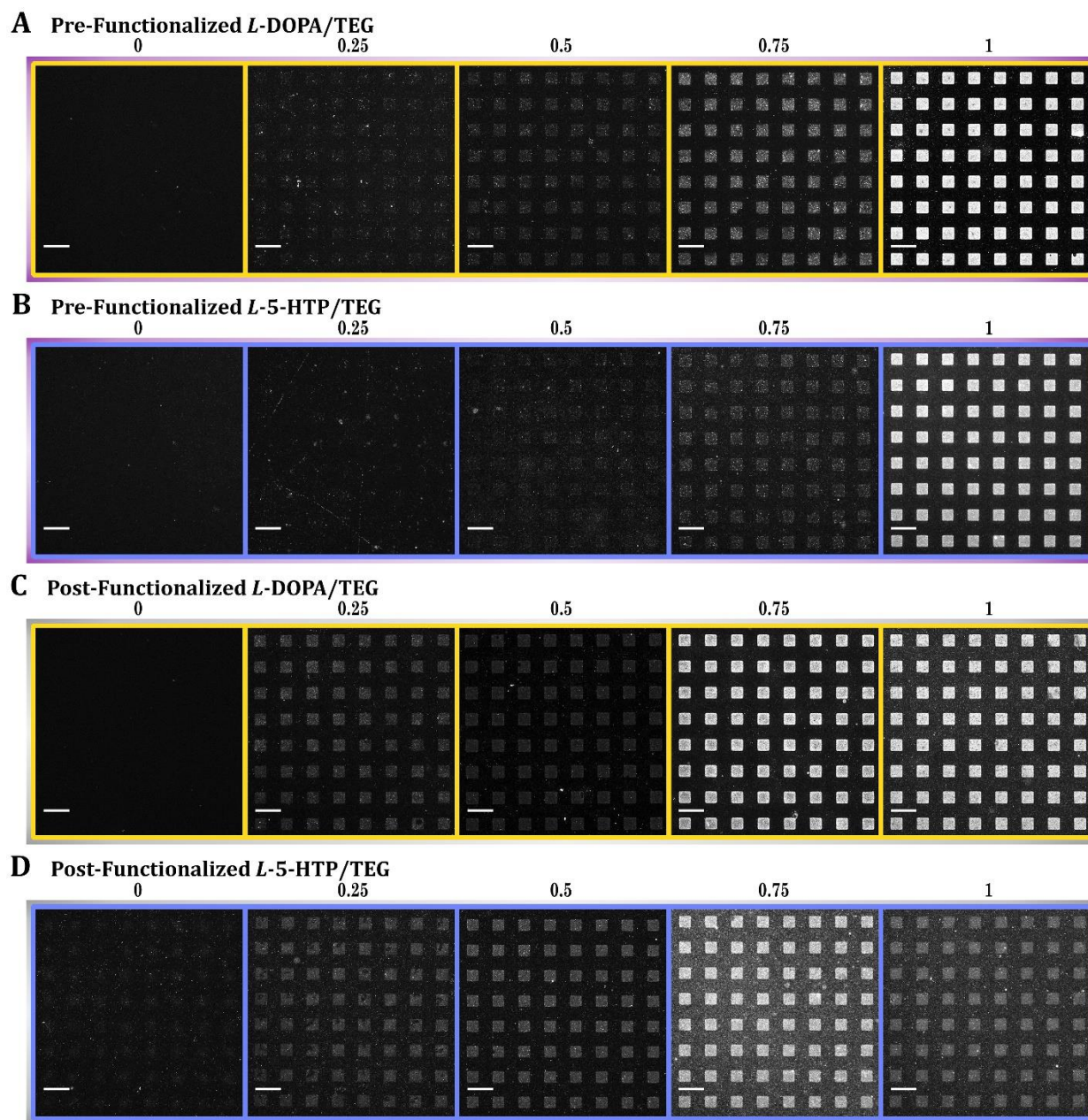


Figure 6-2. Representative fluorescence images showing lift-off lithography patterned self-assembled monolayers (SAMs) consisting of (A,B) inserted neurotransmitter (*i.e.*, *L*-3,4-dihydroxyphenylalanine (*L*-DOPA) and *L*-5-hydroxytryptophan (*L*-5-HTP)) pre-functionalized molecules or (C,D) inserted tethers with post-functionalized neurotransmitters. The ratios of inserted pre-functionalized or post-functionalized molecules to hydroxyl-terminated tri(ethylene glycol)alkanethiol (TEG) are shown above the images. Substrates were imaged at an emission wavelength of 525 nm (AlexaFluor® 488 with excitation at 490 nm) to visualize secondary antibodies, which recognize primary antibodies captured on patterned substrates. Scale bars are 50 μ m.

A number of factors likely contribute to this nonlinear behavior. These include differences in the rates of diffusion of the respective molecules to the surface, steric hindrance arising as the larger pre-functionalized molecules approach the surface, and differences in miscibility (*i.e.*, pre-functionalized molecules may be less miscible with TEG remaining in the lift-off regions). Additionally, pyridyl disulfides are bulkier and require disulfide cleavage upon adsorption on Au surfaces.^{40,50} In fact, previous competitive adsorption studies of thiols *vs.* disulfides have shown that adsorption of thiols is about two orders of magnitude greater than adsorption of disulfides, possibly due to steric hindrance from disulfide head groups in approaching Au surfaces.^{51,52} Thus, co-incubation with TEG does not appear to be needed to dilute pre-functionalized molecules further because the remaining TEG molecules in the post-lift-off regions already provides the necessary dilution to achieve maximal antibody binding.

Similar patterning and antibody capture procedures were carried out for post-patterning functionalization on post-lift-off substrates. Again, control experiments (Figs. 6-S2C,D) produced negligible fluorescence indicating high specific binding (>90%) on post-functionalized *L*-DOPA and *L*-5-HTP patterned substrates. However, behavior with respect to nominal AEG tether/TEG ratios (Fig. 6-2C,D) was different from that observed with pre-functionalized molecules (Fig. 6-2A,B). As quantified in Figures 6-3C, fluorescence signal intensities increased more gradually and approached a plateau at 75-100% *L*-DOPA post-functionalized molecules. For *L*-5-HTP (Fig. 6-3D), fluorescence intensities peaked at the 75% ratio and declined at 100% post-functionalized *L*-5-HTP.

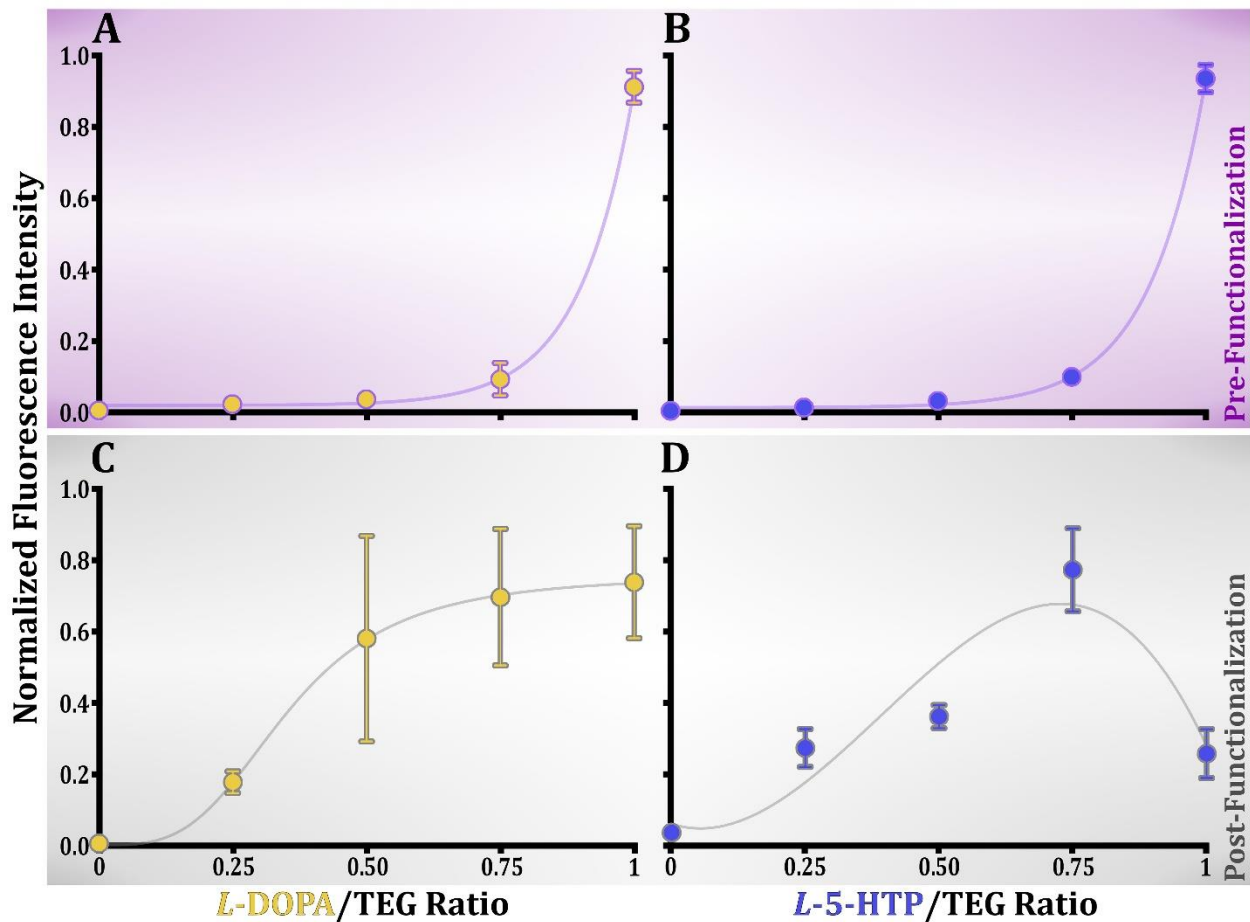


Figure 6-3. Graphs of normalized fluorescence intensities vs fractions of (A,B) pre-functionalized and (C,D) post-functionalized molecules relative to hydroxyl-terminated tri(ethylene glycol)alkane thiol (TEG). Data for *L*-3,4-dihydroxyphenylalanine (*L*-DOPA) are shown in (A,C); data for *L*-5-hydroxytryptophan (*L*-5-HTP) are in (B,D). Relative fluorescence intensities rose slowly with increasing fractions of pre-functionalized molecules suggesting preferential adsorption of TEG except where post-lift-off substrates were exposed to 100% pre-functionalized molecules, which resulted in maximal fluorescence intensities. Relatively small variability in the data in (A,B) suggests reproducible insertion and antibody recognition for pre-functionalized molecules. By contrast, the fluorescence profiles for post-functionalized molecules approached a plateau more slowly in (C) for *L*-DOPA and (D) for *L*-5-HTP where maximal fluorescence was observed at 25%/75% TEG/AEG ratios. Error bars for replicate samples were larger by comparison suggesting greater variability in post-functionalization and/or antibody capture. Error bars represent standard errors of the means with $N=3$ samples per data point.

Because neurotransmitters were conjugated to surface tethers *after* the latter were inserted into post-lift-off regions, antibody binding depends not only on surface tether densities but also on the efficiency of NHS/EDC coupling chemistry in attaching *L*-DOPA and *L*-5-HTP. As stated earlier, residual alkanethiols remain in the contact regions on post-lift-off substrates.⁵³ Unlike pre-functionalized molecules, however, AEG molecules are thiol-terminated and do not possess bulky Fmoc-protected neurotransmitters, so they resemble TEG molecules more closely than pre-functionalized molecules (Scheme 6-1). Thus, insertion behavior of mixed AEG/TEG solutions may more closely follow their nominal ratios.

The behavior of the post-functionalized systems also suggests that besides the densities of surface tethers, the extent of surface conjugation of neurotransmitters may also contribute to antibody binding behavior across different AEG/TEG ratios. For NHS/EDC surface-coupling chemistry, specific conditions including pH, solvents, reagent concentrations, and incubation periods must be optimized for individual probes.³⁰ Side reactions and hydrolysis of NHS esters can lower yields of probe conjugation.^{28,29} Thus, variability in functionalization efficiency might contribute not only to plateau effects but also to the larger error terms for post-functionalized substrates (Fig. 6-3C,D) *vs.* pre-functionalized substrates (Fig. 6-3A,B). Moreover, this same variability could underlie differences in antibody binding behavior between *L*-DOPA and *L*-5-HTP post-functionalized substrates.

6.4.3 Direct Comparisons between Pre- and Post-Functionalized Approaches

The central hypothesis under investigation in this study is that pre-functionalizing neurotransmitters to surface tethers prior to self-assembly improves specific recognition by biomolecule targets. To test this hypothesis directly, we compared the two approaches side by

side on the same substrates to reduce contributions associated with sample-to-sample variation. Moreover, we subjected pre-functionalized molecules to subsequent chemical lift-off patterning and post-functionalization chemistries to test whether pre-functionalized molecules can survive harsh post-functionalization conditions and retain their ability to capture antibodies. Conditions optimized for patterning pre- and post-functionalized molecules were used as determined above. Pre-functionalized molecules were inserted onto post-lift-off substrates at 100%, whereas for post-patterning functionalization, AEG was co-deposited with TEG at a 75%/25% ratio for *L*-5-HTP and at 100% AEG for *L*-DOPA.

Each substrate required double lift-off lithography, thus, there were two patterning routes possible. The first route investigated, as shown in Figure 6-4A, involved inserting AEG tethers into post-lift-off substrates followed by probe conjugation. A second lift-off step was performed in an adjacent region on each substrate and neurotransmitter pre-functionalized molecules were then inserted into these newly generated post-lift-off areas. Probe-conjugation reactions on surfaces are known to disrupt surrounding SAM structures thereby altering the local environment of pre-existing probes tethered on surfaces.^{15,54} By implementing the post-functionalization step *prior* to insertion with pre-functionalized molecules, the matrix environments around the latter should be preserved.

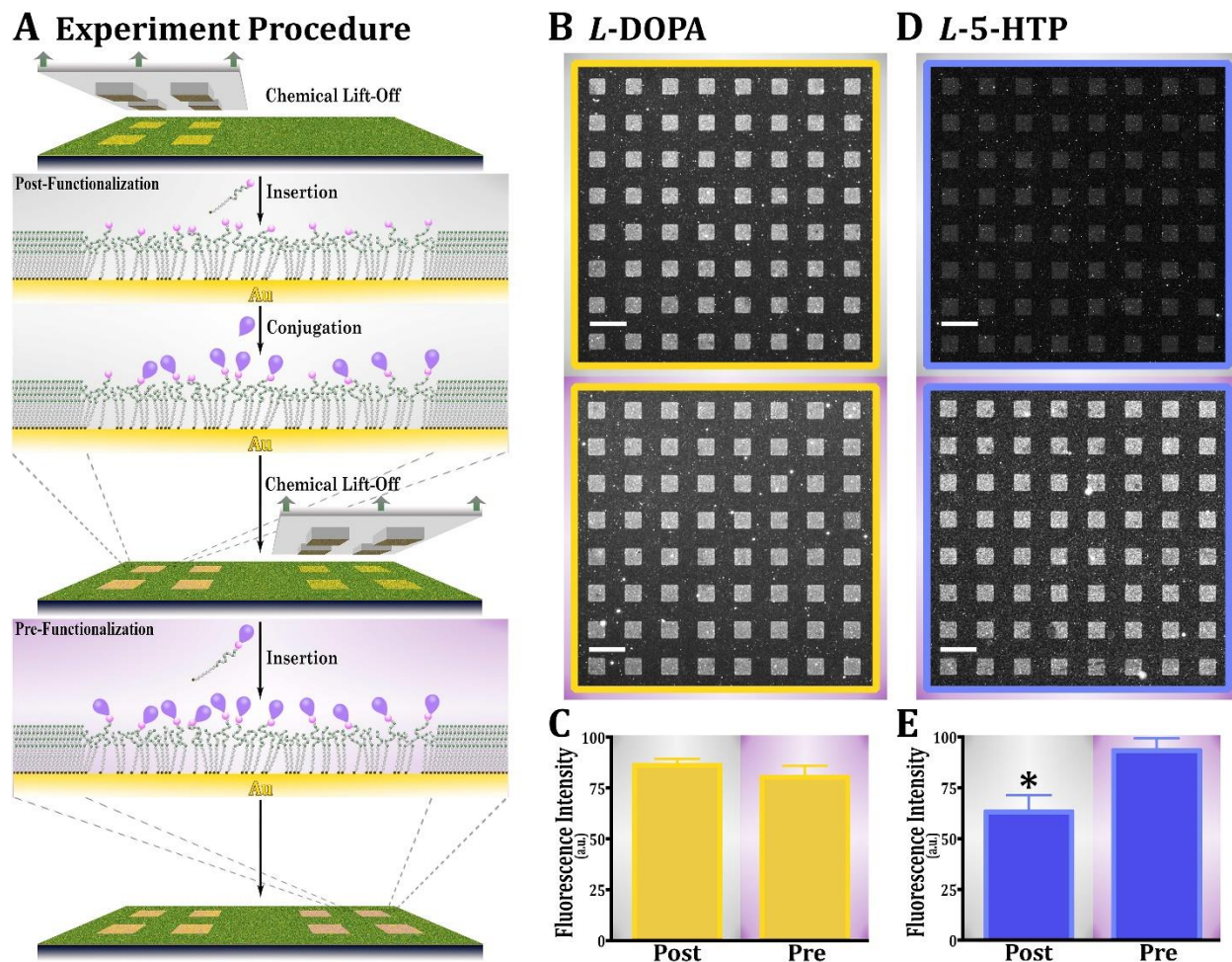


Figure 6-4. (A) Schematic illustrating double lift-off patterning of post- and pre-functionalized molecules. Tether molecules are inserted after the first lift-off step and post-functionalized followed by insertion of pre-functionalized molecules in an adjacent region after a second lift-off step. (B,D) Representative fluorescence images and (C,E) fluorescence intensity graphs for antibody binding on double patterns of (B,C) *L*-3,4-dihydroxyphenylalanine (*L*-DOPA) and (D,E) *L*-5-hydroxytryptophan (*L*-5-HTP). Similar fluorescence intensities were observed in (C) indicating comparable specific antibody binding to *L*-DOPA in pre- vs. post-functionalized regions. However, in (E), higher fluorescence intensities were observed for *L*-5-HTP for pre-functionalized regions in compared to *L*-5-HTP post-functionalized regions indicating improved antibody binding to the former. Substrates were imaged at an emission wavelength of 525 nm (AlexaFluor[®] 488 with excitation at 490 nm). Error bars represent standard errors of the means with $N=3$ samples per group. Mean intensities are significantly different for *L*-5-HTP [$t(4)=3$ * $P<0.05$]. Scale bars are 50 μm .

As shown in Figure 6-4B,6-4C, similar fluorescence intensities were observed for *L*-DOPA when post-functionalized (top image) vs. pre-functionalized (bottom image) approaches were compared. In contrast, relative fluorescence intensities for *L*-5-HTP for pre-functionalized molecules (bottom image) were higher than those for *L*-5-HTP post-functionalized molecules (top image). Control experiments in which capture surfaces were exposed to fluorescently labeled secondary antibodies alone (Fig. 6-S3C-F) showed negligible fluorescence signals indicating highly specific antibody binding (>90%).

For the second patterning route, neurotransmitter pre-functionalized molecules were inserted into post-lift-off regions followed by a second lift-off step in an adjacent region, insertion of AEG tethers, and post-functionalization. This patterning sequence could alter pre-functionalized molecules during the course of the subsequent probe conjugation steps. Nonetheless, similar fluorescence signals were observed for *L*-DOPA pre-functionalized (Fig. 6-S4B (top image) and 6-S4C) and post-functionalized (Fig. 6-S4B (bottom image) and 6-S4C) molecules. Again, improved specific antibody binding was observed for *L*-5-HTP pre-functionalized molecules (Fig. 6-S4D,E). Control experiments where fluorescently labeled secondary antibodies were exposed to capture surfaces in the absence of primary antibodies (Fig. 6-S3G-J) displayed negligible fluorescence.

These results provide additional evidence for improved specific antibody recognition of *L*-5-HTP pre-functionalized molecules in support of the central hypothesis, though antibody binding to *L*-DOPA pre-functionalized molecules did not show similar improvements. One explanation for the latter is that the efficiency of the NHS/EDC coupling chemistry may be more efficient for *L*-DOPA compared to *L*-5-HTP. Thus, antibody binding was maximal for *L*-DOPA post-functionalized substrates and could not be further improved using pre-functionalized

molecules. It is noteworthy that pre-functionalized molecules appeared to be unaffected by post-functionalization chemistries such that they did not lose their ability to capture antibodies.

6.4.4 Multiplexed Neurotransmitter Pre-Functionalized Substrates

Since pre-functionalized molecules provided advantages in the case of some probes (*e.g.*, *L*-5-HTP) and circumvented the need for sequential and compatible on-chip coupling chemistries, these molecules were used to create multiplexed neurotransmitter-modified substrates. Double lift-off lithography was used to pattern *L*-DOPA and *L*-5-HTP pre-functionalized molecules on the same substrates. Substrates were then exposed to mixed primary antibody solutions containing mouse anti-*L*-DOPA monoclonal antibody and rabbit anti-*L*-5-HTP polyclonal antibody. Primary antibody binding was visualized *via* exposure to a mixed AlexaFluor[®] 488 (peak emission at 519 nm; “green”) anti-mouse and AlexaFluor[®] 546 (peak emission at 573 nm; “red”) anti-rabbit secondary antibody solution.

Anti-*L*-DOPA monoclonal antibody displayed 80% selective recognition of surface-tethered *L*-DOPA (Fig. 6-5A,C) over *L*-5-HTP (Fig. 6-5B,C). By contrast, anti-*L*-5-HTP polyclonal antibody displayed poor selectivity and recognized *L*-5-HTP (Fig. 6-5D,F) and *L*-DOPA (Fig. 6-5E,F) equally well. Substrates exposed to fluorescently labeled secondary antibodies alone displayed negligible fluorescence (Fig. 6-S5A,B,C,D) leading to the conclusion that it is anti-*L*-5-HTP *primary* antibodies that cross-react with *L*-DOPA pre-functionalized molecules. Because variations in probe functionalization, which affect specific binding of antibodies to their small-molecule targets, was avoided by using pre-functionalized molecules, the cross-reactivity of polyclonal anti-*L*-5-HTP antibodies likely results from the properties of the antibodies themselves. While monoclonal antibodies are identical and recognize the same

epitope on antigens by design, polyclonal antibodies are polydisperse and recognize multiple different epitopes on antigens.³³ Thus, polyclonal antibodies are more susceptible to cross-reactivity to structurally related epitopes.

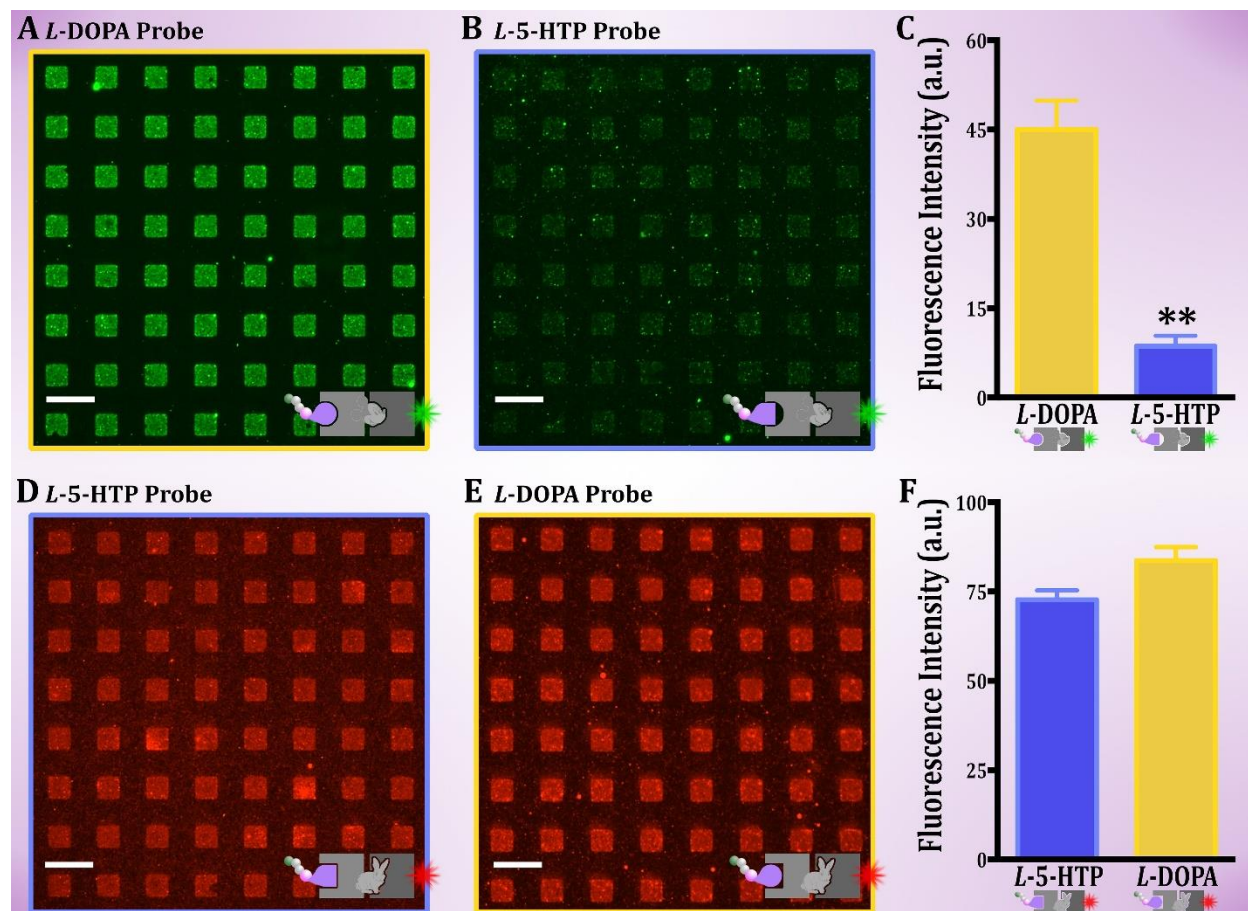


Figure 6-5. (A,B,D,E) Representative fluorescence images and intensity graphs for antibody binding on double chemical lift-off patterns of *L*-3,4-dihydroxyphenylalanine (*L*-DOPA) and *L*-5-hydroxytryptophan (*L*-5-HTP) pre-functionalized molecules. Substrates were imaged at two fluorescence emission wavelengths (525 nm (green, A,B) and 605 nm (red, D,E) for AlexaFluor[®] 488 (excitation at 490 nm) and AlexaFluor[®] 546 (excitation at 556 nm), respectively to visualize recognition of *L*-DOPA vs. *L*-5-HTP by monoclonal anti-*L*-DOPA antibodies in (A,B,C). Recognition of *L*-DOPA and *L*-5-HTP by polyclonal anti-*L*-5-HTP antibodies is seen in (D,E,F). Error bars represent standard errors of the means with $N=3$ samples per group. Means are significantly different for anti-*L*-DOPA antibody binding [$t(4)=7$ $**P<0.01$]. Scale bars are 50 μm .

The differences in specificities between monoclonal and polyclonal antibodies were evident for other pairs of neurotransmitter pre-functionalized molecules. For example, anti-*L*-DOPA monoclonal antibodies showed 90% selective recognition of *L*-DOPA (Fig. 6-6A,C) vs. *L*-His (Fig. 6-6B,C). Similarly, anti-*L*-DOPA monoclonal antibodies showed 60% selective recognition of *L*-DOPA (Fig. 6-6D,F) vs. *L*-Trp (Fig. 6-6E,F). By contrast, both anti-*L*-His and anti-*L*-Trp polyclonal antibodies failed to display selective recognition of *L*-His vs. *L*-DOPA (Fig. 6-S6A,B,C) and *L*-Trp vs. *L*-DOPA (Fig. 6-S6D,E,F), respectively. In all cases, control experiments indicated negligible fluorescence signals associated with fluorescently labeled secondary antibodies in the absence of primary antibodies (Fig. 6-S7A-H).

Together, these results suggest that polyclonal primary antibodies may not have sufficient specificity to differentiate surface-tethered small-molecule probes having similar structures. In contrast, differences between *L*-DOPA and other small-molecule amino acids (*i.e.*, *L*-5-HTP, *L*-His, and *L*-Trp) were readily distinguished by anti-*L*-DOPA monoclonal antibodies. Moreover, anti-*L*-DOPA monoclonal antibodies exhibited 50% selectivity for *L*-DOPA (Fig. 6-6G,I) over closely structured *L*-DOPS (Fig. 6-6H,I). Selective recognition for the *L*-DOPA/*L*-DOPS pair was somewhat poorer than the previous pairs, however, this pair of probes is the most similar of those tested and differs by only a hydroxyl group (Scheme 6-1). Secondary antibodies did not bind to *L*-DOPA/*L*-DOPS-functionalized substrates (Fig. 6-S7I,J). We could not identify commercially available antibodies against *L*-DOPS, so we could not carry out selectivity experiments focused on *L*-DOPS over *L*-DOPA.

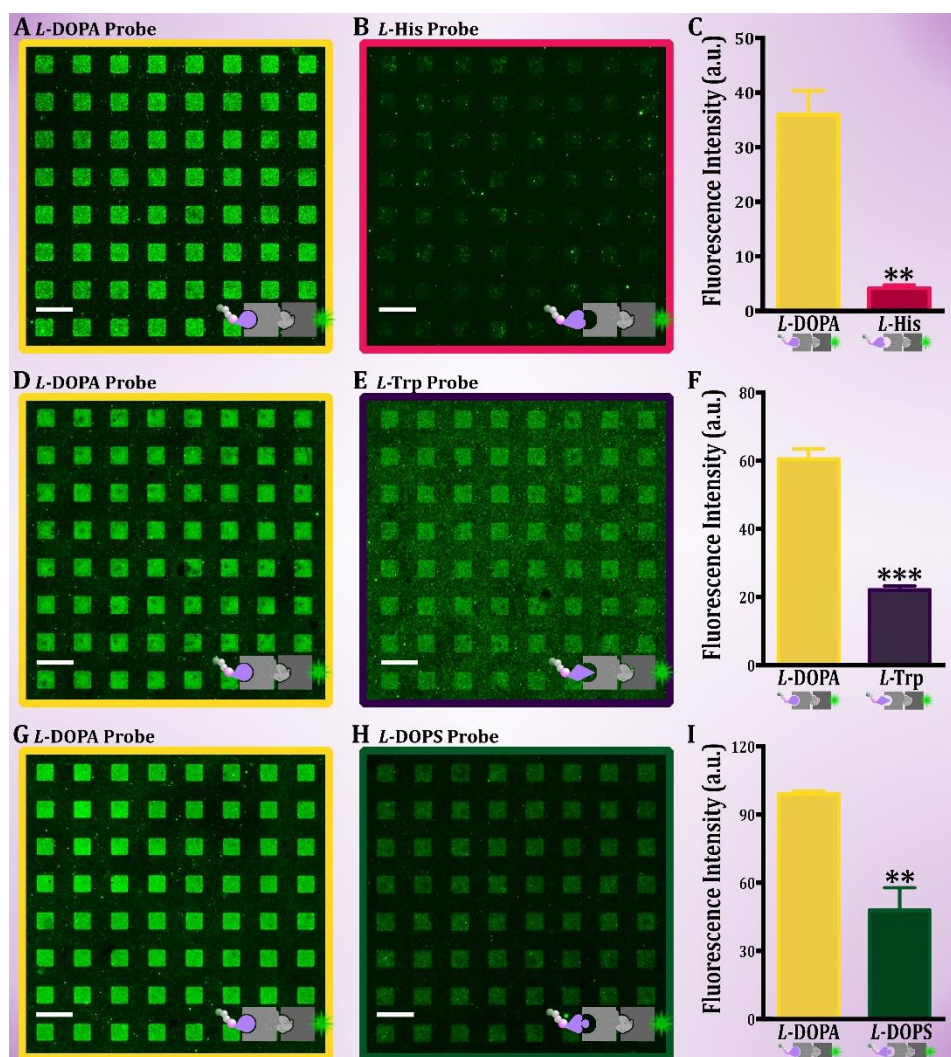


Figure 6-6 Representative fluorescence images and intensity graphs for antibody binding on double chemical lift-off patterns of (A,B) *L*-3,4-dihydroxyphenylalanine (*L*-DOPA)/*L*-histidine (*L*-His), (D,E) *L*-DOPA/*L*-tryptophan (*L*-Trp), and (G,H) *L*-DOPA/*L*-droxidopa (*L*-DOPS) pre-functionalized molecules. Higher fluorescence intensities were observed for monoclonal anti-*L*-DOPA antibody binding to surface tethered *L*-DOPA vs. (C) *L*-His, (F) *L*-Trp, and (I) *L*-DOPS. Imaging was via AlexaFluor® 488 labeled secondary antibodies (excitation at 490 nm and emission of 525 nm (green)). Error bars are standard errors of the means with $N=3$ substrates per group. Means are significantly different for (C) [$t(4)=7$ ** $P<0.01$], (F) [$t(4)=12$ *** $P<0.001$] and (I) [$t(4)=5$ ** $P<0.01$]. Scale bars are 50 μm .

The comparative antibody binding results suggest that monoclonal antibodies may display better selectivity for small-molecule antigens than polyclonal antibodies. However, additional monoclonal antibodies beyond the anti-*L*-DOPA antibodies used here would need to be tested to investigate this hypothesis further. Notably, there are very few commercially available monoclonal antibodies available for small molecules. Moreover, although highly specific recognition (>90%) of surface-bound small-molecule probes was achieved on multiplexed substrates, limitations remain in terms of the cross-reactivity of many of the antibodies examined here. Nonetheless, the use of pre-functionalized molecules greatly reduced variations in probe conjugation, improved specific recognition, and in some cases, when paired with highly specific antibodies, enabled multiplexing.

6.5 Conclusions and Prospects

Designing and controlling recognition parameters for biocapture surfaces are challenging. In this report, we demonstrated that small-molecules pre-functionalized to surface tethers displayed more consistent antibody binding than post-patterning functionalization. Notably, pre-functionalized molecules not only withstood subsequent conditions associated with addition functionalization chemistries but they also improved specific target recognition of some probes. Although multiplexed probes were indiscriminately recognized by polyclonal antibodies against all tested neurotransmitter pre-functionalized molecules, monoclonal antibodies showed selective recognition of *L*-DOPA *vs.* all other neurotransmitters tested, even against *L*-DOPS, which differs from *L*-DOPA by a single hydroxyl moiety.

When it comes to finding a solution to the cross-reactivity issues associated with some biomolecule targets, the ability to reduce nonspecific binding while improving specific binding *via* careful control of surface chemistries appears to be insufficient. Synthetic oligonucleotides or aptamers may be potential game changers as they possess many advantages over antibodies.^{35,36,55} Notably, because aptamers are synthesized *in vitro*, their structures are identical and their affinities can be tuned by modulating oligonucleotide sequences and thus, their 3D conformations.⁵⁶ The advantages of the novel neurotransmitter pre-functionalized molecules synthesized here will facilitate the generation of improved substrates for identifying high-affinity aptamers targeting small-molecule neurotransmitters for neurosensing applications.^{35,57}

6.6 Supplementary Experiments and Figures

Detailed Synthesis Procedures for Neurotransmitter Pre-Functionalized Molecules (see Scheme 6-2 in main text).

Fmoc-*L*-DOPS-OH. A solution of 208.5 mg (0.98 mmol, 1 eq.) of *L*-DOPS in 10 mL of a 2:1 mixture of 10% aqueous Na₂CO₃/ tetrahydrofuran (THF) was cooled to 0 °C in an ice bath and a solution of Fmoc-Cl (278.9 mg, 1.08 mmol, 1.1 eq.) in THF (3.4 mL) was added dropwise. The reaction was stirred overnight at room temperature. Tetrahydrofuran was evaporated under reduced pressure and the compound was extracted with ethyl acetate. The aqueous layer was acidified to pH 2 with 6 M HCl and was then extracted again with ethyl acetate. The organic extract was dried over magnesium sulfate, filtered, and then rotovapped to dryness. The oil was purified by silica gel chromatography (eluent: dichloromethane (DCM)/ethyl acetate 9:1 to 1:9 and DCM/methanol (MeOH) 19:1) to give 344 mg of a light brown solid (79%). ¹H NMR (300 MHz, DMSO-*d*₆, 25 °C): δ (ppm) = 8.80 (s, 1 H), 8.75 (s, 1 H), 7.88 (d, 2 H, J = 7.6 Hz), 7.61-7.71 (m, 2 H), 7.25-7.45 (m, 4 H), 7.07 (d, 1 H, J = 9.2 Hz), 6.78 (s, 1 H), 6.62-6.66 (m, 2 H), 4.94 (m, 1 H), 4.05-4.24 (m, 4 H), 3.17 (d, 1 H, J = 5.04 Hz). Mass analysis (MALDI-TOF): m/z 458.9754 (calculated for C₂₄H₂₁NNaO₇ [M+Na]⁺ m/z 458.1210).

Undec-1-en-11-ylhepta(ethylene glycol) (1). Undec-1-en-11-ylhepta(ethylene glycol) was synthesized as previously described.^{S1} Hepta(ethylene glycol) (4.95 g, 15.2 mmol, 3 eq.) was treated with 606 mg of 50% aqueous sodium hydroxide solution (7.6 mmol, 1.5 eq.) for 30 min at 100 °C under argon, and then 11-bromo-1-undecene (1.18 g, 5.05 mmol, 1 eq.) was added. The solution was stirred for 24 h at 100 °C under argon, then cooled down. The organic mixture was extracted with DCM and purified by silica gel chromatography (eluent: ethyl acetate to remove the di-functionalized molecule, then DCM/MeOH 19:1 to obtain the mono-

functionalized molecule, and finally DCM/MeOH 9:1 to recover the non-modified hepta(ethylene glycol) giving 1.51 g of the mono-functionalized compound **1** (colorless oil, 63%). ¹H NMR (300 MHz, CDCl₃, 25 °C): δ (ppm) = 5.74-5.89 (m, 1 H), 4.89-5.04 (m, 2 H), 3.53-3.77 (m, 28 H), 3.44 (t, 2 H, J = 6.8 Hz), 2.67 (br s, 1 H), 2.04 (q, 2 H, J = 7.1 Hz), 1.57 (quin, 2 H, J = 7.0 Hz), 1.22-1.43 (m, 12 H). Mass analysis (MALDI-TOF): m/z 501.2800 (calculated for C₂₅H₅₀NaO₈ [M+Na]⁺ m/z 501.3398).

[1-[(Methylcarbonyl)thio]undec-11-yl]hepta(ethylene glycol) (2).

([1-[(Methylcarbonyl)thio]undec-11-yl]hepta(ethylene glycol) was synthesized as previously described with slight modifications.^{S1} Compound **1** (587.2 mg, 1.23 mmol, 1 eq.) was dissolved in 4 mL of anhydrous MeOH. Thioacetic acid (351 μL, 4.92 mmol, 4 eq.) and 10 mg of AIBN were added. The mixture was irradiated with a UV lamp (UVP XX-40 BLB, 40-W, 365 nm) overnight. Afterwards, another 10 mg of AIBN was added and the reaction was stirred for an additional 24 h before concentration by rotary evaporation followed by purification by silica gel chromatography (eluent: ethyl acetate, then DCM/MeOH 19:1). Then, 618.7 mg of compound **2** (91%) were obtained as a colorless oil. ¹H NMR (300 MHz, CDCl₃, 25 °C): δ (ppm) = 3.54-3.78 (m, 28 H), 3.44 (t, 2 H, J = 6.8 Hz), 2.86 (t, 2 H, J = 7.3 Hz), 2.77 (br s, 1 H), 2.32 (s, 3 H), 1.50-1.63 (m, 4 H), 1.21-1.41 (m, 14 H). Mass analysis (MALDI-TOF): m/z 577.6519 (calculated for C₂₇H₅₄NaO₉S [M+Na]⁺ m/z 577.3381).

[1-[(Methylcarbonyl)thio]undec-11-yl]-21-(tosyl)oxy-1,4,7,10,13,16,19-heptaoheneicosane

(3). To a solution of compound **2** (1.29 g, 2.32 mmol, 1 eq.) in distilled DCM (2 mL), triethylamine (648 μL, 4.64 mmol, 2 eq.) was added. The solution was cooled to 0 °C in an ice bath and 4-toluenesulfonyl chloride (663 mg, 3.48 mmol, 1.5 eq.) was added. The ice bath was then removed and the solution was allowed to warm to room temperature and react for 24 h. The

resultant mixture was diluted in DCM (50 mL) and washed with 2% acetic acid solution and brine. The organic layer was dried with magnesium sulfate and then rotovapped to remove all remaining liquid. The compound was purified by silica gel chromatography (eluent: DCM/ethyl acetate 4:1-1:1). Then, 1.26 g of compound **3** (76%) were obtained as a colorless oil. ¹H NMR (500 MHz, CDCl₃, 25 °C): δ(ppm) = 7.80 (d, 2 H, J = 8.1 Hz), 7.34 (d, 2 H, J = 8.1 Hz), 4.16 (t, 2 H, J = 4.9 Hz), 3.69 (t, 2 H, 4.9 Hz), 3.56-3.67 (m, 24 H), 3.44 (t, 2 H, J = 6.9 Hz), 2.86 (t, 2 H, J = 7.1 Hz), 2.45 (s, 3 H), 2.32 (s, 3 H), 1.52-1.62 (m, 4 H), 1.22-1.41 (m, 14 H). Mass analysis (MALDI-TOF): m/z 731.3299 (calculated for C₃₄H₆₀NaO₁₁S₂ [M+Na]⁺ m/z 731.3469).

[1-Mercaptoundec-11-yl]-21-azido-1,4,7,10,13,16,19-heptaoxaheneicosane (4). To a solution of compound **3** (1.26 g, 1.77 mmol, 1 eq.) in absolute EtOH (21 mL) was added sodium azide (230 mg, 3.54 mmol, 2 eq.). The solution was stirred at 85 °C overnight under argon. Afterward, the solution was cooled to room temperature. The solvent was carefully evaporated under reduced pressure; then the salts were precipitated in ethyl acetate and removed by filtration. The solution was rotovapped to dryness yielding 902.5 mg (94%) of compound **4** (and its disulfide derivative) as colorless oil. The residue was used as is without further purification. The thioacetate group was cleaved inducing the formation of disulfide bonds (~50%). ¹H NMR (500 MHz, CDCl₃, 25 °C): δ(ppm) = 3.49-3.83 (m, 26 H), 3.44 (t, 2 H, J = 6.7 Hz), 3.39 (t, 2 H, J = 4.7 Hz), 2.68 (t, 2 H, J = 7.3 Hz, CH₂-S-S), 2.52 (q, 2 H, J = 7.2 Hz, CH₂-SH), 1.66 (quin, 2 H, J = 7.3 Hz), 1.57 (quin, 2 H, J = 7.5 Hz), 1.20-1.40 (m, 14 H). Mass analysis (MALDI-TOF): m/z 560.3625 (calculated for C₂₅H₅₁N₃NaO₇S [M+Na]⁺ m/z 560.3345) and m/z 1095.7825 for the disulfide derivative (calculated for C₅₀H₁₀₀N₆NaO₁₄S₂ [M+Na]⁺ m/z 1095.6637).

[1-(Pyridin-2-yl)disulfanyl]undec-11-yl]-21-amino-1,4,7,10,13,16,19-heptaoheneicosane

(amine hepta(ethylene glycol)-terminated undecane-pyridyl disulfide (7EG-PDS) (5). A

solution of compound **4** (902.5 mg, 1.68 mmol, 1 eq.) in anhydrous THF (5 mL) was cooled to 0 °C in an ice bath and triphenylphosphine (818 mg, 3.12 mmol, 1.9 eq.) was added under argon. The ice bath was then removed and the solution was allowed to warm to room temperature and react for 24 h. The solvent was evaporated under reduced pressure and water was added to the mixture. The solution was filtered to remove precipitated triphenylphosphine oxide. The filtrate was then rotovapped to dryness yielding 1.03 g of a crude compound. The residue was dissolved in 20 mL of ammonia solution (7 N in MeOH), and 2-PDS (1.95 g, 8.85 mmol, 5.3 eq.) was added to the mixture under argon. The solution was stirred for 72 h at room temperature. The solvent was removed by rotary evaporation. The resultant mixture was diluted in DCM (100 mL) and washed with water. The organic layer was dried with magnesium sulfate and then rotovapped to dryness. The compound was dissolved in water, washed with hexane (4 times) and lyophilized. Then 474 mg of compound **5** (43%) were obtained as a colorless oil. ¹H NMR (500 MHz, CDCl₃, 25 °C): δ (ppm) = 8.46 (d, 1 H, J = 4.7 Hz), 7.73 (d, 1 H, J = 8.2 Hz), 7.64 (t, 1 H, J = 7.0 Hz), 7.08 (t, 1 H, J = 6.2 Hz), 3.54-3.76 (m, 26 H), 3.44 (t, 2 H, J = 6.8 Hz), 2.99 (t, 2 H, J = 4.1 Hz), 2.79 (t, 2 H, J = 7.2 Hz), 1.68 (quin, 2 H, J = 7.2 Hz), 1.56 (quin, 2 H, J = 6.4 Hz), 1.19-1.45 (m, 14 H). Mass analysis (MALDI-TOF): m/z 621.3679 (calculated for C₃₀H₅₇N₂O₇S₂ [M+H] m/z 621.3602).

General procedure for the coupling of Fmoc-protected neurotransmitter (Fmoc-R) to 7EG-PDS compound. Fmoc-R (1-1.1 eq.) was pre-activated in DCM or DMF (95-105 mM) with DIEA (3 eq.), HOBt (1.2 eq.) and EDC (1.2 eq.) for 30 min under argon. Thereafter, a 95 mM solution of compound **5** in DCM was added to the mixture. The solution was stirred for 24 h

under argon at room temperature. The resultant mixture was diluted in DCM and washed with brine. The organic layer was dried with magnesium sulfate and then rotovapped to remove all remaining liquid. The compound was purified by silica gel chromatography (eluent: DCM/ethyl acetate 9:1 to 1:9 and DCM/MeOH 19:1).

Fmoc-L-DOPA-7EG-PDS. Fmoc-L-DOPA-OH (88 mg, 0.21 mmol, 1.1 eq.) was coupled to amino-PEG-alkanepyridyl disulfide compound (**5**) (120 mg, 0.19 mmol, 1 eq.) according to the general procedure described above. Then, 81 mg of compound **Fmoc-L-DOPA-7EG-PDS** (42%) were obtained as a colorless oil. ¹H NMR (300 MHz, CDCl₃, 25 °C): δ (ppm) = 8.45 (m, 1 H), 7.25-7.76 (m, 10 H), 7.05-7.10 (m, 1 H), 6.56-6.84 (m, 3 H), 6.03 (m, 1 H), 5.70 (m, 1 H), 4.18-4.44 (m, 4 H), 3.51-3.74 (m, 28 H), 3.42 (t, 2 H, J = 6.8 Hz), 3.04-3.20 (m, 2 H), 2.79 (t, 2 H, J = 7.2 Hz), 1.68 (quin, 2 H, J = 7.6 Hz), 1.55 (quin, 2 H, J = 7.0 Hz), 1.20-1.40 (m, 14 H). Mass analysis (MALDI-TOF): m/z 1022.6145 (calculated for C₅₄H₇₆N₃O₁₂S₂ [M+H]⁺ m/z 1022.4865).

Fmoc-L-Trp-7EG-PDS: Fmoc-L-Trp(Boc)-OH (106 mg, 0.20 mmol, 1 eq.) was coupled to amino-PEG-alkanepyridyl disulfide compound (**5**) (125 mg, 0.20 mmol, 1 eq.) according to the general procedure described above with a minor change. Before purification by column chromatography, the Boc protecting group was cleaved with 20% trifluoroacetic acid solution in DCM for 1 h at room temperature. The mixture was diluted with DCM, washed with saturated aqueous sodium bicarbonate (3× eq. vol.), dried with magnesium sulfate, and then rotovapped to dryness. The compound was purified by silica gel chromatography (eluent: DCM/ethyl acetate 9:1 to 1:9 and DCM/MeOH 9:1). Then, 129 mg of compound **Fmoc-L-Trp-7EG-PDS** (63%) were obtained as a colorless oil. ¹H NMR (500 MHz, CDCl₃, 25 °C): δ (ppm) = 9.20 (s, 1 H), 8.45 (m, 1 H), 7.25-7.81 (m, 13 H), 7.04-7.21 (m, 2 H), 5.92 (m, 1 H), 5.83 (m, 1 H), 4.35-4.48

(m, 2 H), 4.23 (t, 1 H, J = 7.4 Hz), 3.45-3.75 (m, 28 H), 3.44 (t, 2 H, J = 6.8 Hz), 3.03-3.38 (m, 2 H), 2.78 (t, 2 H, J = 7.5 Hz), 1.68 (quin, 2 H, J = 7.5 Hz), 1.55 (quin, 2 H, 7.0 Hz) 1.18-1.42 (m, 14 H). Mass analysis (MALDI-TOF): m/z 1029.6008 (calculated for C₅₆H₇₇N₄O₁₀S₂ [M+H]⁺ m/z 1029.5076).

Fmoc-L-His-7EG-PDS: Fmoc-L-His(Trt)-OH (105.3 mg, 0.17 mmol, 1.1 eq.) was coupled to amino-PEG-alkanepyridyl disulfide compound (**5**) (97.4 mg, 0.15 mmol, 1 eq.) according to the general procedure described above with a minor change. Before purification by column chromatography, the Trt protecting group was cleaved with 20% trifluoroacetic acid solution in DCM for 1 h at room temperature. The mixture was diluted with DCM, washed with saturated aqueous sodium bicarbonate (3× eq. vol.), dried with magnesium sulfate, and then rotovapped to dryness. The compound was purified by silica gel chromatography (eluent: DCM/ethyl acetate 9:1 to 1:9 and DCM/MeOH 9:1). Then, 56.3 mg of compound **Fmoc-L-His-7EG-PDS** (37%) were obtained as a colorless oil. ¹H NMR (300 MHz, CDCl₃, 25 °C): δ (ppm) = 8.46 (m, 1 H), 7.25-7.79 (m, 11 H), 7.07 (m, 1 H), 6.96 (m, 1 H), 6.55 (m, 1 H), 4.57 (m, 1 H), 4.32-4.41 (m, 2 H), 4.22 (t, 1 H, J = 7.1 Hz), 3.46-3.72 (m, 28 H), 3.41 (t, 2 H, J = 7.0 Hz), 3.00-3.34 (m, 2 H), 2.79 (t, 2 H, J = 7.1 Hz), 1.68 (quin, 2 H, J = 7.7 Hz), 1.54 (quin, 2 H, J = 6.6 Hz), 1.17-1.45 (m, 14 H). Mass analysis (MALDI-TOF): m/z 1002.4191 (calculated for C₅₁H₇₃N₅NaO₁₀S₂ [M+Na]⁺ m/z 1002.4691).

Fmoc-L-5-HTP-7EG-PDS: Fmoc-L-5-HTP-OH (140.7 mg, 0.32 mmol, 1.1 eq.) was coupled to amino-PEG-alkanepyridyl disulfide compound (**5**) (179.5 mg, 0.29 mmol, 1 eq.) according to the general procedure described above. Then, 133 mg of compound **Fmoc-L-5-HTP-7EG-PDS** (44%) were obtained as a colorless oil. ¹H NMR (500 MHz, CDCl₃, 25 °C): δ (ppm) = 8.73 (s, 1 H), 8.46 (m, 1 H), 7.19-7.80 (m, 12 H), 7.02-7.09 (m, 2 H), 6.80 (m, 1 H), 6.23 (br s, 1 H), 6.14

(br s, 1 H), 5.87 (m, 1 H), 4.35-4.50 (m, 3 H), 4.23 (t, 1 H, J = 7.1 Hz), 3.45-3.71 (m, 28 H), 3.42 (t, 2 H, J = 6.9 Hz), 3.16-3.40 (m, 1 H), 3.00-3.08 (m, 1 H), 2.78 (t, 2 H, J = 7.0 Hz), 1.68 (quin, 2 H, J = 7.3 Hz), 1.55 (quin, 2 H, J = 6.9 Hz), 1.19-1.41 (m, 14 H). Mass analysis (MALDI-TOF): m/z 1067.5042 (calculated for C₅₆H₇₆N₄NaO₁₁S₂ [M+Na]⁺ m/z 1067.4844).

Fmoc-L-DOPS-7EG-PDS: Fmoc-L-DOPS-OH (94.4 mg, 0.22 mmol, 1.1 eq.) was coupled to amino-PEG-alkanepyridyl disulfide compound (**5**) (122.6 mg, 0.21 mmol, 1 eq.) according to the general procedure described above. Then, 76 mg of compound **Fmoc-L-DOPS-7EG-PDS** (37%) were obtained as a colorless oil. ¹H NMR (300 MHz, CDCl₃, 25 °C): δ(ppm) = 8.47 (m, 1 H), 7.25-7.81 (m, 10 H), 7.06-7.15 (m, 2 H), 6.83 (d, 1 H, J = 7.9 Hz), 6.65 (d, 1 H, J = 7.9 Hz), 6.23 (br s, 1 H), 5.87 (br s, 1 H), 4.99 (m, 1 H), 4.46 (m, 2 H), 4.37 (m, 1 H), 4.24 (t, 1 H, J = 6.7 Hz), 3.48-3.78 (m, 28 H), 3.44 (t, 2 H, J = 7.0 Hz), 3.25 (m, 1 H), 2.80 (t, 2 H, J = 7.3 Hz), 1.63-1.79 (m, 2 H), 1.57 (quin, 2 H, J = 7.2 Hz), 1.22-1.42 (m, 14 H). Mass analysis (MALDI-TOF): m/z 1060.1505 (calculated for C₅₄H₇₅N₃NaO₁₂S₂ [M+Na]⁺ m/z 1060.4634).

Insertion Kinetics of Neurotransmitter Pre-Functionalized Molecules on Post-Lift-Off Substrates. Post-lift-off substrates were inserted with *L*-3,4-dihydroxyphenylalanine (*L*-DOPA) pre-functionalized molecules for different periods of time, *i.e.*, 15 min (0.25 h), 30 min (0.5 h), 60 min (1 h), 180 min (3 h), and 1440 min (24 h) as seen in Figures 6-S1. The graph shows the fluorescence intensities resulting from antibody capture by *L*-DOPA pre-functionalized molecules. An early increase (0.25-3 h) followed by a slow rise (after 3 h) in fluorescence intensities indicates that the insertion of pre-functionalized molecule begins to reach saturation at ~3 h of insertion.














Control Experiments for Figures 6-2, 6-4, 6-5, and 6-6 in main text. To determine nonspecific binding, neurotransmitter-functionalized substrates were exposed to fluorescently labeled secondary antibodies in the absence of primary antibodies. Representative fluorescence microscopic images from substrates inserted with 100/0 *L*-DOPA pre-functionalized/TEG molecules, 100/0 *L*-5-HTP pre-functionalized/TEG molecules, 100/0 *L*-DOPA post-conjugated/TEG molecules, and 72/25 *L*-5-HTP post-conjugated/TEG molecules are shown in Figure 6-S2A, B, C, and D, respectively. Other ratios of TEG molecules and neurotransmitters pre- or post-functionalized molecules showed similar results to that in Figure 6-S2. As shown in Figures 6-S2, 6-S3, 6-S5, and 6-S7, negligible fluorescence signals were observed on substrates patterned with neurotransmitter pre- and post-functionalized molecules, indicating minimal nonspecific binding of fluorescently labeled secondary antibodies. Low nonspecific binding was associated with the use of protein-resistant TEG self-assembled monolayers as the background matrix and bovine serum albumin as a blocking agent.^{S2-4}

Comparison of Pre- and Post-Functionalization Approaches on the Same Substrates. As discussed in the main text, neurotransmitter pre-functionalized molecule insertion followed surface tether insertion to avoid alterations to pre-functionalized probes resulting from neurotransmitter conjugation to surface tethers. For the reverse patterning route where pre-functionalized molecule insertion preceded tether insertion and post-functionalization, specific recognition of neurotransmitter pre-functionalized molecules might be altered due to the subsequent neurotransmitter conjugation. Nonetheless, fluorescence results showed equivalent specific binding on substrates patterned with *L*-DOPA pre-functionalized followed by post-functionalized molecules (Fig. 6-S4B,C). Improved specific binding was observed on *L*-5-hydroxytryptophan (*L*-5-HTP) pre-functionalized followed by post-functionalized molecule substrates (Fig. 6-S4D,E). Results in Figure 6-S4 were consistent with those in Figure 6-4 in the main text where post-functionalization preceded pre-functionalization. These results suggest that neurotransmitter pre-functionalized molecules are resistant to harsh post-conjugation reactions. Notably, neurotransmitter pre-functionalized molecules displayed consistent specific antibody binding independent of patterning strategies.

Supplemental Results for Figures 6-6A,B,D,E,G,H (main text). Double chemical lift-off lithography was used to fabricate multiplexed neurotransmitter-modified substrates. Patterns of *L*-DOPA/*L*-histidine (*L*-His) and *L*-DOPA/*L*-tryptophan (*L*-Trp) pre-functionalized molecule pairs were exposed to corresponding mixed primary antibodies followed by mixed fluorescently labeled secondary antibodies. Substrates were imaged at two emission wavelengths of 525 nm (AlexaFluor[®] 488; peak excitation at 490 nm; “green”) and 605 nm (AlexaFluor[®] 546; peak excitation at 556 nm; “red”) to visualize captured anti-*L*-DOPA and anti-*L*-His antibodies. A similar pair of emission wavelengths of 525 nm (AlexaFluor[®] 488; peak excitation 490 nm;

“green”) and 605 nm (AlexaFluor[®] 568; peak excitation 578 nm; “red”) was used to visualize captured anti-*L*-DOPA and anti-*L*-Trp antibodies. All green fluorescence images are shown in Figures 6-6A,B,D,E,G,H in the main text. Red fluorescence images are shown in Figure 6-S6A,B,D,E.

Table 6-S1. Summary of primary antibodies and fluorescently labeled secondary antibodies corresponding to surface-tethered neurotransmitters used in this study.

Surface-Tethered Small-Molecule Probe	Primary Antibodies	Secondary Antibodies
 <i>L</i> -3,4-dihydroxyphenylalanine (<i>L</i> -DOPA)	Mouse monoclonal anti- <i>L</i> -DOPA 	AlexaFluor® 488 goat anti-mouse IgG 
 <i>L</i> -5-hydroxytryptophan (<i>L</i> -5-HTP)	Rabbit polyclonal anti- <i>L</i> -5-HTP 	AlexaFluor® 488 goat anti-rabbit IgG  AlexaFluor® 546 goat anti-rabbit IgG 
 <i>L</i> -histidine (<i>L</i> -His)	Rabbit polyclonal anti- <i>L</i> -His 	AlexaFluor® 546 goat anti-rabbit IgG 
 <i>L</i> -tryptophan (<i>L</i> -Trp)	Rat polyclonal anti- <i>L</i> -Trp 	AlexaFluor® 568 goat anti-rat IgG 

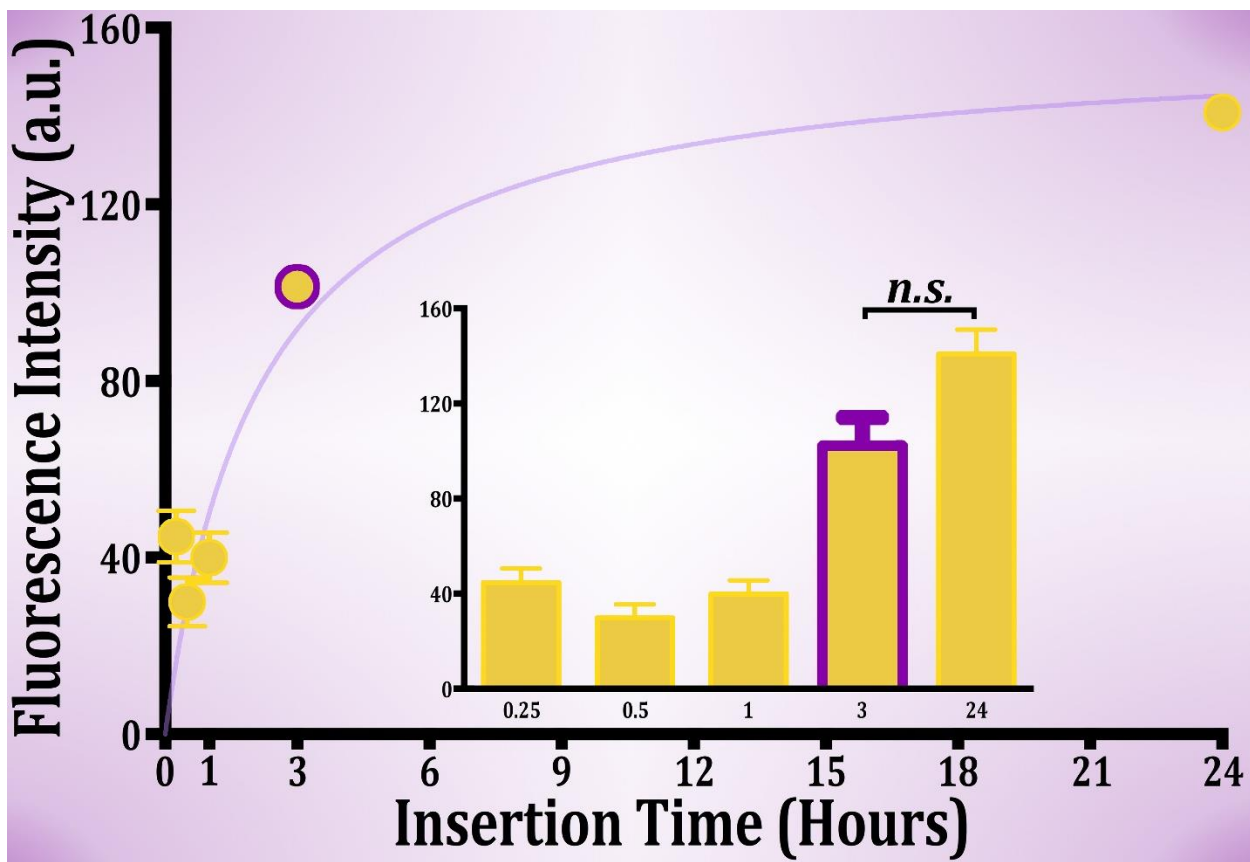


Figure 6-S1. Fluorescence intensities as a function of insertion times. An initial sharp increase (0.25-3 h) followed by a slow rise in fluorescence intensities was associated with different insertion times for L-DOPA pre-functionalized probes. These results, indicate that the insertion of pre-functionalized molecules begins to reach saturation after 3 h of insertion. Patterned substrates were imaged at an emission wavelength of 525 nm (AlexaFluor[®] 488 secondary antibodies; excitation at 490 nm) to visualize the binding of anti-L-DOPA primary antibodies on L-DOPA functionalized substrates. The fluorescence intensity bar graphs in the inset show non-significant differences in fluorescence intensities between 3 h and 24 h insertion times. Error bars represent standard errors of the means with $N=3$ substrates per group.

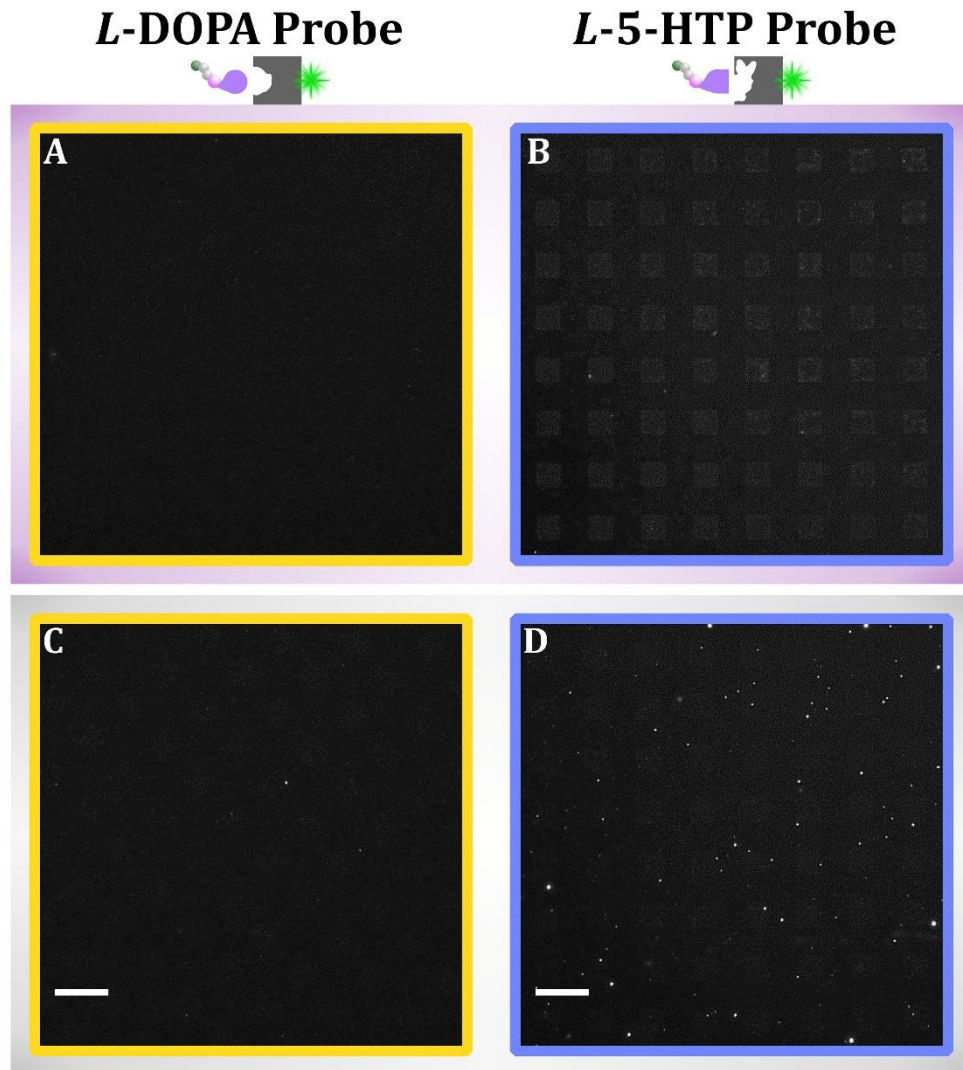


Figure 6-S2 Control experiments for Figure 6-2 (main text). Representative fluorescence images for patterns of pre-/post-functionalized molecules or mixed hydroxyl tri(ethylene glycol)-terminated alkanethiols and pre-/post-functionalized molecules: **(A)** *L*-3,4-dihydroxyphenylalanine (*L*-DOPA) and **(B)** *L*-5-hydroxytryptophan (*L*-5-HTP) pre-functionalization. **(C)** *L*-DOPA and **(D)** *L*-5-HTP post-patterning functionalization, respectively. Patterned substrates were exposed to fluorescently labeled secondary antibodies alone. Negligible fluorescence signals at an emission wavelength of 525 nm (AlexaFluor[®] 488; excitation at 490 nm) indicated nominal nonspecific binding of fluorescently labeled secondary antibodies. Scale bars are 50 μ m.

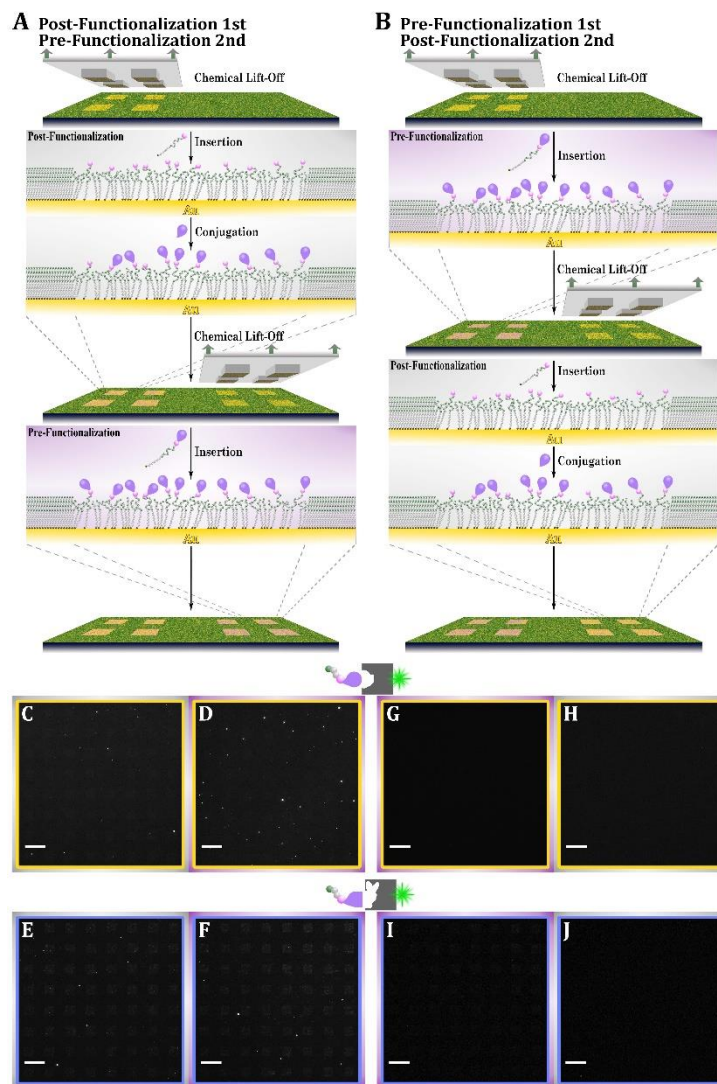


Figure 6-S3 Control experiments corresponding to Figure 6-4 (main text) and Figure 6-S4B (supporting materials). Schematic illustrating double lift-off patterning of (A) post-functionalization followed by pre-functionalization and (B) pre-functionalization followed by post-functionalization. In (A), tether molecules are inserted after the first lift-off step and functionalized (conjugated with neurotransmitter) followed by insertion of pre-functionalized molecules in an adjacent region after a second lift-off step. The procedure is reversed in (B).

Representative fluorescence images for (C,D,G,H) are patterns of L-3,4-dihydroxyphenylalanine (L-DOPA) and (E,F,I,J) are patterns of L-5-hydroxytryptophan (L-5-HTP) on substrates subjected to (C,E) post- followed by (D,F) pre- and (G,I) pre- followed by (H,J) post-functionalization. Substrates were exposed to fluorescently labeled secondary antibodies alone. Negligible fluorescence signals were observed at an emission wavelength of 525 nm (AlexaFluor® 488; excitation at 490 nm) indicating negligible nonspecific binding of fluorescently labeled secondary antibodies on patterned substrates. Scale bars are 50 μm.

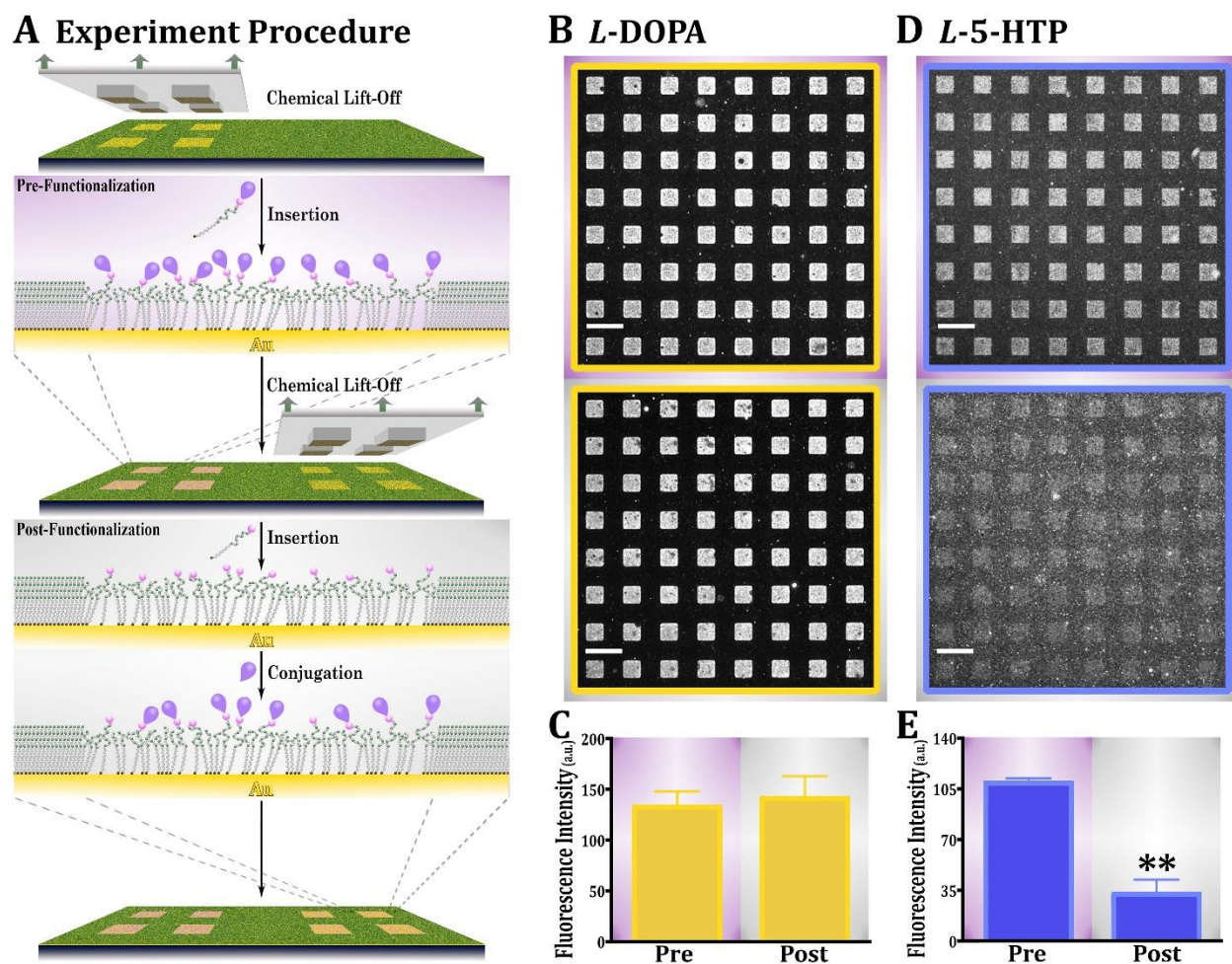


Figure 6-S4. (A) Schematic illustrating double lift-off patterning of pre- followed by post-functionalized molecules. (B,D) Representative fluorescence images and (C,E) fluorescence intensity graphs for antibody binding on double patterns of (B,C) *L*-3,4-dihydroxyphenylalanine (*L*-DOPA) and (D,E) *L*-5-hydroxytryptophan (*L*-5-HTP). (C) Fluorescence intensity graphs showed equivalent fluorescence signals resulting from antibody binding on *L*-DOPA pre- vs. post-functionalized substrates. (E) In contrast, fluorescence signals from antibody binding to *L*-5-HTP pre-functionalized molecules are significantly greater than those for *L*-5-HTP post-patterning functionalization indicating improved specific binding for *L*-5-HTP pre-functionalized molecules. Patterned substrates were imaged at emission wavelength of 525 nm (AlexaFluor[®] 488; excitation at 490 nm). Error bars represent standard errors of the means with $N=3$ samples per group. Mean intensities are significantly different for (E) [$t(4)=8$ ** $P<0.01$]. Scale bars are 50 μm .

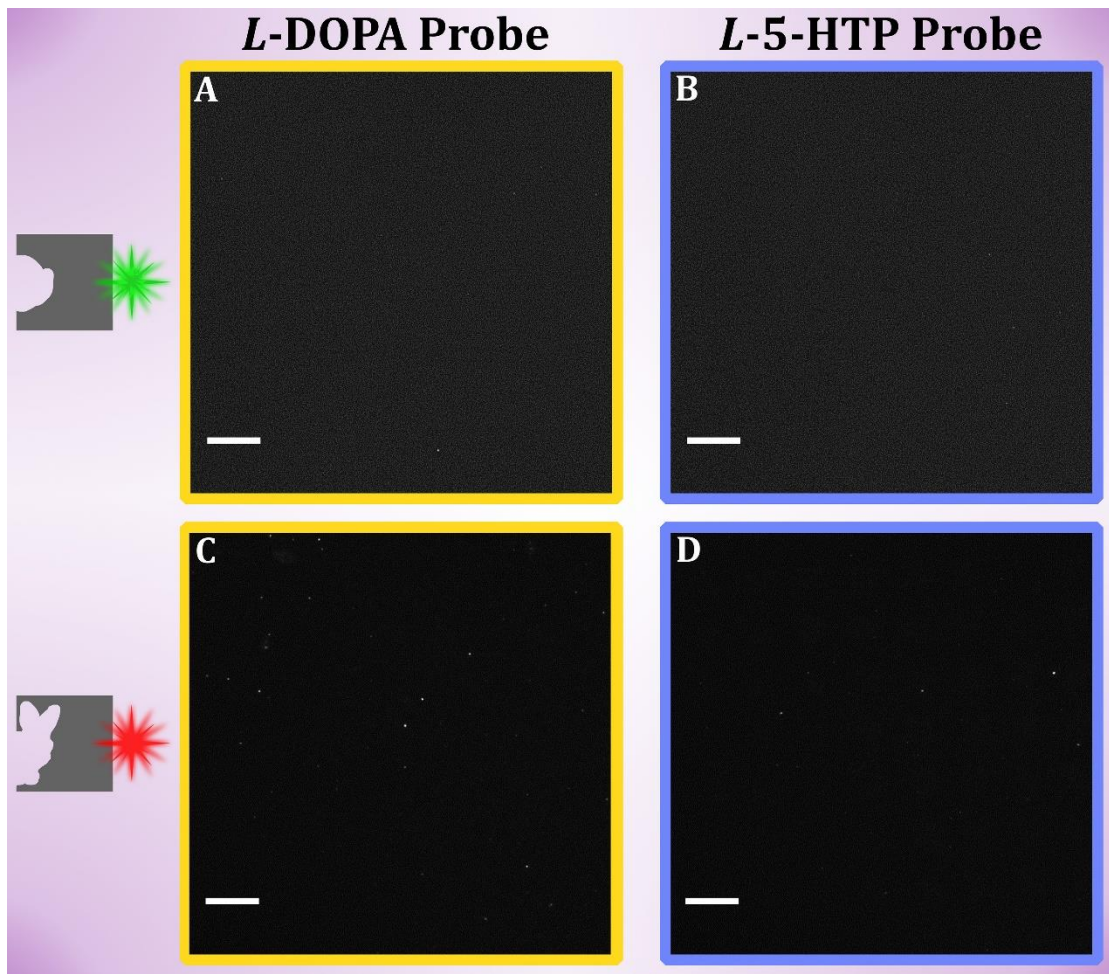


Figure 6-S5 Control experiments for Figure 6-5 (main text). Representative fluorescence microscopic images for substrates double patterning with (A,C) *L*-3,4-dihydroxyphenylalanine (*L*-DOPA) and (B,D) *L*-5-hydroxytryptophan (*L*-5-HTP) pre-functionalized molecules. Patterned substrates were challenged with mixed fluorescently labeled secondary antibodies alone. Negligible fluorescence was observed at two emission wavelengths of (A,B) 525 nm (AlexaFluor[®] 488; excitation at 490 nm) and (C,D) 605 nm (AlexaFluor[®] 546; excitation at 556 nm) indicating minimal nonspecific binding of fluorescently labeled secondary antibodies. Scale bars are 50 μ m.

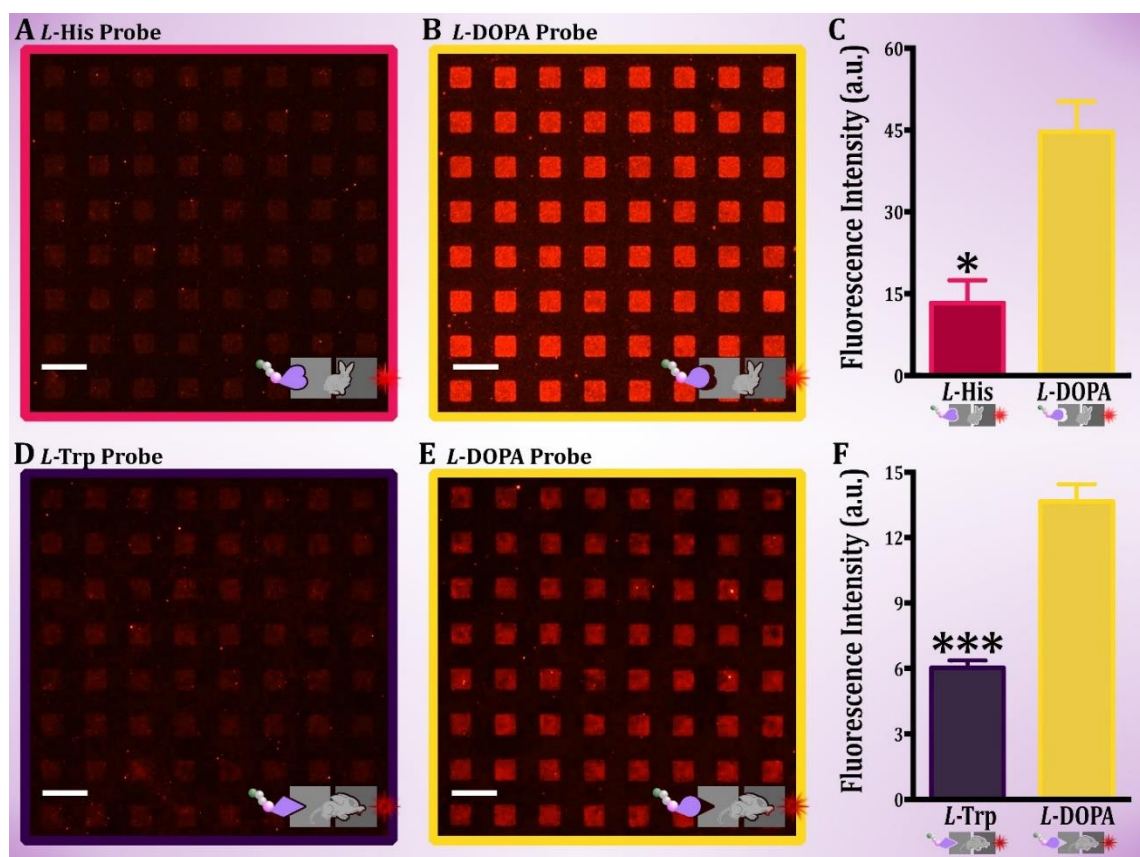


Figure 6-S6 Complementary experiments for Figure 6-6 (main text). Representative fluorescence images for substrates double patterned with (A,B) *L*-3,4-dihydroxyphenylalanine (*L*-DOPA)/*L*-histidine (*L*-His) and (D,E) *L*-DOPA/*L*-tryptophan (*L*-Trp) pre-functionalized molecules. Patterned substrates were exposed to mixed primary antibodies followed by mixed fluorescently labeled secondary antibodies. Substrates were imaged at two emission wavelengths of 525 nm (AlexaFluor[®] 488; excitation 490 nm; green) and 605 nm (AlexaFluor[®] 546; excitation 556 nm; red) to visualize primary antibodies captured on (A,B) *L*-DOPA/*L*-His patterns. Similar fluorescence emission wavelength pairs were used (525 nm for AlexaFluor[®] 488 with excitation at 490 nm and 603 nm for AlexaFluor[®] 568 with excitation at 578 nm) to visualize primary antibodies captured on (D,E) *L*-DOPA/*L*-Trp patterns. Corresponding images for green fluorescence are shown in Figure 6-6 in the main text. Images shown here for red fluorescence visualize binding of (A,B) anti-*L*-His and (D,E) anti-*L*-Trp primary antibodies on double-patterned substrates. (C,F) Fluorescence intensity graphs showed higher binding of anti-*L*-His and anti-*L*-Trp primary antibodies to *L*-DOPA than to *L*-His and *L*-Trp pre-functionalized molecules, suggesting cross-reactivity of primary antibodies. Error bars represent standard errors of the means with $N=3$ substrates per group. Mean intensities are significantly different in (C) [$t(4)=5$ * $P<0.05$] and in (F) [$t(4)=9$ *** $P<0.001$]. Scale bars are 50 μm .

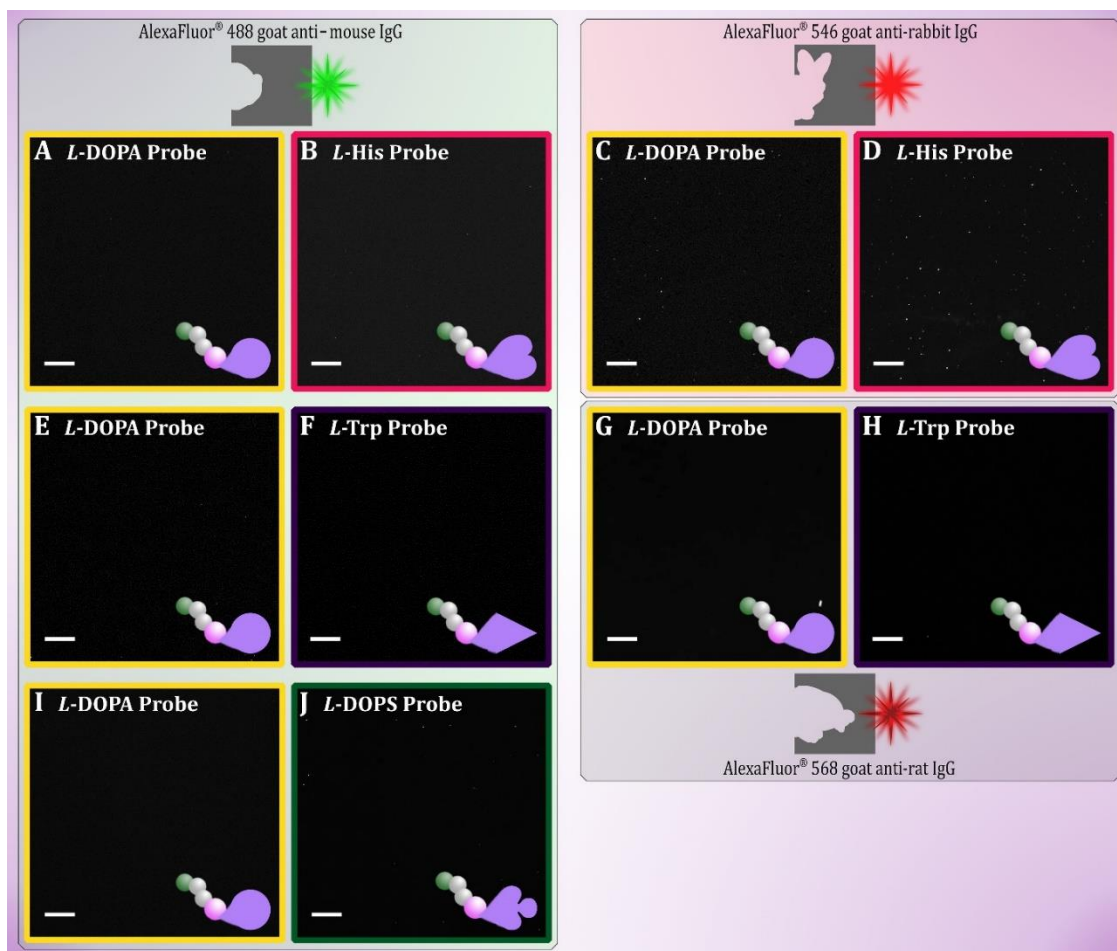


Figure 6-S7 Control experiments for Figure 6-6 (main text) and Figure 6-S6 (supporting materials). Representative fluorescence images for substrates double patterned with (A,B,C,D) *L*-3,4-dihydroxyphenylalanine (*L*-DOPA)/*L*-histidine (*L*-His), (E,F,G,H) *L*-DOPA/*L*-tryptophan (*L*-Trp), and (I,J) *L*-DOPA/*L*-droxidopa (*L*-DOPS) pre-functionalized molecules. Patterned substrates were challenged with fluorescently labeled secondary antibodies in (I,J) and with mixed fluorescently labeled secondary antibodies in (A-H). Negligible fluorescence was observed at two emission wavelengths in (A,B) 525 nm (AlexaFluor® 488; excitation at 490 nm) and (C,D) 605 nm (AlexaFluor® 546; excitation at 556 nm) indicating minimal nonspecific binding of fluorescently labeled secondary antibodies on *L*-DOPA/*L*-His patterns. Similarly, negligible fluorescence signals at two emission wavelengths in (E,F) 525 nm (AlexaFluor® 488; excitation at 490 nm) and (G,H) 605 nm (AlexaFluor® 568; excitation at 578 nm) and at an emission wavelength of 525 nm (AlexaFluor® 488; excitation at 490 nm) in (I,J) indicated negligible nonspecific binding of fluorescently labeled secondary antibodies on (E,F,G,H) *L*-DOPA/*L*-Trp and (I,J) *L*-DOPA/*L*-DOPS patterns, respectively. Scale bars are 50 μm .

6.7 References

1. Farahi, R. H.; Passian, A.; Tetard, L.; Thundat, T. Critical Issues in Sensor Science to Aid Food and Water Safety. *ACS Nano* **2012**, *6*, 4548-4556.
2. Wittenberg, N. J.; Im, H.; Johnson, T. W.; Xu, X.; Warrington, A. E.; Rodriguez, M.; Oh, S.-H. Facile Assembly of Micro- and Nanoarrays for Sensing with Natural Cell Membranes. *ACS Nano* **2011**, *5*, 7555-7564.
3. Neumann, L.; Wohland, T.; Whelan, R. J.; Zare, R. N.; Kobilka, B. K. Functional Immobilization of a Ligand-Activated G-Protein-Coupled Receptor. *ChemBioChem* **2002**, *3*, 993-998.
4. Minic, J.; Grosclaude, J.; Aioun, J.; Persuy, M. A.; Gorojankina, T.; Salesse, R.; Pajot-Augy, E.; Hou, Y. X.; Helali, S.; Jaffrezic-Renault, N.; Bessueille, F.; Errachid, A.; Gomila, G.; Ruiz, O.; Samitier, J. Immobilization of Native Membrane-Bound Rhodopsin on Biosensor Surfaces. *Biochim. Biophys. Acta-Gen. Subjects* **2005**, *1724*, 324-332.
5. Fang, Y.; Peng, J. L.; Ferrie, A. M.; Burkhalter, R. S. Air-Stable G Protein-Coupled Receptor Microarrays and Ligand Binding Characteristics. *Anal. Chem.* **2006**, *78*, 149-155.
6. Bally, M.; Bailey, K.; Sugihara, K.; Grieshaber, D.; Voros, J.; Stadler, B. Liposome and Lipid Bilayer Arrays Towards Biosensing Applications. *Small* **2010**, *6*, 2481-2497.
7. Kwon, Y.; Han, Z. Z.; Karatan, E.; Mrksich, M.; Kay, B. K. Antibody Arrays Prepared by Cutinase-Mediated Immobilization on Self-Assembled Monolayers. *Anal. Chem.* **2004**, *76*, 5713-5720.
8. Lu, B.; Smyth, M. R.; Okennedy, R. Oriented Immobilization of Antibodies and Its Applications in Immunoassays and Immunosensors. *Analyst* **1996**, *121*, R29-R32.

9. Spitznagel, T. M.; Clark, D. S. Surface-Density and Orientation Effects on Immobilized Antibodies and Antibody Fragments. *Bio-Technology* **1993**, *11*, 825-829.
10. Vijayendran, R. A.; Leckband, D. E. A Quantitative Assessment of Heterogeneity for Surface-Immobilized Proteins. *Anal. Chem.* **2001**, *73*, 471-480.
11. MacBeath, G.; Koehler, A. N.; Schreiber, S. L. Printing Small Molecules as Microarrays and Detecting Protein-Ligand Interactions en Masse. *J. Am. Chem. Soc.* **1999**, *121*, 7967-7968.
12. Vegas, A. J.; Fuller, J. H.; Koehler, A. N. Small-Molecule Microarrays as Tools in Ligand Discovery. *Chem. Soc. Rev.* **2008**, *37*, 1385-1394.
13. Shuster, M. J.; Vaish, A.; Gilbert, M. L.; Martinez-Rivera, M.; Nezarati, R. M.; Weiss, P. S.; Andrews, A. M. Comparison of Oligo(Ethylene Glycol)Alkanethiols versus *n*-Alkanethiols: Self-Assembly, Insertion, and Functionalization. *J. Phys. Chem. C* **2011**, *115*, 24778-24787.
14. Liao, W.-S.; Cao, H. H.; Cheunkar, S.; Shuster, M. J.; Altieri, S. C.; Weiss, P. S.; Andrews, A. M. Small-Molecule Arrays for Sorting G-Protein-Coupled Receptors. *J. Phys. Chem. C* **2013**, *117*, 22362-22368.
15. Shuster, M. J.; Vaish, A.; Cao, H. H.; Guttentag, A. I.; McManigle, J. E.; Gibb, A. L.; Martinez, M. M.; Nezarati, R. M.; Hinds, J. M.; Liao, W.-S.; Weiss, P. S.; Andrews, A. M. Patterning Small-Molecule Biocapture Surfaces: Microcontact Insertion Printing vs. Photolithography. *Chem. Commun.* **2011**, *47*, 10641-10643.
16. Vaish, A.; Shuster, M. J.; Cheunkar, S.; Singh, Y. S.; Weiss, P. S.; Andrews, A. M. Native Serotonin Membrane Receptors Recognize 5-Hydroxytryptophan-Functionalized

- Substrates: Enabling Small-Molecule Recognition. *ACS Chem. Neurosci.* **2010**, *1*, 495-504.
17. Vaish, A.; Shuster, M. J.; Cheunkar, S.; Weiss, P. S.; Andrews, A. M. Tuning Stamp Surface Energy for Soft Lithography of Polar Molecules to Fabricate Bioactive Small-Molecule Microarrays. *Small* **2011**, *7*, 1471-1479.
18. Shuster, M. J.; Vaish, A.; Szapacs, M. E.; Anderson, M. E.; Weiss, P. S.; Andrews, A. M. Biospecific Recognition of Tethered Small Molecules Diluted in Self-Assembled Monolayers. *Adv. Mater.* **2008**, *20*, 164-167.
19. Ostuni, E.; Yan, L.; Whitesides, G. M. The Interaction of Proteins and Cells with Self-Assembled Monolayers of Alkanethiolates on Gold and Silver. *Colloids Surf. B. Biointerfaces* **1999**, *15*, 3-30.
20. Harder, P.; Grunze, M.; Dahint, R.; Whitesides, G. M.; Laibinis, P. E. Molecular Conformation in Oligo(Ethylene Glycol)-Terminated Self-Assembled Monolayers on Gold and Silver Surfaces Determines Their Ability to Resist Protein Adsorption. *J. Phys. Chem. B* **1998**, *102*, 426-436.
21. Mullen, T. J.; Srinivasan, C.; Hohman, J. N.; Gillmor, S. D.; Shuster, M. J.; Horn, M. W.; Andrews, A. M.; Weiss, P. S. Microcontact Insertion Printing. *Appl. Phys. Lett.* **2007**, *90*, 063114.
22. Saavedra, H. M.; Mullen, T. J.; Zhang, P. P.; Dewey, D. C.; Claridge, S. A.; Weiss, P. S. Hybrid Strategies in Nanolithography. *Rep. Prog. Phys.* **2010**, *73*, 036501.
23. Liao, W.-S.; Cheunkar, S.; Cao, H. H.; Bednar, H. R.; Weiss, P. S.; Andrews, A. M. Subtractive Patterning *via* Chemical Lift-Off Lithography. *Science* **2012**, *337*, 1517-1521.

24. Alivisatos, A. P.; Andrews, A. M.; Boyden, E. S.; Chun, M.; Church, G. M.; Deisseroth, K.; Donoghue, J. P.; Fraser, S. E.; Lippincott-Schwartz, J.; Looger, L. L.; Masmanidis, S.; McEuen, P. L.; Nurmikko, A. V.; Park, H.; Peterka, D. S.; Reid, C.; Roukes, M. L.; Scherer, A.; Schnitzer, M.; Sejnowski, T. J.; Shepard, K. L.; Tsao, D.; Turrigiano, G.; Weiss, P. S.; Xu, C.; Yuste, R.; Zhuang, X. W. Nanotools for Neuroscience and Brain Activity Mapping. *ACS Nano* **2013**, *7*, 1850-1866.
25. Andrews, A. M. The BRAIN Initiative: Toward a Chemical Connectome. *ACS Chem. Neurosci.* **2013**, *4*, 645-645.
26. Andrews, A. M.; Schepartz, A.; Sweedler, J. V.; Weiss, P. S. Chemistry and the BRAIN Initiative. *J. Am. Chem. Soc.* **2014**, *136*, 1-2.
27. Andrews, A. M.; Weiss, P. S. Nano in the Brain: Nano-Neuroscience. *ACS Nano* **2012**, *6*, 8463-8464.
28. Sam, S.; Touahir, L.; Andresa, J. S.; Allongue, P.; Chazalviel, J. N.; Gouget-Laemmel, A. C.; de Villeneuve, C. H.; Moraillon, A.; Ozanam, F.; Gabouze, N.; Djebbar, S. Semiquantitative Study of the EDC/NHS Activation of Acid Terminal Groups at Modified Porous Silicon Surfaces. *Langmuir* **2010**, *26*, 809-814.
29. Wang, C.; Yan, Q.; Liu, H. B.; Zhou, X. H.; Xiao, S. J. Different EDC/NHS Activation Mechanisms between PAA and PMAA Brushes and the following Amidation Reactions. *Langmuir* **2011**, *27*, 12058-12068.
30. Xia, N.; Xing, Y.; Wang, G. F.; Feng, Q. Q.; Chen, Q. Q.; Feng, H. M.; Sun, X. L.; Liu, L. Probing of EDC/NHSS-Mediated Covalent Coupling Reaction by the Immobilization of Electrochemically Active Biomolecules. *Int. J. Electrochem. Sci.* **2013**, *8*, 2459-2467.

31. Congreve, M.; Langmead, C. J.; Mason, J. S.; Marshall, F. H. Progress in Structure Based Drug Design for G Protein-Coupled Receptors. *J. Med. Chem.* **2011**, *54*, 4283-4311.
32. Seeber, M.; De Benedetti, P. G.; Fanelli, F. Molecular Dynamics Simulations of the Ligand-Induced Chemical Information Transfer in the 5-HT_{1A} Receptor. *J. Chem. Inf. Comput. Sci.* **2003**, *43*, 1520-1531.
33. Lipman, N. S.; Jackson, L. R.; Trudel, L. J.; Weis-Garcia, F. Monoclonal *versus* Polyclonal Antibodies: Distinguishing Characteristics, Applications, and Information Resources. *Ilar J.* **2005**, *46*, 258-268.
34. Mendonsa, S. D.; Bowser, M. T. *In Vitro* Selection of Aptamers with Affinity for Neuropeptide Y Using Capillary Electrophoresis. *J. Am. Chem. Soc.* **2005**, *127*, 9382-9383.
35. McKeague, M.; DeRosa, M. C. Challenges and Opportunities for Small Molecule Aptamer Development. *J. Nucleic Acids* **2012**, *2012*, 1-20.
36. Kim, Y. S.; Gu, M. B. Advances in Aptamer Screening and Small Molecule Aptasensors. *Biosensors Based on Aptamers and Enzymes* **2014**, *140*, 29-67.
37. Banerjee, J.; Nilsen-Hamilton, M. Aptamers: Multifunctional Molecules for Biomedical Research. *J. Mol. Med.* **2013**, *91*, 1333-1342.
38. Svedhem, S.; Hollander, C. A.; Shi, J.; Konradsson, P.; Liedberg, B.; Svensson, S. C. T. Synthesis of a Series of Oligo(Ethylene Glycol)-Terminated Alkanethiol Amides Designed to Address Structure and Stability of Biosensing Interfaces. *J. Org. Chem.* **2001**, *66*, 4494-4503.

39. Palegrosdemange, C.; Simon, E. S.; Prime, K. L.; Whitesides, G. M. Formation of Self-Assembled Monolayers by Chemisorption of Derivatives of Oligo(Ethylene Glycol) of Structure HS(CH₂)₁₁(OCH₂CH₂)Meta-OH on Gold. *J. Am. Chem. Soc.* **1991**, *113*, 12-20.
40. Vazquez-Dorbatt, V.; Tolstyka, Z. P.; Chang, C. W.; Maynard, H. D. Synthesis of a Pyridyl Disulfide End-Functionalized Glycopolymer for Conjugation to Biomolecules and Patterning on Gold Surfaces. *Biomacromolecules* **2009**, *10*, 2207-2212.
41. Prime, K. L.; Whitesides, G. M. Adsorption of Proteins onto Surfaces Containing End-Attached Oligo(Ethylene Oxide) - A Model System Using Self-Assembled Monolayers. *J. Am. Chem. Soc.* **1993**, *115*, 10714-10721.
42. Tolstyka, Z. P.; Richardson, W.; Bat, E.; Stevens, C. J.; Parra, D. P.; Dozier, J. K.; Distefano, M. D.; Dunn, B.; Maynard, H. D. Chemoselective Immobilization of Proteins by Microcontact Printing and Bio-orthogonal Click Reactions. *ChemBioChem* **2013**, *14*, 2464-2471.
43. Booth, C.; Bushby, R. J.; Cheng, Y. L.; Evans, S. D.; Liu, Q. Y.; Zhang, H. L. Synthesis of Novel Biotin Anchors. *Tetrahedron* **2001**, *57*, 9859-9866.
44. Kleinert, M.; Rockendorf, N.; Lindhorst, T. K. Glyco-SAMs as Glycocalyx Mimetics: Synthesis of L-Fucose- and D-Mannose-Terminated Building Blocks. *Eur. J. Org. Chem.* **2004**, 3931-3940.
45. Prats-Alfonso, E.; Oberhansl, S.; Lagunas, A.; Martinez, E.; Samitier, J.; Albericio, F. Effective and Versatile Strategy for the Total Solid-Phase Synthesis of Alkanethiols for Biological Applications. *Eur. J. Org. Chem.* **2013**, 1233-1239.

46. Murray, J.; Nowak, D.; Pukenas, L.; Azhar, R.; Guillorit, M.; Walti, C.; Critchley, K.; Johnson, S.; Bon, R. S. Solid Phase Synthesis of Functionalised SAM-Forming Alkanethiol-Oligoethyleneglycols. *J. Mat. Chem. B* **2014**, *2*, 3741-3744.
47. Islam, N.; Gurgel, P. V.; Rojas, O. J.; Carbonell, R. G. Effects of Composition of Oligo(ethylene glycol)-Based Mixed Monolayers on Peptide Grafting and Human Immunoglobulin Detection. *J. Phys. Chem. C* **2014**, *118*, 5361-5373.
48. Caprioli, F.; Marrani, A. G.; Di Castro, V. Tuning the Composition of Aromatic Binary Self-Assembled Monolayers on Copper: An XPS Study. *Appl. Surf. Sci.* **2014**, *303*, 30-36.
49. Bain, C. D.; Evall, J.; Whitesides, G. M. Formation of Monolayers by the Coadsorption of Thiols on Gold - Variation in the Head Group, Tail Group, and Solvent. *J. Am. Chem. Soc.* **1989**, *111*, 7155-7164.
50. Zareie, H. M.; Boyer, C.; Bulmus, V.; Nateghi, E.; Davis, T. P. Temperature-Responsive Self-Assembled Monolayers of Oligo(Ethylene Glycol): Control of Biomolecular Recognition. *ACS Nano* **2008**, *2*, 757-765.
51. Bain, C. D.; Troughton, E. B.; Tao, Y. T.; Evall, J.; Whitesides, G. M.; Nuzzo, R. G. Formation of Monolayer Films by the Spontaneous Assembly of Organic Thiols from Solution onto Gold. *J. Am. Chem. Soc.* **1989**, *111*, 321-335.
52. Bain, C. D.; Biebuyck, H. A.; Whitesides, G. M. Comparison of Self-Assembled Monolayers on Gold - Coadsorption of Thiols and Disulfides. *Langmuir* **1989**, *5*, 723-727.

53. Cao, H. H.; Nakatsuka, N.; Serino, A. C.; Liao, W.-S.; Cheunkar, S.; Yang, H.; Weiss, P. S.; Andrews, A. M. Controlled DNA Patterning by Chemical Lift-Off Lithography: Matrix Matters. *ACS Nano* **2015**, *9*, 11439–11454.
54. Saavedra, H. M.; Thompson, C. M.; Hohman, J. N.; Crespi, V. H.; Weiss, P. S. Reversible Lability by *in Situ* Reaction of Self-Assembled Monolayers. *J. Am. Chem. Soc.* **2009**, *131*, 2252-2259.
55. Mei, H. C.; Bing, T.; Yang, X. J.; Qi, C.; Chang, T. J.; Liu, X. J.; Cao, Z. H.; Shangguan, D. H. Functional-Group Specific Aptamers Indirectly Recognizing Compounds with Alkyl Amino Group. *Anal. Chem.* **2012**, *84*, 7323-7329.
56. Vallee-Belisle, A.; Plaxco, K. W. Structure-Switching Biosensors: Inspired by Nature. *Curr. Opin. Struct. Biol.* **2010**, *20*, 518-526.
57. Kim, J.; Rim, Y. S.; Chen, H. J.; Cao, H. H.; Nakatsuka, N.; Hinton, H. L.; Zhao, C. Z.; Andrews, A. M.; Yang, Y.; Weiss, P. S. Fabrication of High-Performance Ultrathin In₂O₃ Film Field-Effect Transistors and Biosensors Using Chemical Lift-Off Lithography. *ACS Nano* **2015**, *9*, 4572-4582.
58. Stenlund, P.; Babcock, G. J.; Sodroski, J.; Myszka, D. G. Capture and Reconstitution of G Protein-Coupled Receptors on a Biosensor Surface. *Anal. Biochem.* **2003**, *316*, 243-250.
59. Bailey, K.; Bally, M.; Leifert, W.; Voros, J.; McMurchie, T. G-Protein Coupled Receptor Array Technologies: Site Directed Immobilisation of Liposomes Containing the H₁-Histamine or M₂-Muscarinic Receptors. *Proteomics* **2009**, *9*, 2052-2063.

60. Fruh, V.; Ijzerman, A. P.; Siegal, G. How to Catch a Membrane Protein in Action: A Review of Functional Membrane Protein Immobilization Strategies and Their Applications. *Chem. Rev.* **2011**, *111*, 640-656.

References for Supporting Materials (references S3 and S4 are from references 50 and 14 in the main text)

- S1. Palegrosdemange, C.; Simon, E. S.; Prime, K. L.; Whitesides, G. M. Formation of Self-Assembled Monolayers by Chemisorption of Derivatives of Oligo(Ethylene Glycol) of Structure HS(CH₂)₁₁(OCH₂CH₂)Meta-OH on Gold. *J. Am. Chem. Soc.* **1991**, *113*, 12-20.
- S2. Li, S. S.; Yang, D. Y.; Tu, H. Y.; Deng, H. T.; Du, D.; Zhang, A. D. Protein Adsorption and Cell Adhesion Controlled by the Surface Chemistry of Binary Perfluoroalkyl/Oligo(Ethylene Glycol) Self-Assembled Monolayers. *J. Colloid Interface Sci.* **2013**, *402*, 284-290.
- S3. Zareie, H. M.; Boyer, C.; Bulmus, V.; Nateghi, E.; Davis, T. P. Temperature-Responsive Self-Assembled Monolayers of Oligo(Ethylene Glycol): Control of Biomolecular Recognition. *ACS Nano* **2008**, *2*, 757-765.
- S4. Liao, W. S.; Cao, H. H.; Cheunkar, S.; Shuster, M. J.; Altieri, S. C.; Weiss, P. S.; Andrews, A. M. Small-Molecule Arrays for Sorting G-Protein-Coupled Receptors. *J. Phys. Chem. C* **2013**, *117*, 22362-22368.

Chapter 7

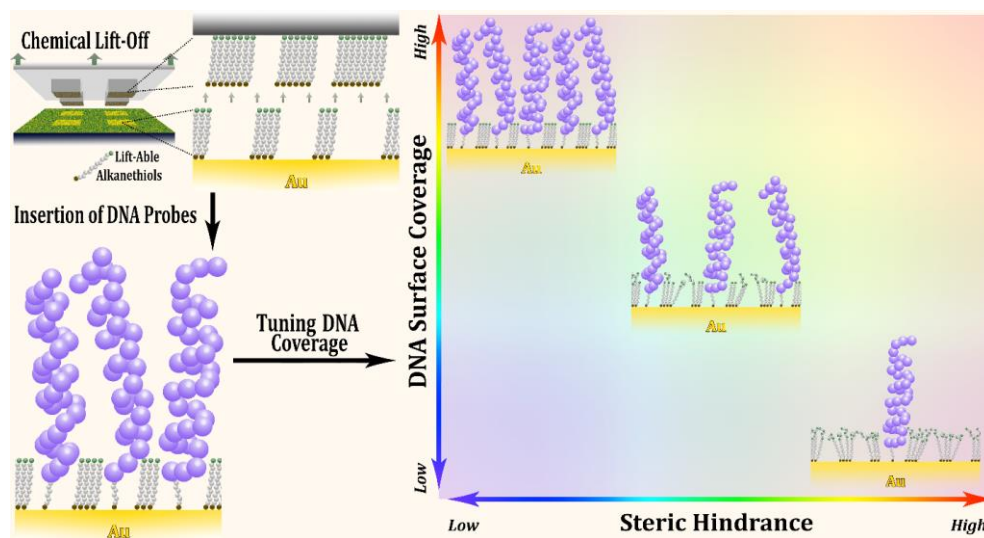
Controlled DNA Patterning by Chemical Lift-Off Lithography: Matrix Matters

The information in this chapter was published in *ACS Nano* **2015**, *9*, 11439-11454

and has been reproduced here in its entirety.

Authors: Cao, H. H., Nakatsuka, N., Serino, A. C.; Liao, W.-S.; Cheunkar, S.; Yang, H.;

Weiss, P. S.; Andrews, A. M.



7.1 Abstract

Nucleotide arrays require controlled surface densities and minimal nucleotide-substrate interactions to enable highly specific and efficient recognition by corresponding targets. We investigated chemical lift-off lithography with hydroxyl- and oligo(ethylene glycol)-terminated alkanethiol self-assembled monolayers as a means to produce substrates optimized for tethered DNA insertion into post-lift-off regions. Residual alkanethiols in the patterned regions after lift-off lithography enabled the formation of patterned DNA monolayers that favored hybridization with target DNA. Nucleotide densities were tunable by altering surface chemistries and alkanethiol ratios prior to lift-off. Lithography-induced conformational changes in oligo(ethylene glycol)-terminated monolayers hindered nucleotide insertion but could be used to advantage *via* mixed monolayers or double lift-off lithography. Compared to thiolated DNA self-assembly alone or with alkanethiol backfilling, preparation of functional nucleotide arrays by chemical lift-off lithography enables superior hybridization efficiency and tunability.

7.2 Introduction

Nucleotide microarrays are widely used to identify specific DNA sequences and to investigate large-scale gene expression.¹ To fabricate arrays, probe nucleotides are immobilized on solid substrates for hybridization with complementary targets from solution. Tethering strategies include covalent binding, electrostatic interaction, biotin-streptavidin linkage, and thiolated nucleotide self-assembly.^{2,3} Alkanethiol (SAMs) on Au have been utilized to regulate surface-probe densities and probe-substrate interactions, thereby enhancing specific recognition of tethered DNA targets and minimizing nonspecific binding.⁴⁻⁸ As such, the use of alkanethiol SAMs modified with DNA probes has advanced understanding of DNA-SAM and DNA-substrate interactions to improve and to optimize the performance of nucleotide-functionalized substrates.⁹⁻¹⁵

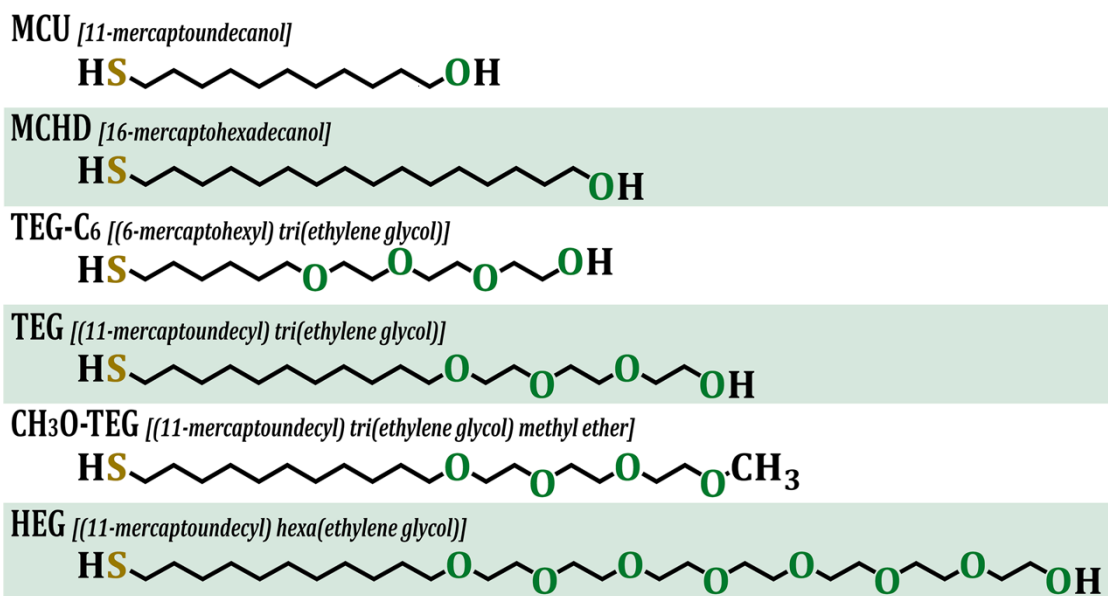
Tarlov *et al.* illustrated the importance of alcohol-terminated alkanethiols on Au substrates to facilitate target DNA hybridization.^{4,16,17} Here, alkanethiol-DNA was self-assembled and then backfilled with mercaptohexanol (MCH) to dilute the DNA and to prevent direct interactions between DNA probes and substrates.^{4,18} Backfilling with alkanethiols also lowers quenching of fluorescently labeled DNA by preventing DNA molecules from lying flat on metal substrates.^{12,19} In addition to MCH, mercaptoundecanol (MCU) and oligo(ethylene glycol)-terminated alkanethiols have been used as diluents.^{6,7,20-22} The presence of the latter reduces nonspecific interactions with proteins and other biomolecules.^{9,23,24} For example, Choi *et al.* demonstrated that DNA substrates created by backfilling with hydroxyl- and carboxyl-terminated oligo(ethylene glycol)-containing alkanethiols and functionalized with cell-adhesion peptides simultaneously promoted peptide-selective cell adhesion and DNA hybridization.²⁵

In lieu of backfilling, thiolated DNA can be inserted into preformed alkanethiol SAMs.^{6,26,27} Insertion is advantageous for a number of reasons. Instead of exposing surface-bound DNA to ethanolic alkanethiol solutions during backfilling, which causes DNA condensation and precipitation, alkanethiols are assembled first followed by insertion of DNA dissolved in aqueous buffers.^{28,29} Insertion also prevents phase separation.^{23,30-33} A recent study of DNA hybridization on Au electrodes demonstrated that surface hybridization was reduced because DNA probes tended to aggregate into domains after backfilling with alcohol-terminated alkanethiols.³⁴ In contrast, tethered DNA molecules inserted into defect sites in preformed SAMs produced dilute coverage wherein individual probe strands were isolated from each other.^{34,35} A low-density environment for surface-bound DNA not only improves hybridization by providing better access for target DNA but it enables investigation of DNA-substrate interactions at the single-molecule level.³⁴⁻³⁷

Insertion-directed chemistries are also beneficial because they can be combined with surface patterning methods.³⁸⁻⁴⁰ We developed microcontact insertion printing for substrate patterning³⁸ and have used this technique to produce dilute coverage of surface-tethered small-molecule ligands on preformed oligo(ethylene glycol)-terminated alkanethiol SAMs.²³ However, using microcontact insertion printing for DNA patterning will require tuning stamp surface chemistries to facilitate insertion of alkanethiol-functionalized DNA into SAMs.⁴¹ Alternately, we illustrate how patterning characterized by dilute DNA surface coverage and reduced DNA-substrate interactions can be achieved straightforwardly using chemical lift-off lithography.⁴² Lift-off lithography takes advantage of the strong interactions formed during stamp-substrate contact between the siloxyl groups on oxygen plasma-treated PDMS stamps and hydroxyl-terminated alkanethiol SAMs. Boxer and co-workers have used similar strategies to remove

molecules from lipid bilayers.⁴³⁻⁴⁵ In lift-off lithography, terminally (ω -)functionalized alkanethiol molecules are removed when stamps are lifted from substrates. Here, we investigated how retained alkanethiols in the contacted regions interact with DNA probes to modulate surface properties. A range of alkanethiols terminated with hydroxyl or oligo(ethylene glycol) functional groups were studied (Scheme 7-1).

We find that following lift-off lithography, hydroxyl-terminated alkanethiol SAMs enable DNA probes greater access to Au substrates compared to oligo(ethylene glycol)-terminated SAMs. Notably, alkanethiol-functionalized DNA inserted into post-lift-off hydroxyl-terminated alkanethiol SAMs showed increased surface hybridization compared to DNA monolayers assembled by backfilling. Moreover, alkanethiol backfilling following patterning *via* lift-off lithography did not improve DNA hybridization efficiency. We discovered that the lift-off process induces conformational changes in oligo(ethylene glycol) moieties resulting in steric



Scheme 7-1. Abbreviations, names, and molecular structures of the alkanethiols used in these studies.

effects that limit DNA-probe access to Au surfaces. As such, we varied hydroxyl-/oligo(ethylene glycol)-terminated alkanethiol SAM ratios *via* codeposition prior to lift-off to tune the amounts of inserted tethered DNA. Ultimately, chemical lift-off lithography, in combination with variable matrix compositions, provides a facile means to regulate and to optimize DNA surface coverage, which is essential for controlling hybridization efficiency and the thermodynamic/kinetic behavior of nucleic acids on surfaces.^{5,46,47}

7.3 Materials and Methods

Materials. Silicon substrates coated with 100-nm-thick Au films overlaying 10-nm-thick Ti adhesive layers were purchased from Platypus Technologies (Madison, WI, USA). 11-Mercaptoundecyl tri(ethylene glycol) (TEG) was purchased from Toronto Research Chemicals Inc. (Toronto, ON, Canada). 11-Mercaptoundecanol (MCU) and 0.01 M phosphate buffered saline (PBS) ([NaCl] = 138 mM, [KCl] = 2.7 mM, and [MgCl₂] = 5 mM, pH 7.4) were purchased from Sigma-Aldrich (St. Louis, MO, USA). 16-Mercaptohexadecanol (MCHD) was purchased from Dojindo Molecular Technologies (Rockville, MD, USA). 11-Mercaptoundecyl hexa(ethylene glycol) (HEG), (6-mercaptohexyl) tri(ethylene glycol) (TEG-C₆), and 11-mercaptoundecyl tri(ethylene glycol) methyl ether (CH₃O-TEG) were purchased from ProChimia Surfaces (Sopot, Poland). Absolute ethanol was purchased from Decon Laboratories, Inc. (King of Prussia, PA, USA). Deionized water (~18 MΩ) was obtained from a Millipore water purifier (Billerica, MA, USA). Short single-stranded DNA thiolated at the 5' end with a hexyl linker (thioMC6-D) (5'-/5ThioMC6-D/GCA CGA AAC CCA AAC CTG ACC TAA CCA ACG TGC T-3' with molecular weight 10647.2 g/mol and melting temperature 67.2 °C), long thiolated single-stranded DNA (5'-/5ThioMC6-D/TTT TTT TTT TTT TTT TTT TTT TTT TTT TTT GCC GGG CGC GGC GCC GGG GCG CCG TTT TTT TTT TTT TTT TTT TTT TTT TGT GGT TTG GTT GTG TGT G-3' with molecular weight 31111.2 g/mol and melting temperature 72.0 °C), Alexa 488 fluorophore-conjugated complementary single-stranded DNA molecules (5'-/5-Alex488N/AGC ACG TTG GTT AGG TCA GGT TTG GGT TTC GTG C-3' with molecular weight 11262.5 g/mol and melting temperature 67.2 °C), and Alexa 488 fluorophore-conjugated noncomplementary, scrambled, single-stranded DNA sequences

(5'-/5-Alex488N/CAT GAA CCA ACC CAA GTC AAC GCA AAC GCA TCA A-3' with molecular weight 11031.4 g/mol and melting temperature 65.3 °C) were purchased from Integrated DNA Technologies (Coralville, IA, USA).⁸³ All DNA solutions were 100 μM as received and were diluted with 0.01 M PBS pH 7.4 to specific concentrations as needed for each experiment.

Substrate and Stamp Preparation. Silicon substrates with Au films were hydrogen-flame annealed. To prepare SAMs, hydroxyl-terminated alkanethiols (MCU, MCHD), hydroxyl tri(ethylene glycol)-terminated alkanethiols (TEG, TEG-C₆, HEG), or methoxy tri(ethylene glycol)-terminated alkanethiol (CH₃O-TEG) in ethanolic solutions (0.5 mM) were self-assembled on Au substrates for 16-18 h. For controlling DNA surface densities, mixed MCU/TEG SAMs were created by varying the ratios of MCU to TEG in solution concentrations as follows (in mM): 1:0, 0.75:0.25, 0.5:0.5, 0.25:0.75, and 0:1. Following self-assembly, substrates were rinsed thoroughly with ethanol and blown dry with nitrogen gas.

Square (25 μm × 25 μm or 2 μm × 2 μm), protruding features on PDMS stamps were fabricated *via* standard photolithography-processed masters. Details on stamp fabrication and oxygen plasma treatment of PDMS stamps have been published previously.^{24,41,42} Briefly, 10:1 mass ratios of SYLGARD 184 silicone elastomer base and curing agent (Ellsworth Adhesives, Germantown, WI, USA) were mixed thoroughly in a plastic cup, degassed under a vacuum, cast onto master substrates in a plastic Petri dish, and then cured in an oven at 70 °C overnight. The polymerized stamps were removed from the masters, cut into appropriate sizes, rinsed with ethanol, and blown dry with nitrogen gas. Stamps were then exposed to oxygen plasma (Harrick Plasma, power 18 W, and oxygen pressure 10 psi) for 30 s, yielding hydrophilic, reactive PDMS surfaces.⁴² After lift-off, PDMS stamps were rinsed with ethanol, wiped with Kimberly-Clark

tissues soaked in ethanol, and dried with nitrogen gas. Cleaned stamps were sealed to clean glass slides for storage before additional use.

Patterning Alkanethiol SAM-Modified Substrates via Chemical Lift-Off Lithography.

Oxygen plasma-treated PDMS stamps were brought into conformal contact with SAM-modified substrates for ~6 h for single lift-off. The contact reactions at the stamp-SAM interfaces caused SAM molecules to be removed specifically in the contact regions once the PDMS stamps were released from the substrates. After patterning, substrates were rinsed with ethanol and dried with nitrogen gas.

Double lift-off on TEG SAMs involved a combination of flat (featureless) and patterned PDMS stamps. The first lift-off step was carried out using flat stamps for 3 h to remove molecules from the entire surface. In the second lift-off step, patterned stamps were sealed to the post-lift-off substrates for another 3 h to remove molecules only in the contact regions between the stamp features and the surfaces. The shorter stamp/substrate contact times (3 h vs. 6 h) were selected to expedite DNA pattern generation. We previously found that patterns were created *via* chemical lift-off at even shorter times (*i.e.*, 1 and 5 min).^{42,82} Thus, exploring short stamp/substrate contact times (<3 h) may be beneficial for practical applications associated with generating lift-off-based DNA arrays.

For fluorescence experiments, substrates were incubated in solutions of 1 μ M DNA probes in 0.01 M PBS pH 7.4 for ~17 h to insert DNA into the post-lift-off exposed Au areas.⁸ After incubation, substrates were rinsed thoroughly with deionized water and blown to dryness with nitrogen gas. To visualize DNA hybridization, substrates were exposed to solutions of 1 μ M target DNA in 0.01 M PBS pH 7.4 for ~1 h. Substrates were processed in pairs for MCU and TEG SAMs. One substrate was incubated with target DNA and the other with

noncomplementary DNA as a control. Each experiment was repeated at least three times over a minimum of three different days. Variations in fluorescence intensities across experiments can arise due to the sensitivity of DNA hybridization to Mg^{2+} concentrations in incubation buffers.⁶⁸ However, this factor should affect all substrates processed in parallel equally within each experiment. Thus, it is important to process samples in parallel as much as possible and to include appropriate control samples (*e.g.*, hybridization to noncomplementary DNA) in all sample runs.

Deionized water was used to rinse the substrates gently before imaging under an inverted fluorescence microscope (Axio Observer.D1, Carl Zeiss MicroImaging, Inc., Thornwood, NY, USA) using a fluorescence filter set (38 HE/high efficiency) having excitation and emission wavelengths of 470 ± 20 nm and 525 ± 25 nm, respectively. Fluorescence intensity was measured with the line profile function in AxioVs40 V 4.7.1.0 software (Carl Zeiss MicroImaging, Inc., Thornwood, USA). The widths of the fluorescence line scans were made to be approximately the same as that of the square patterned features (*i.e.*, 25 μ m). On average, three to four fluorescence line scans were acquired per image. Fluorescence intensity was averaged for each line scan and then for each image. Alternately, for substrates without patterns, fluorescence intensity was measured using a histogram function and similarly defined areas across all fluorescence images. In all cases, three fluorescence measurements were made per substrate. Specific fluorescence intensities measured on post-lift-off substrates are the differences between the DNA hybridization regions (square features) and the alkanethiol backgrounds (absence of DNA probes).

Backfilling experiments following chemical lift-off were performed using the same procedures as those described above with the exception that after DNA probe incubation,

substrates were further incubated with 0.5 mM MCU diluted with 0.01 M PBS pH 7.4 to make 10 μ M MCU solutions for backfilling MCU/DNA SAMs for 30 min.⁷ Similarly, solutions of 0.5 mM TEG were diluted with 0.01 M PBS pH 7.4 to make 50 μ M TEG solutions for backfilling after lift-off.²¹ The traditional backfilling method was carried out by incubating hydrogen-flame annealed Au substrates with 1 μ M DNA-probe solutions for \sim 17 h followed by backfilling with 10 μ M MCU solution for 30 min. Dilution with PBS was used to minimize the deleterious effect that ethanol can have on DNA probes assembled on surfaces.²⁸

For AFM and XPS experiments, post-lift-off substrates were incubated with solutions of 1 μ M long (100 base) or short (34 base) DNA probes in 0.01 M PBS pH 7.4 for \sim 17 h, rinsed gently with deionized water and blown dry with nitrogen gas.⁸ Tapping mode AFM (Dimension 5000, Bruker AXS, Santa Barbara, CA, USA) was used to characterize height differences on DNA/alkanethiol mixed monolayers on the post-lift-off substrates. Topographic AFM images were collected using Si cantilevers with a spring constant of 48 N/m and a resonant frequency of 190 kHz (Veeco Instruments, Santa Barbara, CA, USA).

For XPS experiments, featureless PDMS stamps were used for the chemical lift-off process. All XPS data were collected using an AXIS Ultra DLD instrument (Kratos Analytical Inc., Chestnut Ridge, NY, USA). A monochromatic Al K α X-ray source (10 mA for survey scans and 20 mA for high resolution scans, 15 kV) with a 200 μ m circular spot size and ultrahigh vacuum (10^{-9} Torr) were used.^{41,42} Spectra were acquired at a pass energy of 160 eV for survey spectra and 20 eV for high resolution spectra of C 1s, O 1s, N 1s, P 2p, S 2p, and Au 4f regions using a 200 ms dwell time. Different numbers of scans were carried out depending on the difficulty of identifying each peak vs. background, ranging from 20 scans for C 1s to 100 for

Au 4f. All XPS peaks for each element on Au substrates were referenced to the Au 4f signal at 84.0 eV. Atomic percentages were calculated from peak areas.

Because PDMS is an insulator, a charge neutralizer (flood gun) was used to obtain signals from each element on PDMS stamps. As a result, peaks are shifted slightly from their expected regions (for C 1s this is 4-5 eV lower than the reference at 284.0 eV). Because the number of peaks of interest was small (only Au 4f peaks on PDMS samples), and they were well separated (~ 4 eV), peak shifting did not affect identification. No corrections were carried out during data collection to shift peaks back to particular regions or to scale peaks based on reference locations.

Featureless PDMS stamps were also used for the chemical lift-off process for infrared spectroscopy experiments. Polarization modulation infrared reflection-absorption spectroscopy (PM-IRRAS) was carried out using a Thermo Nicolet 8700 Fourier-transform infrared spectrometer (Thermo Electron Corp., Madison, WI, USA) in reflectance mode using infrared light incident at 80° relative to the surface normal. Spectra with 1024 scans and a resolution of 4 cm^{-1} were collected in all cases. Each PM-IRRAS experiment was carried out at least four times. Polarization modulation infrared reflection-absorption spectroscopy was used to investigate the removal of molecules due to lift-off by monitoring the peak areas of the O-H stretching band associated with hydroxyl terminal groups. This spectroscopic method was also used to detect the conformational changes of oligo(ethylene glycol) moieties in TEG, TEG-C₆, HEG, and CH₃O-TEG alkanethiols.

Statistical Analyses. Data from fluorescence microscopy, XPS atomic percentage, and AFM topography experiments were initially analyzed by one-way or two-way analysis of variance as appropriate, followed by Tukey's multiple group comparisons. *A priori* individual

group comparisons for fluorescence microscopy data were also analyzed by two-tailed unpaired Student's *t*-tests. All statistics were carried out using GraphPad Prism (GraphPad Software Inc., San Diego, USA). Data are reported as means (standard errors of the means with probabilities of $P < 0.05$ considered statistically significant).

7.4 Results and Discussions

7.4.1 Chemical Lift-Off Lithography Facilitates Probe DNA Insertion and Target DNA

Hybridization

Following self-assembly, oxygen-plasma-treated PDMS stamps were used to remove alkanethiols terminated with hydroxyl moieties from Au substrates within the stamp-substrate contact areas.⁴² Previously, we found that ~70% of MCU molecules are removed from the contact regions after lift-off.⁴² Further, we showed that inserting biotin hexa(ethylene glycol)-terminated alkanethiols into the contact areas enabled streptavidin recognition in the biotin-patterned regions with features as small as 40 nm for a single lift-off step and 20 nm for two lift-off lithography steps. The precision of these features reached 2 nm and later results showed that we have not yet reached the resolution limits of the method. Similarly, we reasoned that alkanethiol residues remaining in the contact areas after lift-off would act as diluents when inserting thiolated single-stranded DNA probes.

The chemical lift-off process is illustrated in Figure 7-1. Negative features in SAMs were generated using PDMS stamps with arrays of protruding square-shaped posts. Patterned SAMs were incubated with alkanethiol-functionalized DNA probe solutions to enable insertion into the post-lift-off areas. Substrates were then exposed to fluorescently labeled target DNA. Experiments were carried out using ~17 h (overnight) insertion times. Short insertion times (*i.e.*, <2 h) were associated with linearly increasing hybridization efficiencies, whereas DNA insertion over longer times resulted in near saturation of hybridization efficiency (Figure 7-S1).

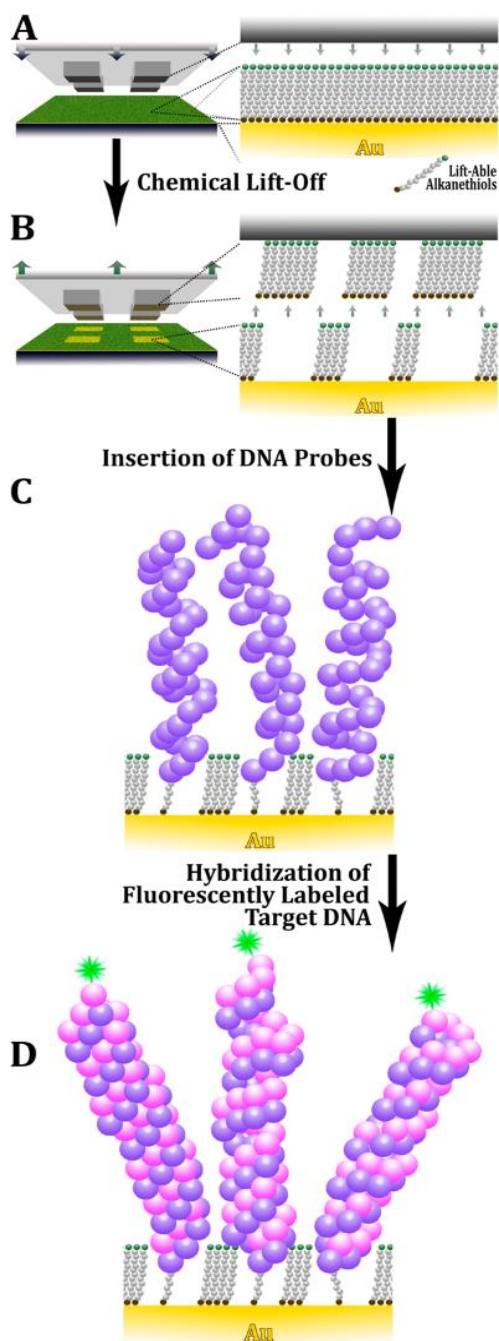


Figure 7-1. Schematic illustration of chemical lift-off/DNA insertion patterning. **(A)** Oxygen plasma-treated polydimethylsiloxane stamps are brought into conformal contact with alkanethiol self-assembled monolayers (SAMs) terminated with functional groups that are reactive toward chemical lift-off. **(B)** As a result of the strong interactions at stamp-substrate interfaces, stamp removal causes lift-off of functionalized alkanethiols, albeit incompletely, from Au substrates. **(C)** The exposed lift-off regions are then insertion-functionalized with alkanethiol-functionalized DNA probes, **(D)** followed by surface hybridization with fluorescently labeled target DNA.

A representative fluorescence image of a DNA array formed on a patterned MCU SAM following hybridization with complementary DNA is shown in Figure 7-2A. Specificity of target DNA hybridization is indicated by the lack of a fluorescence pattern when a similar substrate was challenged with noncomplementary target DNA (Figure 7-2B). The DNA arrays on post-lift-off tri(ethylene glycol)-terminated undecanethiol (TEG) SAMs showed faint yet discernible fluorescent patterns compared to MCU SAMs (Figure 7-2C) and similarly lacked detectable fluorescence when hybridized with noncomplementary target DNA (Figure 7-2D). These results illustrate that hydroxyl-terminated (MCU) and tri(ethylene glycol)-terminated (TEG) molecules in the lift-off regions act as diluting matrices to enable tethered DNA probe insertion and specific hybridization with target DNA, albeit with different efficiencies.

Prior infrared spectral analysis indicated $\sim 70\%$ lift-off yields for MCU.⁴² Here, we compared lift-off efficiencies for MCU *vs.* TEG, which were not significantly different (MCU $64 \pm 7\%$ *vs.* TEG $73 \pm 2\%$; $N=3$; $t(4)=1$; $P>0.05$). Thus, DNA insertion into post-lift-off MCU and TEG SAMs was anticipated to occur at similar levels. Nonetheless, fluorescence signals from DNA surface hybridization on TEG SAMs were substantially lower than those detected on MCU SAMs (Figure 7-2E).

We have used sequential lift-off steps to produce substrate features smaller than actual stamp features in doubly contacted regions.⁴² Here, we employed double lift-off lithography to investigate whether additional TEG molecules could be removed from SAM substrates to improve DNA insertion and hybridization. First, flat stamps were used to lift-off TEG across entire substrates. Patterned PDMS stamps were next employed to remove additional TEG molecules only in the regions contacted by the stamp features. Alkanethiol probe DNA was then inserted followed by exposure to either fully complementary (Figure 7-2F) or noncomplementary

(Figure 7-2G) fluorescently labeled target DNA. Hybridization was specific and greater DNA insertion and/or surface hybridization occurred on post-double-lift-off TEG SAMs compared to post-single-lift-off TEG SAMs (Figure 7-2E). Patterned fluorescence intensities after double lift-off lithography were twice those following single lift-off (Figure 7-2E) and notably, are the differences between DNA hybridization in post-double-lift-off regions vs. the single-lift-off background.

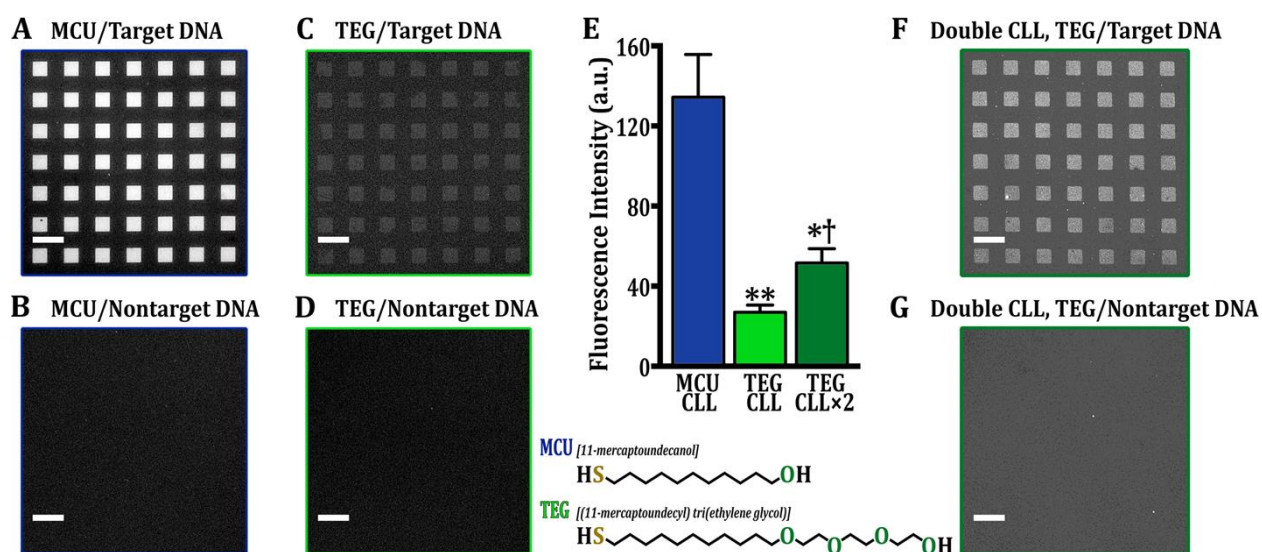


Figure 7-2. Representative fluorescence images displaying (A,C,F) hybridization of surface-bound DNA probes (34 bases) with fluorescently labeled complementary target DNA or (B,D,G) hybridization with noncomplementary DNA (scrambled 34-base sequences). Post-lift-off self-assembled monolayers (SAMs) are (A,B) hydroxyl-terminated alkanethiols (MCU) or (C,D,F,G) tri(ethylene glycol)-terminated (TEG) alkanethiols. The fluorescence patterns in (F,G) represent double lift-off regions against a post-single-lift-off background. Fluorescence patterns in (A,C,F) compared to their absence in (B,D,G) indicate specific hybridization between Alexa Fluor 488-labeled target DNA (excitation at 495 nm) and tethered probe DNA. (E) Patterned specific fluorescence intensities resulting from DNA hybridization on post-lift-off MCU SAMs were higher than those observed on post-lift-off TEG SAMs. (F) Patterned specific fluorescence intensity was increased on post-double-lift-off TEG SAMs. Fluorescence images were taken with the same exposure times of 5 s at an emission wavelength of 517 nm. Stamp features are (25 μm \times 25 μm). Error bars represent standard errors of the means with $N = 3$ samples per group. Mean intensities were significantly different across groups [$F(2,6)=18$; $P<0.01$]. * $P<0.05$ and ** $P<0.01$ vs. MCU/CLL; † $P<0.05$ vs. TEG/CLL. Scale bars are 50 μm .

7.4.2 Oligo(Ethylene Glycol)-Terminated Alkanethiols Reduce DNA Insertion

The findings in Figure 7-2 suggest that ethylene glycol moieties in TEG hinder the numbers of tethered DNA probes inserted into the lift-off regions of patterned substrates. Alternately, the flexible ethylene glycol segments might interfere with tethered probe DNA surface orientations so as to disfavor hybridization. Both scenarios could lower hybridization efficiency. Several studies have found that although oligo(ethylene glycol)-terminated alkanethiols are longer than comparable hydroxyl-terminated alkanethiols, the ethylene glycol moieties do not interfere with DNA orientations favorable for surface hybridization.^{6,21,22,25} In light of this understanding and the double-lift-off findings above, we posited that the ethylene glycol moieties in TEG reduce DNA access to post-lift-off regions during insertion thereby lowering DNA-probe surface densities.

To test this hypothesis, thiolated DNA inserted into post-lift-off hydroxyl-terminated (MCU) *vs.* tri(ethylene glycol)-terminated (TEG) SAMs was compared using atomic force microscopy (AFM). After lift-off, MCU and TEG SAMs displayed similar negative-height topographic features where PDMS stamps had contacted SAMs (Figure 7-3A,B, respectively). Following incubation with DNA probes, positive-height topographic features protruding beyond SAM backgrounds were observed for MCU SAMs (1.5 ± 0.06 nm, Figure 7-3C), indicating that DNA had been inserted. Significantly smaller height increases were observed for DNA inserted on TEG SAMs (0.34 ± 0.02 nm, [$t(8)=19$; $P<0.001$], Figure 7-3D) suggesting that fewer DNA probe molecules had been inserted compared to MCU SAMs.

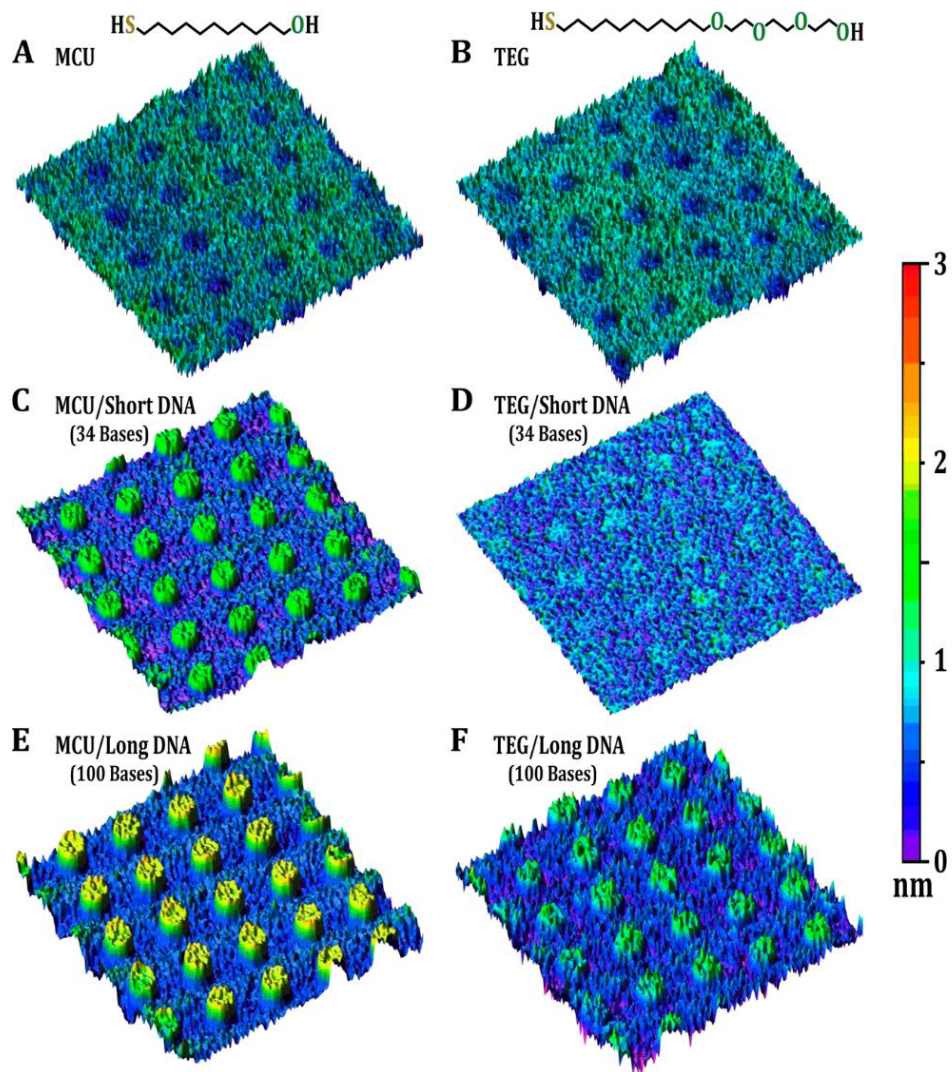


Figure 7-3. Atomic force microscopy images before and after insertion with short or long DNA. Negative SAM features resulting from chemical lift-off of (A) hydroxyl-terminated alkanethiol self-assembled monolayers (SAMs) or (B) tri(ethylene glycol)-terminated SAMs indicate similar degrees of lift-off. After short (34-base) or long (100-base) thiolated DNA was inserted into the lift-off areas, protruding features were observed on (C,E) MCU SAMs, while lower-contrast DNA features appeared on (D,F) TEG SAMs. Differences in topographic heights between (C) vs. (D) and (E) vs. (F) suggest that fewer DNA probe molecules were inserted into the post-lift-off areas of TEG SAMs, regardless of DNA length. Images are representative of $N=4-5$ samples per condition. Image dimensions are $20\ \mu\text{m} \times 20\ \mu\text{m}$.

Although we observed differences in AFM topographic heights between thiolated DNA inserted into post-lift-off MCU *vs.* TEG SAMs, height differences alone do not conclusively indicate that fewer DNA probes were present on post-lift-off TEG SAMs. Because TEG molecules are longer than MCU molecules by three ethylene glycol units, upon insertion, the observed height difference between DNA molecules and the TEG SAM background is expected to be smaller than that observed with the MCU SAM background. Additional AFM experiments were carried out using longer thiolated single-stranded DNA probes (100 bases) to increase AFM topographic contrast over insertion of 34-base DNA probes. An increase in height was observed on post-lift-off MCU SAMs indicating insertion of long DNA probes (2.1 ± 0.07 nm, Figure 7-3E). Observable, yet smaller height increases were found for post-lift-off TEG SAMs (0.78 ± 0.05 nm, Figure 7-3F). Mean topographic heights of MCU/DNA SAMs were again significantly different from TEG/DNA SAMs [$t(6)=16$; $P<0.001$].

The apparent height differences between the patterned and unpatterned regions in Figure 7-3F substantiate DNA-probe insertion on TEG SAMs. However, similar to short DNA, differences in AFM topographic heights where long DNA was inserted into post-lift-off MCU (Figure 7-3E) *vs.* TEG SAMs (Figure 7-3F) might still be due to the smaller height differences between DNA molecules and TEG *vs.* MCU molecules. Assuming a 0.34 nm distance between DNA bases,⁴⁸ fully extended 34- and 100-base single-stranded DNA molecules would be ~12 and 34 nm long, respectively. The protruding features on post-lift-off MCU and TEG SAMs (Figure 7-3C,D,E,F) are substantially smaller than the extended DNA lengths. Since AFM images were collected under dry conditions and the DNA molecules constitute only a fraction of each monolayer, the segments of the inserted DNA that lay beyond the matrices were unlikely to be fully extended. Thus, the relative height differences observed on post-lift-off MCU *vs.* TEG

SAMs do not reflect absolute DNA heights relative to SAMs but instead, indicate relative differences in the numbers of inserted molecules. Below, we use these results to estimate the fractions of monolayers associated with inserted DNA. Beyond these estimates, any potential effects of DNA probe lengths on insertion efficiency into SAMs⁴⁹ cannot be straightforwardly differentiated by AFM.

7.4.3 Chemical Lift-Off Reduces DNA-Substrate Interactions and Improves DNA Hybridization

We used XPS to quantify DNA-associated nitrogen and phosphorus signals on MCU vs. TEG patterned surfaces. Since we were interested in probe DNA inserted into post-lift-off regions, featureless PDMS stamps were used with chemical lift-off lithography for these experiments to maximize lift-off areas. In addition, because we focused on investigating the XPS fingerprints of DNA, only the N 1s and P 2p XPS data are discussed here. The complete XPS data can be found in the Supporting Information (Table 7-S1). The bottom curves in Figure 7-4 indicate that N 1s and P 2p peaks were not present on post-lift-off MCU and TEG SAMs in the absence of DNA probes (*i.e.*, incubation with 0.01 M phosphate-buffered saline), as expected. Both N 1s and P 2p peaks corresponding to 6.9 atomic % and 2.0 atomic %, respectively (Table 7-1), were observed for thiolated DNA inserted into post-lift-off MCU SAMs (lower-middle curves, Figure 7-4A,C). By contrast, these peaks were undetectable for DNA inserted into post-lift-off TEG SAMs (middle curves, Figure 7-4B,D).

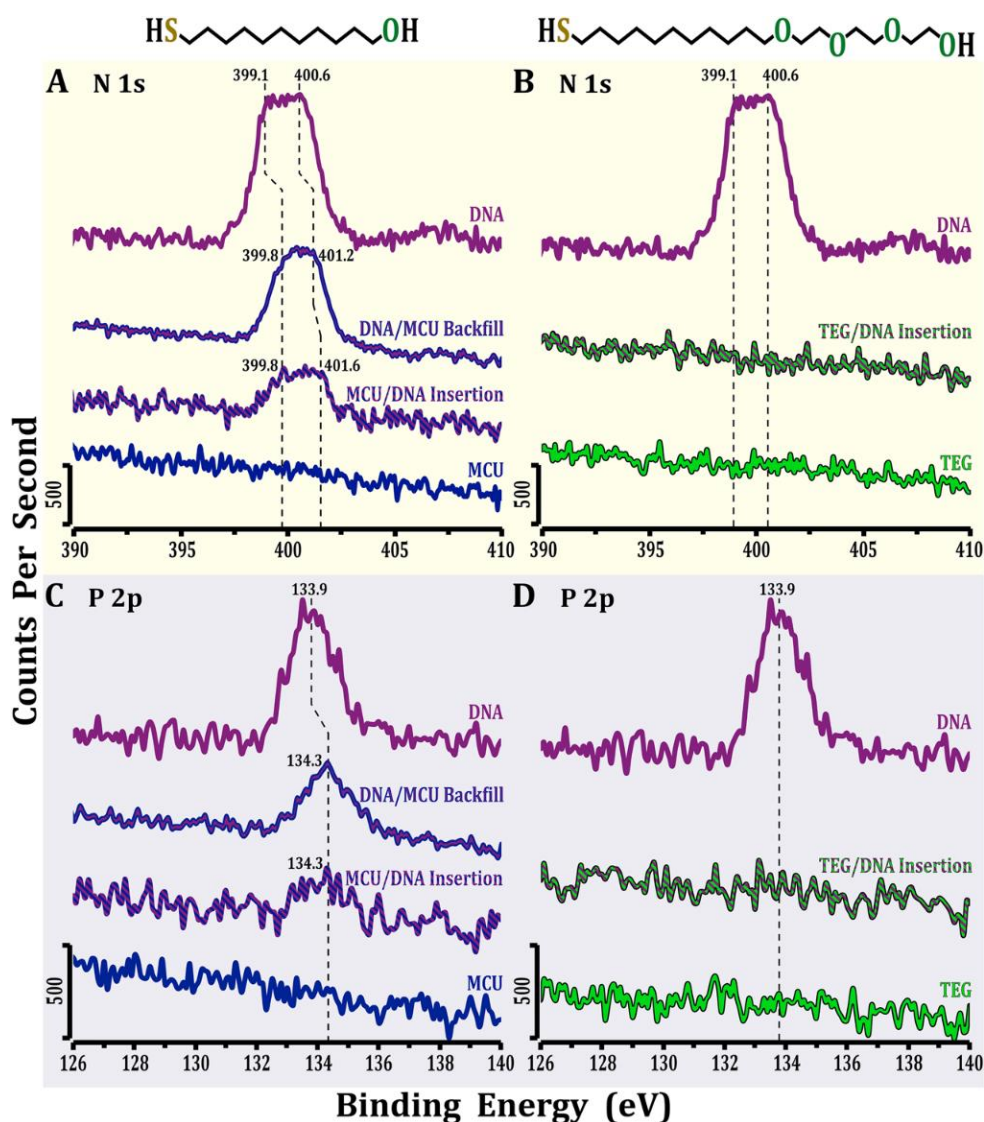


Figure 7-4. Representative X-ray photoelectron spectra of N 1s and P 2p peaks associated with (A,C) hydroxyl-terminated (MCU) and (B,D) tri(ethylene glycol)-terminated (TEG) alkanethiol self-assembled monolayers (SAMs). All bottom curves represent post-lift-off SAMs incubated with 0.01 M phosphate buffered saline devoid of thiolated DNA probes, hence the absence of nitrogen and phosphorus peaks in these curves. The large N 1s and P 2p peaks from pure DNA monolayers (all top curves) are in contrast to the smaller peaks (all middle curves) from MCU/DNA and TEG/DNA mixed SAMs indicating dilute DNA coverage on MCU-backfilled (upper middle curves A,C) and post-lift-off MCU (lower middle curves A,C) SAMs. The apparent shift to lower energies in N 1s (~0.6-1 eV) and P 2p (~0.4 eV) peaks on pure DNA SAMs compared with alkanethiol/DNA SAMs is attributed to greater DNA-substrate interactions associated with the pure DNA SAMs. Spectra are displaced vertically for ease of visualization.

The absence of nitrogen and phosphorus peaks associated with post-lift-off TEG SAMs suggests that DNA insertion into post-lift-off TEG SAMs was either absent or below the XPS detection limit. We conclude the latter case is correct in light of the detectable fluorescence microscopy patterns (Figure 7-2C) and AFM topographies (Figure 7-3D,F) on similar substrates. Consequently, XPS may not be sensitive enough to detect small amounts ($\leq 1\%$ monolayer, *vide infra*) of DNA associated nitrogen and phosphorus on post-lift-off TEG SAMs.

The broad N 1s peak for DNA on post-lift-off MCU SAMs (lower-middle curve, Figure 7-4A) arises from nitrogen peaks associated with heteroaromatic DNA nitrogen at 399.8 eV, and C(=O)-N, N-C(=O)-N, and C(=O)-N-C(=O) moieties at 401.6 eV.⁵⁰ These nitrogen peaks were at higher binding energies (~ 1 eV) in comparison to undiluted tethered DNA monolayers (top vs. lower middle curves in Figure 7-4A). Previous studies have shown that heteroaromatic nitrogen in undiluted DNA monolayers interacts with Au substrates, resulting in lower N 1s binding energies compared to the same nitrogen species in DNA bases that are free from substrate interactions.^{7,21,51} Additionally, the P 2p peaks from post-lift-off MCU/DNA SAMs were at a higher binding energy (~ 0.4 eV) than for pure DNA monolayers (top vs. lower middle curves, Figure 7-4C). Nitrogen and phosphorus XPS peaks shifted to higher energies indicate that DNA base-substrate interactions are reduced in the presence of post-lift-off MCU molecules suggesting that DNA bases are more available to hybridize with complementary bases in target DNA. In contrast, the thiolated DNA molecules in pure DNA monolayers tend to lie down on metal surfaces such that bases interact with Au substrates disfavoring hybridization with target DNA.

We also prepared substrates using the backfilling method wherein thiolated DNA SAMs were subsequently exposed to MCU solutions (upper-middle curves, Figure 7-4A,C). Backfilling

was carried out for 30 min because previous studies showed that this incubation time results in DNA-probe orientations that favor hybridization.⁷ Similar to DNA inserted in post-lift-off MCU SAMs, nitrogen and phosphorus XPS peaks were at higher binding energies (~ 0.4 eV for N 1s and ~ 0.6 eV for P 2p) for MCU-backfilled DNA SAMs compared to undiluted DNA monolayers indicating reduced DNA base-substrate interactions.

Table 7-1. X-Ray Photoelectron Spectroscopy Atomic Percentages^a

Elements	Atomic Percentage	
	N 1s	P 2p
DNA (predicted)	18.1	4.7
DNA (experimental)	15.6 \pm 0.4	3.6 \pm 0.1
DNA/MCU Backfill	13.2 \pm 0.3*	3.1 \pm 0.2
MCU/DNA Insertion	6.9 \pm 0.4 [†]	2.0 \pm 0.1 [†]
TEG/DNA Insertion	N/D (1.0) [†]	N/D (0.3) [†]
MCU	N/D	N/D
TEG	N/D	N/D

^a Predicted X-ray photoelectron spectroscopy (XPS) atomic percentages for undiluted DNA were calculated using the numbers of nitrogen and phosphorus atoms in DNA probe molecules. Atomic percentages for undiluted thiolated DNA monolayers (experimental) and mixed monolayers of hydroxyl- (MCU) and tri(ethylene glycol) (TEG)-terminated alkanethiol/DNA on Au substrates were calculated from XPS peak areas ($N=3-6/\text{group}$). Not detectable XPS signals are indicated by “N/D”. Atomic percentages in parentheses are hypothetical lower limits are based on XPS detection limits of 1% and a P/N ratio of 0.3 and are used for statistical purposes. Entries are means (standard errors of the means. Nitrogen and phosphorus atomic percentages were significantly different across groups ($[F(3,14)=280; P<0.001]$ and $[F(3,14)=135; P<0.001]$, respectively). * $P<0.01$ vs. DNA (experimental). [†] $P<0.001$ vs. DNA/MCU Backfill.

Prior studies have shown that differences in N 1s and P 2p binding energies between undiluted DNA monolayers and DNA/alkanethiol SAMs not only indicate reduced DNA-substrate interactions in the latter but also upright orientation of DNA probes.^{7,15,21} For example, near-edge X-ray absorption fine-structure spectroscopy has been used to show that shifts to higher binding energies for the N 1s and P 2p XPS signals associated with DNA/alkanethiol monolayers are accompanied by upright probe orientations on Au surfaces.^{7,21,52} The N 1s and P 2p peak areas (Table 7-1) from post-lift-off MCU/DNA SAMs (6.9 atomic % nitrogen and 2.0 atomic % phosphorus) vs. those of MCU-backfilled DNA SAMs (13.2 atomic % nitrogen and 3.1 atomic % phosphorus) and undiluted DNA monolayers (15.6 atomic % nitrogen and 3.6 atomic % phosphorus (Figure 7-4A,C) indicate lower surface coverages of DNA probes on post-lift-off MCU SAMs. Compared with pure DNA monolayers, DNA probes are diluted by ~50% on post-lift-off MCU SAMs, in agreement with previous studies.^{6,7,21} These surface coverage estimates, however, are only relative because XPS signals are affected not only by the numbers of molecules on the substrates but also by X-ray attenuation lengths.⁵¹

Since the XPS data in Figure 7-4 show that various methods result in different amounts of surface-assembled DNA, we investigated whether this translated into differential DNA hybridization. Fluorescence resulting from target DNA hybridization on substrates prepared using lift-off lithography followed by probe-DNA insertion was significantly greater than fluorescence intensities from hybridization on undiluted DNA monolayers (Figure 7-5A). Moreover, there was greater fluorescence on post-lift-off MCU SAMs compared to MCU-backfilled DNA SAMs. Considering that post-lift-off MCU SAMs had the *lowest* numbers of DNA probe molecules compared to pure DNA monolayers and MCU-backfilled DNA SAMs (Table 7-1 and Figure 7-4A,C), these results indicate improved DNA hybridization efficiency

associated with the chemical lift-off lithography-DNA insertion approach (Figure 7-5B), in agreement with studies using other insertion methods.^{34,35} Notably, the coefficients of variation (%CV) for hybridization were significantly lower for the lift-off-insertion approach signifying improved reproducibility (Figure 7-5A; 4.5% MCU/DNA insertion, 25% DNA/MCU backfill, 37% undiluted DNA).

Hybridization efficiencies on Au films and nanoparticles have been determined by various quantification methods including fluorescence-based methods,^{7,53,54} electrochemical techniques,^{16,49,55,56} “quantitative” XPS,⁵¹ neutron reflectivity measurements,¹⁷ radiometric assays,⁵⁷ and surface plasmon resonance spectroscopy.^{5,6,21,46} Here, because quantification from fluorescence images and XPS atomic percentages do not provide absolute numbers of DNA

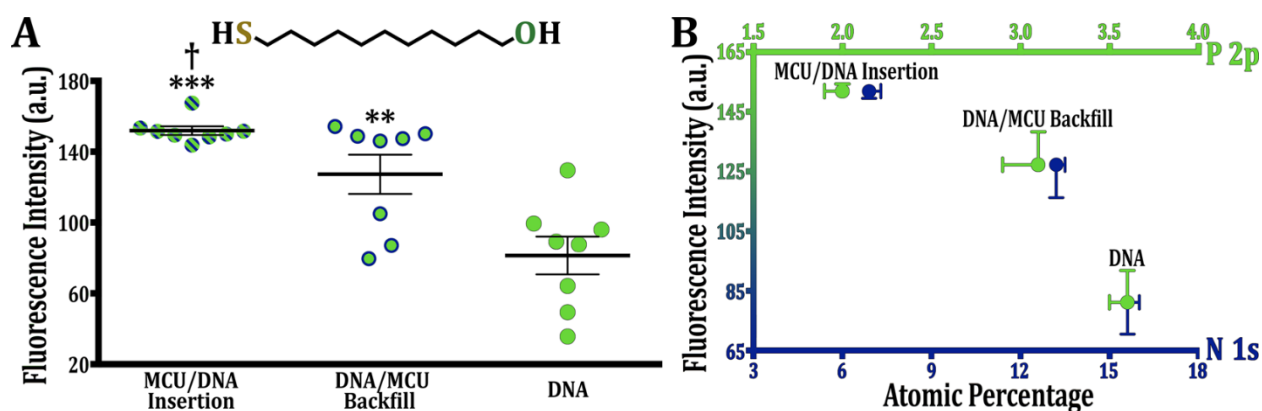


Figure 7-5. (A) Fluorescence intensities resulting from hybridization of surface-bound DNA probes and fluorescently labeled complementary DNA target strands on post-lift-off hydroxyl-terminated alkanethiol (MCU) self-assembled monolayers (SAMs) (MCU/DNA Insertion), MCU-backfilled DNA SAMs (DNA/MCU Backfill), and pure DNA SAMs (DNA). Mean fluorescence intensities were significantly different across groups [$F(2,21)=6$; $P<0.001$]. ** $P<0.01$ and *** $P<0.001$ vs. DNA; † $P<0.05$ vs. DNA/MCU Backfill. Error bars represent standard errors of the means with $N = 8$ substrates per group. (B) Correlations are between fluorescence resulting from DNA hybridization vs. X-ray photoelectron spectroscopy atomic percentages [N 1s (bottom/blue x-axis)/P 2p (top/green x-axis)]. Higher fluorescence intensities were correlated with lower DNA probe numbers. Thus, hybridization efficiencies were MCU/DNA Insertion > DNA/MCU Backfill > DNA alone.

probes and targets, we examined relative relationships *via* correlation analysis (Figure 7-5B) and determined that improved hybridization efficiency is associated with the lift-off lithography-based DNA insertion approach compared to undiluted DNA monolayers and MCU-backfilled DNA SAMs.

7.4.4 Backfilling Reduces Inserted DNA on Post-Lift-Off Alkanethiol SAMs

Backfilling with MCU or TEG has been shown to increase target DNA hybridization for Au substrates functionalized first with thiolated probe DNA (Figure 7-5B).^{6,7,21} Here, we investigated the effects of backfilling following lift-off and DNA insertion on MCU and particularly, TEG SAMs. After lift-off and insertion of thiolated DNA probes, we exposed MCU/DNA or TEG/DNA SAMs to additional MCU or TEG molecules, respectively, *via* solution deposition. Backfilling was hypothesized to reduce any remaining DNA-substrate interactions and to increase fluorescence due to greater surface hybridization. On the contrary, we observed decreases in the fluorescence intensities of patterns on both post-lift-off MCU (Figure 7-6A,B) and TEG (Figure 7-6C,D) SAMs after additional backfilling suggesting that DNA probes were instead removed from substrates.

Removal of DNA probes by backfilling with alkanethiols has been reported.^{6,7,21} The purpose of alkanethiol backfilling is to reduce steric interactions between DNA probes and to decrease DNA-substrate interactions. However, when substrates are exposed to alkanethiol backfilling solutions for extended times (>1 h), DNA molecules are displaced and fluorescence decreases due to reduced numbers of surface-bound DNA molecules. Studies by others have shown that DNA probes on MCU-backfilled SAMs diluted by ~50% from pure DNA monolayers required >5 h of backfilling.^{7,57} The XPS data above (Table 7-1, Figure 7-4A vs.

7-4C) indicate ~50% dilution of post-lift-off MCU/DNA *vs.* undiluted DNA monolayers. Thus, DNA surface coverages on post-lift-off substrates might be in the regime where additional alkanethiol backfilling removes inserted DNA probes instead of reducing DNA-substrate interactions, which are already presumably minimized. Decreases in fluorescence after backfilling (Figure 7-6E) suggest that additional incorporation of MCU or TEG molecules reduced the numbers of DNA probe molecules. For TEG, the already low numbers of DNA probes on post-lift-off DNA/SAM-modified substrates were further reduced with additional TEG solution exposure. Therefore, we conclude that alkanethiol backfilling is not advantageous when patterning DNA on Au substrates *via* chemical lift-off lithography.

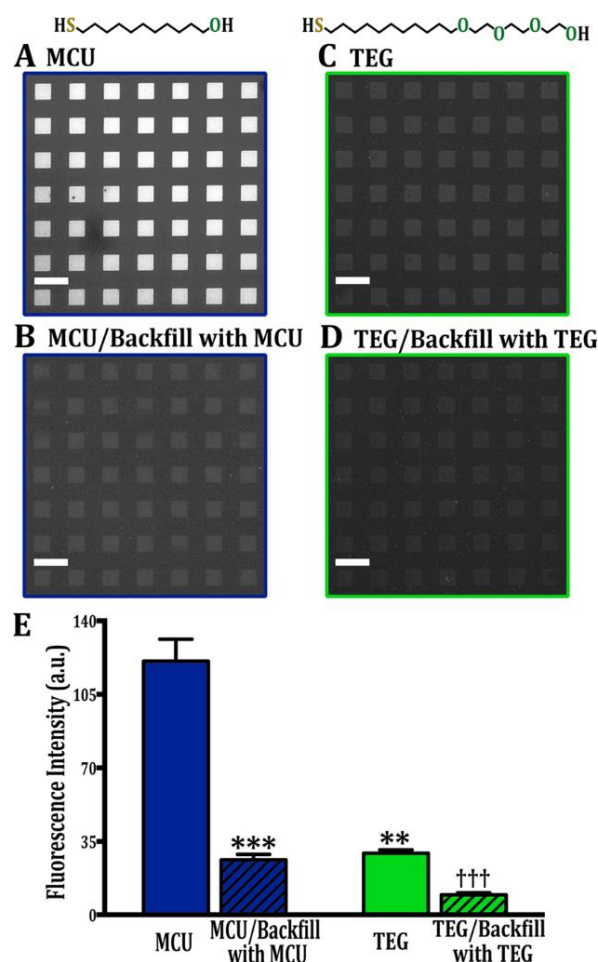


Figure 7-6. Representative fluorescence images displaying hybridization of thiolated single-stranded DNA probes with Alexa Fluor 488-labeled target DNA (excitation at 495 nm) on (A,B) hydroxyl-terminated alkanethiol (MCU) or (C,D) tri(ethylene glycol)-terminated alkanethiol (TEG) self-assembled monolayers (SAMs) after lift-off lithography and without or with backfilling with additional respective alkanethiol molecules following probe DNA insertion. After exposing post-lift-off MCU/DNA SAMs to additional MCU, fluorescence was decreased in (B) compared to (A) suggesting that thiolated DNA is displaced by subsequent exposure to additional MCU. Similarly, a weaker fluorescent pattern (D) was observed for backfilled post-lift-off TEG/DNA SAMs compared to the pattern after hybridization on a post-lift-off-alone TEG SAM (C). Fluorescence images (shown with the same exposure times of 5 s) were taken at an emission wavelength of 517 nm. (E) Mean intensities were significantly different for post-lift-off MCU vs. TEG surfaces without backfilling (A,C) again indicating significant differences with respect to target hybridization (independent replication vs. Figure 2, two-way ANOVA interaction term [$F(1,4)=37$, $P<0.01$]). Error bars represent standard errors of the means with $N=3$ samples per group. ** $P<0.01$ and *** $P<0.001$ vs. MCU; ††† $P<0.001$ vs. TEG. Scale bars are 50 μm .

7.4.5 DNA Arrays Patterned via Lift-Off Lithography Using Longer Functionalized Alkanethiols

Three terminal ethylene glycol units differentiate TEG from MCU molecules. The additional molecular length of TEG vs. MCU might reduce DNA access to Au surfaces. Alternately, the presence of the ethylene glycol moieties might have greater influence on alkanethiol-DNA insertion. To differentiate these possibilities, molecules longer than MCU and TEG, namely mercaptohexadecanol (MCHD) and hexa(ethylene glycol) undecanethiol (HEG) were investigated (Scheme 7-1). The alkyl backbone of MCHD is five carbon atoms longer than MCU, whereas HEG has the same alkyl backbone as TEG but contains three additional ethylene glycol units.

Previously, we showed by XPS that oxygen plasma treatment of PDMS stamps is needed to lift-off alkanethiols terminated with hydroxyl or amine tail groups.⁴² Because interactions at stamp-SAM and SAM-Au interfaces are stronger than Au-Au substrate bonds, post-lift-off PDMS stamps showed Au 4f XPS signals. In contrast, PDMS stamps following conformal contact with relevant SAMs in the absence of oxygen plasma pretreatment did not show Au 4f XPS signals. Here, the chemical lift-off lithography process was carried out on MCHD and HEG SAMs. Post-lift-off PDMS stamps from these SAMs showed Au 4f signals in the XPS spectra (Figure 7-S2A,B) indicating that MCHD and HEG are lift-able molecules. While intense fluorescent patterns were observed for MCHD/DNA SAMs (Figure 7-S3A), such patterns were indiscernible for HEG/DNA SAMs (Figure 7-S3B). Thus, although MCHD and HEG molecules are each longer than the corresponding MCU and TEG molecules, respectively, the thicker SAMs formed by MCHD did not hinder DNA probes from accessing Au surfaces. Since the principal differences between MCHD and HEG are the ethylene glycol moieties in the latter, the

important finding is that differences in physical lengths between SAM molecules do not by themselves underlie variations in the numbers of tethered DNA probes inserted into post-lift-off regions and associated target DNA hybridization. Instead, ethylene glycol moieties appear to play key roles in limiting the numbers of DNA molecules on post-lift-off oligo(ethylene glycol)-terminated alkanethiol-modified Au surfaces.

7.4.6 Spectroscopic Evidence for Lift-Off-Induced Conformation Changes in Oligo(Ethylene Glycol) Moieties

Together, information gleaned from investigating the various hypotheses above suggests that steric hindrance originates from the ethylene glycol moieties of TEG (and HEG). To explore the origin of this effect, polarization-modulation infrared reflection-absorption spectroscopy (PM-IRRAS) was used to monitor the characteristic vibrational feature of ethylene glycol moieties, namely the C–O–C vibrational stretch, before and after chemical lift-off. As for the XPS experiments above, featureless PDMS stamps were used to maximize lift-off areas. For alkanethiols with (ethylene glycol)_n ($n \leq 4$), the –vibrational band is the dominant IR feature characterizing ethylene glycol moieties.⁵⁸

As shown in Figure 7-7A, the C–O–C vibrational band displayed a strong, sharp peak at $\sim 1138 \text{ cm}^{-1}$ for pristine TEG SAMs (top curve), indicating a predominantly all-*trans* conformation for the ethylene glycol moieties.⁵⁹ However, after lift-off, the C–O–C peak was shifted to $\sim 1132 \text{ cm}^{-1}$ and the peak area was decreased (Figure 7-7A, bottom curve). Infrared absorption spectra are affected by surface coverage and molecular conformations.⁵⁹ While the reduced peak

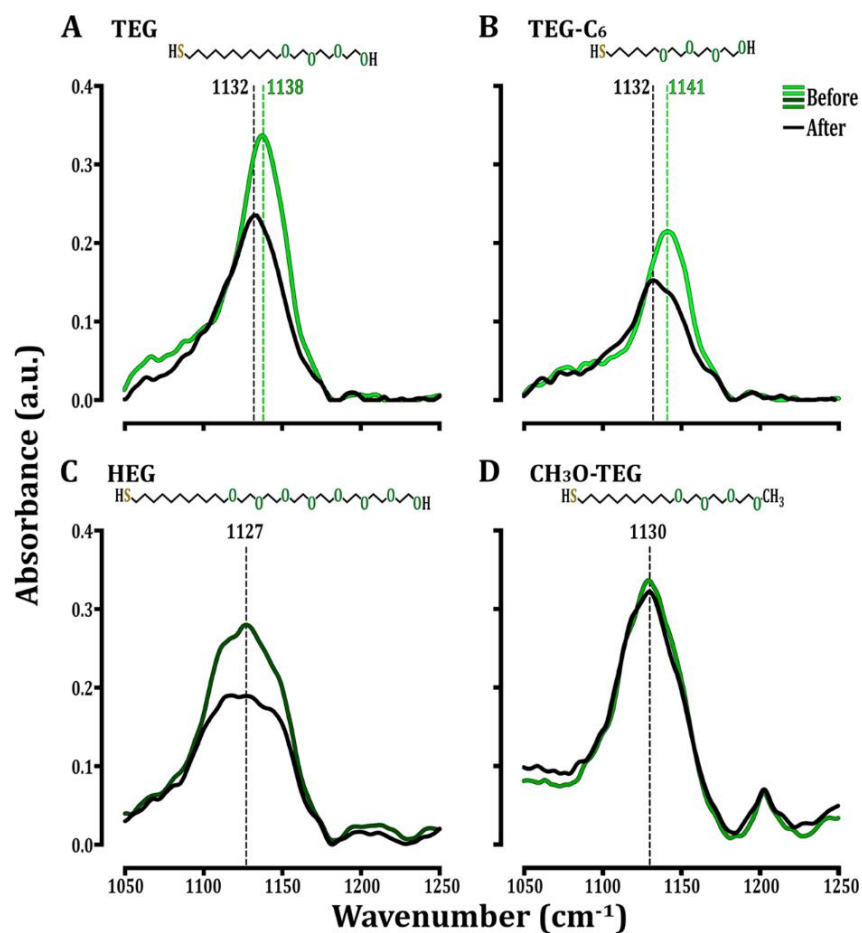


Figure 7-7. Representative polarization modulation infrared reflection-absorption spectra of (A) tri(ethylene glycol) undecanethiol (TEG), (B) tri(ethylene glycol) hexanethiol (TEG-C₆), (C) hexa(ethylene glycol) undecanethiol (HEG), and (D) methoxy tri(ethylene glycol) undecanethiol (CH₃O-TEG) self-assembled monolayers (SAMs) before (top curves) and after (bottom curves) contact with fully oxidized PDMS stamps. Strong C–O–C vibrational bands at ~1138 cm⁻¹ and ~1141 cm⁻¹ are characteristic of ordered all-*trans* tri(ethylene glycol) conformations in (A) TEG and (B) TEG-C₆ SAMs prior to lift-off, respectively. (C) A broad C–O–C vibrational band at ~1127 cm⁻¹ is characteristic of disordered helical hexa(ethylene glycol) moieties in HEG SAMs after self-assembly and prior to lift-off. (D) A strong C–O–C vibrational band at ~1130 cm⁻¹ characteristic of amorphous helical tri(ethylene glycol) moieties is also seen with CH₃O-TEG SAMs. Peak-area decreases in (A), (B), and (C) indicate the removal of alkanethiol molecules due to lift-off. (D) Because methoxy groups are not lift-able, the peak area of the C–O–C stretch of CH₃O-TEG SAMs remains the same before and after lift-off. The post-lift-off C–O–C bands in (A) and (B) appear shifted from pre-lift-off positions at ~1138 cm⁻¹ and ~1141 cm⁻¹ for TEG and TEG-C₆, respectively, to a new position at ~1132 cm⁻¹ indicating conformational changes in tri(ethylene glycol) moieties to disordered helical conformations.

area is likely the result of decreased surface coverage due to the removal of TEG molecules, which is known to occur (*vide supra*), the peak shift is potentially the result of conformational changes in SAM molecules following lift-off. Studies have shown that a C–O–C band at $\sim 1140\text{ cm}^{-1}$ is attributable to a predominantly all-*trans* conformation, whereas red shifts in the C–O–C stretch indicate transitions to disordered helical conformations.^{59,60} The spectroscopic shift from 1138 to 1132 cm^{-1} suggests that TEG molecules undergo rearrangement from ordered nearly all-*trans* to disordered helical conformations following lift-off (Figure 7-8A), which would reduce DNA probe access to Au surfaces. In contrast, such conformational changes do not occur for MCU SAMs post-lift-off due to the absence of oligo(ethylene glycol) moieties (Figure 7-8B).

As an additional test that chemical lift-off lithography induces conformational changes in oligo(ethylene glycol) moieties, we investigated tri(ethylene glycol) hexanethiol (TEG-C₆) SAMs using infrared spectroscopy before and after lift-off. The TEG-C₆ molecules are similar to TEG except their aliphatic backbones consist of 6 vs. 11 carbons (Scheme 7-1). As shown in Figure 7-7B, a C–O–C band was observed at $\sim 1141\text{ cm}^{-1}$ for pristine TEG-C₆ SAMs (top curve). The peak area was reduced after lift-off and shifted to $\sim 1132\text{ cm}^{-1}$ (bottom curve). Similar to TEG SAMs, these results show that alkanethiols were removed from Au surfaces (smaller peak area). Moreover, the shifted C–O–C band observed with TEG-C₆ is characteristic of conformational changes in oligo(ethylene glycol) from pre-lift-off ordered all-*trans* to post-lift-off disordered helical conformations.

For HEG molecules, a broad C–O–C stretch for pre-lift-off SAMs (Figure 7-7C, top curve) was observed at $\sim 1127\text{ cm}^{-1}$, which indicates initial predominantly disordered helical

conformations for alkanethiols with six or greater ethylene glycol units, in agreement with previous studies.^{60,61} After lift-off, the C–O–C peak area decreased due to removal of SAM molecules (Figure 7-7C, bottom curve). Notably, the C–O–C band did not show a redshift similar to TEG and TEG-C₆. This result suggests that HEG SAMs retain the same relative conformation after lift-off. Although HEG molecules did not show conformational changes associated with lift-off lithography, the disordered helical conformation prevented DNA insertion (Figure 7-S3B).

To investigate whether PDMS contact with oligo(ethylene glycol)-terminated SAMs by itself produces disordered ethylene glycol conformations, we monitored the C–O–C stretch arising from methoxy tri-(ethylene glycol)-terminated alkanethiol (CH₃O-TEG) SAMs with infrared spectroscopy before and after conformal contact with oxygen plasma-treated PDMS stamps. The CH₃O-TEG molecules were selected because they are identical to TEG except for the terminal methoxy group (Scheme 7-1), which prevents subtractive patterning.⁴² A sharp C–O–C band was observed at $\sim 1130\text{ cm}^{-1}$ for pristine CH₃O-TEG SAMs, suggestive of initial helical conformations⁶⁰ (top curve, Figure 7-7D). Neither the peak position nor the peak area changed post-lift-off (bottom curve, Figure 7-7D). The lack of a decrease in peak area indicates that CH₃O-TEG molecules were not removed from Au surfaces by contact with activated PDMS stamps. The invariant peak position implies that conformal contact with activated PDMS stamps by itself did not change the conformation of the ethylene glycol moieties. However, the peak position at 1130 cm^{-1} indicates that the CH₃O-TEG molecules adopted helical conformations in both pre- and post-lift-off SAMs. Thus, CH₃O-TEG SAMs are not ideally suited to testing whether stamp contact alone (vs. lift-off) underlies the shift from all-*trans* to helical

oligo(ethylene glycol) conformations. We have yet to identify oligo(ethylene glycol) alkanethiols best suited for isolating the effects of stamp contact *vs.* actual lift-off. These molecules would possess a terminal group not amenable to lift-off yet oligo(ethylene glycol) moieties would adopt an all-*trans* conformation after surface assembly.

The overriding observation from the spectral studies of oligo(ethylene glycol)-terminated alkanethiols is that chemical lift-off lithography induces conformational changes in ethylene glycol segments from ordered to disordered states when the former exist following self-assembly. For TEG and TEG-C₆, ordered all-*trans* conformations were converted to disordered helical conformations after lift-off. For HEG, the helical conformation remained the same before and after lift-off. For CH₃O-TEG, no conformational or lift-off-related changes occurred. The results of this study as a whole lead to the conclusion that disordered states of oligo(ethylene glycols) existing either prior to lift-off (HEG) or as a result of lift-off (TEG, TEG-C₆) are associated with steric hindrance so as to reduce (TEG, TEG-C₆) or to prevent (HEG) thiolated DNA insertion into post-lift-off SAMs. Furthermore, greater numbers of ethylene glycol units appear to interfere to a greater extent with DNA insertion following patterning by lift-off lithography. Conversely, increased DNA insertion and/or hybridization can be achieved on TEG SAMs *via* double-lift-off lithography (Figure 7-2F).

7.4.7 Mixed MCU/TEG SAMs Modulate DNA Surface Coverage

Since DNA surface densities are affected differently by MCU *vs.* TEG due to the ethylene glycol units in the latter, we examined whether variable combinations of these two types of molecules could be used to advantage to tune DNA access to Au substrates. Mixed composition SAMs have been used to create dilute surface coverages wherein surface tethers are

separated and exposed for subsequent chemical modifications, instead of phase segregated.^{10,23,39,41,62} As shown in Figure 7-8C, fluorescence due to surface hybridization between tethered DNA probes and DNA targets increases with respect to solution concentration ratios of MCU vs. TEG. This relationship indicates that as the fraction of MCU in monolayers increases, steric hindrance from the ethylene glycol moieties in TEG decreases, enabling greater DNA access to the Au surfaces. These results are consistent with the hypothesis that oligo(ethylene glycol) moieties are key factors in regulating DNA surface coverage on post-lift-off SAMs. They further demonstrate that the steric effects resulting from chemical lift-off lithography-induced conformational changes in oligo(ethylene glycol) can be used judiciously to control DNA probe surface coverages.

Fluorescence in Figure 7-8C resulted from DNA hybridization between surface-bound probes and fluorescently labeled target-DNA. Notably, fluorescence intensities may not directly reflect the actual numbers of surface-bound DNA probes associated with different mixed SAM compositions. Probes already hybridized with target strands may preclude hybridization of additional DNA targets from solution. As such, DNA hybridization may require extended amounts of time (>1 h) to reach saturation at higher probe densities.⁶³ Also, because we investigated complementary strands with complete base-pair match, some target strands could have cross-hybridized with two DNA probes at higher probe densities. In such a case, part of a target strand hybridizes with the top segment of one DNA probe and the bottom segment of a neighboring probe. Nonetheless, the data in Figure 7-8C indicate the dependence and general trends of DNA hybridization on mixed SAM compositions.

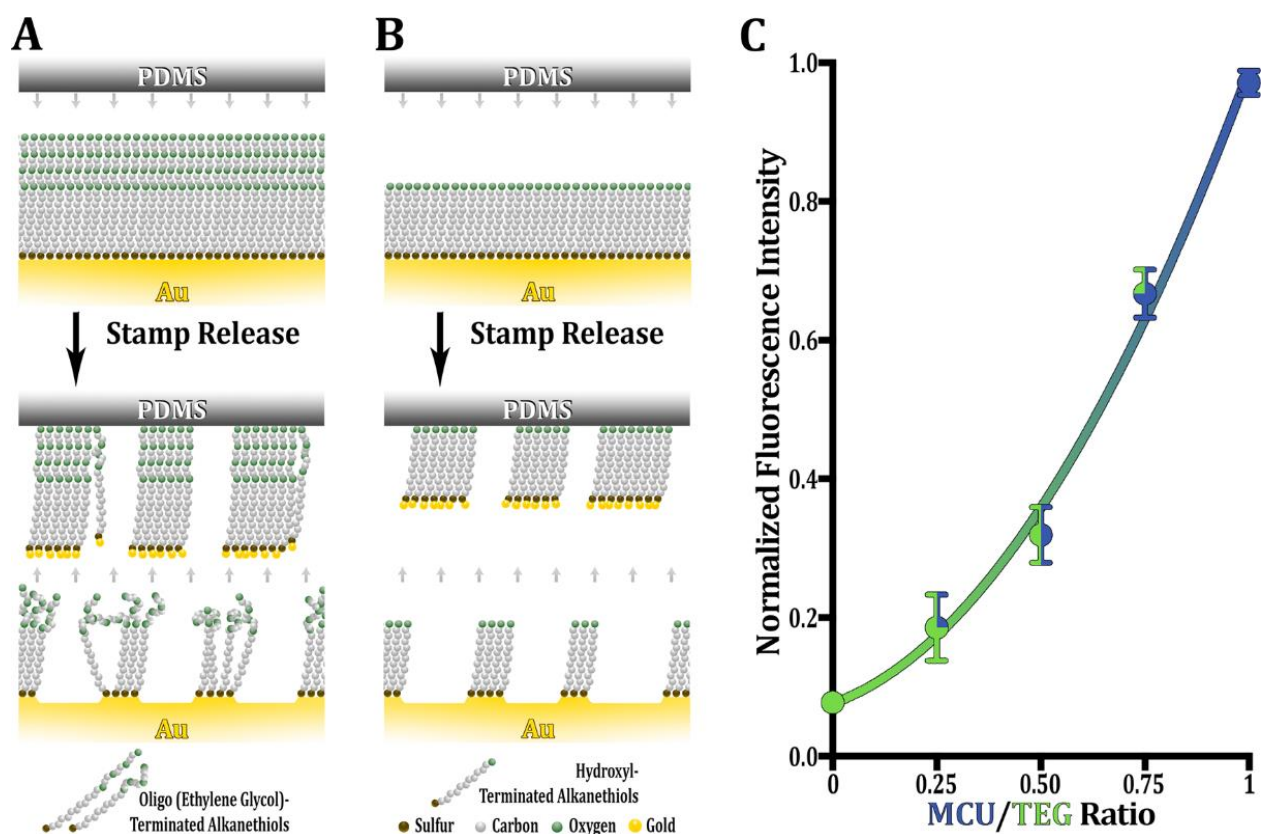


Figure 7-8. Schematic (not to scale) illustrating changes in self-assembled monolayers (SAMs) of (A) tri(ethylene glycol)-terminated (TEG) or (B) hydroxyl-terminated (MCU) alkanethiols following conformal contact between oxygen plasma-treated stamps and SAM-modified substrates. The spectroscopic evidence in Figure 7-7 suggests that ethylene glycol moieties of TEG SAMs undergo conformational changes from ordered *all-trans* conformations prior to chemical lift-off to disordered helical conformations afterward, limiting DNA probe access to Au substrates. In contrast, these conformational changes do not occur for post-lift-off MCU SAMs due to the lack of ethylene glycol moieties. (C) Normalized fluorescence intensities arising from surface hybridization of thiolated DNA probes with fluorescently labeled target DNA vs. ratios (prior to self-assembly) of MCU molecules in mixed solutions with TEG molecules. The best-fit curve ($R^2 > 0.97$) indicates that by varying the nominal concentration ratios, steric effects resulting from ethylene glycol moieties are controlled to tune surface probe densities and thus, DNA hybridization. Error bars represent standard errors of the mean with $N=3$ samples per ratio.

Using the MCH backfilling method, Peterson *et al.* reported a DNA surface density of 3×10^{12} molecules/cm² on Au surfaces.⁵ Furthermore, Lee *et al.* have reported values of 1.7×10^{13} molecules/cm² and 3.6×10^{13} molecules/cm² for backfilled MCH and oligo(ethylene glycol)-terminated alkanethiols, respectively.^{7,21} In contrast, by inserting thiolated DNA into preformed MCH SAMs, Murphy *et al.* and Josephs *et al.* reported low surface densities of 1.1×10^{10} molecules/cm² and 9.5×10^{10} molecules/cm², respectively.^{34,35} The extent of insertion depends strongly on the preparation of the matrix into which molecules are placed.^{33,38,62} We have previously targeted and reached surface densities between $\sim 2 \times 10^{12}$ molecules/cm² and 8×10^{13} molecules/cm² *via* insertion.^{38,39} In comparison to the backfilling method, correlation analysis of XPS atomic percentages and fluorescence hybridization intensities showed improved hybridization efficiency associated with lower DNA probe surface coverages when using the insertion approach. Thus, we expect that the numbers of DNA probes inserted into post-lift-off MCU or MCHD SAMs are below the upper limit determined for backfilling. Estimations using volume fractions in AFM measurements (shown in Figure 7-3), with all of the caveats described above, indicate that the tri(ethylene glycol)-terminated (TEG) and hydroxyl-terminated (MCU) SAMs, as prepared and under the conditions described, lead to tethered DNA densities of $3\text{-}4 \times 10^{12}$ molecules/cm² (5-7 pmol/cm²) and $0.8\text{-}2 \times 10^{13}$ molecules/cm² (10-30 pmol/cm²), respectively. These values are consistent with what others and we have observed for insertion of other molecules into SAM matrices.^{31,33,64}

7.5 Conclusions and Prospects

Subtractive patterning by chemical lift-off lithography relies on strong interactions at stamp-substrate interfaces to remove preassembled alkanethiol SAM molecules from Au substrates. A fundamental advantage of this patterning method is that not all alkanethiol molecules are removed after lift-off within the contacted areas. The remaining molecules create an optimized environment for subsequent insertion and assembly of thiolated DNA probes such that undesirable interactions with substrates are reduced and surface hybridization with target DNA is favored. The extent to which nucleotide surface densities are modulated by post-lift-off SAM molecules depends on specific matrix chemistries and in some cases, the conformations of the terminal SAM moieties.

By creating mixed MCU/TEG SAMs, the surface densities of alkanethiol-DNA probes were tuned according to the nominal concentrations of the two-component SAMs. While post-lift-off TEG SAMs represented the lower limits of tethered DNA surface coverages (with HEG appearing to have negligible DNA inserted), post-lift-off MCU (and to a greater extent MCHD) SAMs represented the upper limits of DNA coverages for the range of SAM molecules investigated here. Expansion of additional parameters such as employing alkanethiols with a wider range of functional groups, altering lengths of ethylene glycol moieties or DNA linkers, and tuning alkanethiol surface coverages and/or packing densities, may enable even greater control of DNA insertion into post-lift-off SAMs. This could broaden the upper and lower limits of DNA surface densities while maintaining highly efficient hybridization.

It is noteworthy that conformational changes in ethylene glycol moieties have been shown to vary with hydration, chain-length, temperature-driven processes, packing densities, surface coverage, and storage conditions.^{59,65-67} Our findings show that (ethylene glycol)-

terminated alkanethiol conformational changes in SAMs can also be induced by the chemical lift-off process. Moreover, ionic strength, salt concentration, pH, multipoint binding dendrimers, alkyl linkers, and nucleotide-block spacers have been reported to influence thiolated DNA probe coverage.^{8,13,63,68} Here, we show that chemical lift-off lithography, in combination with tunable mixed SAM compositions, provides a facile means by which to regulate DNA surface densities.

Probe DNA inserted into native MCH SAM defects has been reported to produce more uniformly distributed DNA monolayers *vs.* surface-bound DNA backfilled with MCH.³⁵ However, it was difficult to achieve high DNA surface densities for practical sensing purposes using insertion alone because of the limited numbers of intrinsic SAM defects. Here, we show that by using lift-off lithography, large-area, high-density DNA patterns can be fabricated by inserting alkanethiol-functionalized DNA probes into post-lift-off alkanethiol SAMs. These findings advance DNA insertion methods toward more practical applications for creating DNA-based sensors. While a single lift-off step removes a large fraction of the preformed SAM molecules, multiple lift-off steps presumably remove additional SAM molecules and/or create additional defects providing greater surface availability for insertion compared to intrinsic SAM/substrate defects.⁴² Thus, “artificial defects” introduced into the post-lift-off regions beyond intrinsic defects are key to a highly feasible and advantageous DNA insertion method.

The “artificial defects” created by chemical lift-off lithography appear to comprise a new class of defect site that is serendipitously optimized for insertion and biorecognition. In the future, molecular-resolution information about the post-lift SAM regions will enable a deeper understanding of their structure. This type of information will also shed light on potential limitations and improve control. The use of scanning probe microscopies to interrogate these SAM structures will be difficult because of their molecular lengths, corrugation, degree of

disorder, and association with water molecules under ambient conditions.⁶⁹⁻⁷² A more precise quantification of the SAM molecules remaining in the stamp-contact regions is feasible using electrochemical reductive desorption, which is sensitive to domain sizes and interaction strengths with different molecules desorbing at different electrochemical potentials.⁷³⁻⁷⁵ Electrochemical reductive desorption measurements will also be useful for determining the numbers and arrangements of alkanethiol molecules remaining on substrates after multiple lift-off steps.

Because lift-off lithography patterning reduces DNA-substrate interactions, when coupled with automated processes for generating arrays, this technique should be applicable for fabricating high-throughput platforms to study aptamer-ligand interactions.^{76,77} Notably, the ability to control the surface properties of DNA, the sub-40 nm nanopatterning capabilities of chemical lift-off lithography, and the ability to fabricate high-performance field-effect transistor-based biosensors also *via* lift-off lithography will render single-molecule DNA nanoarrays feasible for bioelectronics and other applications.⁷⁸⁻⁸²

7.6 Supplementary Experiments and Figures

Experiments were carried out to determine optimal DNA insertion times. Similar to the conditions in the experimental procedures in the main text, chemical lift-off was carried out on MCU SAMs followed by thiolated DNA probe insertion for 0 min, 0.5 min, 2 min, 5 min, 40 min, 120 min (2 h), or 1020 min (17 h). Surface DNA probes were hybridized with fluorescently tagged complementary DNA. Normalized fluorescence intensities for DNA hybridization vs. DNA insertion times are shown in Figure 7-S1.

Atomic percentages determined from XPS peak areas for carbon, oxygen, sulfur, nitrogen, and phosphorus are shown in Table 7-S1. With the exception of nitrogen and phosphorus, which are XPS fingerprints for DNA molecules, XPS signals from carbon, oxygen and sulfur are present in both DNA and matrix molecules. Moreover, X-ray attenuation lengths further complicate the interpretation of these XPS signals. Thus, while reported in Table 7-S1 for completeness, these peak areas are not suitable for determining relative surface coverages of DNA probes.

Additionally, XPS experiments were carried out to determine whether hydroxyl-terminated hexadecanethiol (MCHD) and hexa(ethylene glycol)-terminated undecanethiol (HEG) molecules were removed from Au surfaces by chemical lift-off. We showed previously that alkanethiol SAM molecules removed by lift-off resulted in Au 4f XPS signals on post-lift-off PDMS stamps indicating that Au atoms bound to alkanethiols are also removed. Here, Au 4f XPS signals were observed on post-lift-off PDMS stamps, as shown in Figures S2A (MCHD) and S2B (HEG). Control experiments were carried out wherein oxygen plasma-treated PDMS stamps were not contacted with MCHD and HEG SAMs. Here, no Au 4f signals were observed,

as shown in Figure 7-S2C. Similar to other XPS experiments in this study, featureless PDMS stamps were used for these experiments.

Additional fluorescence microscopy experiments were carried out to explore an alternative mechanism regarding steric effects of ethylene glycol moieties in TEG molecules induced by the lift-off process. Because TEG molecules are longer than MCU molecules by three ethylene glycol units, it is possible that thicker TEG SAMs might hinder DNA probes from accessing Au surfaces. Therefore, if longer alkanethiols, such as hydroxyl-terminated hexadecanethiol (MCHD) and hexa(ethylene glycol)-terminated undecanethiol (HEG) are used, one would expect that the resulting thicker SAMs would obstruct DNA probes from reaching Au surfaces to a greater extent compared to MCU and TEG SAMs, respectively. For example, if SAM thickness alone blocked DNA probes from accessing Au surfaces, then weaker fluorescence patterns would be expected following DNA surface hybridization on either MCHD or HEG SAMs *vs* MCU or TEG SAMs, respectively. Similar to the conditions in the main text experimental procedures, chemical lift-off was carried out on MCHD and HEG SAMs followed by DNA probe insertion and hybridization with fluorescently tagged complimentary DNA. Representative fluorescence microscopy images are shown in Figures 7-S3A (MCHD/DNA SAMs) and 7-S3B (HEG/DNA SAMs).

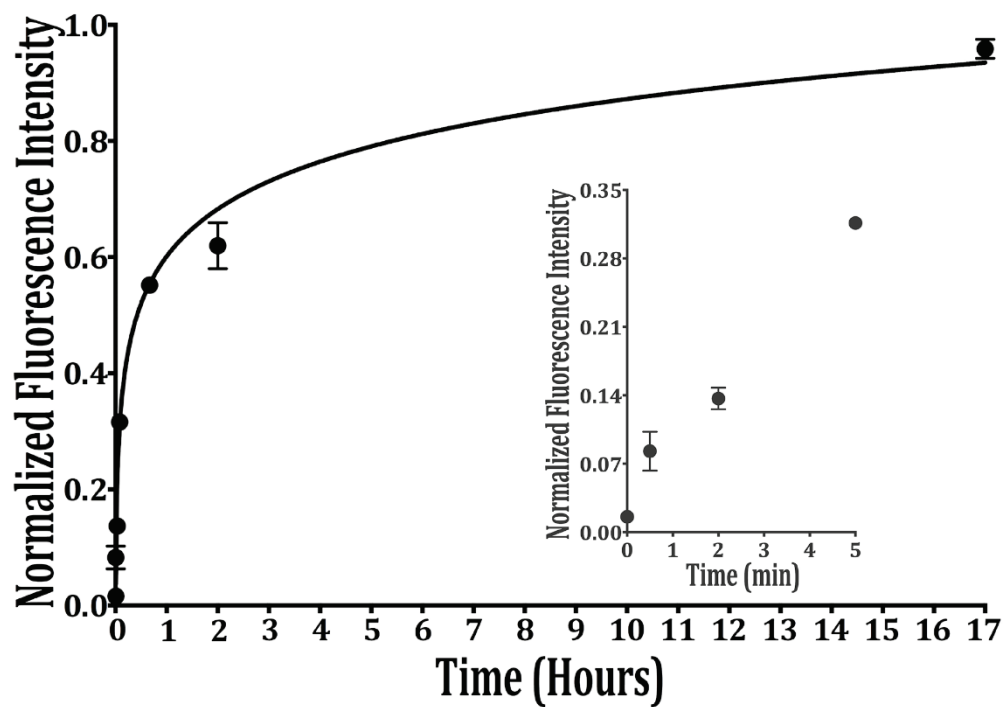


Figure 7-S1. Normalized fluorescence intensities resulting from target DNA hybridization vs. DNA probe insertion times. An initial sharp increase in hybridization (0-2 h) was followed by a slow rise in fluorescence intensities, suggesting that DNA probe surface coverages start to approach saturation after ~2 h of insertion. The inset shows DNA probe insertion behavior at the early time points

Elements	Atomic Percentage		
	C 1s	O 1s	S 2p
DNA (predicted)	45.7	31.2	0.3
DNA (experimental)	31.9±0.7	48.8±0.4	N/D
DNA/MCU Backfill	40.7±0.5	41.2±0.2	1.7±0.2
MCU/DNA Insertion	52.7±1.5	35.0±1.3	3.4±0.2
TEG/DNA Insertion	52.4±0.6	44.9±0.7	2.6±0.1
MCU	62.6±3.5	26.4±2.2	5.3±0.4
TEG	51.9±0.5	45.0±1.0	2.6±0.0

Table 7-S1. Predicted X-ray photoelectron spectroscopy atomic percentages for undiluted DNA were calculated using the numbers of C, O, and S atoms in DNA probe molecules. Atomic percentages for pure DNA monolayers (experimental) and mixed monolayers of hydroxyl- (MCU) and tri(ethylene glycol) (TEG)-terminated alkanethiol/DNA on Au substrates were calculated from XPS peak areas ($N=3-6/\text{group}$). Not detectable XPS signals are indicated by "N/D". Entries are means \pm standard errors of the means.

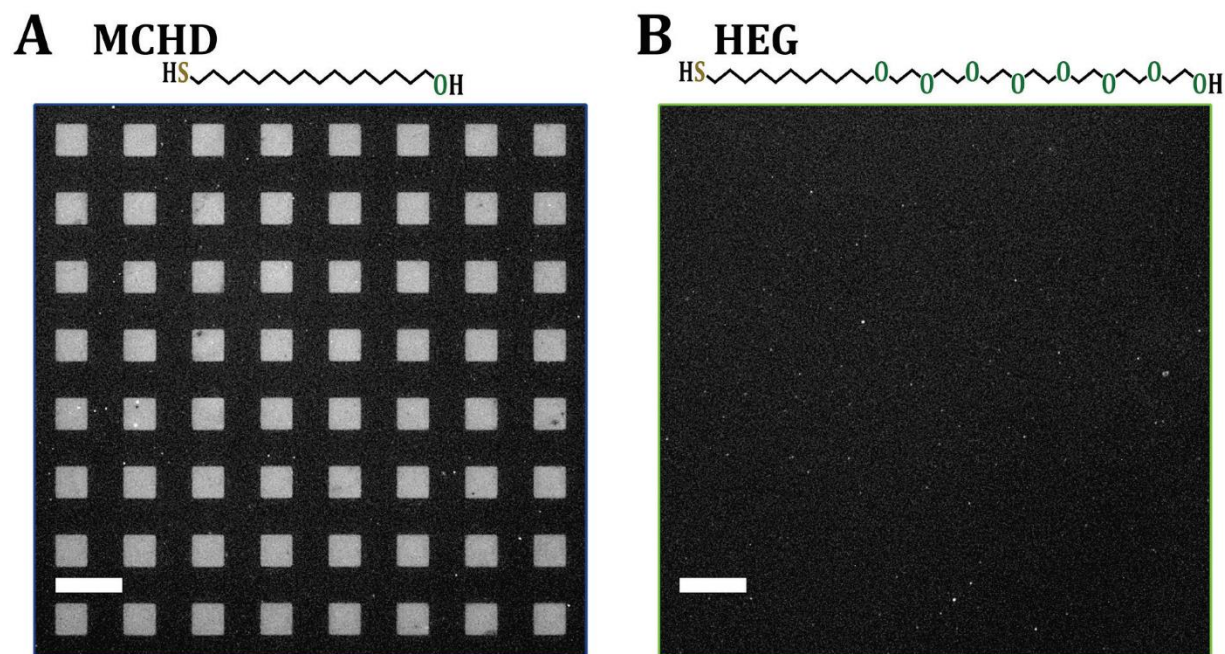


Figure 7-S3. Representative fluorescence images displaying hybridization of thiolated DNA probes with Alexa Fluor 488 (excitation at 495 nm)-labeled complementary DNA targets on (A) hydroxyl-terminated hexadecanethiol (MCHD) and (B) hexa(ethylene glycol)-terminated undecanethiol (HEG) self-assembled monolayers (SAM). The bright square patterns in (A) indicate that substantial numbers of DNA probes inserted into the post-lift-off MCHD SAM and were available for hybridization. By contrast, the lack of a discernable pattern in (B) suggests that insertion does not occur to an appreciable extent on HEG SAMs. The fact that a similar fluorescent square pattern is not visible in (B) implies that the increased numbers of ethylene glycol moieties in HEG SAMs impose greater steric hindrance compared to TEG SAMs; HEG molecules are three ethylene glycol units longer than TEG molecules. The fluorescence images (shown with the same exposure time of 5 s) were taken at an emission wavelength of 517 nm. Scale bars are 50 μm .

7.7 References

1. Lockhart, D. J.; Winzler, E. A. Genomics, Gene Expression and DNA Arrays. *Nature* **2000**, *405*, 827–836.
2. Caruso, F.; Rodda, E.; Furlong, D. N.; Haring, V. DNA Binding and Hybridization on Gold and Derivatized Surfaces. *Sens. Actuators, B* **1997**, *41*, 189–197.
3. Sassolas, A.; Leca-Bouvier, B. D.; Blum, L. J. DNA Biosensors and Microarrays. *Chem. Rev.* **2008**, *108*, 109–139.
4. Herne, T. M.; Tarlov, M. J. Characterization of DNA Probes Immobilized on Gold Surfaces. *J. Am. Chem. Soc.* **1997**, *119*, 8916–8920.
5. Peterson, A. W.; Heaton, R. J.; Georgiadis, R. M. The Effect of Surface Probe Density on DNA Hybridization. *Nucleic Acids Res.* **2001**, *29*, 5163–5168.
6. Boozer, C.; Chen, S. F.; Jiang, S. Y. Controlling DNA Orientation on Mixed ssDNA/OEG SAMs. *Langmuir* **2006**, *22*, 4694–4698.
7. Lee, C.-Y.; Gong, P.; Harbers, G. M.; Grainger, D. W.; Castner, D. G.; Gamble, L. J. Surface Coverage and Structure of Mixed DNA/Alkylthiol Monolayers on Gold: Characterization by XPS, NEXAFS, and Fluorescence Intensity Measurements. *Anal. Chem.* **2006**, *78*, 3316–3325.
8. Day, B. S.; Fiegland, L. R.; Vint, E. S.; Shen, W.; Morris, J. R.; Norton, M. L. Thiolated Dendrimers as Multi-Point Binding Headgroups for DNA Immobilization on Gold. *Langmuir* **2011**, *27*, 12434–12442.
9. Ostuni, E.; Yan, L.; Whitesides, G. M. The Interaction of Proteins and Cells with Self-Assembled Monolayers of Alkane thiolates on Gold and Silver. *Colloids Surf., B* **1999**, *15*, 3–30.

10. Shuster, M. J.; Vaish, A.; Cao, H. H.; Guttentag, A. I.; McManigle, J. E.; Gibb, A. L.; Martinez, M. M.; Nezarati, R. M.; Hinds, J. M.; Liao, W.-S.; Weiss, P. S.; Andrews, A. M. Patterning Small-Molecule Biocapture Surfaces: Microcontact Insertion Printing vs. Photolithography. *Chem. Commun.* **2011**, *47*, 10641–10643.
11. Huang, E.; Zhou, F. M.; Deng, L. Studies of Surface Coverage and Orientation of DNA Molecules Immobilized onto Preformed Alkanethiol Self-Assembled Monolayers. *Langmuir* **2000**, *16*, 3272–3280.
12. Rant, U.; Arinaga, K.; Fujita, S.; Yokoyama, N.; Abstreiter, G.; Tornow, M. Structural Properties of Oligonucleotide Monolayers on Gold Surfaces Probed by Fluorescence Investigations. *Langmuir* **2004**, *20*, 10086–10092.
13. Opdahl, A.; Petrovykh, D. Y.; Kimura-Suda, H.; Tarlov, M. J.; Whitman, L. J. Independent Control of Grafting Density and Conformation of Single-Stranded DNA Brushes. *Proc. Natl. Acad. Sci. U. S. A.* **2007**, *104*, 9–14.
14. Kaufmann, R.; Averbukh, I.; Naaman, R.; Daube, S. S. Controlling the Reactivity of Adsorbed DNA on Template Surfaces. *Langmuir* **2008**, *24*, 927–931.
15. Howell, C.; Zhao, J. L.; Koelsch, P.; Zharnikov, M. Hybridization in ssDNA Films A Multi-Technique Spectroscopy Study. *Phys. Chem. Chem. Phys.* **2011**, *13*, 15512–15522.
16. Steel, A. B.; Herne, T. M.; Tarlov, M. J. Electrochemical Quantitation of DNA Immobilized on Gold. *Anal. Chem.* **1998**, *70*, 4670–4677.
17. Levicky, R.; Herne, T. M.; Tarlov, M. J.; Satija, S. K. Using Self-Assembly to Control the Structure of DNA Monolayers on Gold: A Neutron Reflectivity Study. *J. Am. Chem. Soc.* **1998**, *120*, 9787–9792.

18. Kimura-Suda, H.; Petrovykh, D. Y.; Tarlov, M. J.; Whitman, L. J. Base-Dependent Competitive Adsorption of Single-Stranded DNA on Gold. *J. Am. Chem. Soc.* **2003**, *125*, 9014–9015.
19. Arinaga, K.; Rant, U.; Tornow, M.; Fujita, S.; Abstreiter, G.; Yokoyama, N. The Role of Surface Charging During the Coadsorption of Mercaptohexanol to DNA Layers on Gold: Direct Observation of Desorption and Layer Reorientation. *Langmuir* **2006**, *22*, 5560–5562.
20. Lai, R. Y.; Seferos, D. S.; Heeger, A. J.; Bazan, G. C.; Plaxco, K. W. Comparison of the Signaling and Stability of Electrochemical DNA Sensors Fabricated from 6- or 11-Carbon Self-Assembled Monolayers. *Langmuir* **2006**, *22*, 10796–10800.
21. Lee, C.-Y.; Gamble, L. J.; Grainger, D. W.; Castner, D. G. Mixed DNA/Oligo (Ethylene Glycol) Functionalized Gold Surfaces Improve DNA Hybridization in Complex Media. *Biointerphases* **2006**, *1*, 82–92.
22. Boozer, C.; Ladd, J.; Chen, S. F.; Yu, Q.; Homola, J.; Jiang, S. Y. DNA Directed Protein Immobilization on Mixed ssDNA/Oligo(Ethylene Glycol) Self-Assembled Monolayers for Sensitive Biosensors. *Anal. Chem.* **2004**, *76*, 6967–6972.
23. Shuster, M. J.; Vaish, A.; Szapacs, M. E.; Anderson, M. E.; Weiss, P. S.; Andrews, A. M. Biospecific Recognition of Tethered Small Molecules Diluted in Self-Assembled Monolayers. *Adv. Mater.* **2008**, *20*, 164–167.
24. Liao, W.-S.; Cao, H. H.; Cheunkar, S.; Shuster, M. J.; Altieri, S. C.; Weiss, P. S.; Andrews, A. M. Small-Molecule Arrays for Sorting G-Protein-Coupled Receptors. *J. Phys. Chem. C* **2013**, *117*, 22362–22368.

25. Choi, S.; Murphy, W. L. Multifunctional Mixed SAMs That Promote Both Cell Adhesion and Noncovalent DNA Immobilization. *Langmuir* **2008**, *24*, 6873–6880.
26. Satjapipat, M.; Sanedrin, R.; Zhou, F. M. Selective Desorption of Alkanethiols in Mixed Self-Assembled Monolayers for Subsequent Oligonucleotide Attachment and DNA Hybridization. *Langmuir* **2001**, *17*, 7637–7644.
27. Aqua, T.; Naaman, R.; Daube, S. S. Controlling the Adsorption and Reactivity of DNA on Gold. *Langmuir* **2003**, *19*, 10573–10580.
28. Fang, Y.; Spisz, T. S.; Hoh, J. H. Ethanol-Induced Structural Transitions of DNA on Mica. *Nucleic Acids Res.* **1999**, *27*, 1943–1949.
29. Kick, A.; Boensch, M.; Kummer, K.; Vyalikh, D. V.; Molodtsov, S. L.; Mertig, M. Controlling Structural Properties of Self-Assembled Oligonucleotide-Mercaptohexanol Monolayers. *J. Electron Spectrosc. Relat. Phenom.* **2009**, *172*, 36–41.
30. Bumm, L. A.; Arnold, J. J.; Cygan, M. T.; Dunbar, T. D.; Burgin, T. P.; Jones, L.; Allara, D. L.; Tour, J. M.; Weiss, P. S. Are Single Molecular Wires Conducting? *Science* **1996**, *271*, 1705–1707.
31. Cygan, M. T.; Dunbar, T. D.; Arnold, J. J.; Bumm, L. A.; Shedlock, N. F.; Burgin, T. P.; Jones, L.; Allara, D. L.; Tour, J. M.; Weiss, P. S. Insertion, Conductivity, and Structures of Conjugated Organic Oligomers in Self-Assembled Alkanethiol Monolayers on Au{111}. *J. Am. Chem. Soc.* **1998**, *120*, 2721–2732.
32. Shuster, M. J.; Vaish, A.; Gilbert, M. L.; Martinez-Rivera, M.; Nezarati, R. M.; Weiss, P. S.; Andrews, A. M. Comparison of Oligo(Ethylene Glycol)Alkanethiols *versus* *n*-Alkanethiols: Self-Assembly, Insertion, and Functionalization. *J. Phys. Chem. C* **2011**, *115*, 24778–24787.

33. Claridge, S. A.; Liao, W.-S.; Thomas, J. C.; Zhao, Y.; Cao, H. H.; Cheunkar, S.; Serino, A. C.; Andrews, A. M.; Weiss, P. S. From the Bottom Up: Dimensional Control and Characterization in Molecular Monolayers. *Chem. Soc. Rev.* **2013**, *42*, 2725–2745.
34. Murphy, J. N.; Cheng, A. K. H.; Yu, H.-Z.; Bizzotto, D. On the Nature of DNA Self-Assembled Monolayers on Au: Measuring Surface Heterogeneity with Electrochemical *in Situ* Fluorescence Microscopy. *J. Am. Chem. Soc.* **2009**, *131*, 4042–4050.
35. Josephs, E. A.; Ye, T. Nanoscale Spatial Distribution of Thiolated DNA on Model Nucleic Acid Sensor Surfaces. *ACS Nano* **2013**, *7*, 3653–3660.
36. Josephs, E. A.; Ye, T. A Single-Molecule View of Conformational Switching of DNA Tethered to a Gold Electrode. *J. Am. Chem. Soc.* **2012**, *134*, 10021–10030.
37. Josephs, E. A.; Ye, T. Electric-Field Dependent Conformations of Single DNA Molecules on a Model Biosensor Surface. *Nano Lett.* **2012**, *12*, 5255–5261.
38. Mullen, T. J.; Srinivasan, C.; Hohman, J. N.; Gillmor, S. D.; Shuster, M. J.; Horn, M. W.; Andrews, A. M.; Weiss, P. S. Microcontact Insertion Printing. *Appl. Phys. Lett.* **2007**, *90*, 0631141–0631143.
39. Vaish, A.; Shuster, M. J.; Cheunkar, S.; Singh, Y. S.; Weiss, P. S.; Andrews, A. M. Native Serotonin Membrane Receptors Recognize 5-Hydroxytryptophan-Functionalized Substrates: Enabling Small-Molecule Recognition. *ACS Chem. Neurosci.* **2010**, *1*, 495–504.
40. Saavedra, H. M.; Mullen, T. J.; Zhang, P. P.; Dewey, D. C.; Claridge, S. A.; Weiss, P. S. Hybrid Strategies in Nanolithography. *Rep. Prog. Phys.* **2010**, *73*, 0365011–03650140.

41. Vaish, A.; Shuster, M. J.; Cheunkar, S.; Weiss, P. S.; Andrews, A. M. Tuning Stamp Surface Energy for Soft Lithography of Polar Molecules to Fabricate Bioactive Small-Molecule Microarrays. *Small* **2011**, *7*, 1471–1479.
42. Liao, W.-S.; Cheunkar, S.; Cao, H. H.; Bednar, H. R.; Weiss, P. S.; Andrews, A. M. Subtractive Patterning *via* Chemical Lift-Off Lithography. *Science* **2012**, *337*, 1517–1521.
43. Kung, L. A.; Kam, L.; Hovis, J. S.; Boxer, S. G. Patterning Hybrid Surfaces of Proteins and Supported Lipid Bilayers. *Langmuir* **2000**, *16*, 6773–6776.
44. Hovis, J. S.; Boxer, S. G. Patterning Barriers to Lateral Diffusion in Supported Lipid Bilayer Membranes by Blotting and Stamping. *Langmuir* **2000**, *16*, 894–897.
45. Hovis, J. S.; Boxer, S. G. Patterning and Composition Arrays of Supported Lipid Bilayers by Microcontact Printing. *Langmuir* **2001**, *17*, 3400–3405.
46. Peterson, A. W.; Heaton, R. J.; Georgiadis, R. Kinetic Control of Hybridization in Surface Immobilized DNA Monolayer Films. *J. Am. Chem. Soc.* **2000**, *122*, 7837–7838.
47. Rao, A. N.; Grainger, D. W. Biophysical Properties of Nucleic Acids at Surfaces Relevant to Microarray Performance. *Biomater. Sci.* **2014**, *2*, 436–471.
48. Damaschun, G.; Damaschun, H.; Misselwitz, R.; Pospelov, V. A.; Zalenskaya, I. A.; Zirwer, D.; Muller, J. J.; Vorobev, V. I. How Many Base-Pairs per Turn Does DNA Have in Solution and in Chromatin - an Answer from Wide-Angle X-Ray Scattering. *Biochim. Acta* **1983**, *42*, 697–703.
49. Steel, A. B.; Levicky, R. L.; Herne, T. M.; Tarlov, M. J. Immobilization of Nucleic Acids at Solid Surfaces: Effect of Oligonucleotide Length on Layer Assembly. *Biophys. J.* **2000**, *79*, 975–981.

50. May, C. J.; Canavan, H. E.; Castner, D. G. Quantitative X-Ray Photoelectron Spectroscopy and Time-Of-Flight Secondary Ion Mass Spectrometry Characterization of the Components in DNA. *Anal. Chem.* **2004**, *76*, 1114–1122.
51. Petrovykh, D. Y.; Kimura-Suda, H.; Tarlov, M. J.; Whitman, L. J. Quantitative Characterization of DNA Films by X-Ray Photoelectron Spectroscopy. *Langmuir* **2004**, *20*, 429–440.
52. Lee, C. Y.; Nguyen, P. C. T.; Grainger, D. W.; Gamble, L. J.; Castner, D. G. Structure and DNA Hybridization Properties of Mixed Nucleic Acid/Maleimide-Ethylene Glycol Monolayers. *Anal. Chem.* **2007**, *79*, 4390–4400.
53. Cederquist, K. B.; Keating, C. D. Hybridization Efficiency of Molecular Beacons Bound to Gold Nanowires: Effect of Surface Coverage and Target Length. *Langmuir* **2010**, *26*, 18273–18280.
54. Demers, L. M.; Mirkin, C. A.; Mucic, R. C.; Reynolds, R. A.; Letsinger, R. L.; Elghanian, R.; Viswanadham, G. A Fluorescence-Based Method for Determining the Surface Coverage and Hybridization Efficiency of Thiol-Capped Oligonucleotides Bound to Gold Thin Films and Nanoparticles. *Anal. Chem.* **2000**, *72*, 5535–5541.
55. Gorodetsky, A. A.; Buzzeo, M. C.; Barton, J. K. DNA-Mediated Electrochemistry. *Bioconjugate Chem.* **2008**, *19*, 2285–2296.
56. Kelley, S. O.; Jackson, N. M.; Hill, M. G.; Barton, J. K. Long-Range Electron Transfer through DNA Films. *Angew. Chem., Int. Ed.* **1999**, *38*, 941–945.
57. Gong, P.; Lee, C. Y.; Gamble, L. J.; Castner, D. G.; Grainger, D. W. Hybridization Behavior of Mixed DNA/Alkylthiol Monolayers on Gold: Characterization by Surface Plasmon Resonance and P-32 Radiometric Assay. *Anal. Chem.* **2006**, *78*, 3326–3334.

58. Valiokas, R.; Malysheva, L.; Onipko, A.; Lee, H.-H.; Ruzele, Z.; Svedhem, S.; Svensson, S. C. T.; Gelius, U.; Liedberg, B. On the Quality and Structural Characteristics of Oligo(Ethylene Glycol) Assemblies on Gold: An Experimental and Theoretical Study. *J. Electron Spectrosc. Relat. Phenom.* **2009**, *172*, 9–20.
59. Skoda, M. W. A.; Jacobs, R. M. J.; Willis, J.; Schreiber, F. Hydration of Oligo(Ethylene Glycol) Self-Assembled Monolayers Studied Using Polarization Modulation Infrared Spectroscopy. *Langmuir* **2007**, *23*, 970–974.
60. Harder, P.; Grunze, M.; Dahint, R.; Whitesides, G. M.; Laibinis, P. E. Molecular Conformation in Oligo(Ethylene Glycol)-Terminated Self-Assembled Monolayers on Gold and Silver Surfaces Determines Their Ability to Resist Protein Adsorption. *J. Phys. Chem. B* **1998**, *102*, 426–436.
61. Zorn, S.; Martin, N.; Gerlach, A.; Schreiber, F. Real-Time PMIRRAS Studies of *in Situ* Growth of C₁₁Eg₆OMe on Gold and Immersion Effects. *Phys. Chem. Chem. Phys.* **2010**, *12*, 8986–8991.
62. Weck, M.; Jackiw, J. J.; Rossi, R. R.; Weiss, P. S.; Grubbs, R. H. Ring-Opening Metathesis Polymerization from Surfaces. *J. Am. Chem. Soc.* **1999**, *121*, 4088–4089.
63. Wong, E. L. S.; Chow, E.; Gooding, J. J. DNA Recognition Interfaces: The Influence of Interfacial Design on the Efficiency and Kinetics of Hybridization. *Langmuir* **2005**, *21*, 6957–6965.
64. Smith, R. K.; Nanayakkara, S. U.; Woehrlé, G. H.; Pearl, T. P.; Blake, M. M.; Hutchison, J. E.; Weiss, P. S. Spectral Diffusion in the Tunneling Spectra of Ligand-Stabilized Undecagold Clusters. *J. Am. Chem. Soc.* **2006**, *128*, 9266–9267.

65. Valiokas, R.; Svedhem, S.; Ostblom, M.; Svensson, S. C. T.; Liedberg, B. Influence of Specific Intermolecular Interactions on the Self-Assembly and Phase Behavior of Oligo(Ethylene Glycol)-Terminated Alkanethiolates on Gold. *J. Phys. Chem. B* **2001**, *105*, 5459–5469.
66. Zorn, S.; Skoda, M. W. A.; Gerlach, A.; Jacobs, R. M. J.; Schreiber, F. On the Stability of Oligo(Ethylene Glycol) (C₁₁EG₆OMe) SAMs on Gold: Behavior at Elevated Temperature in Contact with Water. *Langmuir* **2011**, *27*, 2237–2243.
67. Zorn, S.; Dettinger, U.; Skoda, M. W. A.; Jacobs, R. M. J.; Peisert, H.; Gerlach, A.; Chasse, T.; Schreiber, F. Stability of Hexa(Ethylene Glycol) SAMs towards the Exposure to Natural Light and Repeated Reimmersion. *Appl. Surf. Sci.* **2012**, *258*, 7882–7888.
68. Ravan, H.; Kashanian, S.; Sanadgol, N.; Badoei-Dalfard, A.; Karami, Z. Strategies for Optimizing DNA Hybridization on Surfaces. *Anal. Biochem.* **2014**, *444*, 41–46.
69. Esplandiu, M. J.; Hagenstrom, H.; Kolb, D. M. Functionalized Self-Assembled Alkanethiol Monolayers on Au(111) Electrodes: 1. Surface Structure and Electrochemistry. *Langmuir* **2001**, *17*, 828–838.
70. Liu, Y. F.; Yang, Y. C.; Lee, Y. L. Assembly Behavior and Monolayer Characteristics of OH-Terminated Alkanethiol on Au(111): *In Situ* Scanning Tunneling Microscopy and Electrochemical Studies. *Nanotechnology* **2008**, *19*, 065609.
71. Liu, Y. F.; Lee, Y. L. Adsorption Characteristics of OH-Terminated Alkanethiol and Arenethiol on Au(111) Surfaces. *Nanoscale* **2012**, *4*, 2093–2100.
72. Abel, G. R.; Josephs, E. A.; Luong, N.; Ye, T. A Switchable Surface Enables Visualization of Single DNA Hybridization Events with Atomic Force Microscopy. *J. Am. Chem. Soc.* **2013**, *135*, 6399–6402.

73. Mullen, T. J.; Dameron, A. A.; Weiss, P. S. Directed Assembly and Separation of Self-Assembled Monolayers *via* Electrochemical Processing. *J. Phys. Chem. B* **2006**, *110*, 14410–14417.
74. Dameron, A. A.; Mullen, T. J.; Hengstebeck, R. W.; Saavedra, H. M.; Weiss, P. S. Origins of Displacement in 1-Adamantanethiolate Self-Assembled Monolayers. *J. Phys. Chem. C* **2007**, *111*, 6747–6752.
75. Kim, M.; Hohman, J. N.; Serino, A. C.; Weiss, P. S. Structural Manipulation of Hydrogen-Bonding Networks in Amide-Containing Alkanethiolate Monolayers *via* Electrochemical Processing. *J. Phys. Chem. C* **2010**, *114*, 19744–19751.
76. Gao, P.; Cai, Y. G. Aptamer Fiber Anchored on the Edge of a Protein Pattern: A Template for Nanowire Fabrication. *ACS Nano* **2009**, *3*, 3475–3484.
77. Sheng, W. A.; Chen, T.; Tan, W. H.; Fan, Z. H. Multivalent DNA Nanospheres for Enhanced Capture of Cancer Cells in Microfluidic Devices. *ACS Nano* **2013**, *7*, 7067–7076.
78. Wilson, N. A.; Abu-Shumays, R.; Gyarfás, B.; Wang, H.; Lieberman, K. R.; Akesson, M.; Dunbar, W. B. Electronic Control of DNA Polymerase Binding and Unbinding to Single DNA Molecules. *ACS Nano* **2009**, *3*, 995–1003.
79. Yasui, T.; Rahong, S.; Motoyama, K.; Yanagida, T.; Wu, Q.; Kaji, N.; Kanai, M.; Doi, K.; Nagashima, K.; Tokeshi, M.; Taniguchi, M.; Kawano, S.; Kawai, T.; Baba, Y. DNA Manipulation and Separation in Sublithographic-Scale Nanowire Array. *ACS Nano* **2013**, *7*, 3029–3035.
80. Fu, Y. M.; Zeng, D. D.; Chao, J.; Jin, Y. Q.; Zhang, Z.; Liu, H. J.; Li, D.; Ma, H. W.; Huang, Q.; Gothelf, K. V.; Fan, C. H. Single-Step Rapid Assembly of DNA Origami

- Nanostructures for Addressable Nanoscale Bioreactors. *J. Am. Chem. Soc.* **2013**, *135*, 696–702.
81. Liao, W. S.; Chen, X.; Yang, T. L.; Castellana, E. T.; Chen, J. X.; Cremer, P. S. Benchtop Chemistry for the Rapid Prototyping of Label-Free Biosensors: Transmission Localized Surface Plasmon Resonance Platforms. *Biointerphases* **2009**, *4*, 80–85.
82. Kim, J.; Rim, Y. S.; Chen, H. J.; Cao, H. H.; Nakatsuka, N.; Hinton, H. L.; Zhao, C. Z.; Andrews, A. M.; Yang, Y.; Weiss, P. S. Fabrication of High-Performance Ultrathin In₂O₃ Film Field-Effect Transistors and Biosensors Using Chemical Lift-Off Lithography. *ACS Nano* **2015**, *9*, 4572–4582.
83. Yang, X. J.; Bing, T.; Mei, H. C.; Fang, C. L.; Cao, Z. H. Shangguan, D. H. Characterization and Application of a DNA Aptamer Binding to L-Tryptophan. *Analyst* **2011**, *136*, 577–585.

Chapter 8

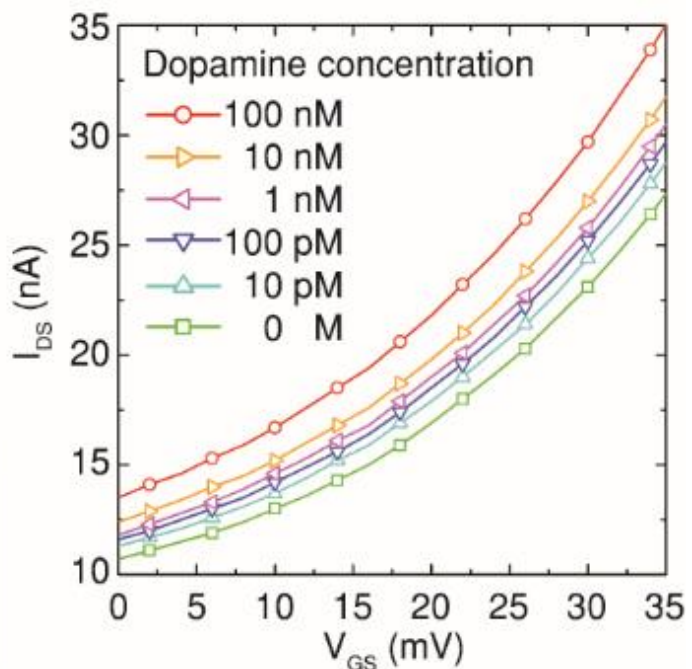
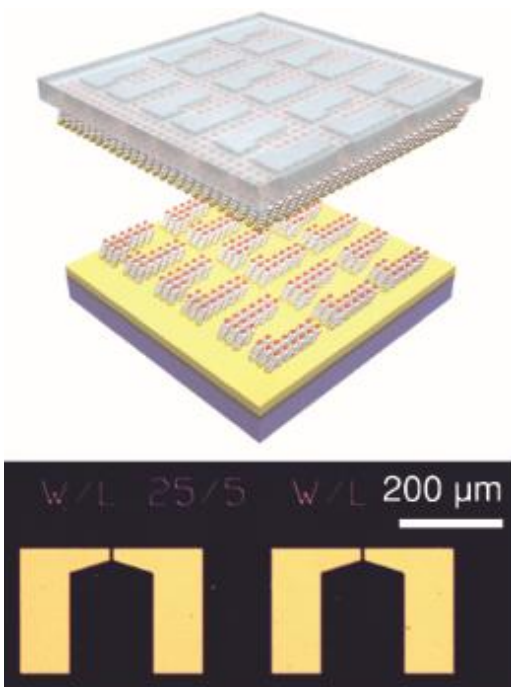
Fabrication of High-Performance Ultrathin In₂O₃ Film Field-Effect Transistors and Biosensors Using Chemical Lift-Off Lithography

The information in this chapter was published in *ACS Nano* **2015**, *9*, 4572-4582

and has been reproduced here in its entirety.

Authors: Kim, J.; Rim, Y. S.; Chen, H.; Cao, H. H.; Nakatsuka, N.; Hinton, H. L.; Zhao, C.;

Andrews, A. M.; Yang, Y.; Weiss, P. S.



8.1 Abstract

We demonstrate straightforward fabrication of highly sensitive biosensor arrays based on field-effect transistors, using an efficient high-throughput, large-area patterning process. Chemical lift-off lithography is used to construct field-effect transistor arrays with high spatial precision suitable for the fabrication of both micrometer- and nanometer-scale devices. Sol-gel processing is used to deposit ultrathin (~ 4 nm) In_2O_3 films as semiconducting channel layers. The aqueous sol-gel process produces uniform In_2O_3 coatings with thicknesses of a few nanometers over large areas through simple spin-coating, and only low-temperature thermal annealing of the coatings is required. The ultrathin In_2O_3 enables construction of highly sensitive and selective biosensors through immobilization of specific aptamers to the channel surface; the ability to detect subnanomolar concentrations of dopamine is demonstrated.

8.2 Introduction

Field-effect transistors (FETs) have key advantages over optical or electrochemical platforms for biosensing applications, including low detection limits, real-time and label-free detection, and simple integration with standard semiconductor-device processing.¹⁻⁴ Biosensors based on FETs are typically constructed by immobilizing specific receptors on the surfaces of semiconducting channels. Upon specific interactions with target biomolecules, these receptors electrostatically gate the underlying channels and produce electronic signals such as changes in channel conductance and/or drain current. As the electronic signals of FET-based biosensors arise from the surface binding events between receptors and analytes, the sensitivity of devices is enhanced as the surface-to-volume ratio of the semiconducting channels increases. Therefore, nanomaterials with reduced dimensionalities and large surface areas are advantageous for the design of highly sensitive biosensors.

Notably, one-dimensional (1D) nanomaterials such as Si nanowires (SiNWs)⁵⁻¹⁰ or carbon nanotubes (CNTs)¹¹⁻¹⁷ have been employed as the channel components of FET-based biosensors and shown to be highly effective in detecting biomolecules including proteins,^{5,8,9,12-15} DNAs,^{6,17} viruses,¹⁸ and neurotransmitters.^{7,10,19} More recently, two-dimensional (2D) nanomaterials such as graphene²⁰⁻²⁴ and MoS₂^{25,26} have attracted attention for biosensing applications as they are composed of surfaces only and can thus provide remarkably large surface-to-volume ratios and high sensitivity.

One major challenge of using nanomaterials for FET-based biosensing applications is the complexity of the processes involved in their synthesis and integration into device platforms. For instance, both SiNWs and CNTs are typically synthesized by chemical vapor deposition (CVD),²⁷⁻³⁰ which requires precise control of the growth parameters to produce high-quality 1D

nanomaterials suitable for FETs. In the case of CNTs, the CVD process usually produces a mixture of nanotubes with varying electrical properties, and additional purification steps are needed to separate from the mixture the metallic CNTs that are not compatible with FET channel materials.³¹⁻³³ For large-scale applications of 2D nanostructures, both graphene³⁴⁻³⁶ and MoS₂^{37,38} are typically grown by CVD as well. After growth, transfer steps are required that can leave undesirable polymer residue on the surface that degrades device characteristics and/or the surface immobilization of receptors.³⁹⁻⁴²

Once nanomaterials are synthesized and placed on the desired substrates, lithography techniques are used to define device areas and to complete FET fabrication. Although conventional nanofabrication techniques such as photolithography or electron-beam lithography are effective in producing suitable electrode patterns for FET devices, they require the use of specialized equipment in clean, well-controlled environments. As such, there is a trade-off between spatial precision, cost, and throughput, limiting the scalability of high spatial precision patterning.

Here, we find that ultrathin (~4 nm), amorphous metal-oxide semiconductor films produced *via* simple sol-gel chemistry are effective for the fabrication of highly sensitive FET-based biosensors. Oxide semiconductor thin films were formed over large areas through a simple spin-coating process. This fabrication step was followed by functionalization with biologically receptive moieties through oxide surface chemistry attachment. To define the electrode patterns and to construct the devices, we employed chemical lift-off lithography⁴³ using SAMs of alkanethiols on Au as soft masks. Through covalent interactions formed at the interfaces between hydroxyl-terminated alkanethiol SAMs and “activated” PDMS stamps, thiol

molecules were selectively removed from predefined areas, exposing the underlying bare Au surfaces for subsequent wet-etching.

Chemical lift-off lithography provides an efficient tool for high-throughput prototyping of FET devices over large areas without the use of sophisticated instruments, producing device features with high spatial precision suitable for the fabrication of micrometer- and submicrometer-scale devices. By combining ultrathin oxide semiconductor layers with chemical lift-off lithography, we demonstrate simple and straightforward fabrication of highly sensitive biosensors toward the detection of the small-molecule neurotransmitter dopamine down to physiological subnanomolar concentrations.

8.3 Materials and Methods

Materials. The DNA aptamer for dopamine was synthesized by Integrated DNA Technologies, Inc. (Coralville, IA). SYLGARD 184 from Dow Corning Corporation was used to make PDMS stamps throughout the work. All other chemicals were purchased from Sigma-Aldrich and used as received. Water was deionized before use (18.2 M Ω cm) using a Milli-Q system (Millipore, Billerica, MA).

Chemical Lift-off Lithography. Thin Au films (typically ~50 nm) were deposited on target substrates by electron-beam evaporation (CHA Industries, Fremont, CA) with Ti adhesion layers (5 nm). To deposit SAMs on Au surfaces, the substrates were immersed in 1 mM ethanolic solutions of 11-mercapto-1-undecanol and incubated overnight unless described otherwise. The PDMS stamps with defined patterns were prepared over masters fabricated by standard photolithography or electron-beam lithography. The stamps were exposed to oxygen plasma (Harrick Plasma, Ithaca, NY) at a power of 18 W and an oxygen pressure of 10 psi for 40 s to yield fully hydrophilic reactive surfaces, and brought into conformal contact with the SAM-modified Au surfaces. After 1 h, unless described otherwise, the stamps were carefully removed from the substrates, and an aqueous solution of 20 mM iron nitrate and 30 mM thiourea was applied to the substrates to etch Au films selectively from the area where the SAM was removed. Ti was removed from the exposed area using a 1:2 (v/v) solution of ammonium hydroxide and hydrogen peroxide. The substrates were rinsed with deionized water and dried under nitrogen gas before use.

Fabrication of Field-Effect Transistors and Biosensors. Chemical lift-off lithography was performed to pattern source and drain Au electrodes on a heavily doped silicon wafer covered with a 100-nm-thick thermally grown SiO₂ layer. Aqueous solutions of varying

indium(III) nitrate hydrate (99.999%) concentrations were spin-coated onto the substrates at 3000 rpm for 30 s. The substrates were then prebaked at 100 °C for 5 min followed by thermal annealing at 250 °C for 1 h. For top-contact devices, In₂O₃ layers and Au thin films were deposited successively by spin-coating and electron-beam evaporation, respectively, and lift-off lithography was performed to pattern source and drain electrodes. To make biosensors, a DNA aptamer that selectively binds to dopamine was immobilized on In₂O₃ layers with a top-contact device configuration. Briefly, chemical lift-off was used to pattern interdigitated Au source and drain electrodes atop the In₂O₃ layer deposited on a SiO₂/Si substrate. The substrate was then briefly exposed to oxygen plasma to remove the hydroxyl-terminated alkanethiols from the Au surface, followed by incubation in a 1 mM ethanolic solution of 1-dodecanethiol for 1 h. After thorough rinsing with ethanol, (3-aminopropyl)trimethoxysilane and trimethoxy(propyl)silane (1:9, v/v) were thermally evaporated to the In₂O₃ surface at 40 °C for 1 h, and the substrate was immersed in a 1 mM solution of 3-maleimidobenzoic acid *N*-hydroxysuccinimide ester dissolved in 1:9 (v/v) mixture of dimethyl sulfoxide and 1× PBS for 30 min. To anchor the DNA aptamer, the substrate was rinsed with deionized water, immersed in a 1 μM solution of thiolated DNA in 1× PBS for 1 h, rinsed again with deionized water and blown dried with nitrogen gas.

Characterization. Optical microscopy images were taken with Olympus BX51M. Atomic force microscopy imaging was performed on a Bruker Dimension Icon system under tapping mode. X-ray diffraction and XRR measurements were performed on a PANalytical X'Pert Pro system and a Bede D1 diffractometer, respectively. X-ray photoelectron spectra were collected on a Kratos Axis Ultra DLD system. Cyclic voltammetry was performed using a PAR EG&G 273A Potentiostat with a Ag/AgCl electrode, a platinum foil, and a platinum wire as a reference

electrode, a counter electrode, and a working electrode, respectively. The measurement was performed in a 0.1× PBS at a voltage sweep rate of 50 mV s⁻¹. All electrical measurements were performed on a probe station equipped with an Agilent 4155C semiconductor analyzer. At least 10 devices were tested for each biosensing experiment, and the five best devices in terms of stable (*i.e.*, low drift) baseline currents were selected to obtain statistical data.

8.4 Results and Discussions

8.4.1 Preparation and Characterization of Ultrathin In₂O₃ Film on SiO₂/Si substrates

We employed In₂O₃ as the channel material because its nanostructure has been shown to function effectively in biosensing platforms.^{14,44-46} Moreover, thin films of In₂O₃ can be formed *via* simple aqueous sol-gel chemistry, resulting in few organic contaminants and enabling low-temperature processing.⁴⁷ We dissolved varying amounts of an indium precursor, indium(III) nitrate hydrate (99.999%), in water and spin-coated the solutions onto heavily doped Si substrates covered with 100 nm-thick, thermally grown SiO₂ dielectric layers. The substrates were then annealed at above 200 °C for 1 h to solidify the films.

As the indium precursor concentrations were increased, the color of the coated substrates changed from blue to light blue suggesting that the thicknesses of the deposited thin films increased. For the films prepared from solutions with low precursor concentrations (≤ 0.1 M), the color change was barely noticeable. When examined under an optical microscope, however, we found that solutions containing less than 0.1 M of indium precursor produced large pinholes in the resulting thin films (left panel, Figure 8-1a), which can cause discontinuous electrical conduction and are thus not suitable for thin-film devices. We determined that an indium precursor concentration of 0.1 M was the lower limit for spin-coating of uniform In₂O₃ films over large areas without pinholes (right panel, Figure 8-1a). Figure 8-1b and c show atomic force microscope (AFM) images of the resulting thin films. Even though the apparent thicknesses of these films were only ~ 4 nm (Figure 8-1b), they showed high uniformity over large areas ($30 \mu\text{m} \times 30 \mu\text{m}$ in Figure 8-1c), and the root-mean-square roughness was calculated to be 0.4 nm.

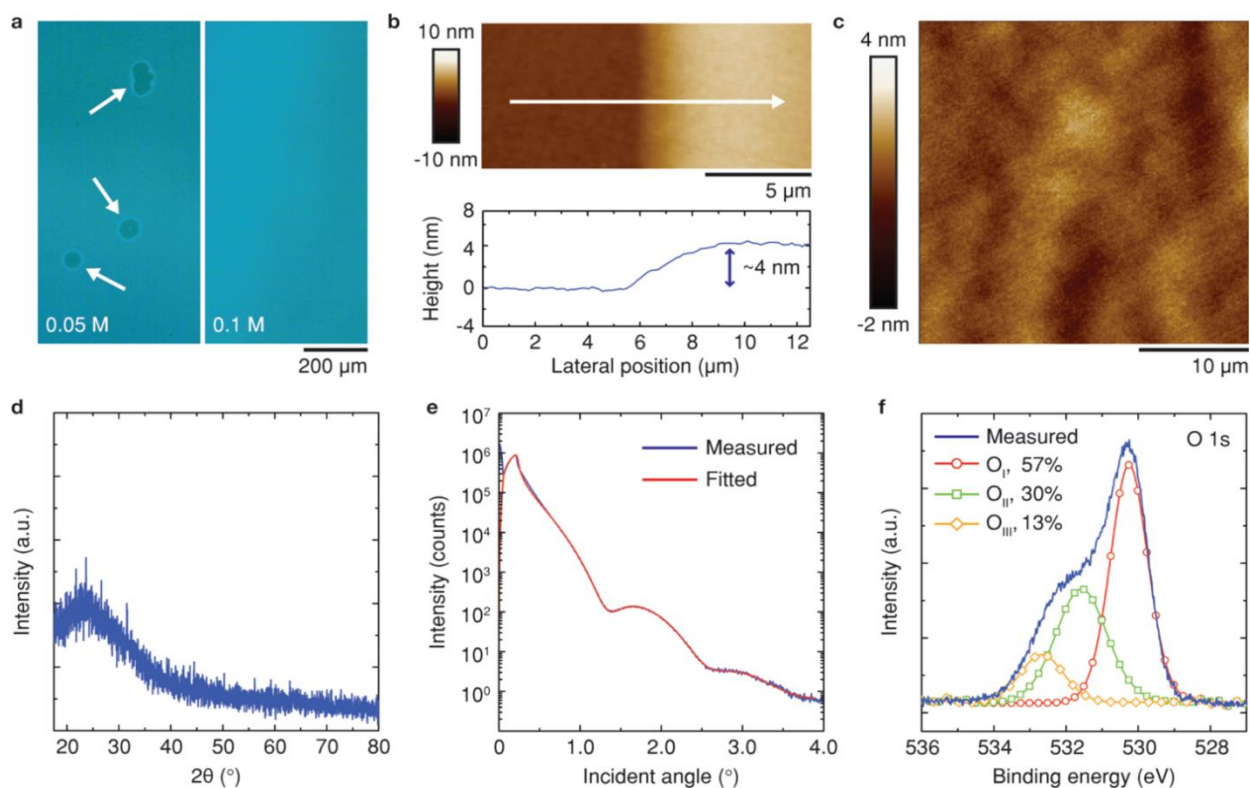


Figure 8-1. Sol-gel-processed In_2O_3 ultrathin films. Simple spin-coating of indium precursor solutions followed by thermal annealing enabled uncomplicated deposition of In_2O_3 layers with thicknesses measuring a few nanometers. **(a)** While a precursor solution containing 0.05 M of indium(III) nitrate produced a thin film with large pinholes (left, indicated by white arrows), a 0.1 M precursor solution produced a uniform thin film over large areas. **(b, c)** Atomic force microscope images of In_2O_3 thin film produced from a 0.1 M precursor solution; the sol-gel process produced a uniform film over large areas, with **(b)** an apparent thickness of 4 nm and **(c)** a root-mean-square roughness of 0.4 nm. **(d)** No characteristic peaks were observed in the X-ray diffraction pattern, suggesting the amorphous nature of the thin film. **(e)** The thickness, mass density, and interface roughness of the sol-gel processed In_2O_3 film were estimated to be 3.8 nm, 5.90 g cm^{-3} , and 0.4 nm, respectively, by fitting (red line) the X-ray reflectivity measurements (blue line) to a standard model. **(f)** The X-ray photoelectron O 1s spectrum of the ultrathin In_2O_3 layer shows that most of the peak can be assigned to O in the oxide lattice (O_I : O in oxide lattice without vacancies, O_{II} : O in oxide lattice with vacancies), while only 13% of O can be assigned to unreacted metal hydroxide species (O_{III}).

We further examined these In_2O_3 films using nondestructive X-ray metrology. Figure 8-1d shows an X-ray diffraction (XRD) pattern of an In_2O_3 thin film prepared on a glass slide. Even after thermal annealing of the spin-coated film, no characteristic peak of In_2O_3 was observed, suggesting that the film was largely amorphous (a broad shoulder at around $2\theta \approx 25^\circ$ corresponds to the background signal from the glass substrate). The thickness, mass density, and interface roughness of In_2O_3 films deposited on SiO_2/Si substrates were extracted by fitting X-ray reflectivity (XRR) curves to a standard model (Figure 8-1e). Film thicknesses were determined to be ~ 3.8 nm, which agrees well with the apparent thickness measured by AFM (Figure 8-1b). The mass density of the films was estimated to be 5.90 g cm^{-3} , which is equivalent to 82.2% of the theoretical value of structurally perfect In_2O_3 crystals (7.18 g cm^{-3}). The roughness of the interface between In_2O_3 and SiO_2 was calculated to be ~ 0.4 nm. In general, the interface roughness is indicative of the interface trap density, which has direct effects on the electron-transport properties of FET devices.⁴⁸ With an interface roughness below 0.5 nm, the In_2O_3 films deposited on the SiO_2 dielectric layers are expected to show good switching behavior, as demonstrated in subsequent experiments. Figure 8-1f shows the O 1s spectrum of the annealed In_2O_3 films obtained by X-ray photoelectron spectroscopy (XPS). The spectrum was fit with and deconvoluted into three distinct peaks at 530.4, 531.5, and 532.6 eV, which correspond to O in the oxide lattice without vacancies (O_I), O in the oxide lattice with vacancies (O_II), and metal hydroxides (O_III), respectively.⁴⁷ We found that most of the O atoms reside in the oxide lattice while only 13% of O was assigned to unreacted metal hydroxide species, which is comparable to In_2O_3 films produced *via* organic-solvent-based approaches and annealed at high temperature.⁴⁷ On the basis of the XRD, XRR, and XPS measurements, we conclude that the

aqueous-medium-based sol-gel process can produce, at relatively low temperatures, high-density amorphous In_2O_3 ultrathin films that are suitable for electronic applications.

8.4.2 Fabricating Micrometer-Scale FET Devices with Chemical Lift-Off Lithography

To construct FET devices using the sol-gel-processed In_2O_3 films, we employed chemical lift-off lithography as a high-throughput, large-scale tool to pattern Au source and drain contacts on SiO_2/Si substrates.⁴³ Figure 8-2a shows a schematic diagram depicting the lift-off process. First, PDMS stamps with predesigned negative images of source-drain patterns were activated by oxygen plasma treatment and brought into conformal contact with hydroxyl-terminated alkanethiol SAMs, 11-mercapto-1-undecanol, deposited on Au surfaces (step 1). When the PDMS stamps were removed from the Au surfaces after 1 h of contact, thiol molecules in direct contact with the reactive PDMS surfaces were selectively removed owing to condensation reactions between the hydroxyl groups of the PDMS surfaces and the SAMs (step 2). The remaining SAMs on the Au surfaces acted as soft masks against subsequent chemical reactions, where the exposed bare Au surfaces and underlying Ti adhesion layers were selectively removed by wet etching (step 3). Remaining SAM molecules were then removed using oxygen plasma treatment (step 4), and ultrathin In_2O_3 layers were deposited on top of the electrode patterns *via* the sol-gel process (step 5). After thermal annealing, In_2O_3 films outside the channel areas were removed by 1 M HCl using photolithography-patterned masks (step 6).

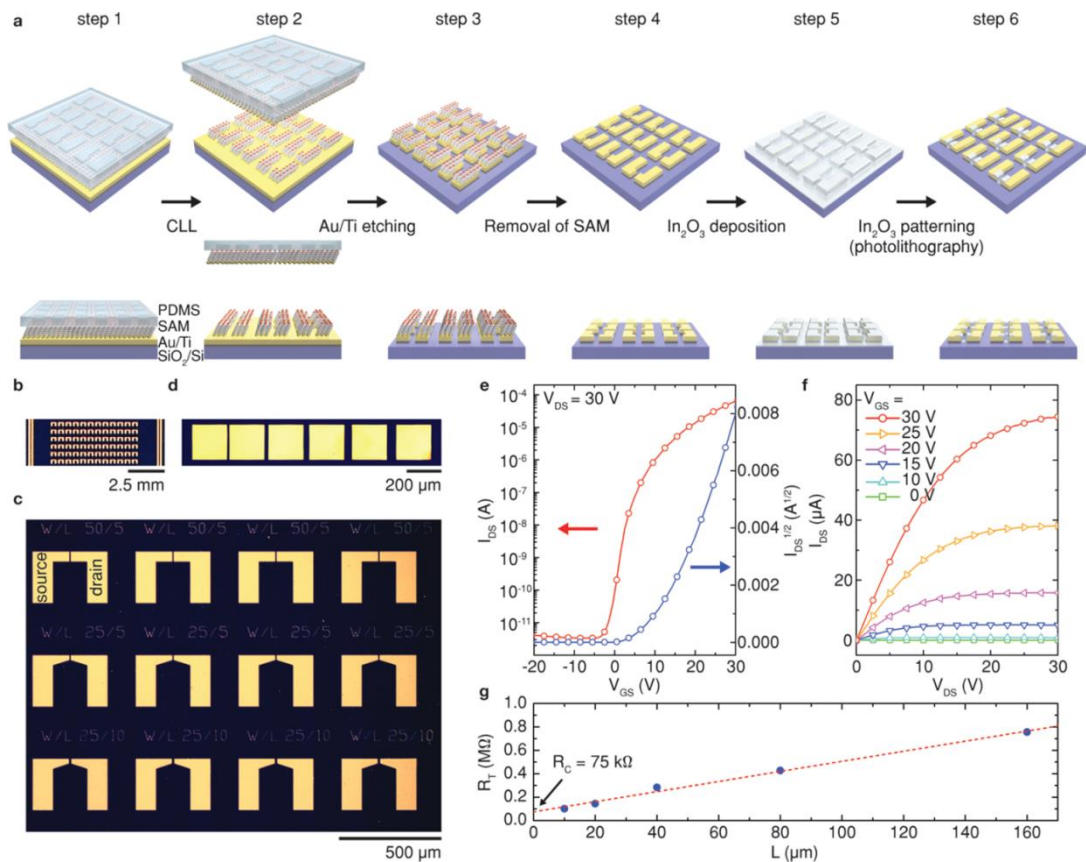


Figure 8-2. Field-effect transistor (FET) fabrication using chemical lift-off lithography (CLL). (a) Schematic illustration of FET fabrication steps using CLL. First, polydimethylsiloxane (PDMS) stamps with arrays of source and drain patterns were activated by oxygen plasma and brought into conformal contact with Au surfaces covered with self-assembled monolayers (SAMs) of hydroxyl-terminated alkanethiols (step 1). Through a condensation reaction between the hydroxyl groups of the PDMS surfaces and the SAMs, alkanethiol molecules in direct contact with the PDMS surfaces were selectively removed (step 2), leaving molecular patterns that served as soft masks during the following wet-etching of Au and Ti (step 3). After the metals were etched from the unprotected areas, the SAMs were removed by oxygen plasma (step 4) and ultrathin In_2O_3 layers were deposited through a sol-gel process (step 5). After thermal annealing, In_2O_3 films outside the channel areas were removed by wet-etching using photolithography-patterned masks (step 6). (b) Photograph showing 72 FET device patterns produced by CLL on a 100 nm SiO_2 layer on a Si substrate. (c, d) Optical microscope images of the CLL-produced device patterns over large areas showing (c) well-defined source and drain electrodes with channel gaps measuring a few micrometers and (d) a transmission line measurement (TLM) pattern with varying channel lengths. (e) Transfer and (f) output characteristics of the ultrathin In_2O_3 film FETs constructed atop the CLL-produced device patterns; the FETs showed good device performance with n-type pinch-off behavior with μ_{sat} of $11.5 \pm 1.3 \text{ cm}^2 \text{ V}^{-1} \text{ s}^{-1}$ and $I_{\text{ON}}/I_{\text{OFF}}$ of ~ 107 . (g) R_C between In_2O_3 and the Au electrodes was estimated to be $\sim 75 \text{ k}\Omega$ using the TLM pattern shown in (d).

Chemical lift-off lithography employs a strategy that is the inverse of conventional microcontact printing⁴⁹ as it leaves soft molecular masks on metal surfaces by subtractively patterning preformed SAMs. Compared to microcontact printing, which relies on the transfer of molecular inks from PDMS stamps to metal surfaces, both lateral diffusion and gas-phase deposition of ink molecules are avoided in lift-off lithography.^{50,51} Thus, chemical lift-off produces high spatial precision, high-fidelity molecular masks that can be used to pattern underlying metal substrates. Figure 8-2b shows a photograph of 72 pairs of FET source-drain electrodes patterned over an area of 0.25 cm² using chemical lift-off lithography. An optical microscope image of the Au patterns (Figure 8-2c) shows that the source and drain electrodes were well-defined and separated by channel gaps measuring a few micrometers. While we typically incubated Au surfaces in thiol solutions overnight and left the PDMS stamps on the substrates for 1 h, we found that this process could be shortened significantly. The patterns obtained after 5 min of SAM deposition and a 5 min stamping process also showed clear definition, comparable to patterns produced with longer processing times for the same spatial precision (see Supporting Information, Figure 8-S1). The PDMS stamps could be used multiple times after simple rinsing and reactivation, reproducing patterns with similar qualities. A series of electrodes with varying channel lengths was also patterned on the same substrate for in-depth FET analysis (Figure 8-2d). Scanning electron microscope (SEM) images of the channel regions are shown in Figure 8-S2 (see Supporting Information).

Figure 8-2e and f show representative transfer and output characteristics of bottom-gate bottom-contact (BGBC) In₂O₃ FET devices fabricated using chemical-lift-off-patterned Au electrodes on SiO₂/Si substrates. In this structure, the channel width and length were 35 and 15 μm, respectively, and heavily doped Si substrates were used as gate electrodes. Different

annealing conditions were tested and optimized device performance was obtained after the In₂O₃ thin films were annealed at 250 °C for 1 h (see Supporting Information, Figure 8-S3). The optimized In₂O₃ FETs showed high field-effect mobilities (μ_{sat}) of $11.5 \pm 1.3 \text{ cm}^2 \text{ V}^{-1} \text{ s}^{-1}$ (averaged over 50 devices) and on/off current ratios ($I_{\text{ON}}/I_{\text{OFF}}$) above 10^7 . These performance characteristics are comparable to FETs with thicker In₂O₃ films fabricated *via* either organic-solvent-based sol-gel approaches⁵²⁻⁵⁵ or sputtering^{56,57} (see Supporting Information, Table 8-S1).

The output characteristics of the FET devices (Figure 8-2f) showed n-type pinch-off behavior. The contact resistance (R_{C}) between In₂O₃ channels and Au electrodes was estimated by transmission-line measurements (TLMs; Figure 8-2g) using the pattern with varying channel lengths created by lift-off lithography (Figure 8-2d). Contact resistance was determined to be $\sim 75 \text{ k}\Omega$. We also fabricated bottom-gate top-contact (BGTC) In₂O₃ FETs by performing chemical lift-off on Au/Ti deposited on top of the semiconducting layers (see Supporting Information, Figure 8-S4). The BGTC FETs showed better device performance compared to BGBC FETs, with $\mu_{\text{sat}} = 12.1 \pm 3.5 \text{ cm}^2 \text{ V}^{-1} \text{ s}^{-1}$ and $I_{\text{ON}}/I_{\text{OFF}} \sim 108$. This improved performance was attributed to more favorable energy-level alignment at the interface between In₂O₃ channels and the Ti adhesion layers.⁴⁸ Detailed device parameters of BGBC ultrathin In₂O₃ film FETs processed under different annealing conditions and optimized BGTC devices are summarized in Table 8-S2 (see Supporting Information).

8.4.3 Fabricating Submicrometer-Scale FET Devices with Chemical Lift-Off Lithography

Next, we scaled down the FET dimensions further and examined device performance of ultrathin In_2O_3 film FETs with submicrometer-scale channel lengths. Field-effect transistor miniaturization is integral for high-density device integration and enables low-voltage, low-power device operation. In a common laboratory setting, studies of FETs with submicrometer channel lengths are typically carried out with the aid of electron-beam lithography, which produces patterns with much finer features than photolithography. However, unlike photolithography, electron-beam lithography is a serial process and requires a considerable amount of time for patterning multiple devices over large areas. Chemical lift-off lithography enables facile prototyping of nanoscale devices as it enables parallel patterning of multiple devices over large areas with a spatial precision that can reach <20 nm.⁴³

Figure 8-3a shows 12 Au source-drain electrode pairs with submicrometer channel lengths produced by chemical lift-off lithography on a SiO_2/Si substrate. Bow-tie patterns with a large pad size were designed and used to ensure easy access by external electrodes. The top panels in Figure 8-3b and c show SEM images of the channel regions with gap lengths measuring 300 and 150 nm, respectively. High-magnification SEM images of the channel regions are shown in Figure 8-S5 (see Supporting Information). Transfer characteristics of ultrathin In_2O_3 film FETs fabricated on the corresponding electrode patterns are shown in the bottom panels. Compared to devices with micrometer-scale channel lengths (Figure 8-2), the nm-gap FETs can be operated at a significantly lower drain voltage (V_{DS}) of 4 V since the channel component of the series resistance scales down with decreasing channel lengths. Field-effect transistors with channel lengths of 300 nm (Figure 8-3b) showed steep switching behavior with a subthreshold swing (SS) of 0.3 ± 0.1 V dec⁻¹, which is significantly improved compared to the

long-channel devices (Figure 8-2e; $SS = 1.6 \pm 0.1 \text{ V dec}^{-1}$). We hypothesize that this behavior is due to the reduced number of charge traps along the lateral direction and a decrease in sheet resistance as the channel length was decreased. The values of μ_{sat} and $I_{\text{ON}}/I_{\text{OFF}}$ for these smaller FETs were $0.6 \pm 0.3 \text{ cm}^2 \text{ V}^{-1} \text{ s}^{-1}$ and ~ 107 , respectively. Further reduction of the channel length to 150 nm (Figure 8-3c) resulted in considerable degradation of device performance, with SS , μ_{sat} , and $I_{\text{ON}}/I_{\text{OFF}}$ values of $0.6 \pm 0.1 \text{ V dec}^{-1}$, $0.4 \pm 0.1 \text{ cm}^2 \text{ V}^{-1} \text{ s}^{-1}$, and ~ 105 , respectively. We attribute these adverse effects to drain-induced barrier lowering associated with short-channel FETs,⁴⁸ as evidenced by the negative shift in the turn-on voltage from -4 V (300 nm-channel FET) to -5 V (150 nm-channel FET). We expect that the performance of ultrathin In_2O_3 film FETs with submicrometer channel lengths can be further improved by employing advanced device architectures including lightly doped drains⁴⁸ or structures with double active layers.⁵⁸

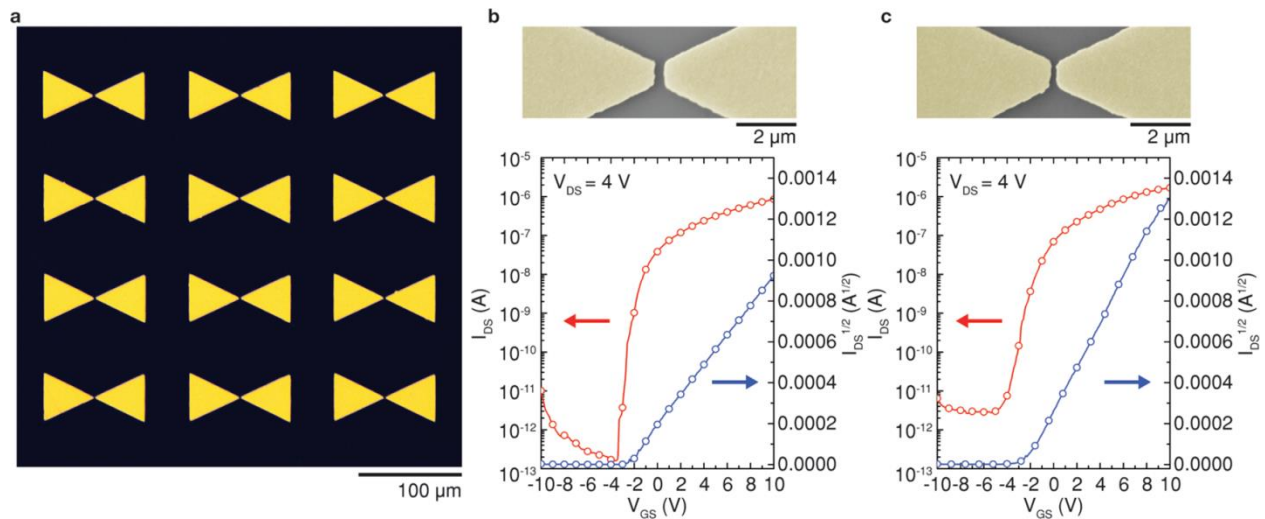


Figure 8-3. Fabrication of submicrometer-channel field-effect transistors (FETs) using chemical lift-off lithography (CLL). **(a)** Bow-tie device patterns with submicrometer channel lengths produced by CLL. **(b, c)** The top panels show scanning electron micrographs of the channel regions of the CLL-produced device patterns, with gap lengths measuring **(b)** 300 nm and **(c)** 150 nm. Transfer characteristics of the ultrathin (~ 4 nm) In_2O_3 film FETs fabricated atop the corresponding patterns are shown in the bottom panels. Compared to FETs with channel lengths measuring a few micrometers (Figure 8-2e), ultrathin In_2O_3 film FETs with submicrometer channel lengths can be operated at much lower V_{DS} . Reduction of the channel length to **(c)** 150 nm led to considerable degradation in device performance because of the short-channel effect. The values of μ_{sat} , $I_{\text{ON}}/I_{\text{OFF}}$, and SS of **(b)** 300 nm-channel FETs were calculated to be $0.6 \pm 0.3 \text{ cm}^2 \text{ V}^{-1} \text{ s}^{-1}$, $\sim 10^7$, $0.3 \pm 0.1 \text{ V dec}^{-1}$, respectively, while those for **(c)** 150 nm-channel FETs were calculated to be $0.4 \pm 0.1 \text{ cm}^2 \text{ V}^{-1} \text{ s}^{-1}$, $\sim 10^5$, $0.6 \pm 0.1 \text{ V dec}^{-1}$, respectively.

8.4.4 Fabricating FET-Based Aptamer Biosensors for *In Vitro* Dopamine Sensing

As charge transport through sol-gel-processed In_2O_3 thin films is confined within a few nanometers in the surface normal direction, electronic perturbation at the surface can significantly affect FET characteristics of the underlying metal oxide layer. Furthermore, various surface functionalization strategies available to metal oxides can be readily used to immobilize biospecific receptors on In_2O_3 thin films for selective detection of target molecules.⁴⁵ Therefore, ultrathin In_2O_3 layers can serve as platforms to construct highly sensitive and selective FET-based biosensors. To test the ultrathin In_2O_3 FETs fabricated by chemical lift-off lithography for biosensing applications, we investigated molecular recognition of the neurotransmitter dopamine using a previously identified dopamine aptamer (Figure 8-4a).⁵⁹⁻⁶¹ We investigated dopamine as a prototypical analyte because (i) it is a key neurotransmitter involved in brain reward and movement circuitries; dopaminergic neurons are known to degenerate in Parkinson's disease,⁶²⁻⁶⁵ and (ii) dopamine is a primary amine that carries a single positive charge at physiological pH, far less charge than that associated with biologically important macromolecular analytes such as proteins. Therefore, molecular recognition of dopamine at FET surfaces is expected to cause significantly less electronic perturbation than proteins. As such, dopamine is representative of an important class of biologically relevant small molecules that includes endogenous signaling molecules and drugs that are difficult to measure with simple devices.

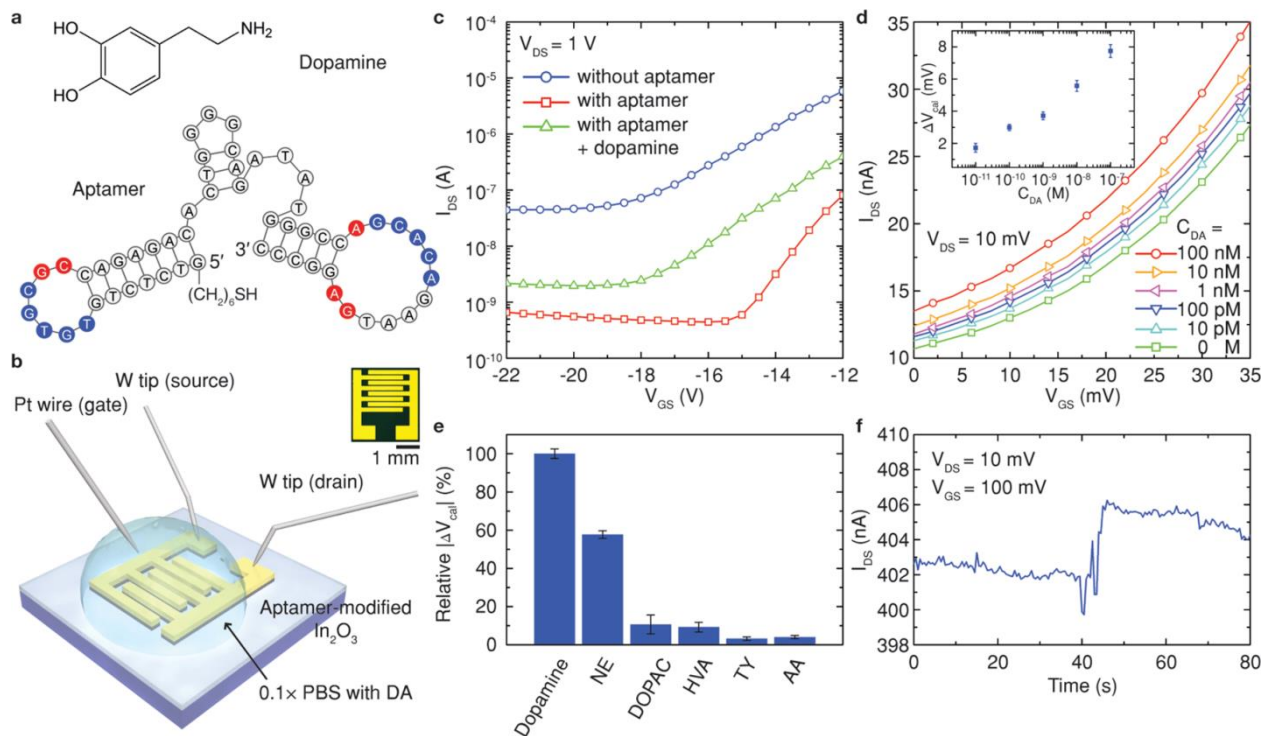


Figure 8-4. Aptamer–In₂O₃ biosensors for subnanomolar dopamine detection. The ultralow thickness of the sol-gel-processed In₂O₃ enabled the construction of highly sensitive dopamine biosensors by immobilizing (a) a DNA aptamer (bottom) that had specific binding with dopamine (top) on the oxide surface. The complementary and invariant bases for dopamine binding are indicated in blue and red, respectively. (b) Schematic diagram of the sensing setup; the aptamer–In₂O₃ biosensors operated with a liquid gate. The inset shows an interdigitated electrode pattern, fabricated using chemical lift-off lithography, used for the biosensors. (c) Dry state, Si back-gating measurements show that upon immobilization of the aptamer on the oxide surface, the transfer characteristics of ultrathin In₂O₃ film field-effect transistors (blue line) shifted downward (red line) and the turn-on voltage shifted toward positive values because of the electrostatic gating effect of negatively charged DNA on n-type In₂O₃. Positively charged dopamine binding to the aptamer partially recovered the drain current, with a shift of the turn-on voltage toward negative values (green line). (d) For the liquid-gate sensing experiments, the addition of dopamine to the liquid electrolyte also led to an increase in the drain current, and the linear working range of the aptamer–In₂O₃ biosensors was determined to be 10⁻¹¹–10⁻⁷ M (inset, ΔV_{cal}: calibrated response). (e) Calibrated responses of the aptamer–In₂O₃ biosensors upon exposure to 1 nM each of ascorbic acid (AA), tyramine (TY), homovanillic acid (HVA), 3,4-dihydroxyphenylacetic acid (DOPAC), and norepinephrine (NE). (f) Real-time sensing recording of 100 pM dopamine in 0.1× PBS, showing an increase in current upon exposure.

To construct dopamine biosensors, we employed the BGTC structure that showed more favorable device characteristics (see Supporting Information, Table 8-S2). To obtain large active sensor areas and uniform current distribution, interdigitated source and drain electrodes were used for biosensors. We first deposited ultrathin In_2O_3 layers on SiO_2/Si substrates, followed by Au/Ti deposition using electron-beam evaporation. The Au/Ti films were then patterned into interdigitated source and drain electrodes using chemical lift-off lithography (Figure 8-4b). Subsequently, the hydroxyl-terminated alkanethiol SAMs used for chemical lift-off were removed by brief exposure to oxygen plasma, and 1-dodecanethiol was self-assembled on the Au surfaces to protect the electrodes from ensuing receptor immobilization. A thiol-terminated tethered DNA aptamer that recognizes dopamine, $\text{HS}(\text{CH}_2)_6\text{-5}'\text{-GTC TCT GTG TGC GCC AGA GAC ACT GGG GCA GAT ATG GGC CAG CAC AGA ATG AGG CCC-3}'$ (Figure 8-4a),⁵⁹⁻⁶¹ was immobilized on In_2O_3 surfaces using (3-aminopropyl)trimethoxysilane and 3-maleimidobenzoic acid *N*-hydroxysuccinimide ester as linkers to complete the biosensor fabrication.¹⁰ Organosilanes form SAMs on various metal oxide surfaces with in-plane cross-linked Si-O-Si networks promoting dense molecular packing.⁶⁶⁻⁷⁰ As the size of DNA aptamers is on the order of a few nanometers, steric hindrance may prohibit effective ligand-receptor binding unless aptamers are well-separated.¹⁰ Therefore, trimethoxy(propyl)silane was codeposited on In_2O_3 surfaces and used as a spacer to optimize the surface density of aptamers for effective biosensing (see the Experimental Methods section).

Figure 8-4b shows a schematic illustration of the electrical measurement setup used for dopamine-sensing experiments. $0.1\times$ phosphate-buffered saline (PBS, pH 7.4) was used as a liquid gate to detect signals effectively without severe Debye screening (Debye length ~ 2.3 nm). Gate bias (V_{GS}) was applied through a Pt wire. Specific amounts of dopamine in $0.1\times$ PBS were

injected into the electrolyte solution to modulate dopamine concentrations in the liquid environment. To study the effect of the aptamer attachment to the channel surface, we first used highly doped Si substrates and 100 nm-thick SiO₂ layers as a back gate and a dielectric layer, respectively, and examined the changes in FET characteristics in a dry state upon aptamer immobilization (Figure 8-4c). We found that the attachment of aptamers to the channel surfaces caused over an order of magnitude decreases in the drain currents and positive shifts in the turn-on voltages (from -19 to -15 V). We attributed these effects to electrostatic gating effects of negatively charged DNA on the channel surfaces that result in decreases in carrier concentration of the *n*-type In₂O₃ layer. Upon incubation of the device in a 1 mM solution of dopamine for 1 h, the drain current partially recovered and the turn-on voltage shifted back to -18 V.

In general, aptamers undergo significant conformational changes upon binding with ligands,⁷¹⁻⁷⁵ which should affect the conductance modulation of underlying channel layers substantially. Since aptamers carry much greater charge than small molecules such as dopamine, their conformational changes are typically expected to dominate surface charge densities and surface charge density changes, as compared to the electrostatic gating effects of analytes. However, a previous study suggests that the dopamine-specific aptamer used in this work undergoes insufficient structural reorganization for electronic beacon approaches upon ligand binding.⁶¹ Further studies will be needed to determine the specific charge redistribution and charge-sensing mechanism of our dopamine aptamer-based sensors, which will be critical to generalizing chemical sensing with these arrays.

Figure 8-4d shows the transfer characteristics of liquid-gated aptamer-In₂O₃ biosensors measured at various dopamine concentrations (C_{DA}) in solution. As in the case of measurements in a dry state, using a back-gated FET (Figure 8-4c), exposure of the biosensors to dopamine in a

liquid-gate setup resulted in increased drain current. As C_{DA} was increased from 10 pM to 100 nM, the transfer characteristics of the device continuously shifted upward. No significant redox behavior of dopamine was observed in our device operating range (see Supporting Information, Figure 8-S6), and the leakage current through the $0.1\times$ PBS electrolyte was confirmed to be negligible (see Supporting Information, Figure 8-S7). While further increases of C_{DA} to 1 μ M or more resulted in continued upshift of the drain current, we found that nonspecific binding of dopamine to the channel surface became significant, and the drain current increased even without aptamer functionalization on the channel surface in this concentration range (see Supporting Information, Figure 8-S8). To reduce device-to-device variations in sensor response, the change in drain current was converted to a change in gate voltage (calibrated response, ΔV_{cal}),⁴⁶ and the linear working range of the aptamer– In_2O_3 biosensor was determined to be 10^{-11} – 10^{-7} M, as shown in the inset of Figure 8-4d. We also constructed devices using an aptamer with mutations at identified dopamine binding sites (mut-DA-aptamer, HS(CH₂)₆-5'-GTC TCT GTG TGC **TTC** AGA GAC ACT GGG GCA GAT ATG GGC CTG CAC AGA ATT TGG CCC-3', mutated bases are highlighted in bold), as well as DNA with a random base sequence (scrambled-DNA, HS(CH₂)₆-5'-CAT AAA TAC TAG GAT GTG CAT ACT TAG ACT GGA GAT TGT ATC CCT ACA CAC ACC CTA-3'). Upon exposure of both devices to 10 nM dopamine in $0.1\times$ PBS, we measured a ΔV_{cal} of less than 15% of the responses measured at devices constructed using the correct aptamer sequence (see Supporting Information, Figure 8-S9). These results strongly suggest that sensor responses are based on specific interactions between dopamine and its cognate aptamer.

To test the selectivity of the aptamer–In₂O₃ biosensors, we exposed devices to 1 nM solutions of other similarly structured small molecules found in the brain extracellular environment.⁷⁶ Ascorbic acid (AA), tyramine (TY), homovanillic acid (HVA), 3,4-dihydroxyphenylacetic acid (DOPAC), and norepinephrine (NE) were dissolved in 0.1× PBS. Calibrated responses were then compared to responses to dopamine (Figure 8-4e). Although NE caused significant ΔV_{cal} that reached $58 \pm 2\%$ of the response to dopamine, all other tested biomolecules were associated with relative responses that were below 10% of the dopamine response. Cross reactivity of this aptamer with norepinephrine has been previously observed and reported.^{10,61,77} We note that dopamine, NE, and TY caused increases in the drain current while AA, HVA, and DOPAC caused decreases, as the former group of molecules carry positive charges at physiological pH while the latter carry negative charges.

Finally, we performed real-time detection of dopamine in 0.1× PBS. The drain current of the aptamer–In₂O₃ device was continuously monitored at $V_{\text{DS}} = 10$ mV and $V_{\text{GS}} = 100$ mV while dopamine was introduced into the buffer solution. Figure 8-4f shows representative real-time sensing measurements obtained when the biosensor was exposed to a solution of 100 pM dopamine at $t = 0$. After a short delay associated with diffusion of dopamine to the channel surface, a sharp increase in drain current was observed. In comparison, the addition of buffer solution devoid of dopamine did not yield measurable changes in the drain current (data not shown).

8.5 Conclusions and Prospects

A high-throughput and high spatial precision soft-lithography technique, chemical lift-off lithography, was employed to produce device patterns with both micrometer- and submicrometer-scale feature sizes over large areas. This patterning method can be integrated with other processes to produce electronic device and biosensor arrays. Here, we have demonstrated that ultrathin In_2O_3 layers, produced by simple aqueous sol-gel processing, can be used as semiconducting active layers to construct high-performance FETs and biosensors. The as-fabricated In_2O_3 FETs showed effective device performance with μ_{sat} exceeding $10 \text{ cm}^2 \text{ V}^{-1} \text{ s}^{-1}$. The ultrathin In_2O_3 layers enabled construction of highly sensitive and selective aptamer-based biosensors capable of detecting subnanomolar concentrations of dopamine. The latter are more than sufficient to detect dopamine in the physiological range of basal extracellular brain levels.⁷⁸ Given this straightforward and effective device-fabrication strategy, we anticipate that chemical-lift-off-patterned, sol-gel-processed metal-oxide FETs will enable platforms for the construction of both biological and nonbiological sensors that can detect subtle yet important chemical perturbations at interfaces.

8.6 Supplementary Experiments and Figures

An optical micrograph of device patterns produced by chemical lift-off lithography with shorter processing times, scanning electron microscope images of chemical-lift-off-patterned devices, transfer characteristics of BGBC ultrathin In_2O_3 film FETs processed under different annealing conditions, a device performance chart of previously reported In_2O_3 field-effect transistors, transfer and output characteristics of optimized BGTC devices, a summary of detailed device performance parameters, a cyclic voltammogram of a Pt wire in $0.1\times$ PBS, a leakage current measurement through the liquid electrolyte, and responses of In_2O_3 FETs to dopamine exposures with modified aptamer sequences and without aptamer immobilization.

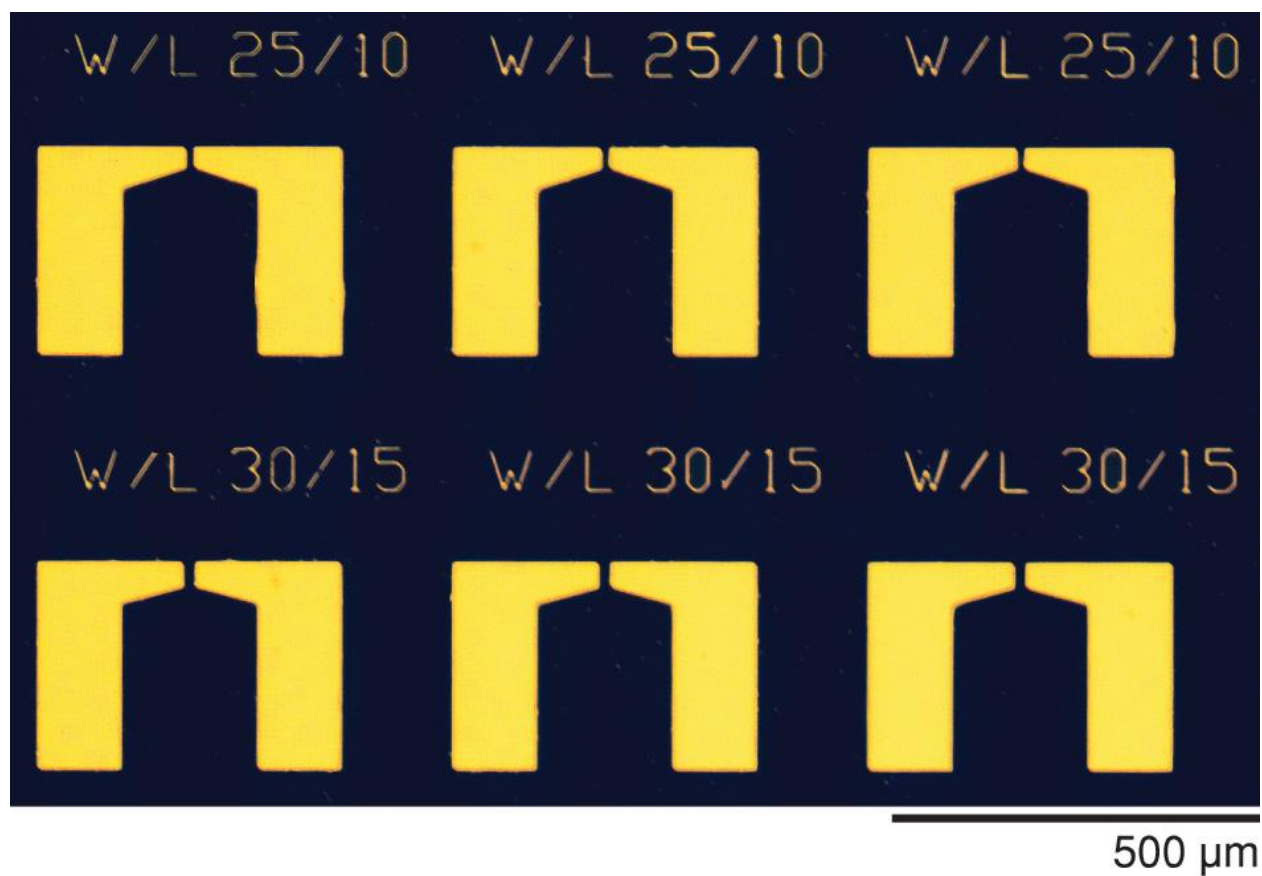


Figure 8-S1. Field-effect transistor device patterns on a SiO₂/Si substrate produced by chemical lift-off lithography with a short processing time (5 min self-assembled monolayer deposition, 5 min stamping process).

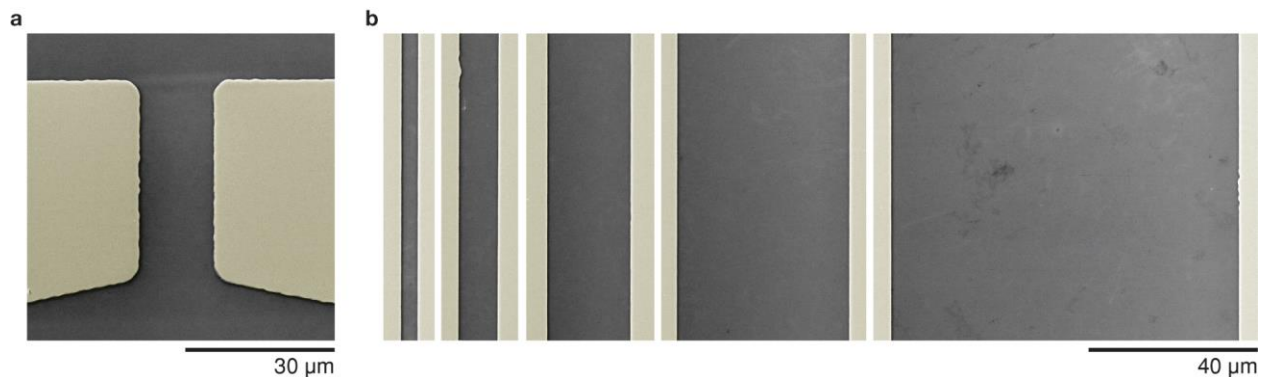


Figure 8-S2. Scanning electron microscope images of channel regions. (a) A representative source-drain electrode pair used for device fabrication. **(b)** A transmission line measurement (TLM) pattern with varying channel lengths.

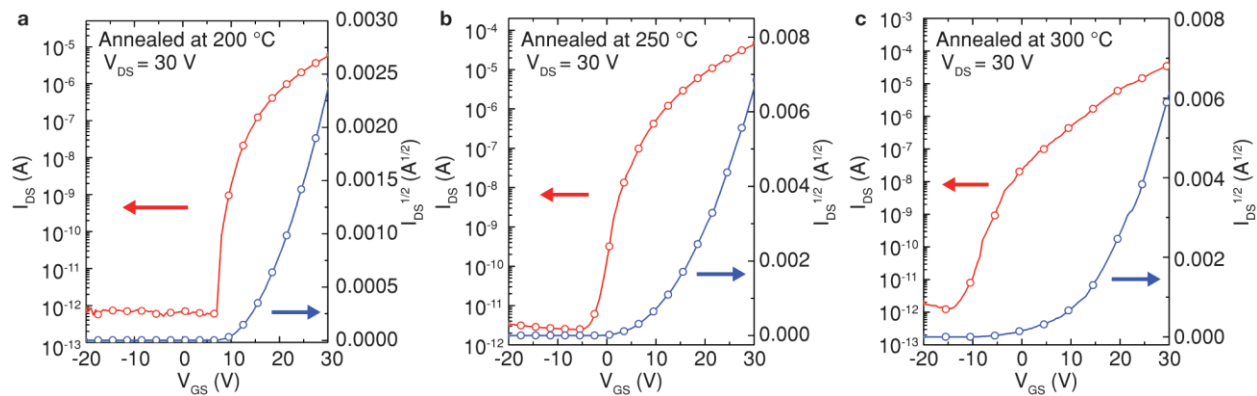


Figure 8-S3. Bottom-gate bottom-contact field-effect transistor transfer characteristics of ultrathin In_2O_3 layers annealed at (a) 200 °C, (b) 250 °C, and (c) 300 °C for 1 h.

Table 8-S1. Device performance of previously reported In₂O₃ field-effect transistors.

Coating Method	Channel Thickness (nm)	μ_{sat} (cm ² V ⁻¹ s ⁻¹)	$I_{\text{ON}}/I_{\text{OFF}}$	SS (V dec ⁻¹)	Ref.
Sol-gel	4	12	10 ⁷	1.6	Our work
Sol-gel	30	0.7	10 ⁶	5.7	S1
Sol-gel	25	2.24	10 ⁸	0.45	S2
Sol-gel	6	7.5	10 ⁷	N/A	S3
Sol-gel	30	3.37	10 ⁷	N/A	S4
Sputtering	8	15.3	10 ⁸	0.25	S5
Sputtering	10	15	10 ⁶	N/A	S6

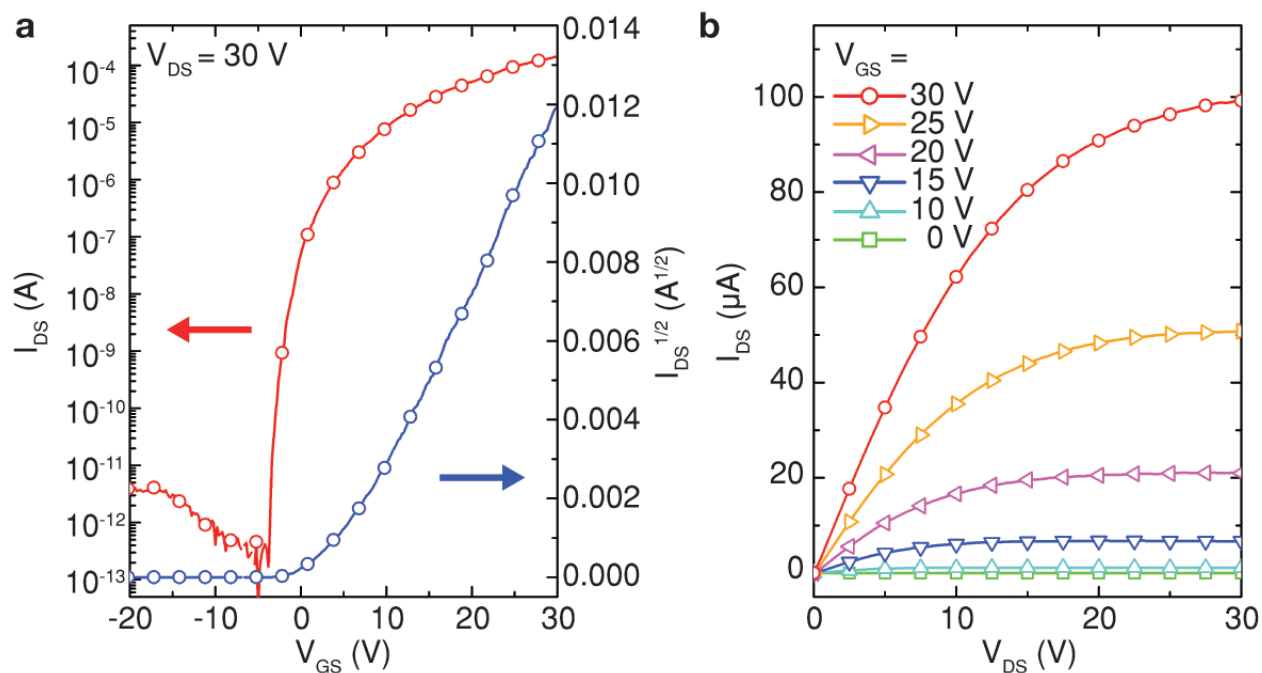


Figure 8-S4. Bottom-gate top-contact field-effect transistor. (a) transfer and (b) output characteristics of ultrathin In₂O₃ layers.

Table 8-S2. Summary of In₂O₃ field-effect transistor device performance with the following geometries bottom-gate bottom-contact (BGBC) and bottom-gate top-contact (BGTC).

Geometry	Annealing Temperature (°C)	μ_{sat} (cm ² V ⁻¹ s ⁻¹)	$I_{\text{ON}}/I_{\text{OFF}}$	SS (V dec ⁻¹)	V_{th} (V) ^a
BGBC	200	2.3 ± 0.2	~10 ⁶	1.2 ± 0.1	19.5 ± 2.1
BGBC	250	11.5 ± 1.3	~10 ⁷	1.6 ± 0.1	15.6 ± 2.0
BGBC	300	10.4 ± 1.8	~10 ⁷	2.7 ± 0.9	18.2 ± 1.2
BGTC	250	12.1 ± 3.5	~10 ⁸	0.9 ± 0.2	9.5 ± 2.7

^aThreshold voltage

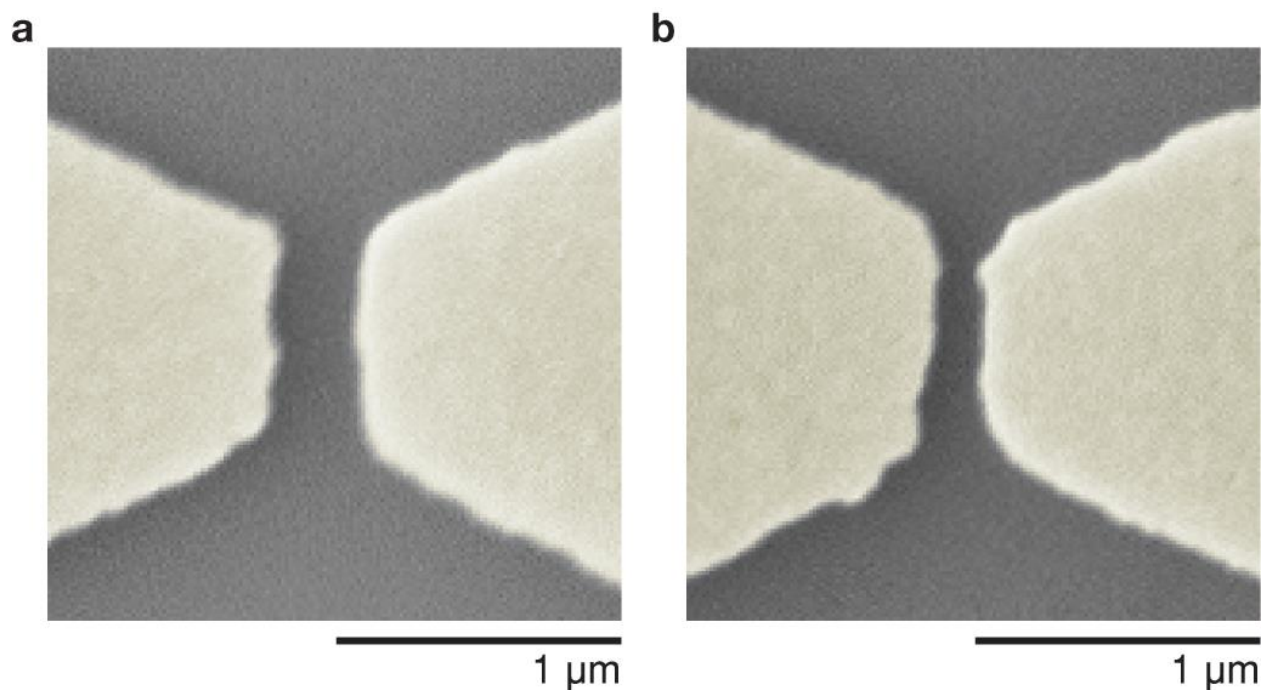


Figure 8-S5. Scanning electron microscope images of submicrometer-channel devices with gap lengths measuring (a) 300 nm and (b) 150 nm.

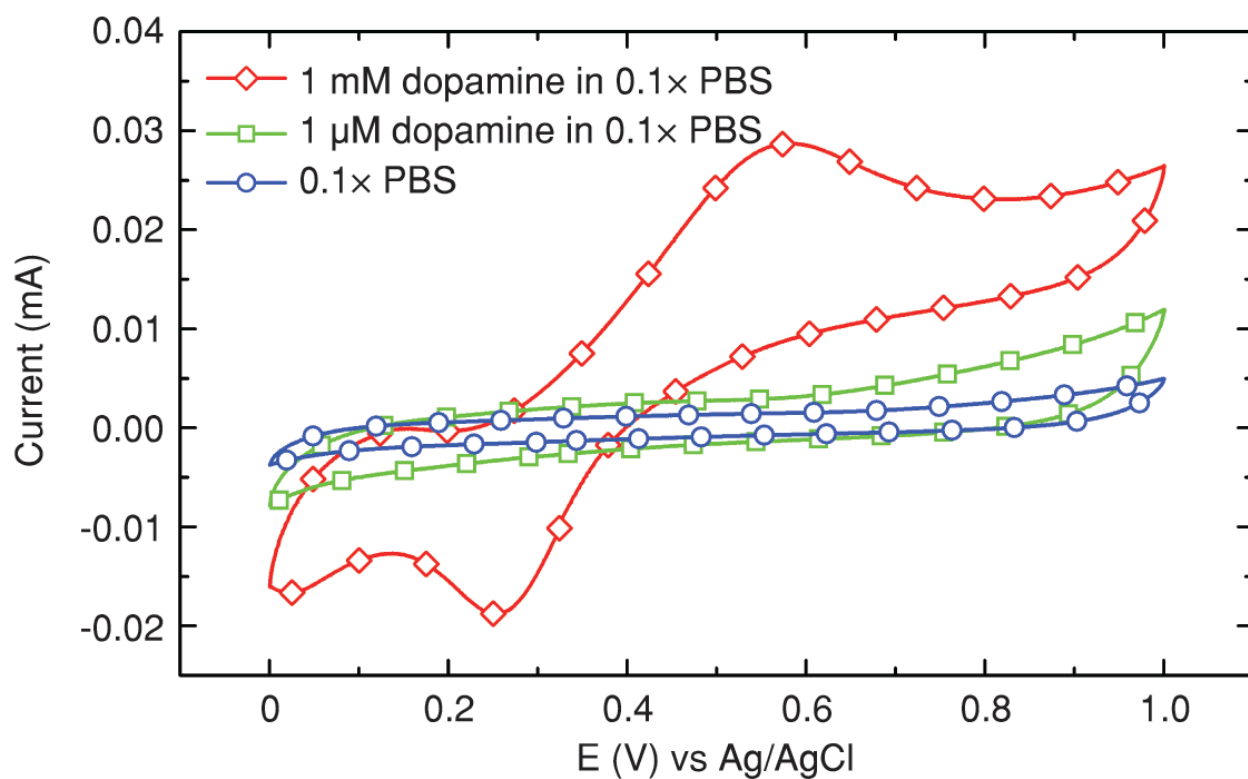


Figure 8-S6. Cyclic voltammogram of a Pt wire in 0.1× PBS with (red: $C_{DA} = 1$ mM, green: $C_{DA} = 1$ μM) or without (blue) dopamine.

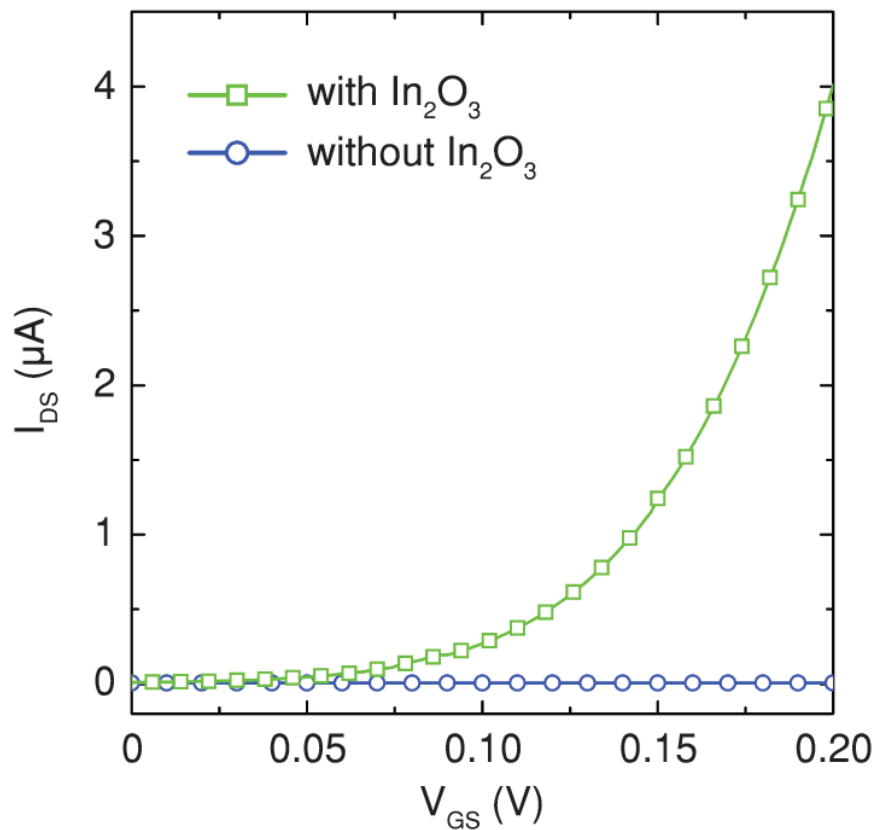


Figure 8-S7. Transfer characteristics of devices with (green) or without (blue) the In_2O_3 channel layer, confirming that the leakage current through a liquid electrolyte (blue) is negligible.

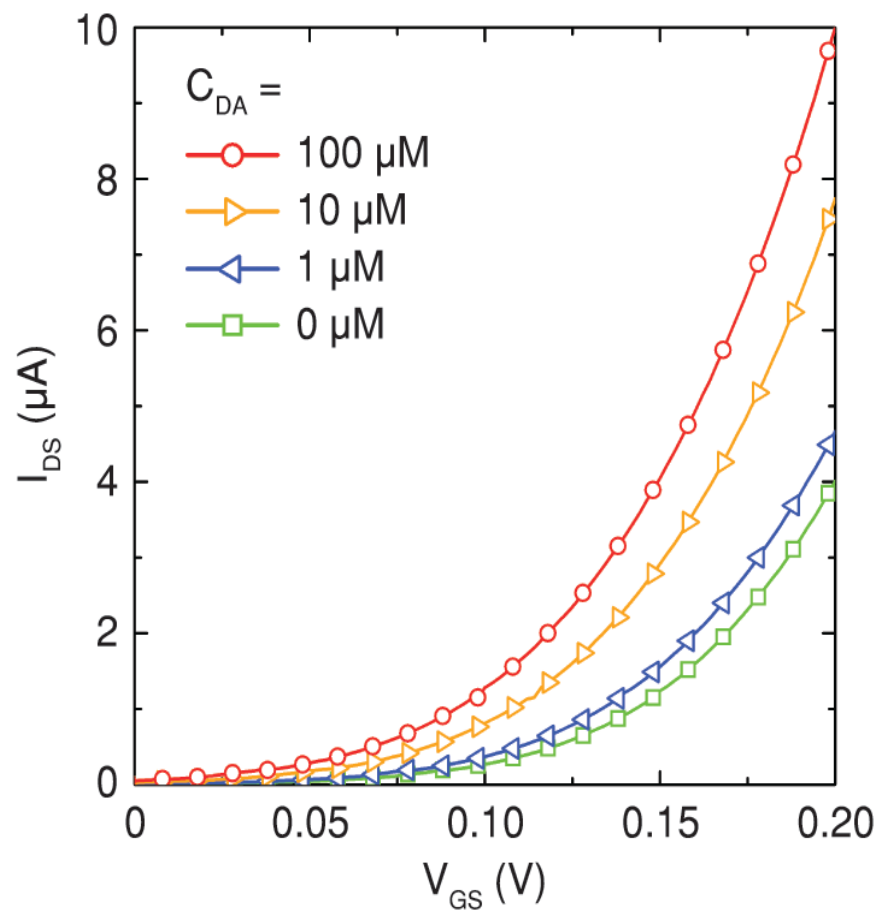


Figure 8-S8. Transfer characteristics of In_2O_3 field-effect transistors without aptamer immobilization. For $C_{DA} \geq 1 \mu M$, non-specific binding of dopamine on the channel surface becomes significant and causes upward shift in the drain current even without aptamer functionalization. No significant change in drain current was observed for $C_{DA} < 1 \mu M$.

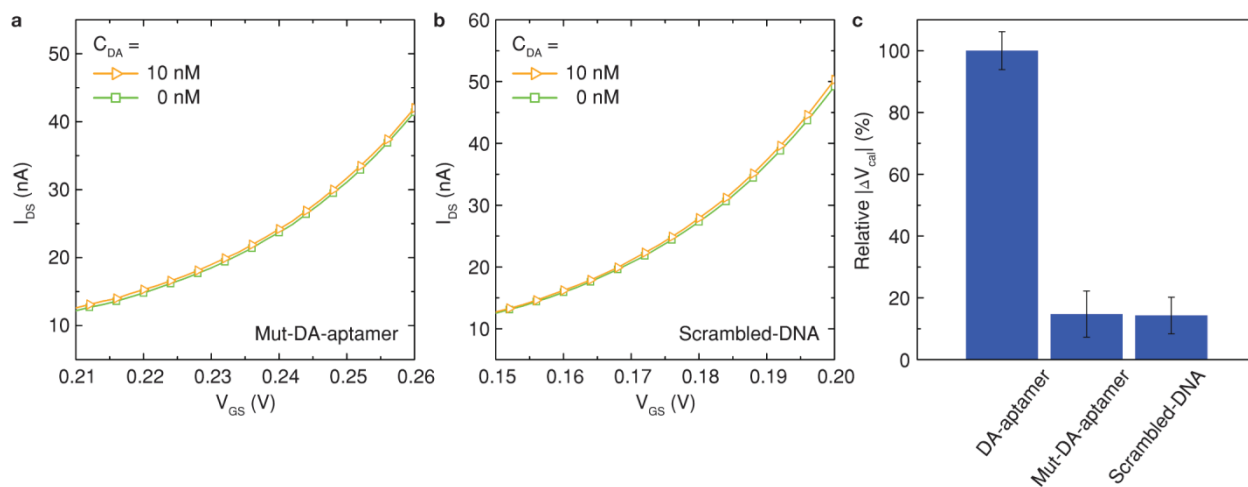


Figure 8-S9. Transfer characteristics of In_2O_3 field-effect transistors constructed using (a) an aptamer with mutations at the binding sites or (b) a DNA with a random base sequence. In both cases, the addition of 10 nM dopamine to $0.1\times$ PBS induced only small changes in drain currents. (c) ΔV_{cal} of both devices were measured to be less than 15% of the responses from devices constructed using the correct dopamine (DA) aptamer.

8.7 References

1. Schoning, M. J.; Poghossian, A. Recent Advances in Biologically Sensitive Field-Effect Transistors (BioFETs). *Analyst* **2002**, *127*, 1137–1151.
2. Patolsky, F.; Lieber, C. M. Nanowire Nanosensors. *Mater. Today* **2005**, *8*, 20–28.
3. Allen, B. L.; Kichambare, P. D.; Star, A. Carbon Nanotube Field-Effect-Transistor-Based Biosensors. *Adv. Mater.* **2007**, *19*, 1439–1451.
4. Curreli, M.; Rui, Z.; Ishikawa, F. N.; Chang, H.-K.; Cote, R. J.; Chongwu, Z.; Thompson, M. E. Real-Time, Label-Free Detection of Biological Entities Using Nanowire-Based FETs. *IEEE Trans. Nanotechnol.* **2008**, *7*, 651–667.
5. Cui, Y.; Wei, Q.; Park, H.; Lieber, C.M. Nanowire Nanosensors for Highly Sensitive and Selective Detection of Biological and Chemical Species. *Science* **2001**, *293*, 1289–1292.
6. Hahn, J.-I.; Lieber, C. M. Direct Ultrasensitive Electrical Detection of DNA and DNA Sequence Variations Using Nanowire Nanosensors. *Nano Lett.* **2003**, *4*, 51–54.
7. Wang, W. U.; Chen, C.; Lin, K.-H.; Fang, Y.; Lieber, C. M. Label-Free Detection of Small-Molecule-Protein Interactions by Using Nanowire Nanosensors. *Proc. Natl. Acad. Sci. U. S. A.* **2005**, *102*, 3208–3212.
8. Zheng, G.; Patolsky, F.; Cui, Y.; Wang, W. U.; Lieber, C. M. Multiplexed Electrical Detection of Cancer Markers with Nanowire Sensor Arrays. *Nat. Biotechnol.* **2005**, *23*, 1294–1301.
9. Stern, E.; Klemic, J. F.; Routenberg, D. A.; Wyrembak, P. N.; Turner-Evans, D. B.; Hamilton, A. D.; LaVan, D. A.; Fahmy, T. M.; Reed, M. A. Label-Free Immunodetection with CMOS-Compatible Semiconducting Nanowires. *Nature* **2007**, *445*, 519–522.

10. Li, B.-R.; Hsieh, Y.-J.; Chen, Y.-X.; Chung, Y.-T.; Pan, C.-Y.; Chen, Y.-T. An Ultrasensitive Nanowire-Transistor Biosensor for Detecting Dopamine Release from Living PC12 Cells under Hypoxic Stimulation. *J. Am. Chem. Soc.* **2013**, *135*, 16034–16037.
11. Besteman, K.; Lee, J.-O.; Wiertz, F. G. M.; Heering, H. A.; Dekker, C. Enzyme-Coated Carbon Nanotubes as Single-Molecule Biosensors. *Nano Lett.* **2003**, *3*, 727–730.
12. Chen, R. J.; Bangsaruntip, S.; Drouvalakis, K. A.; Kam, N. W. S.; Shim, M.; Li, Y.; Kim, W.; Utz, P. J.; Dai, H. Noncovalent Functionalization of Carbon Nanotubes for Highly Specific Electronic Biosensors. *Proc. Natl. Acad. Sci. U. S. A.* **2003**, *100*, 4984–4989.
13. So, H.-M.; Won, K.; Kim, Y. H.; Kim, B.-K.; Ryu, B. H.; Na, P. S.; Kim, H.; Lee, J.-O. Single-Walled Carbon Nanotube Biosensors Using Aptamers as Molecular Recognition Elements. *J. Am. Chem. Soc.* **2005**, *127*, 11906–11907.
14. Tang, T.; Liu, X.; Li, C.; Lei, B.; Zhang, D.; Rouhanizadeh, M.; Hsiai, T.; Zhou, C. Complementary Response of In₂O₃ Nanowires and Carbon Nanotubes to Low-Density Lipoprotein Chemical Gating. *Appl. Phys. Lett.* **2005**, *86*, 103903.
15. Maehashi, K.; Katsura, T.; Kerman, K.; Takamura, Y.; Matsumoto, K.; Tamiya, E. Label-Free Protein Biosensor Based on Aptamer-Modified Carbon Nanotube Field-Effect Transistors. *Anal. Chem.* **2006**, *79*, 782–787.
16. Kim, S. N.; Rusling, J. F.; Papadimitrakopoulos, F. Carbon Nanotubes for Electronic and Electrochemical Detection of Biomolecules. *Adv. Mater.* **2007**, *19*, 3214–3228.
17. Martínez, M. T.; Tseng, Y.-C.; Ormategui, N.; Loinaz, I.; Eritja, R.; Bokor, J. Label-Free DNA Biosensors Based on Functionalized Carbon Nanotube Field Effect Transistors. *Nano Lett.* **2009**, *9*, 530–536.

18. Patolsky, F.; Zheng, G.; Hayden, O.; Lakadamyali, M.; Zhuang, X.; Lieber, C. M. Electrical Detection of Single Viruses. *Proc. Natl. Acad. Sci. U. S. A.* **2004**, *101*, 14017–14022.
19. Alivisatos, A. P.; Andrews, A. M.; Boyden, E. S.; Chun, M.; Church, G. M.; Deisseroth, K.; Donoghue, J. P.; Fraser, S. E.; Lippincott-Schwartz, J.; Looger, L. L.; Masmanidis, S.; McEuen, P. L.; Nurmikko, A. V.; Park, H.; Peterka, D. S.; Reid, C.; Roukes, M. L.; Scherer, A.; Schnitzer, M.; Sejnowski, T. J.; Shepard, K. L.; Tsao, D.; Turrigiano, G.; Weiss, P. S.; Xu, C.; Yuste, R.; Zhuang, X. W. Nanotools for Neuroscience and Brain Activity Mapping. *ACS Nano* **2013**, *7*, 1850–1866.
20. Ohno, Y.; Maehashi, K.; Matsumoto, K. Label-Free Biosensors Based on Aptamer-Modified Graphene Field-Effect Transistors. *J. Am. Chem. Soc.* **2010**, *132*, 18012–18013.
21. Huang, Y.; Dong, X.; Shi, Y.; Li, C. M.; Li, L.-J.; Chen, P. Nanoelectronic Biosensors Based on CVD Grown Graphene. *Nanoscale* **2010**, *2*, 1485–1488.
22. Yang, W.; Ratinac, K. R.; Ringer, S. P.; Thordarson, P.; Gooding, J. J.; Braet, F. Carbon Nanomaterials in Biosensors: Should You Use Nanotubes or Graphene? *Angew. Chem., Int. Ed.* **2010**, *49*, 2114–2138.
23. Pumera, M. Graphene in Biosensing. *Mater. Today* **2011**, *14*, 308–315.
24. He, Q.; Sudibya, H. G.; Yin, Z.; Wu, S.; Li, H.; Boey, F.; Huang, W.; Chen, P.; Zhang, H. Centimeter-Long and Large-Scale Micropatterns of Reduced Graphene Oxide Films: Fabrication and Sensing Applications. *ACS Nano* **2010**, *4*, 3201–3208.
25. Sarkar, D.; Liu, W.; Xie, X.; Anselmo, A. C.; Mitragotri, S.; Banerjee, K. MoS₂ Field-Effect Transistor for Next-Generation Label-Free Biosensors. *ACS Nano* **2014**, *8*, 3992–4003.

26. Wang, L.; Wang, Y.; Wong, J. I.; Palacios, T.; Kong, J.; Yang, H. Y. Functionalized MoS₂ Nanosheet-Based Field-Effect Biosensor for Label-Free Sensitive Detection of Cancer Marker Proteins in Solution. *Small* **2014**, *10*, 1101–1105.
27. Morales, A. M.; Lieber, C. M. A Laser Ablation Method for the Synthesis of Crystalline Semiconductor Nanowires. *Science* **1998**, *279*, 208–211.
28. Hochbaum, A. I.; Fan, R.; He, R.; Yang, P. Controlled Growth of Si Nanowire Arrays for Device Integration. *Nano Lett.* **2005**, *5*, 457–460.
29. Fan, S.; Chapline, M. G.; Franklin, N. R.; Tomblor, T. W.; Cassell, A. M.; Dai, H. Self-Oriented Regular Arrays of Carbon Nanotubes and Their Field Emission Properties. *Science* **1999**, *283*, 512–514.
30. Hata, K.; Futaba, D. N.; Mizuno, K.; Namai, T.; Yumura, M.; Iijima, S. Water-Assisted Highly Efficient Synthesis of Impurity-Free Single-Walled Carbon Nanotubes. *Science* **2004**, *306*, 1362–1364.
31. Hersam, M. C. Progress Towards Monodisperse Single-Walled Carbon Nanotubes. *Nat. Nanotechnol.* **2008**, *3*, 387–394.
32. Arnold, M. S.; Green, A. A.; Hulvat, J. F.; Stupp, S. I.; Hersam, M. C. Sorting Carbon Nanotubes by Electronic Structure Using Density Differentiation. *Nat. Nanotechnol.* **2006**, *1*, 60–65.
33. Zheng, M.; Jagota, A.; Strano, M. S.; Santos, A. P.; Barone, P.; Chou, S. G.; Diner, B. A.; Dresselhaus, M. S.; Mclean, R. S.; Onoa, G. B.; Samsonidze, G. G.; Semke, E. D.; Usrey, M.; Walls, D. J. Structure-Based Carbon Nanotube Sorting by Sequence-Dependent DNA Assembly. *Science* **2003**, *302*, 1545–1548.

34. Sun, Z.; Yan, Z.; Yao, J.; Beitler, E.; Zhu, Y.; Tour, J. M. Growth of Graphene from Solid Carbon Sources. *Nature* **2010**, *468*, 549–552.
35. Li, X.; Cai, W.; An, J.; Kim, S.; Nah, J.; Yang, D.; Piner, R.; Velamakanni, A.; Jung, I.; Tutuc, E.; Banerjee, S. K.; Colombo, L.; Ruoff, R. S. Large-Area Synthesis of High-Quality and Uniform Graphene Films on Copper Foils. *Science* **2009**, *324*, 1312–1314.
36. Bai, J.; Liao, L.; Zhou, H.; Cheng, R.; Liu, L.; Huang, Y.; Duan, X. Top-Gated Chemical Vapor Deposition Grown Graphene Transistors with Current Saturation. *Nano Lett.* **2011**, *11*, 2555–2559.
37. Lee, Y.-H.; Zhang, X.-Q.; Zhang, W.; Chang, M.-T.; Lin, C.-T.; Chang, K.-D.; Yu, Y.-C.; Wang, J. T.-W.; Chang, C.-S.; Li, L.-J.; Lin, T.-W. Synthesis of Large-Area MoS₂ Atomic Layers with Chemical Vapor Deposition. *Adv. Mater.* **2012**, *24*, 2320–2325.
38. Lee, Y.-H.; Yu, L.; Wang, H.; Fang, W.; Ling, X.; Shi, Y.; Lin, C.-T.; Huang, J.-K.; Chang, M.-T.; Chang, C.-S.; Dresselhaus, M.; Palacios, T.; Li, L.-J.; Kong, J. Synthesis and Transfer of Single-Layer Transition Metal Disulfides on Diverse Surfaces. *Nano Lett.* **2013**, *13*, 1852–1857.
39. Li, X.; Zhu, Y.; Cai, W.; Borysiak, M.; Han, B.; Chen, D.; Piner, R. D.; Colombo, L.; Ruoff, R. S. Transfer of Large-Area Graphene Films for High-Performance Transparent Conductive Electrodes. *Nano Lett.* **2009**, *9*, 4359–4363.
40. Lee, Y.; Bae, S.; Jang, H.; Jang, S.; Zhu, S.-E.; Sim, S. H.; Song, Y. I.; Hong, B. H.; Ahn, J.-H. Wafer-Scale Synthesis and Transfer of Graphene Films. *Nano Lett.* **2010**, *10*, 490–493.
41. Lin, Y.-C.; Lu, C.-C.; Yeh, C.-H.; Jin, C.; Suenaga, K.; Chiu, P.-W. Graphene Annealing: How Clean Can It Be? *Nano Lett.* **2011**, *12*, 414–419.

42. Pirkle, A.; Chan, J.; Venugopal, A.; Hinojos, D.; Magnuson, C. W.; McDonnell, S.; Colombo, L.; Vogel, E. M.; Ruoff, R. S.; Wallace, R. M. The Effect of Chemical Residues on the Physical and Electrical Properties of Chemical Vapor Deposited Graphene Transferred to SiO₂. *Appl. Phys. Lett.* **2011**, *99*, 122108.
43. Liao, W.-S.; Cheunkar, S.; Cao, H. H.; Bednar, H. R.; Weiss, P. S.; Andrews, A. M. Subtractive Patterning *via* Chemical Lift-Off Lithography. *Science* **2012**, *337*, 1517–1521.
44. Ishikawa, F. N.; Chang, H.-K.; Curreli, M.; Liao, H.-I.; Olson, C. A.; Chen, P.-C.; Zhang, R.; Roberts, R. W.; Sun, R.; Cote, R. J.; Thompson, M. E.; Zhou, C. Label-Free, Electrical Detection of the SARS Virus N-Protein with Nanowire Biosensors Utilizing Antibody Mimics as Capture Probes. *ACS Nano* **2009**, *3*, 1219–1224.
45. Curreli, M.; Li, C.; Sun, Y.; Lei, B.; Gundersen, M. A.; Thompson, M. E.; Zhou, C. Selective Functionalization of In₂O₃ Nanowire Mat Devices for Biosensing Applications. *J. Am. Chem. Soc.* **2005**, *127*, 6922–6923.
46. Ishikawa, F. N.; Curreli, M.; Chang, H.-K.; Chen, P.-C.; Zhang, R.; Cote, R. J.; Thompson, M. E.; Zhou, C. A Calibration Method for Nanowire Biosensors to Suppress Device-to- Device Variation. *ACS Nano* **2009**, *3*, 3969–3976.
47. Hwang, Y. H.; Seo, J.-S.; Yun, J. M.; Park, H.; Yang, S.; Park, S.-H. K.; Bae, B.-S. An 'Aqueous Route' for the Fabrication of Low-Temperature-Processable Oxide Flexible Transparent Thin-Film Transistors on Plastic Substrates. *NPG Asia Mater.* **2013**, *5*, e45.
48. Sze, S. M.; Ng, K. K. *Physics of Semiconductor Devices*, 3rd ed.; Wiley-Interscience: Hoboken, NJ, **2007**; pp 293–373.

49. Kumar, A.; Whitesides, G. M. Features of Gold Having Micrometer to Centimeter Dimensions Can Be Formed through a Combination of Stamping with an Elastomeric Stamp and an Alkanethiol "Ink" Followed by Chemical Etching. *Appl. Phys. Lett.* **1993**, *63*, 2002–2004.
50. Srinivasan, C.; Mullen, T. J.; Hohman, J. N.; Anderson, M. E.; Dameron, A. A.; Andrews, A. M.; Dickey, E. C.; Horn, M. W.; Weiss, P. S. Scanning Electron Microscopy of Nanoscale Chemical Patterns. *ACS Nano* **2007**, *1*, 191–201.
51. Braunschweig, A. B.; Huo, F.; Mirkin, C. A. Molecular Printing. *Nat. Chem.* **2009**, *1*, 353–358.
52. Kim, H. S.; Byrne, P. D.; Facchetti, A.; Marks, T. J. High Performance Solution-Processed Indium Oxide Thin-Film Transistors. *J. Am. Chem. Soc.* **2008**, *130*, 12580–12581.
53. Rim, Y. S.; Lim, H. S.; Kim, H. J. Low-Temperature Metal-Oxide Thin-Film Transistors Formed by Directly Photopatternable and Combustible Solution Synthesis. *ACS Appl. Mater. Interfaces* **2013**, *5*, 3565–3571.
54. Choi, C.-H.; Han, S.-Y.; Su, Y.-W.; Fang, Z.; Lin, L.-Y.; Cheng, C.-C.; Chang, C.-H. Fabrication of High-Performance, Low-Temperature Solution Processed Amorphous Indium Oxide Thin-Film Transistors Using a Volatile Nitrate Precursor. *J. Mater. Chem. C* **2015**, *3*, 854–860.
55. Kim, M.-G.; Kanatzidis, M. G.; Facchetti, A.; Marks, T. J. Low-Temperature Fabrication of High-Performance Metal Oxide Thin-Film Electronics *via* Combustion Processing. *Nat. Mater.* **2011**, *10*, 382–388.

56. Joo Hyon, N.; Seung Yoon, R.; Sung Jin, J.; Chang Su, K.; Sung-Woo, S.; Rack, P. D.; Dong-Joo, K.; Hong Koo, B. Indium Oxide Thin-Film Transistors Fabricated by RF Sputtering at Room Temperature. *IEEE Electron Device Lett.* **2010**, *31*, 567–569.
57. Jiao, Y.; Zhang, X.; Zhai, J.; Yu, X.; Ding, L.; Zhang, W. Bottom-Gate Amorphous In₂O₃ Thin Film Transistors Fabricated by Magnetron Sputtering. *Electron. Mater. Lett.* **2013**, *9*, 279–282.
58. Rim, Y. S.; Chen, H.; Kou, X.; Duan, H.-S.; Zhou, H.; Cai, M.; Kim, H. J.; Yang, Y. Boost Up Mobility of Solution-Processed Metal Oxide Thin-Film Transistors via Confining Structure on Electron Pathways. *Adv. Mater.* **2014**, *26*, 4273–4278.
59. Mannironi, C.; Di Nardo, A.; Fruscoloni, P.; Tocchini- Valentini, G. P. *In Vitro* Selection of Dopamine RNA Ligands. *Biochemistry* **1997**, *36*, 9726–9734.
60. Walsh, R.; DeRosa, M. C. Retention of Function in the DNA Homolog of the RNA Dopamine Aptamer. *Biochem. Biophys. Res. Commun.* **2009**, *388*, 732–735.
61. Farjami, E.; Campos, R.; Nielsen, J. S.; Gothelf, K. V.; Kjems, J.; Ferapontova, E. E. RNA Aptamer-Based Electrochemical Biosensor for Selective and Label-Free Analysis of Dopamine. *Anal. Chem.* **2012**, *85*, 121–128.
62. Giros, B.; Jaber, M.; Jones, S. R.; Wightman, R. M.; Caron, M. G. Hyperlocomotion and Indifference to Cocaine and Amphetamine in Mice Lacking the Dopamine Transporter. *Nature* **1996**, *379*, 606–612.
63. Kim, J.-H.; Auerbach, J. M.; Rodriguez-Gomez, J. A.; Velasco, I.; Gavin, D.; Lumelsky, N.; Lee, S.-H.; Nguyen, J.; Sanchez- Pernaute, R.; Bankiewicz, K.; McKay, R. Dopamine Neurons Derived from Embryonic Stem Cells Function in an Animal Model of Parkinson's Disease. *Nature* **2002**, *418*, 50–56.

64. Phillips, P. E. M.; Stuber, G. D.; Heien, M. L. A. V.; Wightman, R. M.; Carelli, R. M. Subsecond Dopamine Release Promotes Cocaine Seeking. *Nature* **2003**, *422*, 614–618.
65. Unger, E. L.; Eve, D. J.; Perez, X. A.; Reichenbach, D. K.; Xu, Y.; Lee, M. K.; Andrews, A. M. Locomotor Hyperactivity and Alterations in Dopamine Neurotransmission Are Associated with Overexpression of A53T Mutant Human R-Synuclein in Mice. *Neurobiol. Dis.* **2006**, *21*, 431–443.
66. Aswal, D. K.; Lenfant, S.; Guerin, D.; Yakhmi, J. V.; Vuillaume, D. Self-Assembled Monolayers on Silicon for Molecular Electronics. *Anal. Chim. Acta* **2006**, *568*, 84–108.
67. Helmy, R.; Fadeev, A. Y. Self-Assembled Monolayers Supported on TiO₂: Comparison of C₁₈H₃₇SiX₃ (X = H, Cl, OCH₃), C₁₈H₃₇Si(CH₃)₂Cl, and C₁₈H₃₇PO(OH)₂. *Langmuir* **2002**, *18*, 8924–8928.
68. Kim, J. S.; Park, J. H.; Lee, J. H.; Jo, J.; Kim, D.-Y.; Cho, K. Control of the Electrode Work Function and Active Layer Morphology via Surface Modification of Indium Tin Oxide for High Efficiency Organic Photovoltaics. *Appl. Phys. Lett.* **2007**, *91*, 112111.
69. Chung, Y.; Verploegen, E.; Vailionis, A.; Sun, Y.; Nishi, Y.; Murmann, B.; Bao, Z. Controlling Electric Dipoles in Nanodielectrics and Its Applications for Enabling Air-Stable n-Channel Organic Transistors. *Nano Lett.* **2011**, *11*, 1161–1165.
70. Song, C. K.; Luck, K. A.; Zhou, N.; Zeng, L.; Heitzer, H. M.; Manley, E. F.; Goldman, S.; Chen, L. X.; Ratner, M. A.; Bedzyk, M. J. “Supersaturated” Self-Assembled Charge-Selective Interfacial Layers for Organic Solar Cells. *J. Am. Chem. Soc.* **2014**, *136*, 17762–17773.
71. Baker, B. R.; Lai, R. Y.; Wood, M. S.; Doctor, E. H.; Heeger, A. J.; Plaxco, K. W. An Electronic, Aptamer-Based Small-Molecule Sensor for the Rapid, Label-Free Detection

- of Cocaine in Adulterated Samples and Biological Fluids. *J. Am. Chem. Soc.* **2006**, *128*, 3138–3139.
72. Ferapontova, E. E.; Olsen, E. M.; Gothelf, K. V. An RNA Aptamer-Based Electrochemical Biosensor for Detection of Theophylline in Serum. *J. Am. Chem. Soc.* **2008**, *130*, 4256–4258.
73. Fan, C.; Plaxco, K. W.; Heeger, A. J. Electrochemical Interrogation of Conformational Changes as a Reagentless Method for the Sequence-Specific Detection of DNA. *Proc. Natl. Acad. Sci. U. S. A.* **2003**, *100*, 9134–9137.
74. Zuo, X.; Song, S.; Zhang, J.; Pan, D.; Wang, L.; Fan, C. A Target-Responsive Electrochemical Aptamer Switch (TREAS) for Reagentless Detection of Nanomolar ATP. *J. Am. Chem. Soc.* **2007**, *129*, 1042–1043.
75. Farjami, E.; Clima, L.; Gothelf, K.; Ferapontova, E. E. “Off-On” Electrochemical Hairpin-DNA-Based Genosensor for Cancer Diagnostics. *Anal. Chem.* **2011**, *83*, 1594–1602.
76. Singh, Y. S.; Sawarynski, L. E.; Dabiri, P. D.; Choi, W. R.; Andrews, A. M. Head-to-Head Comparisons of Carbon Fiber Microelectrode Coatings for Sensitive and Selective Neurotransmitter Detection by Voltammetry. *Anal. Chem.* **2011**, *83*, 6658–6666.
77. Zheng, Y.; Wang, Y.; Yang, X. Aptamer-Based Colorimetric Biosensing of Dopamine Using Unmodified Gold Nanoparticles. *Sens. Actuators, B* **2011**, *156*, 95–99.
78. Mathews, T. A.; Fedele, D. E.; Coppelli, F. M.; Avila, A. M.; Murphy, D. L.; Andrews, A. M. Gene Dose-Dependent Alterations in Extraneuronal Serotonin but Not Dopamine in Mice with Reduced Serotonin Transporter Expression. *J. Neurosci. Methods* **2004**, *140*, 169–181.

Supplementary Information References

- S1. Kim, H. S.; Byrne, P. D.; Facchetti, A.; Marks, T. J. High Performance Solution-Processed Indium Oxide Thin-Film Transistors. *J. Am. Chem. Soc.* **2008**, *130*, 12580-12581.
- S2. Rim, Y. S.; Lim, H. S.; Kim, H. J. Low-Temperature Metal-Oxide Thin-Film Transistors Formed by Directly Photopatternable and Combustible Solution Synthesis. *ACS Appl. Mater. Inter.* **2013**, *5*, 3565-3571.
- S3. Choi, C.-H.; Han, S.-Y.; Su, Y.-W.; Fang, Z.; Lin, L.-Y.; Cheng, C.-C.; Chang, C.-H. Fabrication of High-Performance, Low-Temperature Solution Processed Amorphous Indium Oxide Thin-Film Transistors Using a Volatile Nitrate Precursor. *J. Mater. Chem. C* **2015**, *3*, 854-860.
- S4. Kim, M.-G.; Kanatzidis, M. G.; Facchetti, A.; Marks, T. J. Low-Temperature Fabrication of High-Performance Metal Oxide Thin-Film Electronics *via* Combustion Processing. *Nat. Mater.* **2011**, *10*, 382-388.
- S5. Joo Hyon, N.; Seung Yoon, R.; Sung Jin, J.; Chang Su, K.; Sung-Woo, S.; Rack, P. D.; Dong-Joo, K.; Hong Koo, B. Indium Oxide Thin-Film Transistors Fabricated by RF Sputtering at Room Temperature. *IEEE Electron Device Lett.* **2010**, *31*, 567-569.
- S6. Jiao, Y.; Zhang, X.; Zhai, J.; Yu, X.; Ding, L.; Zhang, W. Bottom-Gate Amorphous In₂O₃ Thin Film Transistors Fabricated by Magnetron Sputtering. *Electron. Mater. Lett.* **2013**, *9*, 279-282.

Chapter 9

Prospects to the Realization of Functional Neurotransmitter Chips

9.1 Highlights and Prospects

9.1.1 Neurochip Project

We do not yet fully comprehend the complexity of the human brain; however, we continue to try to shed light on the mechanisms of neural signaling and brain circuitry. Perhaps the goal to monitor electrical and chemical signaling processes underlying communication between neurons across all brain regions is too ambitious and impractical. Nonetheless, in the early 1900's, it was ambitious to think that people could fly in the sky. Also, it was impossible to imagine that people could see and communicate with others through a (computer) monitor. What was considered far-fetched then is reality today.

As with other aspects of life, every scientific investigation begins with small steps that gradually build into larger leaps and eventually transform our ambitious dreams into practical realities. The “neurochip” project in our group aims to construct nanoscale neurosensors combining receptor-ligand recognition and transistor-based biosensing platforms to enable multiplexed *in vivo* measurements of neurotransmitters.¹⁻⁵ This ambitious research endeavor began with small steps where we worked with the surface chemistries of self-assembly and has grown into a larger leap where we have developed a repertoire of chemical patterning tools to investigate the binding of biomolecular receptors at solid/liquid interfaces and to build *functional* screening platforms to identify artificial receptors for biosensing purposes. For over a decade, postdoctoral fellows and graduate students, including myself, have joined together to accomplish these first steps on this long, strenuous, but exciting journey.

Along the way, we discovered a number of important physical/chemical design rules dictating biorecognition at solid/liquid interfaces. For example, the native defects of alkanethiol SAMs have been used to advantage for molecular insertion to enable biospecific recognition of

surface-tethered ligands diluted (<10% of a monolayer) in the background matrices.^{6,7} Oligo(ethylene glycol) moieties were incorporated into the tethering molecules and the background matrices to reduce nonspecific protein-substrate interactions.⁶ Moreover, my contribution was to combine BSA with oligo(ethylene glycol)-modified alkanethiol SAMs to reduce further nonspecific protein-substrate interactions to <10% vs. total protein binding.^{8,9} This discovery improved the visualization of biopatterns using fluorescence microscopy and enabled better quantification of biomolecule binding on biocapture substrates.

We also discovered that for surface-tethered neurotransmitters to capture native membrane-associated receptors in solutions, the ligands had to mimic endogenous molecules in the biological milieu of neural synapses.¹⁰ Specifically, additional ectopic functional groups were introduced for surface tethering to preserve the essential epitopes for biorecognition. Thus, I was able to utilize this ingenious strategy to expand the library of surface-tethered small molecules mimicking endogenous neurotransmitters and to develop microfluidics-based small-molecule arrays for future high-throughput screening of artificial receptors.⁹

I also developed improved surface functionalization strategies for small-molecule ligands. Although our approach of functionalizing surface tethers on-chip with ligands of interest is generalizable, it has limitations. For multiplexed biocapture platforms, not only did it require multiple ligands to be functionalized on substrates, it demanded different *chemically compatible* functionalization strategies. We discovered that the functionalization chemistries of later ligands could alter the extent of functionalization of ligands placed earlier on substrates.⁸ Thus, in collaboration with the Kasko group from the Department of Bioengineering at the University of California, Los Angeles, we focused on developing an alternate strategy whereby small-molecule ligands were pre-functionalized to tethers prior to surface assembly, circumventing the problem

of functionalization compatibility. My results indicate that neurotransmitter pre-functionalized molecules showed more consistent and improved specific recognition by antibodies. In addition, the multiplexed substrates created with pre-functionalized molecules demonstrated the ability to capture and to sort antibodies from mixed solutions of biomolecules.

I explored other strategies to mitigate the underlying causes of problems associated with fabricating and interrogating multiplexed substrates. For example, to circumvent problems associated with visualizing captured receptors *via* primary-receptor antibodies and complementary secondary antibodies, I looked into using green/yellow fluorescent protein and SNAP/CLIP protein tagging technologies to label receptors directly with fluorophores for visualization.¹¹⁻¹⁶ The motivation stems from my discovery that the primary antibodies used to label native membrane-associated receptors also displayed some affinity for surface-tethered ligands,⁹ which confounded the measurements of receptor-specific binding. Studies using the latter will be followed up in the future and we acquired high quantum-yield fluorescent dyes that are SNAP-tagged from Dr. Luke Lavis at Janelia Farms for this purpose.¹⁷

Now that many of the physical and chemical motifs dictating biomolecule-ligand interactions at solid/liquid interfaces have been uncovered, we are ready to use the high-throughput screening platforms developed here to identify the artificial receptors needed for *in vivo* neurosensing. Currently, those continuing to work on the neurochip project are utilizing functional neurotransmitter chips to screen for aptamer-based receptors targeting small-molecule neurotransmitters. In addition, our previous results have shown that an existing aptamer with modest affinity for the small-molecule neurotransmitter dopamine could be coupled to FET-based biosensors to detect subnanomolar dopamine concentrations.¹⁸ Thus, the next phase in the neurochip project will be to incorporate newly identified high-affinity aptamers from the

neurochip screening process into FET-based biosensors for *in vitro* studies, and ultimately for *in vivo* neurosensing.¹⁹⁻²³

9.1.2 Chemical Patterning

In addition to designing motifs to improve substrate-mediated biomolecule-ligand recognition, we developed novel chemical patterning methods to place bioactive probes in spatially defined geometries on substrates. These capabilities not only permitted the investigation of biomolecule binding on ligand functionalized *vs.* unfunctionalized regions on the same substrate, they enabled multiplexed patterning of small-molecule ligands for investigating biomolecule specificity. Our chemical patterning repertoire includes microcontact insertion printing, microfluidics-based addressing, and chemical lift-off lithography.^{8-10,24-28}

Microcontact insertion printing was previously invented in our group to enable the insertion-directed placement of tethered ligands diluted in protein-resistant alkanethiol SAMs.^{8,10,24,25} However, this approach is held hostage by the need for compatible sequential functionalization chemistries for various ligands.⁸ Moreover, insertion printing requires the tuning of surface properties of PDMS stamps to enable effective insertion of tethers of varying hydrophilicity into preformed SAMs.²⁵ These drawbacks impede μ CIP from being used to create multiplexed substrates. Using microfluidics, we circumvented these issues by utilizing microscale conduits to place multiple ligands simultaneously on the same substrates.⁹ The advantage here comes from restricting ligand functionalization in individual channels, thus obviating the need for functionalization compatibility and surface property tuning for insertion. Nevertheless, because tethered molecules in the microfluidic-based approach are diluted in the background matrix by co-deposition of mixed SAMs, phase separation of tethered molecules can still result in steric hindrance and induce multivalent nonspecific interactions with biomolecules.^{6,29-33}

I co-invented chemical lift-off lithography, wherein patterned substrates are produced by removing molecules from preformed hydroxyl-terminated alkanethiol SAMs.²⁶ The key step here is the formation of covalent stamp/SAM interactions, which are stronger than Au-Au bonds on the surface of Au substrates, when oxygen plasma-treated PDMS stamps are in conformal contact with hydroxyl-terminated SAMs. Lifting stamps from the substrates removes terminally functionalized alkanethiolates. Utilizing the subtractive nature of chemical lift-off, we created patterns of tethered biotin probes to capture streptavidin down to sub-40 nm and sub-20 nm feature sizes with single and double lift-off, respectively.²⁶

Infrared spectral analysis indicated that ~70% of preformed SAM molecules are removed *via* chemical lift-off lithography.^{26,34} The available vacancies created by the removed molecules in the contact regions appear to be highly amenable to subsequent insertion-directed surface assembly. For example, I was able to show that the retained alkanethiols in the contact regions enabled insertion of thiolated DNA molecules.³⁴ The resulting DNA patterns were characteristic of dilute DNA surface coverage and reduced DNA-substrate interactions. As such, they greatly improved DNA hybridization efficiency beyond that associated with the convention backfilling method. I also discovered that DNA surface-coverage and hybridization efficiencies were controlled by varying pre-lift-off SAM compositions. In addition to single- and double-lift-off to pattern DNA for hybridization, I carried out triple lift-off lithography (Figure 9-1). Here, we found that additional SAM molecules could be removed even after the third lift-off step. I envision that the next phase of this project will be to investigate how different SAM parameters *i.e.*, terminal groups, chain lengths, conformations, and inter-molecular forces can be used to tune further DNA surface hybridization or DNA interactions with small-molecule ligands.³⁵⁻³⁷ Moreover, lift-off-based DNA patterning should be used to determine whether target DNA with

single base-pair mismatches can be detected.³⁸⁻⁴¹ This is important if these types of arrays are to be used for single nucleotide polymorphism analysis. Also, compared with nucleic acid studies in solution, which have been more thoroughly investigated, DNA behaviors on surfaces is still not well understood.³⁵ Thus, it will be interesting to investigate the effects of SAM compositions on the thermodynamic and kinetic behaviors of nucleic acids on surfaces to provide understanding of the key parameters dictating the properties of surface-tethered DNAs.^{35,42-46}

In addition to inserting DNA molecules, small-molecule functionalized alkanethiols were inserted into post-lift-off substrates. I discovered that chemical lift-off creates a new class of defects for molecular insertion beyond native SAM/substrate defects critical for μ CIP.³⁴ Moreover, lift-off lithography obviated tuning of stamp surface properties needed for inserting individual types of molecules *via* μ CIP.²⁵ The insertion-directed chemistry of lift-off lithography also overcame potential phase-separation associated with co-deposition methods.^{6,27,47,48} As such, I explored the ability of chemical lift-off lithography to create multiplexed platforms. For example, side-by-side patterning of biotin and small molecules mimicking endogenous neurotransmitters on the same substrate illustrated sorting of proteins and antibodies from mixed solutions.

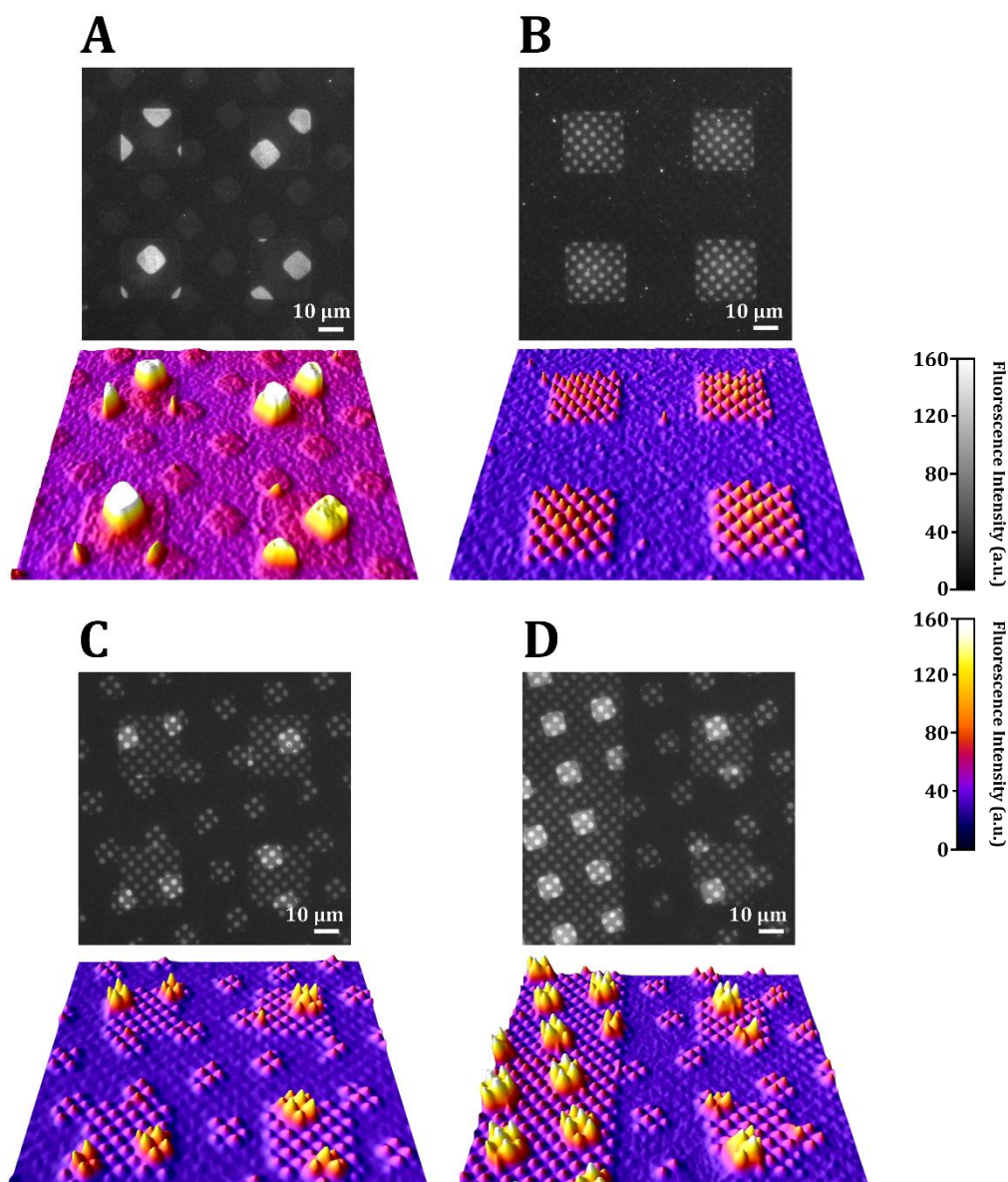


Figure 9-1. Representative fluorescence images and 3D surface plots. **(A,B)** Double and **(C,D)** triple lift-off lithography on hydroxyl-terminated tri(ethylene glycol)alkanethiol SAMs. Post-lift-off substrates were inserted with thiolated DNA probes followed by hybridization with AlexaFluor[®] 488-labeled complementary DNA hybridization. The brightest and dimmer features are doubly and singly contacted, respectively in **(A,B)**, which correspond to higher and lower numbers of inserted DNA probes, respectively. Similarly, the brighter and dimmer features are triply and doubly contacted in **(C,D)**. Fluorescence resulting from DNA insertion into the post-single-lift-off features is difficult to observe due to the small features ($2 \mu\text{m}^2$ in **B,C,D**) but is easier to see in the 3D surface plots **(B,C,D)** and for the larger features ($10 \mu\text{m}^2$ in **A**).

Although chemical functionalization of post-lift-off substrates has shown excellent results for nucleic acid hybridization and biomolecule-ligand recognition, a number of questions remain. For example, because insertion-directed surface assembly on post-lift-off substrates depends on the lift-off yield, it will be crucial to devise new experimental techniques to quantify the amounts of molecules removed in each lift-off step.³⁴ In addition, systematic studies are needed to investigate how different parameters associated with the stamps, including varying oxygen plasma conditions, stamp/substrate contact times, and the use of polymeric materials other than PDMS for lift-off can be used to control the lift-off yield. Because oxygen plasma has been known to cause cracks on PDMS surfaces in addition to oxidation,^{49,50} alternate strategies are essential to activate stamps without damaging them to improve conformal stamp/substrate contact and subsequently, lift-off yield.⁵¹⁻⁵³

Additional factors associated with SAMs and substrates in chemical lift-off lithography are also of interest. For example, varying the terminal groups, chain lengths, intermolecular forces, and head groups of thiolated SAM molecules or varying substrate materials beyond Au will provide essential tuning possibilities and new opportunities to expand the versatility and generalizability of lift-off lithography. X-ray photoelectron spectroscopy has been used to detect the presence of Au atoms bound to alkanethiols, which are removed when PDMS stamps are released from substrates.²⁶ Examining post-lift-off PDMS stamps with XPS showed Au 4f peaks when lift-off was carried out on alkanethiol SAMs terminated with hydroxyl (OH), hydroxyl/amine/carboxylic acid-terminated oligo(ethylene glycol) (OH-(C₂H₄O)_{n=3,6} and NH₂/COOH-(C₂H₄O)_{n=6}), and phosphonate (PO(OH)₂), indicating that these functional groups are amenable to lift-off (Chart 9-1). In contrast, functional groups including methoxy-terminated tri(ethylene glycol) (CH₃O-(C₂H₄O)₃), biotin-terminated hexa(ethylene glycol)

(C₁₀H₁₅O₂N₂S)-(C₂H₄O)₆), and bromine (Br) and methyl (CH₃) tail groups did not show Au 4f XPS peaks on post-lift-off PDMS stamps suggesting that these moieties are not lift-able. These unpublished results are consistent with the hypothesized stamp/SAM reactivity. The use of polycrystalline *vs.* single-crystal facet Au substrates will also be interesting to investigate regarding the effects of surface crystallinity on chemical lift-off process.

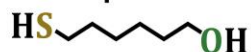
Additionally, the ability to perform lift-off lithography on single-crystal (*i.e.*, Au(111)) substrates will be beneficial for STM studies to resolve the structures and arrangements of molecules in the post-lift-off regions. However, the use of scanning probe microscopies to investigate the structures of post-lift-off SAMs terminated with hydroxyl/amine/carboxylic acid/phosphonate tail groups or oligo(ethylene glycol) moieties will be challenging because of their molecular length, degree of disorder, and association with water molecules under ambient conditions.⁵⁴⁻⁵⁶ Several studies have shown that *in situ* STM coupled with electrochemical measurements is capable of characterizing SAMs terminated with hydrophilic tail groups under aqueous conditions.⁵⁷⁻⁵⁹ These instrumental capabilities may enable insightful structural information regarding post-lift-off SAMs. Alternately, electrochemical reductive desorption measurements also could be used to quantify the SAM molecules remaining in the stamp-contact regions because such measurements are sensitive to domain sizes and interaction strengths with different molecules desorbing at different electrochemical potentials.⁶⁰⁻⁶² Additional computational studies, along with STM investigation, will help to elucidate the lift-off mechanisms and provide new insights into the structures of defects created by chemical lift-off lithography.

Finally, because chemical lift-off relies on the strong contact-induced stamp/SAM interactions and covalent SAM-Au bonds to rupture Au-Au bonds on the surface of Au

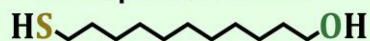
substrates, the removed alkanethiols also carry with them the underlying Au atoms from the substrates.²⁶ This finding provides strong evidence supporting the presence of Au adatoms beneath alkanethiol SAMs, which leads to facile Au-Au bond breakage because of the reduced coordination of the adatoms⁶³⁻⁶⁵ and the mobility of Au thiolates within SAMs observed in several previous STM studies.^{29,66,67} Rough estimates of the topographic differences between lift-off vs. non-lift-off regions on post-lift-off hydroxyl-terminated tri(ethylene glycol)alkanethiol SAMs is on average 2.0 ± 0.3 nm.²⁶ The TEG SAM thickness measured by ellipsometry is 1.6 ± 0.1 nm. Thus, the difference between these two values is roughly the thickness of a single atomic Au-atom layer. It will be important to investigate the structures and associated optical, electrical, and magnetic properties of these ultrathin Au films because they may represent the next-generation graphene-like two-dimensional materials.⁶⁸⁻⁷¹

Lift-Able

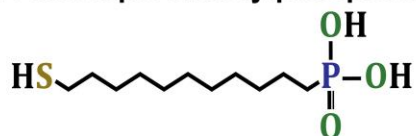
6-Mercaptohexanol



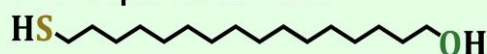
11-Mercaptoundecanol



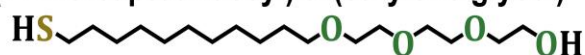
11-Mercaptoundecylphosphonic Acid



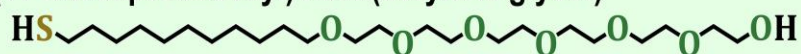
16-Mercaptohexadecanol



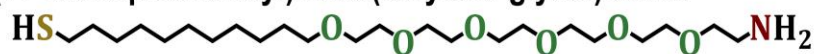
(11-Mercaptoundecyl) tri(ethylene glycol)



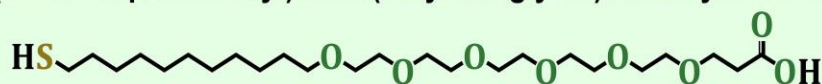
(11-Mercaptoundecyl) hexa(ethylene glycol)



(11-Mercaptoundecyl) hexa(ethylene glycol)amine

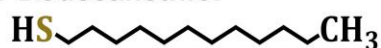


(11-Mercaptoundecyl) hexa(ethylene glycol)carboxylic Acid



Non-Lift-Able

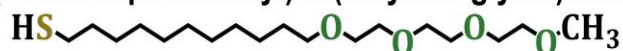
1-Dodecanethiol



11-Bromo-1-undecanethiol



(11-Mercaptoundecyl) tri(ethylene glycol)methyl ether



(11-Mercaptoundecyl) hexa(ethylene glycol)biotin

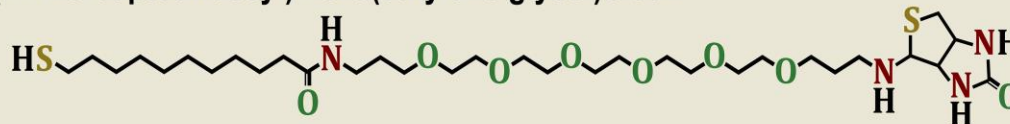


Chart 9-1. A list of lift-able and non-lift-able alkanethiols investigated *via* X-ray photoelectron spectroscopy to detect the presence/absence of Au 4f peaks on post-lift-off polydimethylsiloxane stamps

9.2 References

1. Andrews, A. M.; Weiss, P. S. Nano in the Brain: Nano-Neuroscience. *ACS Nano* **2012**, *6*, 8463-8464.
2. Alivisatos, A. P.; Andrews, A. M.; Boyden, E. S.; Chun, M.; Church, G. M.; Deisseroth, K.; Donoghue, J. P.; Fraser, S. E.; Lippincott-Schwartz, J.; Looger, L. L.; Masmanidis, S.; McEuen, P. L.; Nurmikko, A. V.; Park, H.; Peterka, D. S.; Reid, C.; Roukes, M. L.; Scherer, A.; Schnitzer, M.; Sejnowski, T. J.; Shepard, K. L.; Tsao, D.; Turrigiano, G.; Weiss, P. S.; Xu, C.; Yuste, R.; Zhuang, X. W. Nanotools for Neuroscience and Brain Activity Mapping. *ACS Nano* **2013**, *7*, 1850-1866.
3. Alivisatos, A. P.; Chun, M.; Church, G. M.; Deisseroth, K.; Donoghue, J. P.; Greenspan, R. J.; McEuen, P. L.; Roukes, M. L.; Sejnowski, T. J.; Weiss, P. S.; Yuste, R. The Brain Activity Map. *Science* **2013**, *339*, 1284-1285.
4. Andrews, A. M. The BRAIN Initiative: Toward a Chemical Connectome. *ACS Chem. Neurosci.* **2013**, *4*, 645-645.
5. Andrews, A. M.; Schepartz, A.; Sweedler, J. V.; Weiss, P. S. Chemistry and the BRAIN Initiative. *J. Am. Chem. Soc.* **2014**, *136*, 1-2.
6. Shuster, M. J.; Vaish, A.; Szapacs, M. E.; Anderson, M. E.; Weiss, P. S.; Andrews, A. M. Biospecific Recognition of Tethered Small Molecules Diluted in Self-Assembled Monolayers. *Adv. Mater.* **2008**, *20*, 164-167.
7. Shuster, M. J.; Vaish, A.; Gilbert, M. L.; Martinez-Rivera, M.; Nezarati, R. M.; Weiss, P. S.; Andrews, A. M. Comparison of Oligo(Ethylene Glycol)Alkanethiols versus *n*-Alkanethiols: Self-Assembly, Insertion, and Functionalization. *J. Phys. Chem. C* **2011**, *115*, 24778-24787.

8. Shuster, M. J.; Vaish, A.; Cao, H. H.; Guttentag, A. I.; McManigle, J. E.; Gibb, A. L.; Martinez, M. M.; Nezarati, R. M.; Hinds, J. M.; Liao, W.-S.; Weiss, P. S.; Andrews, A. M. Patterning Small-Molecule Biocapture Surfaces: Microcontact Insertion Printing vs. Photolithography. *Chem. Commun.* **2011**, *47*, 10641-10643.
9. Liao, W. S.; Cao, H. H.; Cheunkar, S.; Shuster, M. J.; Altieri, S. C.; Weiss, P. S.; Andrews, A. M. Small-Molecule Arrays for Sorting G-Protein-Coupled Receptors. *J. Phys. Chem. C* **2013**, *117*, 22362-22368.
10. Vaish, A.; Shuster, M. J.; Cheunkar, S.; Singh, Y. S.; Weiss, P. S.; Andrews, A. M. Native Serotonin Membrane Receptors Recognize 5-Hydroxytryptophan-Functionalized Substrates: Enabling Small-Molecule Recognition. *ACS Chem. Neurosci.* **2010**, *1*, 495-504.
11. Milligan, G. Exploring the Dynamics of Regulation of G Protein-Coupled Receptors Using Green Fluorescent Protein. *Br. J. Pharmacol.* **1999**, *128*, 501-510.
12. He, Y.; Yu, L. P.; Jin, G. Z. Differential Distributions and Trafficking Properties of Dopamine D₁ and D₅ Receptors in Nerve Cells. *Neurosci. Bull.* **2009**, *25*, 43-53.
13. Renner, U.; Zeug, A.; Woehler, A.; Niebert, M.; Dityatev, A.; Dityateva, G.; Gorinski, N.; Guseva, D.; Abdel-Galil, D.; Frohlich, M.; Doring, F.; Wischmeyer, E.; Richter, D. W.; Neher, E.; Ponimaskin, E. G. Heterodimerization of Serotonin Receptors 5-HT_{1A} and 5-HT₇ Differentially Regulates Receptor Signalling and Trafficking. *J. Cell Sci.* **2012**, *125*, 2486-2499.
14. Keppler, A.; Pick, H.; Arrivoli, C.; Vogel, H.; Johnsson, K. Labeling of Fusion Proteins with Synthetic Fluorophores in Live Cells. *Proc. Natl. Acad. Sci. U. S. A.* **2004**, *101*, 9955-9959.

15. Schultz, C.; Kohn, M. Simultaneous Protein Tagging in Two Colors. *Chem. Biol.* **2008**, *15*, 91-92.
16. Emami-Nemini, A.; Roux, T.; Leblay, M.; Bourrier, E.; Lamarque, L.; Trinquet, E.; Lohse, M. J. Time-Resolved Fluorescence Ligand Binding for G Protein-Coupled Receptors. *Nat. Protoc.* **2013**, *8*, 1307-1320.
17. Grimm, J. B.; English, B. P.; Chen, J. J.; Slaughter, J. P.; Zhang, Z. J.; Revyakin, A.; Patel, R.; Macklin, J. J.; Normanno, D.; Singer, R. H.; Lionnet, T.; Lavis, L. D. A General Method to Improve Fluorophores for Live-Cell and Single-Molecule Microscopy. *Nat. Meth.* **2015**, *12*, 244-250.
18. Kim, J.; Rim, Y. S.; Chen, H. J.; Cao, H. H.; Nakatsuka, N.; Hinton, H. L.; Zhao, C. Z.; Andrews, A. M.; Yang, Y.; Weiss, P. S. Fabrication of High-Performance Ultrathin In₂O₃ Film Field-Effect Transistors and Biosensors Using Chemical Lift-Off Lithography. *ACS Nano* **2015**, *9*, 4572-4582.
19. Baker, B. R.; Lai, R. Y.; Wood, M. S.; Doctor, E. H.; Heeger, A. J.; Plaxco, K. W. An Electronic, Aptamer-Based Small-Molecule Sensor for the Rapid, Label-Free Detection of Cocaine in Adulterated Samples and Biological Fluids. *J. Am. Chem. Soc.* **2006**, *128*, 3138-3139.
20. Pavlovic, E.; Lai, R. Y.; Wu, T. T.; Ferguson, B. S.; Sun, R.; Plaxco, K. W.; Soh, H. T. Microfluidic Device Architecture for Electrochemical Patterning and Detection of Multiple DNA Sequences. *Langmuir* **2008**, *24*, 1102-1107.
21. Du, J. G.; Blanche, T. J.; Harrison, R. R.; Lester, H. A.; Masmanidis, S. C. Multiplexed, High Density Electrophysiology with Nanofabricated Neural Probes. *PLoS One* **2011**, *6*, e26204.

22. Yufei, M.; Chi On, C. Transient Measurement Approaches to Differentiate Non-Specific Binding in Affinity-Based Bioanalytical Assays. *J. Appl. Phys.* **2012**, *112*, 024702.
23. Shoorideh, K.; Chui, C. O. On the Origin of Enhanced Sensitivity in Nanoscale FET-Based Biosensors. *Proc. Natl. Acad. Sci. U. S. A.* **2014**, *111*, 5111-5116.
24. Mullen, T. J.; Srinivasan, C.; Hohman, J. N.; Gillmor, S. D.; Shuster, M. J.; Horn, M. W.; Andrews, A. M.; Weiss, P. S. Microcontact Insertion Printing. *Appl. Phys. Lett.* **2007**, *90*, 063114.
25. Vaish, A.; Shuster, M. J.; Cheunkar, S.; Weiss, P. S.; Andrews, A. M. Tuning Stamp Surface Energy for Soft Lithography of Polar Molecules to Fabricate Bioactive Small-Molecule Microarrays. *Small* **2011**, *7*, 1471-1479.
26. Liao, W. S.; Cheunkar, S.; Cao, H. H.; Bednar, H. R.; Weiss, P. S.; Andrews, A. M. Subtractive Patterning *via* Chemical Lift-Off Lithography. *Science* **2012**, *337*, 1517-1521.
27. Claridge, S. A.; Liao, W. S.; Thomas, J. C.; Zhao, Y. X.; Cao, H. H.; Cheunkar, S.; Serino, A. C.; Andrews, A. M.; Weiss, P. S. From the Bottom Up: Dimensional Control and Characterization in Molecular Monolayers. *Chem. Soc. Rev.* **2013**, *42*, 2725-2745.
28. Saavedra, H. M.; Mullen, T. J.; Zhang, P. P.; Dewey, D. C.; Claridge, S. A.; Weiss, P. S. Hybrid Strategies in Nanolithography. *Rep. Prog. Phys.* **2010**, *73*, 036501.
29. Stranick, S. J.; Parikh, A. N.; Tao, Y. T.; Allara, D. L.; Weiss, P. S. Phase-Separation of Mixed-Composition Self-Assembled Monolayers into Nanometer-Scale Molecular Domains. *J. Phys. Chem.* **1994**, *98*, 7636-7646.
30. Lewis, P. A.; Smith, R. K.; Kelly, K. F.; Bumm, L. A.; Reed, S. M.; Clegg, R. S.; Gunderson, J. D.; Hutchison, J. E.; Weiss, P. S. The Role of Buried Hydrogen Bonds in

- Self-Assembled Mixed Composition Thiols on Au{111}. *J. Phys. Chem. B* **2001**, *105*, 10630-10636.
31. Lahiri, J.; Isaacs, L.; Grzybowski, B.; Carbeck, J. D.; Whitesides, G. M. Biospecific Binding of Carbonic Anhydrase to Mixed SAMs Presenting Benzenesulfonamide Ligands: A Model System for Studying Lateral Steric Effects. *Langmuir* **1999**, *15*, 7186-7198.
32. Lahiri, J.; Isaacs, L.; Tien, J.; Whitesides, G. M. A Strategy for the Generation of Surfaces Presenting Ligands for Studies of Binding Based on an Active Ester as a Common Reactive Intermediate: A Surface Plasmon Resonance Study. *Anal. Chem.* **1999**, *71*, 777-790.
33. Kwon, Y.; Han, Z. Z.; Karatan, E.; Mrksich, M.; Kay, B. K. Antibody Arrays Prepared by Cutinase-Mediated Immobilization on Self-Assembled Monolayers. *Anal. Chem.* **2004**, *76*, 5713-5720.
34. Cao, H. H.; Nakatsuka, N.; Serino, A. C.; Liao, W.-S.; Cheunkar, S.; Yang, H.; Weiss, P. S.; Andrews, A. M. Controlled DNA Patterning by Chemical Lift-Off Lithography: Matrix Matters. *ACS Nano* **2015**, *9*, 11439-11454.
35. Rao, A. N.; Grainger, D. W. Biophysical Properties of Nucleic Acids at Surfaces Relevant to Microarray Performance. *Biomater. Sci.* **2014**, *2*, 436-471.
36. Ravan, H.; Kashanian, S.; Sanadgol, N.; Badoei-Dalfard, A.; Karami, Z. Strategies for Optimizing DNA Hybridization on Surfaces. *Anal. Biochem.* **2014**, *444*, 41-46.
37. Wong, E. L. S.; Chow, E.; Gooding, J. J. DNA Recognition Interfaces: The Influence of Interfacial Design on the Efficiency and Kinetics of Hybridization. *Langmuir* **2005**, *21*, 6957-6965.

38. Ozkumur, E.; Ahn, S.; Yalcin, A.; Lopez, C. A.; Cevik, E.; Irani, R. J.; DeLisi, C.; Chiari, M.; Unlu, M. S. Label-Free Microarray Imaging for Direct Detection of DNA Hybridization and Single-Nucleotide Mismatches. *Biosens. Bioelectron.* **2010**, *25*, 1789-1795.
39. Jung, Y. K.; Kim, J.; Mathies, R. A. Microfluidic Linear Hydrogel Array for Multiplexed Single Nucleotide Polymorphism (SNP) Detection. *Anal. Chem.* **2015**, *87*, 3165-3170.
40. Qian, X. T.; Pu, D.; Liu, B. C.; Xiao, P. F. Effect of Oligonucleotide Probes Substituted by Deoxyinosines on the Specificity of SNP Detection on the DNA Microarray. *Electrophoresis* **2015**, *36*, 263-270.
41. Wan, L.; Sun, K. L.; Ding, Q.; Cui, Y. H.; Li, M.; Wen, Y. L.; Elston, R. C.; Qian, M. P.; Fu, W. J. J. Hybridization Modeling of Oligonucleotide SNP Arrays for Accurate DNA Copy Number Estimation. *Nucleic Acids Res.* **2009**, *37*, e117.
42. Monserud, J. H.; Schwartz, D. K. Mechanisms of Surface-Mediated DNA Hybridization. *ACS Nano* **2014**, *8*, 4488-4499.
43. Carlon, E.; Heim, T. Thermodynamics of RNA/DNA Hybridization in High-Density Oligonucleotide Microarrays. *Phys. A* **2006**, *362*, 433-449.
44. Sedighi, A.; Li, P. C. H.; Pekcevik, I. C.; Gates, B. D. A Proposed Mechanism of the Influence of Gold Nanoparticles on DNA Hybridization. *ACS Nano* **2014**, *8*, 6765-6777.
45. Weckx, S.; Carlon, E.; De Vuyst, L.; Van Hummelen, P. Thermodynamic Behavior of Short Oligonucleotides in Microarray Hybridizations Can Be Described Using Gibbs Free Energy in a Nearest-Neighbor Model. *J. Phys. Chem. B* **2007**, *111*, 13583-13590.

46. Halperin, A.; Buhot, A.; Zhulina, E. B. On the Hybridization Isotherms of DNA Microarrays: The Langmuir Model and Its Extensions. *J. Phys. Condens. Matter* **2006**, *18*, S463-S490.
47. Bumm, L. A.; Arnold, J. J.; Cygan, M. T.; Dunbar, T. D.; Burgin, T. P.; Jones, L.; Allara, D. L.; Tour, J. M.; Weiss, P. S. Are Single Molecular Wires Conducting? *Science* **1996**, *271*, 1705-1707.
48. Cygan, M. T.; Dunbar, T. D.; Arnold, J. J.; Bumm, L. A.; Shedlock, N. F.; Burgin, T. P.; Jones, L.; Allara, D. L.; Tour, J. M.; Weiss, P. S. Insertion, Conductivity, and Structures of Conjugated Organic Oligomers in Self-Assembled Alkanethiol Monolayers on Au{111}. *J. Am. Chem. Soc.* **1998**, *120*, 2721-2732.
49. Langowski, B. A.; Uhrich, K. E. Oxygen Plasma-Treatment Effects on Si Transfer. *Langmuir* **2005**, *21*, 6366-6372.
50. Bodas, D.; Khan-Malek, C. Hydrophilization and Hydrophobic Recovery of PDMS by Oxygen Plasma and Chemical Treatment - An SEM Investigation. *Sens. Actuators B Chem.* **2007**, *123*, 368-373.
51. Efimenko, K.; Wallace, W. E.; Genzer, J. Surface Modification of Sylgard-184 Poly(Dimethyl Siloxane) Networks by Ultraviolet and Ultraviolet/Ozone Treatment. *J. Colloid Interface Sci.* **2002**, *254*, 306-315.
52. Koh, K. S.; Chin, J.; Chia, J.; Chiang, C. L. Quantitative Studies on PDMS-PDMS Interface Bonding with Piranha Solution and Its Swelling Effect. *Micromachines* **2012**, *3*, 427-441.

53. Sui, G. D.; Wang, J. Y.; Lee, C. C.; Lu, W. X.; Lee, S. P.; Leyton, J. V.; Wu, A. M.; Tseng, H. R. Solution-Phase Surface Modification in Intact Poly(Dimethylsiloxane) Microfluidic Channels. *Anal. Chem.* **2006**, *78*, 5543-5551.
54. Esplandiu, M. J.; Hagenstrom, H.; Kolb, D. M. Functionalized Self-Assembled Alkanethiol Monolayers on Au(111) Electrodes: 1. Surface Structure and Electrochemistry. *Langmuir* **2001**, *17*, 828-838.
55. Liu, Y. F.; Lee, Y. L. Adsorption Characteristics of OH-Terminated Alkanethiol and Arenethiol on Au(111) Surfaces. *Nanoscale* **2012**, *4*, 2093-2100.
56. Liu, Y. F.; Yang, Y. C.; Lee, Y. L. Assembly Behavior and Monolayer Characteristics of OH-Terminated Alkanethiol on Au(111): *In Situ* Scanning Tunneling Microscopy and Electrochemical Studies. *Nanotechnology* **2008**, *19*, 065609.
57. Wang, Y.; Chi, Q. J.; Hush, N. S.; Reimers, J. R.; Zhang, J. D.; Ulstrup, J. Gold Mining by Alkanethiol Radicals: Vacancies and Pits in the Self-Assembled Monolayers of 1-Propanethiol and 1-Butanethiol on Au(111). *J. Phys. Chem. C* **2011**, *115*, 10630-10639.
58. Wang, Y.; Chi, Q. J.; Hush, N. S.; Reimers, J. R.; Zhang, J. D.; Ulstrup, J. Scanning Tunneling Microscopic Observation of Adatom-Mediated Motifs on Gold-Thiol Self-Assembled Monolayers at High Coverage. *J. Phys. Chem. C* **2009**, *113*, 19601-19608.
59. Rudnev, A. V.; Yoshida, K.; Wandlowski, T. Electrochemical Characterization of Self-Assembled Ferrocene-Terminated Alkanethiol Monolayers on Low-Index Gold Single Crystal Electrodes. *Electrochim. Acta* **2013**, *87*, 770-778.
60. Kim, M.; Hohman, J. N.; Serino, A. C.; Weiss, P. S. Structural Manipulation of Hydrogen-Bonding Networks in Amide-Containing Alkanethiolate Monolayers *via* Electrochemical Processing. *J. Phys. Chem. C* **2010**, *114*, 19744-19751.

61. Dameron, A. A.; Mullen, T. J.; Hengstebeck, R. W.; Saavedra, H. M.; Weiss, P. S. Origins of Displacement in 1-Adamantanethiolate Self-Assembled Monolayers. *J. Phys. Chem. C* **2007**, *111*, 6747-6752.
62. Mullen, T. J.; Dameron, A. A.; Weiss, P. S. Directed Assembly and Separation of Self-Assembled Monolayers via Electrochemical Processing. *J. Phys. Chem. B* **2006**, *110*, 14410-14417.
63. Maksymovych, P.; Sorescu, D. C.; Yates, J. T. Gold-Adatom-Mediated Bonding in Self-Assembled Short-Chain Alkanethiolate Species on the Au(111) Surface. *Phys. Rev. Lett.* **2006**, *97*, 146103.
64. Moore, A. M.; Mantooh, B. A.; Donhauser, Z. J.; Yao, Y. X.; Tour, J. M.; Weiss, P. S. Real-Time Measurements of Conductance Switching and Motion of Single Oligo(Phenylene Ethynylene) Molecules. *J. Am. Chem. Soc.* **2007**, *129*, 10352-10353.
65. Han, P.; Kurland, A. R.; Giordano, A. N.; Nanayakkara, S. U.; Blake, M. M.; Pochas, C. M.; Weiss, P. S. Heads and Tails: Simultaneous Exposed and Buried Interface Imaging of Monolayers. *ACS Nano* **2009**, *3*, 3115-3121.
66. Poirier, G. E.; Tarlov, M. J. The c(4x2) Superlattice of *n*-Alkanethiol Monolayers Self-Assembled on Au(111). *Langmuir* **1994**, *10*, 2853-2856.
67. Poirier, G. E.; Tarlov, M. J. Molecular Ordering and Gold Migration Observed in Butanethiol Self-Assembled Monolayers Using Scanning Tunneling Microscopy. *J. Phys. Chem.* **1995**, *99*, 10966-10970.
68. Butler, S. Z.; Hollen, S. M.; Cao, L. Y.; Cui, Y.; Gupta, J. A.; Gutierrez, H. R.; Heinz, T. F.; Hong, S. S.; Huang, J. X.; Ismach, A. F.; Johnston-Halperin, E.; Kuno, M.; Plashnitsa, V. V.; Robinson, R. D.; Ruoff, R. S.; Salahuddin, S.; Shan, J.; Shi, L.; Spencer, M. G.;

- Terrones, M.; Windl, W.; Goldberger, J. E. Progress, Challenges, and Opportunities in Two-Dimensional Materials Beyond Graphene. *ACS Nano* **2013**, *7*, 2898-2926.
69. Das, S.; Robinson, J. A.; Dubey, M.; Terrones, H.; Terrones, M. Beyond Graphene: Progress in Novel Two-Dimensional Materials and van der Waals Solids. *Annu. Rev. Mater. Res.* **2015**, *45*, 1-27.
70. Kim, J.; Cote, L. J.; Huang, J. X. Two Dimensional Soft Material: New Faces of Graphene Oxide. *Acc. Chem. Res.* **2012**, *45*, 1356-1364.
71. Zhang, H. Ultrathin Two-Dimensional Nanomaterials. *ACS Nano* **2015**, *9*, 9451-9469.

9.3 Full Publication List

A. *Peer-Reviewed Articles* (corresponding authors underlined)

1. **Cao, H. H.**; Nakatsuka, N.; Serino, A. C.; Liao, W.-S.; Cheunkar, S.; Yang, H.; Weiss, P. S.; Andrews, A. M. Controlled DNA Patterning by Chemical Lift-Off Lithography: Matrix Matters. *ACS Nano* **2015**, *9*, 11439–11454.
2. Kim, J.; Rim, Y. S.; Chen, H.; **Cao, H. H.**; Nakatsuka, N.; Hinton, H. L.; Zhao, C.; Andrews, A. M.; Yang, Y.; Weiss, P. S. Fabrication of High-Performance Ultrathin In₂O₃ Film Field-Effect Transistors and Biosensors Using Chemical Lift-Off Lithography. *ACS Nano* **2015**, *9*, 4572-4582.
3. Liao, W.-S.; **Cao, H. H.**; Cheunkar, S.; Shuster, M. J.; Altieri, S. C.; Weiss, P. S.; Andrews, A. M. Small-Molecule Arrays for Sorting G-Protein-Coupled Receptors. *Journal of Physical Chemistry C* **2013**, *117*, 22362-22368.
4. Claridge, S. A.; Liao, W.-S.; Thomas, J. C.; Zhao, Y.; **Cao, H. H.**; Cheunkar, S.; Serino, A. C.; Andrews, A. M.; Weiss, P. S. From the Bottom Up: Dimensional Control and Characterization in Molecular Monolayers. *Chemical Society Reviews* **2013**, *42*, 2725-2745.
5. Liao, W.-S.; Cheunkar, S.; **Cao, H. H.**; Bednar, H.; Andrews, A. M.; Weiss, P. S. Subtractive Patterning *via* Chemical Lift-Off Lithography. *Science* **2012**, *337*, 1517-1521.
6. Shuster, M. J.; Vaish, A.; **Cao, H. H.**; Guttentag, A; McManigle, J.; Gibb, A.; Martinez, M.; Nezarati, R.; Hinds, J.; Liao, W. S.; Weiss P. S.; Andrews, A. M. Patterning Small-Molecule Biocapture Surfaces: Microcontact Insertion Printing *vs.* Photolithography. *Chemical Communications* **2011**, *47*, 10641-10643.

7. Norton, M. L.; Day, B. S.; **Cao, H. H.**; Rahman, M.; Gin, A. Arrays of Nanoarrays: Elements of Binding. *IEEE Sensors Journal* **2008**, *8*, 874-879.
8. Hong, S.; Jauregui, L. A.; Rangel, N. L.; **Cao, H. H.**; Day, B. S.; Norton, M. L.; Sinitskii, A. S.; Seminario, J. M. Impedance Measurements on a DNA Junction. *Journal of Chemical Physics* **2008**, *128*, 201103

B. Conference Proceedings (presenting author underlined)

9. Norton, M. L.; Rahman, M.; Day, B. S.; Huffman, C.; **Cao, H. H.**; Neff, D.; Butts, H.; Gin, A.; Recent Advances in Molecular Lithography. *Proceedings of SPIE* **2007**, 6769, 67690M.
10. Norton, M. L.; Neff, D.; Towler, I.; Day, B. S.; Grambos, Z. T.; Shremshock, M.; Butts, H. M.; Meadows, C.; Samiso, Y.; **Cao, H. H.**; Rahman, M.; Designed Self-Organization for Molecular Optoelectronics. *Proceedings of SPIE* **2006**, 6212, 621203.
11. Rahman, M.; Day, B. S.; **Cao, H. H.**; Butts, H. M.; Norton, M. L. Ordered DNA Arrays Prepared via Soft Lithography. *Proceedings of SPIE* **2006**, 6370, 637012.
12. Norton, M. L.; Neff, D.; Day, B. S.; Grambos, Z. T.; Shremshock, M.; Butts, H. M.; **Cao, H. H.** Single Molecule Substrates for Lithography. *Proceedings of IEEE NANO* **2006**, *2*, 531-533.

C. Submitted Manuscripts (corresponding authors underlined)

13. Image Segmentation with Dynamic Artifacts Detection and Bias Correction. Zosso, D.; An, J.; Stevick, J.; Takaki, N.; Weiss, M.; Slaughter, L. S.; **Cao, H. H.**; Weiss, P. S.; Bertozzi, A. L. Submitted to *American Institute of Mathematical Sciences Journal*

D. Manuscripts in Preparation (corresponding authors underlined)

14. Enabling Multiplexed Small-Molecule Patterning *via* Pre-Functionalized Alkanethiols.
Cao, H. H.; Deshayes, S.; Nakatsuka, N.; Yang, H.; Weiss, P. S.; Kasko, A. M.;
Andrews, A. M. *To be submitted.*
15. Toward Multiplexed Biocapture Substrates *via* Chemical Lift-Off Lithography. **Cao, H. H.**;
Liao, W.-S.; Serino, A. C.; Cheunkar, S.; Yang, H.; Weiss, P. S.; Andrews, A. M. *To be submitted.*
16. Chemical Fabrication of Patterned Transparent Gold-Coated Polydimethylsiloxane.
Slaughter, L. S.; **Cao, H. H.**; Yang, Q.; Young, T. D.; Cheung, K. M.; Serino, A. C.;
Zosso, D.; An, J.; Stevick, J.; Takaki, N.; Weiss, M.; Bertozzi, A. L.; Andrews, A. M.;
Weiss, P. S. *In preparation.*